JAERI-M
87-115

JAERI TANDEM, LINAC & V.D.G.

ANNUAL REPORT

1986

April 1, 1986—March 31, 1987

August 1987

Department of Physics

JAERI TANDEM, LINAC & V.D.G.

Annual Report

1986

April 1, 1986 - March 31, 1987

Department of Physics

Tokai Research Establishment

Japan Atomic Energy Research Institute

Tokai-mura, Naka-gun, Ibaraki-ken, Japan

This annual report describes research activities which have been performed with the JAERI tandem accelerator, the electron linear accelerator and the Van de Graaff accelerator from April 1, 1986 to March 31, 1987. Summary reports of 55 papers, and list of publications, personnel and cooperative researches with universities are contained.

Editors   Naomoto Shikazono

Mitsuhiko Ishii

Yuuki Kawarasaki

Yukio Kazumata

Chiaki Kobayashi

Yohta Nakai

Yoichi Suto

原研タンデム，リニアック，バンデグラフ加速器1986年度年次報告

日本原子力研究所東海研究所物理部
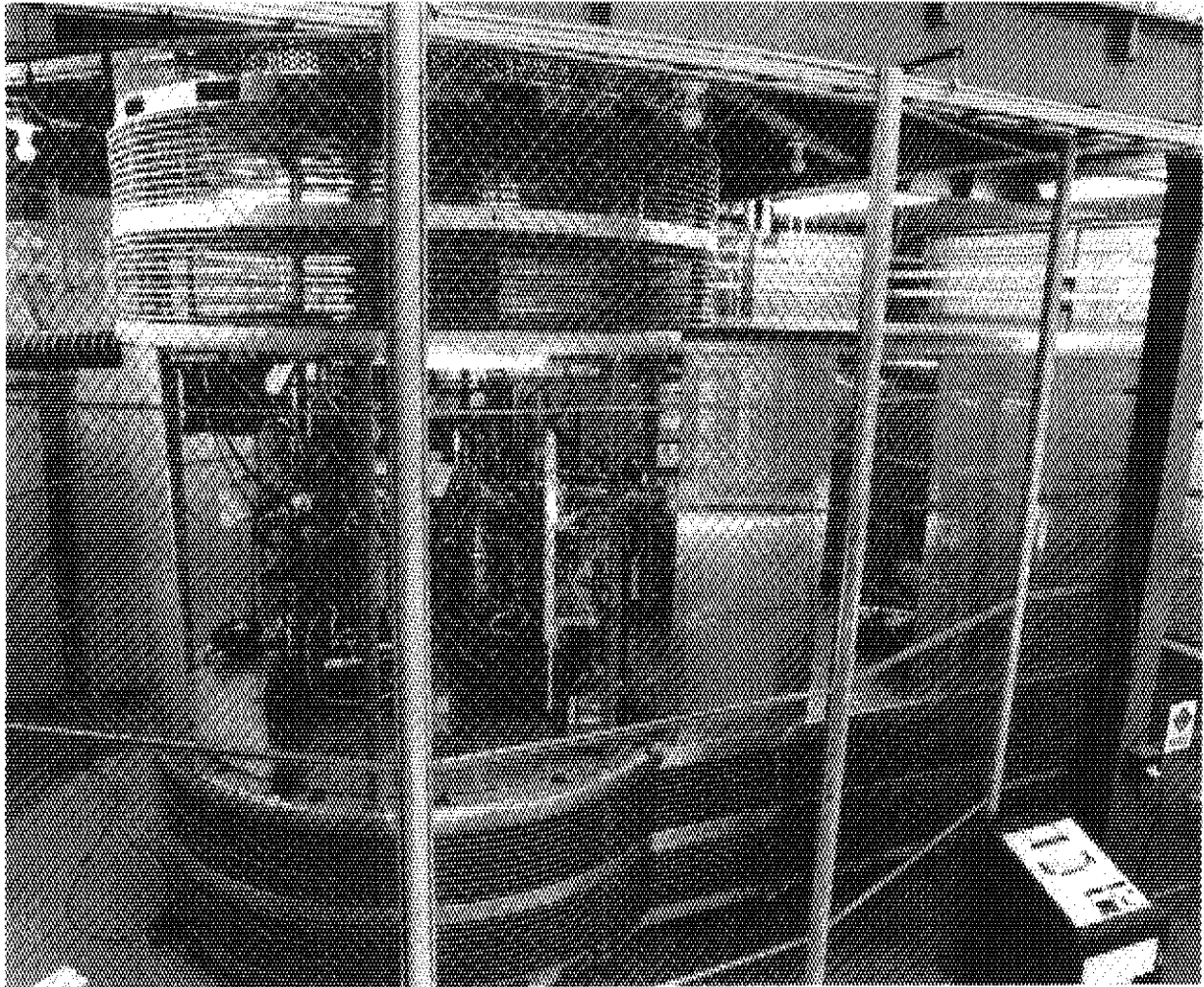
　本年次報告は，原研タンデム，リニアック及びバンデグラフ加速器で，1986年4月1日から1987年3月31日までの間に東海研で行われた研究活動をとりまとめたものである。
　1）加速器運転と開発研究，2）原子及び固体物理，3）材料の放射線損傷，4）核化学，5）核物理　及び6）中性子物理の6部門にまたがる55編の研究報告，公表された文献，関与した職員及び大学との協力研究のリストを収録している。

Negative Ion Injector of Tandem Accelerator

PREFACE

This report covers the research and development activities carried out
with accelerators of Department of Physics JAERI during the period from
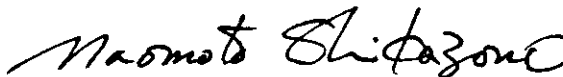April 1 1986 through March 31 1987.

All the accelerators, i.e. the tandem accelerator, the electron
linear accelerator and the Van de Graaff accelerator, have been operated
satisfactorily throughout the period. The tandem accelerator, with which
a majority of the research activities have been performed, operated on a
regular schedule in accordance with the cycle of three months operation
for research studies and the one month for the maintenance. A progress of
developing a superconducting quater wave resonator for the tandem heavy ion
booster has been made. The final goal is to obtain a 30MV of accelerating
voltage by using the 40 quater wave resonators. The electron linear
accelerator and the Van de Graaff accelerator have been used for some of the
research of neutron physics and solid state physics, respectively. In this
period, a design study of a superconducting electron linear accelerator for
free electron laser and related studies have started.

Main subjects of our research activities are as follows.
1) Atomic and solid state physics
2) Radiation effects in materials
3) Nuclear Chemistry
4) Nuclear Physics
5) Neutron Physics

During the period, more than 60 staff members of JAERI have worked in
the above five fields of researches, and about 100 colleagues of
universities and institutions outside JAERI have joined and collaborated in
these studies.

A joint seminar on atomic physics, solid state physics and material
science in the energy region of tandem accelerators was held at Tokai
Research Establishment of JAERI, January 8 - 10, 1987. Some of the
experimental results presented in the seminar are included in this annual
report.

Naomoto Shikazono
Directror,
Depatment of Physics

CONTENTS

I ACCELERATOR OPERATION AND DEVELOPMENT

1.1 TANDEM ACCELERATOR OPERATION

Tandem Accelerator Group

Department of physics, JAERI

Accelerator operation

During the year from April 1, 1986 to March 31, 1987 the tandem accelerator has run very well and almost 100 percent of scheduled experimental programs were performed. In this period, two scheduled maintenance and four unexpected repairs under tank opening are included. The following are summary of the operation and the maintenance.

1) Time distribution by terminal voltage

17-18 MV	2 days	0.9 %		11-12 MV	5 days	2.3 %
16-17	56	25.5		10-11	10	4.5
15-16	57	25.9		9-10	9	4.1
14-15	31	14.1		8- 9	5	2.3
13-14	11	5.0		7- 8	4	1.8
12-13	11	5.0		< 7	5	8.6

2) Time distribution by projectile

H	4 days	1.9 %		Si	10 days	4.8 %
D	15	7.2		S	35	16.8
B	2	1.0		Cl	48	23.1
C	17	8.2		Ni	12	5.8
N	6	2.9		Cu	1	.5
O	33	15.9		Br	5	2.4
F	16	7.7		I	4	1.9

3) Time distribution by activity

Operation for research		225 days	61.6 %
Atomic and solid state physics	(	56 days	)
Radiation effects in materials	(	26	)
Nuclear chemistry	(	39	)
Nuclear physics	(	71	)
Fast neutron physics	(	16	)

Accelerator development	(17)	
Voltage conditioning	21	5.8 %
Operation training	4	1.1
Scheduled maintenance	68	18.6
Unexpected repair	11	3.0
Holidays and vacation	36	9.9

Tank openings

The scheduled maintenance and major troubles, requiring six tank openings, were as follows.

1) April 19-23, 1986

   Lost communication with upper dead section caused by the CAMAC module trouble.

2) May 27-June 19, 1986

   Scheduled opening.

   Reload of the terminal stripper foils.

   Regular maintenance for the chains and the rotating shafts.

   Replacement of the isolation valve between the low energy tube and the terminal stripper foil chamber by a newly designed valve.

3) June 30-July 2, 1986

   The trouble of the terminal pulsing system caused by poor wiring in a terminal pulsing amplifier.

4) October 27-November 25, 1986

   Scheduled maintenance.

   Replacement of the foil stripper chamber by that of modified type. It has viewing ports for observing foils at the beam position by means of TV camera.

   Renewal of Ti sublimation elements for the terminal gas stripper.

   Renewal of two charging chains.

   Regular maintenance for the rotating shafts.

5) December 9-14, 1986

   Lost communication with the terminal caused by trouble of the light link receiver.

6) January 6-10, 1987

   The trouble of the lower dead section generator caused by the bearing damage.

Improvement and development

By observing the stripper foil directly during the ion beam irradiation, we can expect to get many information about it. On October 1986, we installed a small TV camera system, black and white camera and transmitter, on the terminal and laid a plastic fiber along the column to transfer video signals to the ground potential. No trouble has occurred on the system so far. Now we are testing for sapphire sight glasses, strong enough for SF_6 gas pressure, for the foil chamber.

The new vacuum isolation valve between the low energy tube and the foil stripper chamber increases reliability and easy handling. It has a silver seat and is guaranteed for the open-close handling of over 4000 times or over.

A number of improvements have been carried out for the second negative ion injector system and the accelerator control system. For the former system, an insulating deck, an inflection magnet, aninsulation transformer and a part of vacuum system have been assembled so far, and still under construction.

A new computer program for the latter system has completed on December 1986.

1.2 ELECTRON LINAC OPERATION AND IMPROVEMENTS

Electron Linac Group

Department of Physics, JAERI

Operation

The 120 MeV JAERI electron linear accelerator (linac) has been operated without any major troubles during the fiscal year of 1986. The new experimental programs using high energy electron beams have started last year in addition to the continuous programs of neutron cross section measurements and the preparatory study of low energy neutron mirror guide for the JRR-3 (Japan Research Reactor-3) facility. The new research programs are (1) the study of the irradiation damage in solid at the liquid helium temperature, (2) the mono-energetic positron emission and its application for material researches and (3) the free electron laser (FEL) experiment.

The machine time for the ordinary neutron cross section measurements has been decreased last year due to the start-up of the new research programs which have required the machine times for the preparations of the equipments and facilities. The machine times of linac operation itself were mainly for the test of the buncher and prebuncher which had been designed and constructed in 1985, and for the beam adjustment of the FEL experiments which needed the fine beam condition.

Table 1 Machine Time and Output Beam for Research Programs in 1986

Research Program	Time (h)	Ratio (%)	Energy (MeV)	Rate (pps)	Length (nsec)	Ave. Current (μA)
Development of Research Reactor (Development of Neutron Mirror)	737	56.2	100	50	1000	~24
Neutron Cross Section (Time of Flight Method)	441	33.6	120	150	25	12
Solid State Physics (Low Temperature Electron Irradiation)	21	1.6	55	50	1000	~2
Development of Free Electron Laser (Measurement of Spontaneous Emission)	28	2.2	120~140	12.5	1000	0.075
Positron Experiment (Emission of mono-energetic positron)	9	0.7	100	50	1000	12
Tuning and Test Operation	75	5.7	100~180	50~150	~1000	~30
Total	1311	100.0				

Maintenance

The number of the unscheduled shut-downs due to the machine troubles was reduced last year because the linac was operated with the low repetition rate of 50 pps and 150 pps. The causes of troubles were as follows: (1) break-down of a filament of the electron gun, (2) vacuum leak from the bellows in the connection tube between the accelerator structures, and (3) damage of a magnetic braker.

Several parts of the linac components are replaced or overhauled as the scheduled maintenance. The replaced parts are as follows (the number of the parts replaced is shown in the parenthesis): (a) Focusing coil(1) and main klystron(1), (b) Ion pumps of 10 l/s(2) and 40 l/s(2), (c) Power supplies for quadruple magnets with the GP-IB interface(6), (d) Power supplies for bending magnets(3), (e) IVR (20 kVA) drive motor(1) and (f) Wiring including the interlock systems. Parts which were overhauled are as follows: (a) pump units of 600 l/s(1) and 450 l/s(1) for water cooling, (b) ion pumps(2) and (c) beam transport tube.

Improvements

The several modifications of the components were also carried out. (1) The buncher and prebuncher, were installed and become operational. The 2a value (bore radius) of the new buncher is decreased by 5.15 % and the Q value of the prebuncher is increased from 500 to 1000 compared to those in the previous injector system. (2) The whole interlock systems which consist of 240 sensing points, have been replaced by adding new 80 points. All the interlock systems are connected with the GP-IB interface to the micro computer PC-8801, which monitors and displays the operational conditions and carries out data logging. (3) The parts of the linac transport tube in the straight beam line are replaced from stainless steel tube to aluminum tube in order to reduce the radio activities with long half lives. (4) The recording system for personnels who enter into or exit from the radiation controlled area is newly prepared. This new system uses the bar-code reader which checks the number of the individual film budges.

The test of the accelerator characteristics

(1) stationary mode operation

After the new buncher and prebuncher were installed, the test of the accelerator characteristics were carried out. Under the stationary mode
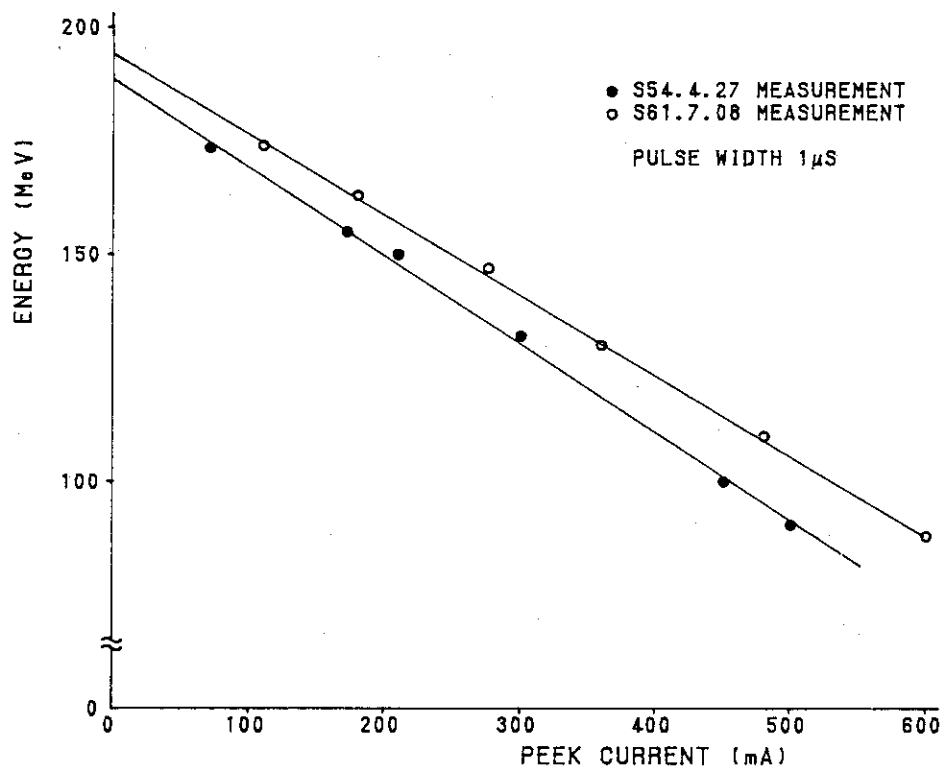
Fig. 1 JAERI LINAC E-I CHARACTERISTICS

operation (pulse width 1 μs), the beam current of 100 MeV electron was
increased by 20 % compared to the old buncher. The E-I curve (Energy vs
current) is shown in Fig. 1, when the linac was operated with a pulse width
of 1 μs.

(2) Transient mode operation

The transient mode operation with an energy of 120 MeV, a pulse width of
25 ns, a repetition rate of 150 pps and a beam current of 12 μA was tested.
The peak current of the electron beam was 3.5 A, if the pulse shape was
assumed to be triangular. This beam current was 80 % of the maximum
current achieved previously with the old injector system. The loss of the
electron current was observed with the core monitor at the end position of
the # 1 accelerator structure. In order to improve the beam current, the
focusing system for the whole injector system and the # 1 accelerator tube
must be improved.

(3) FEL experiments

The FEL experiments were carried out in collaboration with Nuclear
Engineering Research Laboratory, University of Tokyo. The electron beams
were carefully adjusted to meet the requirements for the optical apparatus
such as a wiggler magnet producing the spontaneous emission in the visible

light region. The peak electron current of 12 mA (1 μs) was accelerated with the 1.7 % energy spread at 126.7 MeV. After the FEL experiment, the beam energy resolution was further improved to be 0.96 % with the higher peak current of 36 mA as shown in Fig. 2.
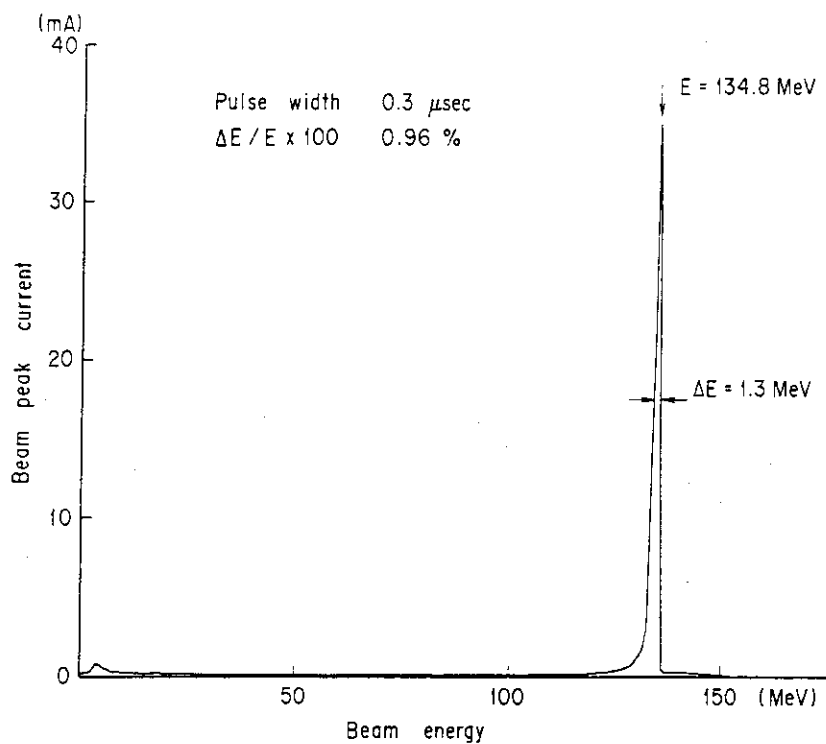
Fig. 2   Energy Resolution of JAERI Linac

References

1) Electron Linac Group: JAERI-M 86-112 (1986) 18.

2) K.Mashiko et al.: Proceedings of the 11th Meeting on Linac in Tsukuba (1986) 12.

1.3 CONTROL SYSTEM FOR THE JAERI TANDEM ACCELERATOR

Susumu HANASHIMA, Isao OHUCHI, Katsuzo HORIE, Susumu KANDA, and Yoshihiro TSUKIHASHI

Department of Physics, JAERI

As previously reported, renewal of the control system[1,2,3] was completed. It was mainly intended to adopt the system to high level control of the accelerator and partially intended to improve reliability of the system. The outlooking of the new system is similar to the previous one[4], but the internal structure is different. All programs were newly written in the new system. More reliable technics of the programming were used than the previous. Data independency of the programs were greatly improved. Maintenance of the programs and data for the accelerator became easy.

A concept of beam line primitive's(abbreviated as BLP's) was newly introduced to point to one of the elementary manipulations of the functions of the devices. They have mnemonic names, CAMAC addresses, data formats, conversion coefficients between physical values and CAMAC representations, etc. These are described in a file called "CAMAC directory". The basic control program reads all of them to start control of the accelerator. Name of the BLP and the notation of the physical value are extensively used. A fast access mechanism to a BLP referenced by the name is realized with a so called hashing technic[5].

In the system, other programs than the basic control programs can run concurrently for the high level control . Four procedures are prepared for a programmer of the high level control, which implement control and monitor of the BLP's. These are the procedures for status control, status monitor, control of numerical value and monitor of numerical value, respectively. He need not know about the CAMAC address and the CAMAC representation of the BLP's to get access to the accelerator.

The system started its service in December of the last year with limited functions. The full functions were implemented in March of this year. No system down occurred with exception of three hardware troubles since the start of the new system(Two of them occurred because of the primary power failure. The other one occurred because of puncture of an I.C..).

Now, we are going to implement the high level control features. Especially, scaling method for the automated beam transport is planed to implement, whose feasibility tests[2,6,7] were successfully made in the past 5 years.

References

1) S. Hanashima et al.: JAERI Tandem Annual Report 1983, JAERI-M 84_129(1984) pp.10-11.

2) S. Hanashima et al.: JAERI Tandem, Linac and V.D.G. Annual Report 1984, JAERI-M 85-104(1985) pp.10-12.

3) S. Hanashima et al.: JAERI Tandem, Linac & V.D.G. Annual Report 1985, JAERI-M 86-112(1986) pp.6-7.

4) M. Maruyama: Proc. 3rd Int. Symp. on Electrostatic Accelerator Technology, Oak Ridge, Tenesse(1981) pp.17.

5) Any tutorial book for computer programing, for example N. Wirth: Algolithms+Data structures = Programs, Prentice-Hall, England Cliffs, New Jersey.

6) S. Hanashima et al.: Automated Control of the JAERI Tandem Accelerator, Proc. of the 5th Symp. on Accelerator Science and Technology, Japan(1984) pp.420.

7) S. Hanashima and E. Minehara: Scaling of the Optical Parameters for the JAERI Tandem Accelerator, Rev. Sci. Instrum. 57(5)(1886) pp.787.

1.4 THE SECOND INJECTOR FOR JAERI TANDEM ACCELERATOR

Eisuke MINEHARA, Tadashi YOSHIDA, Shinichi ABE,
Katsuzo HORIE, Yoshihiro TSUKIHASHI, Susumu KANDA,
Shuhei KANAZAWA and Susumu HANASHIMA

Accelerators Division, Department of Physics,
Japan Atomic Energy Research Institute,

The JAERI 350kV negative ion injector was extended to increase reliability of all devices in the injector, to exclude completely any unsafe operation, and to add a capability of simultaneous operation of plural ion sources in 1984. After the extended injector became available, we have been able to run the injector very steadily, and we have had few troubles concerning about all items of the extension[1].

In order to obtain a full strength of resistance against any sudden troubles in the injector, we will construct another negative ion injector for the JAERI tandem accelerator. In addition to the backing up the first injector, the second injector was designed to realize better transmission, higher mass resolution, and lower aberration than the first injector by utilizing a double focusing 90 degree analyzing magnet instead of a four port switching magnet in the first.

As a schematic view of the JAERI negative ion injectors, and the ion source room layout are shown in figs.1 and 2, the second injector will be installed in front of the established one. The layout of the first and the second injector are shown in figs.3 and 4.
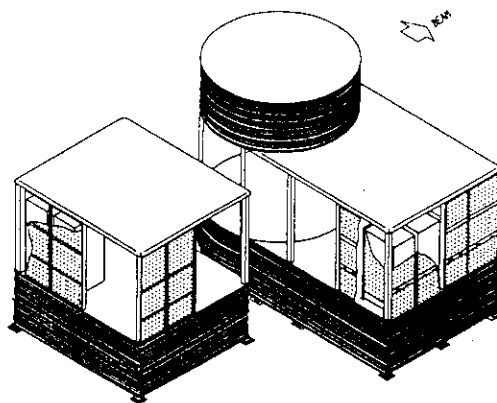
The decision to put the ana-lyzing magnet inside the high

Fig.1 Schematic view of the JAERI negative ion injectors.

voltage platform of the second injector has been made by de-

creasing the current
load to the 300kV
preacceleration tube,
cost consideration,
and mass analysis
independent with the
first injector
operation. The double
focusing 90 degree
analyzing magnet is
chosen because of the
better optical
properties than
smaller bending angle
magnets. A pole gap
of 43mm with a
clearence from the
vacuum chamber of at
least 35mm has been
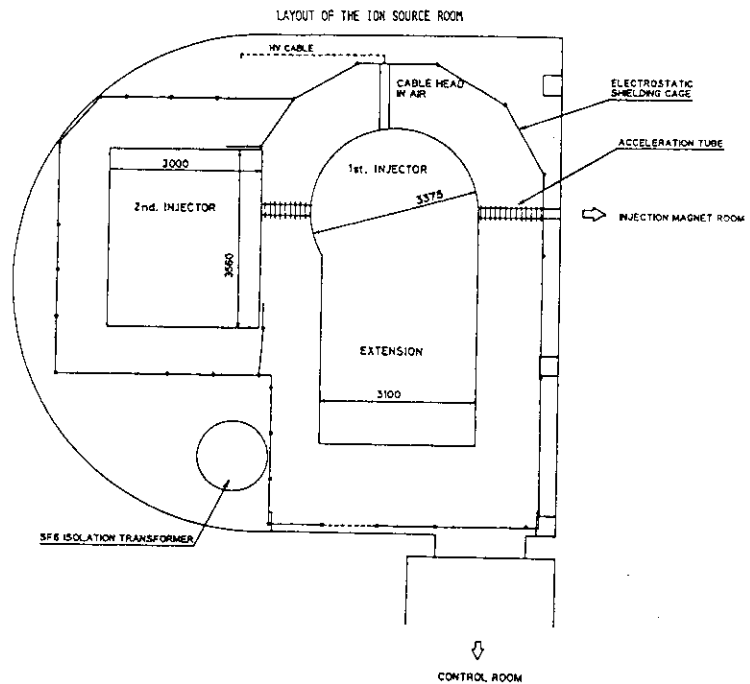
Fig.2 Layout of the ion source room.

chosen so as to increase the acceptance of the analyzing system.
The main characteristics of the analyzing magnet are listed in
table 1.
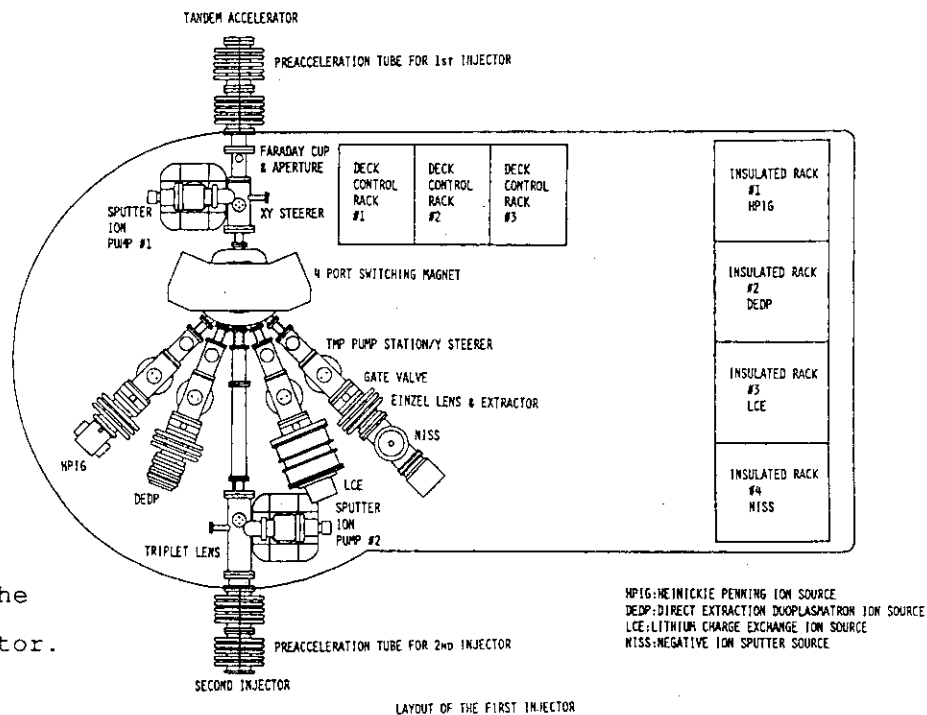
Fig.3 Layout of the
first injector.

HPIG:HEINICKIE PENNING ION SOURCE
DEDP:DIRECT EXTRACTION DUOPLASMATRON ION SOURCE
LCE:LITHIUM CHARGE EXCHANGE ION SOURCE
NISS:NEGATIVE ION SPUTTER SOURCE

Table 1 Main Characteristics of the 90 degree Double Focusing
Magnet.

bending angle	90 degrees
bending radius	300 mm
entrance angle of pole face	26.57 degrees
exit angle of pole face	26.57 degrees
maxium field	14.4kGauss
pole gap	43 mm
vacuum chamber inner gap	35 mm

An einzel lens and extractor unit
is used to produce an image of the source
aperture around the defining slit at a
distance of about 0.6 m from the magnet.
The resolving power of the analyzing
system strongly depends on its acceptance
and on the source position.   The beam
envelop shown in fig.5 has been obtained
with an ion source aperture-magnet
distance of about 1.2m and the system
acceptance to about 4mm mrad (MeV)$^{1/2}$ in
the vertical and horizontal planes.

LAYOUT OF THE SECOND INJECTOR

Fig.4 Layout of the second injector.

Under such conditions, a high mass resolution of M/dM~=150 can be
obtained.

An electrostatic triplet lens will be installed in the beam
line just after the second injector's acceleration tube.   The triplet
lens realizes a waist just after the first injector's tube so as to
keep small beam dimension along the injection line.

The expected goal of the second injector vacuum system is to
produce a working vacuum of $1x10^{-7}$ to $1x10^{-6}$ torr.   The system which
is nearly the same as the first injector's consists of a 520 l/s
turbomolecular pump and a 400 l/s sputter ion pump mounted before
and after the analyzing magnet, and a 120 l/s sputter ion pump after
the triplet lens.

The 400kV high voltage generator consists of a 16 kHz, 30kV
driver powering a multiplier and rectifier column that is contained

Fig.5 Beam envelop for the first and second injectors.

in a SF6 filled FRP pressure vessel. This power supply is characterized by a very low ripple(less than 1×10^{-4}) and a sturdiness against heavy arc discharges.

The maximum power needed to feed all the equipment at the platform has been evaluated to about 20 kVA. Such power will be supplied by a SF6 gas and epoxy resin insulated isolation transformer through a polyethylene insulated high voltage coaxial cable[2].

All power supplies will be equiped with remote control setting and readout in 12 or 16 bit resolution. A CAMAC crate, placed in the high voltage platform, will communicate by optical glass fibers, with other crates driven by a main computer(Perkin Elmer 7/32C) at ground potential[3].

References

(1) E.Minehara, T.Yoshida, S.Abe, S.Kanazawa, Y.Tsukihashi, K.Horie and S.Hanashima, Rev. Sci. Instrum. 58, 215(1987).
(2) E.Minehara,Nucl. Instr. and Meth. A249(1986)137.
(3) S.Hanashima, K.Horie, S.Kanda, I.Ohuchi,Y.Tsukihashi and E.Minehara, Proc. 5th Symp. on Accelerator Science and Technology(1984) Tsukuba, Japan, p.420.

1.5 A PROTOTYPE SUPERCONDUCTING QUARTER WAVE RESONATOR FOR HEAVY ION BOOSTOR

Suehiro TAKEUCHI, Tetsuro ISHII, Hiroshi IKEZOE
Makio OHKUBO, Naomoto SHIKAZONO

Department of Physics, JAERI

A superconducting niobium quarter wave resonator shown in Fig. 1 was fabricated successfully, which was designed as a prototype accelerating structure of the proposed JAERI tandem superconducting heavy ion boostor. After the surface treatment of the inner wall of niobium and the performance test at liquid helium temperature were repeated several times, the resonator could generate an accelerating field level of 4.6 MV/m with 1.6 watts rf input at 4.2K. The progress to this result is described below.

The fabrication at the manufacturer, Mitsubishi Electric Company at Kobe, finished up at the end of June in 1986 with the final electron beam welding joining the center conductor part and the outer conductor. The resonator was expected to be moderately electropolished as the final surface treatment. However, a number of small spots were found on the drift tube and the shorting(upper) end plate. They seemed to be created by mistake in the final high temperature(1000°C) anneal treatment in vacuum. They were removed with sand papers and heavy electropolishing. The resonator viewed from the bottom end is shown in Fig. 2.

Fig. 1 Cut away view of a superconducting quarter wave resonator.

The first cool-down in the test cryostat was performed in August. The resonator put under the helium dewar of the test cryostat is shown in Fig. 3. The intrinsic quality factor Q and the accelerating field level E_a measured at 4.2K in the consecutive performance tests from August to December in 1986 are shown in Fig. 4. At the first test, as indicated by
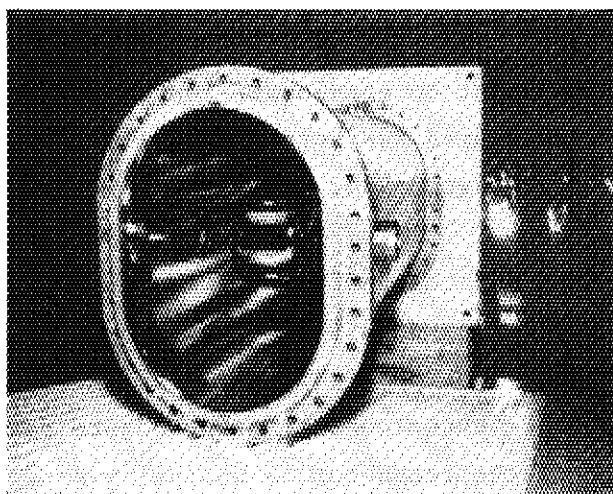
Fig. 2 Quarter wave resonator viewed from the bottom open end.

Fig. 3 Quarter wave resonator being set into a test cryostat.

curve 1, a high maximum field level of 3.6 MV/m was obtained, though the Q was not so high. The test was done without a magnetic shield against the earth's magnetic field. The curve 2 and the remainings are the results taken with a shield of Permalloy. Approximately 50 % increase on Q was yielded by the shield. It is known that dc magnetic flux is frozen in the superconductor if it exists during a cooling across the critical temperature. The frozen-in magnetic flux increases the rf surface resistance and degrades the Q.

The curve 3 was the result after an electropolishing surface treatment was done in order to get a higher field level and a higher Q. It brought about a poor result. We found that it was caused by dirt on the niobium wall surface which happened to enter through a small hole after the surface treatment. The hole was generated by mistake at an outermost point on the top end circumference of the outer conductor in an elecron beam welding process.

The curve 4 is the result obtained by a very careful final rinse with deionized water and drying after a light electropolishing. The field level together with the Q increased to a level satisfying us enough. The curve 5 was obtained after one week outgasing at 75 °C. The Q was improved

appreciablly at lower levels. In consequence of these tests, the importance of surface cleanness was reconfirmed.

The frequency stability is very important to accelerate ion beams stably. The static frequency stability measured was better than + 0.15 Hz. This excellent stability will be advantageous for the fast rf phase tuning to the beam phase.

We can conclude from the fabrication and the performance tests of this prototype resonator that explosive bonding of niobium and copper plates, machining, electron beam welding, electropolishing were all developed to a high level enough to produce superconducting resonators for the tandem booster and that the design of the resonator is basically good.

In addition, a superconducting post buncher consisting of two quarter wave resonator is under construction. The control units involving slow and fast tuners are being developed for the buncher. The resonators and the cryostat were designed so as to pass the domestic high pressure gas law.
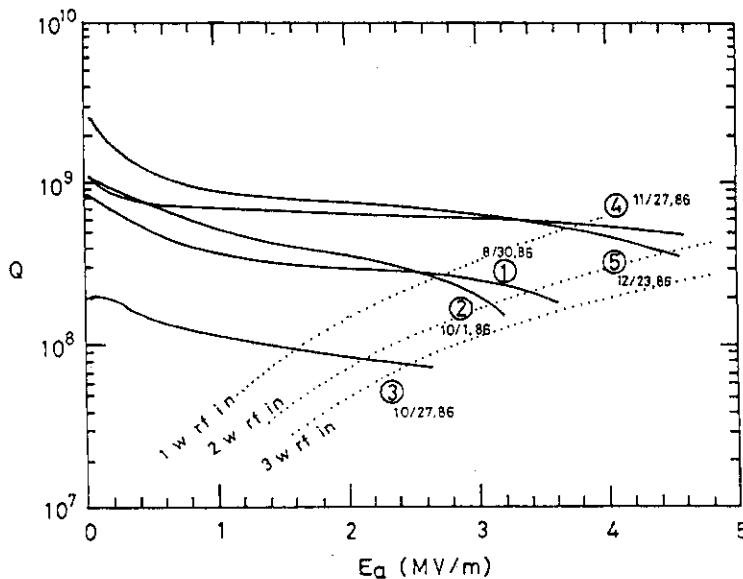
Fig. 4 Performance of the prototype quarter wave resonator at 4.2K. The details are described in the text.

1.6 OBSERVATION OF SPONTANEOUS EMISSION
OF RADIATION AT A VISIBLE WAVELENGTH

Yuuki KAWARASAKI, Makio OHKUBO, Katsuo MASHIKO,
Motoharu MIZUMOTO, Hirotada O'HASHI*, Hitoshi
KOBAYASHI*, Tohru UEDA*, Toshiaki KOBAYASHI*,
Chihiro TSUKISHIMA* and Maki KISHIMOTO*

Department of Physics, JAERI, * Faculty of
Engineering, University of Tokyo

Spontaneous, incoherent synchrotron radiation at a visible wavelength has been observed from a 130-MeV electron beam passing through a 4-cm period wiggler magnet.

Introduction

At the beginning of an experimental study on free electron laser (FEL), many laboratories have first tried the observation of spontaneous emission of radiation from the available electron beam passing through an originally designed wiggler magnet. This implies that the process to FEL can conventionally be divided into three steps; spontaneous emission (incoherent synchrotron radiation), stimulated emission(amplification) and saturation (oscillation).

The wavelength of emitted radiation from the fixed period wiggler magnet is inversely proportional to the square of the electron beam energy. The combination of around 30-MeV electron beam with a 4-cm period wiggler yields in emission of infrared region, while the visible light from the same wiggler requires higher than 100-MeV electron beam. The radiation at a visible wavelength is much easier than that at an invisible wavelength to observe.

From the observation experience, much information on the beam characteristic will effectively be obtained, because the emitted spectrum is sensitively affected by it.

Experimentals

Fig.1 shows schematically an experimental arrangement. From the left

side in the figure, the electron beam from the JAERI linac passed to the right, being bended by 5 degree through the bending magnet BM1 to the right-handed beam port (we have three beam ports totally at this position). Two beam slits were prepared; one had a larger aperture and another inserted for this experiment just in front of the wiggler magnet had an aperture of 6 mm in diameter. The quadrupole magnets were turned off to prevent the deteriorations of the energy spread and emittance.
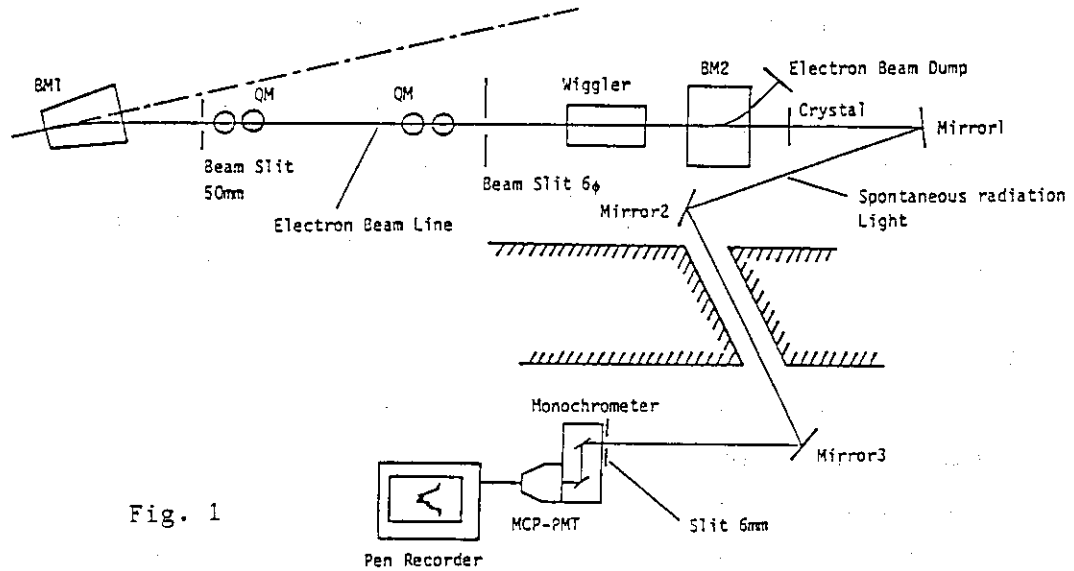
Fig. 1

The second beam bending magnet, BM2, was used for beam dump. The field strength was roughly 0.7 T. The beam bending causes to emit synchrotron radiation, SR. Thus, without the wiggler magnet in the beam course, visible light can be observed as SR. Comparison of the radiation spectrum and intensity between with and without the wiggler magnet was made.

Table 1

Wiggler	Wave Length : λ_w	4 cm
	Max Magnetic Field on Axis : B_w	0.351 T
	Wiggler Parameter : K	0.926
	Number of Period : N_w	10
Electron Beam	Energy : E	126.7 MeV
	Lorentz factor : γ	248.9
	Current : I	24 mA
	Spectrum Band Width : $\Delta E/E$	1.66 %
	Pulse Width	0.2 μs
	Beam Size	7 mm × 5 mm
Spontaneous Radiation	Peak Wave Length : λ_{sp}	590 nm
	Homogeneous Band Width : $\Delta\lambda$	29.5 nm

The experimental parameters, including the specification of the wiggler magnet which has been assembled by members of University of Tokyo, are listed in Table 1. The centeral wavelength of radiation and homogeneous band width are estimated by the formula cited in a textbook .

Result and discussion

A picture shown on page 23 has been photographed, using a telephoto-lens at the position of the monochrometer, flat mirrors being replaced by concave mirrors (f=1000 mm). On axis we see the fundamental radiation of 590 nm(yellow) with larger wavelengths emitted at larger off-axis(yellow to red). Superposed on this fundamental spectrum is the second harmonic spectrum, which first becomes visible as the violet ring at larger angle, because its central region is in the utraviolet. For the fundamental spectrum, at larger angle than the red ring is also invisible, infrared.

The measured spectrum for the fundamental is shown in Fig. 2. This shows wider half width by 4.7 than that of homogeneous broadening. The inhomogeneous broadening is due to beam energy dispersion, beam emittance (beam size and divergence) and field inuniformity of the wiggler magnet.

Fig. 2
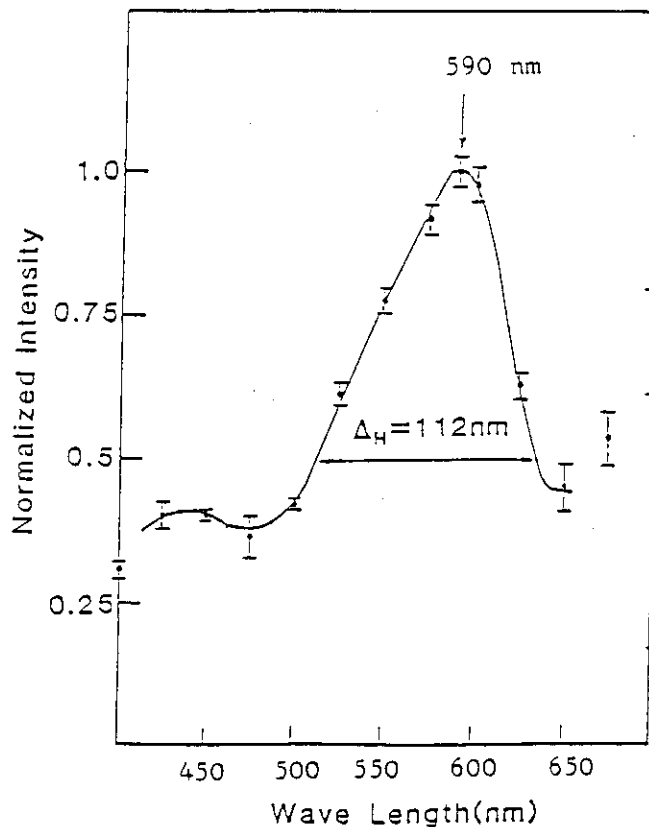
An estimation on the inhomogeneous broadening due to the above three fac-
tors are summarized in Table 2 and meets the experimental spectrum. The
energy dispersion was experimentally checked, and the beam emittance and
size were estimated from beam optics[1] and the field inuniformity previously
measured.[2] The second factor, the beam emittance, gives the most serious
influence to the broadening.

Table 2

Energy Dispersion	$\sigma_E = 0.034$
Emittance/ Beam Diameter	$\sigma_r = 0.10$
Magnetic Field Accuracy	$\sigma_B = 0.014$
$\sigma_{(Inhomogeneous)} = \left(\sigma_E{}^2 + \sigma_r{}^2 + \sigma_B{}^2\right)^{1/2} = 0.107$	

The spectrum and intensity of SR radiation emitted from the BM2 were
almost flat and smaller by 2 order of magnitude than that from the wiggler
magnet.

1) H.Kobayashi and C.Tsukishima: private communication
2) H.O'hashi: private communication

Photograph

−25〜(26)−

Ⅱ ATOMIC AND SOLID STATE PHYSICS

2.1 TIME-OF-FLIGHT MEASUREMENT OF MULTIPLE IONIZATION IN ION-ATOM COLLISION

Yasuaki SUGIZAKI, Masao SATAKA, Kiyoshi KAWATSURA
and Yohta NAKAI

Department of Physics, JAERI

Multiple ionization processes in ion-atom collisions are interesting subjects not only in atomic physics, but also in astrophysics and plasma physics. Most of ionization cross sections for targets, which are based on the yield of electrons and/or recoil ions collected at electrodes by condenser method, are measured as weighted averages over all final charge states of ions produced in collisions.[1] In the last decade, some studies of ionization processes have been made with taking account of the final charge states of both projectiles and recoil ions.[2-4] Fast heavy-ion imact produces multiple-ionized recoil ions in a single collision. It is important in comparison between experimental results and theoretical calculations to know the charge distribution of multiple-ionized recoil ions created in collisions, and further the correlation of the final charge state of both projectile and target atoms.

We have constructed an experimental apparatus at 2MV Van de Graaff (2MV VdG) facility of JAERI. This apparatus is aimed to measure absolute multiple ionization cross sections correlated to the final charge states of projectile and recoil ions by using a time-of-flight(TOF) coincidence method. In this paper, we report the performance of this apparatus.

The experimental apparatus is shown schematically in Fig. 1. It consists of three chambers, which contain a gas cell, a TOF drift tube and a charge selector. The gas cell in the first chamber is defined by entrance (1 mm in diameter) and exit (2 mm in diameter) apertures. The second chamber contains the TOF drift tube to analyze the charge state and the mass of recoil ions, and the charge selector in the third chamber is a pair of deflector plates to choose the charge states of postcollision projectile ions. These chambers are differentially evacuated by turbomolecular pump systems. The base pressure of the gas cell chamber is 1×10^{-8} Torr. The working pressure, which is monitored by a capacitance

manometer, is of the order of 10^{-4} Torr, where a single ion-atom collision condition is confirmed in the gas cell. The pressure of two other chambers are the order of 10^{-7} Torr during experiments. Charge change processes of postcollision projectile and recoil ions are neglegibly small under such vacuum conditions.

A monoenergetic incident beam from 2MV VdG accelerator is brought through an aperture into a target region containing a gas with a transverse electric field of about 400 V/cm, which extracts recoil ions of the target gas created by projectile impact. The recoil ions are extracted through an aperture of 2 mm in diameter from the gas cell and accelerated perpendicular to the incident beam by a 1.6 kV potential in a TOF drift tube. The channel electron multiplier(CEM) at the end of the drift tube detects recoil ions and the amplified signal from this detector provides a start trigger for a time-to-amplitude converter(TAC). The projectile ion after exiting the gas cell is immediately analyzed for its charge state by a pair of deflector plates and finally detected by a CEM. This electric field is variable to 20 kV/cm and is adjusted to select the charge state of interest. The projectile signal, which is delayed electrically with a few microseconds is used as a stop signal for the TAC because of decreasing of TAC duty cycles. The flight time of projectile ion over path from the gas cell to the CEM detector is constant for all charge states. The correlation time measured by the TAC depends only on the flight time of a recoil ion travelling through the drift tube, and is proportional to $\sqrt{m/q}$ where m and q are the mass and the charge state of the recoil ion. Each collision event in the time sequence is characterized by the specific delay time, and the specified charge states of both projectile and recoil ions created in the same collision are recognized by this coincident time.

To examine the performance of this experimental apparatus, we measured the charge distribution of recoil Ar ions for the reaction as follows,

$$He^{+}(1.0 \ MeV) \ + \ Ar \ \rightarrow \ He^{2+} \ + \ Ar^{q+}.$$

Fig. 2 shows the TOF spectrum of Ar ions produced by 1.0 MeV He^{+} impact. The measurement was made with coincidence between He^{2+} ion and each charge state of multiple-ionized Ar^{q+} ion. Peaks of Ar ions with the charge state from 1+ to 5+ are identified in the TOF spectrum. Higher charge state components were not clearly observed because of insufficiency of these

abundance. Background due to ionized fragments of residual gases such as H_2O^+, N_2^+ and O_2^+ were not remarkably appeared. Therefore, it is very easy to evaluate the peak area of each charge state which is proportional to the charge distribution of multiple-ionized Ar ions.

The performance of the experimental apparatus has been carefully examined. We intend to investigate multiple ionization processes by using this apparatus.
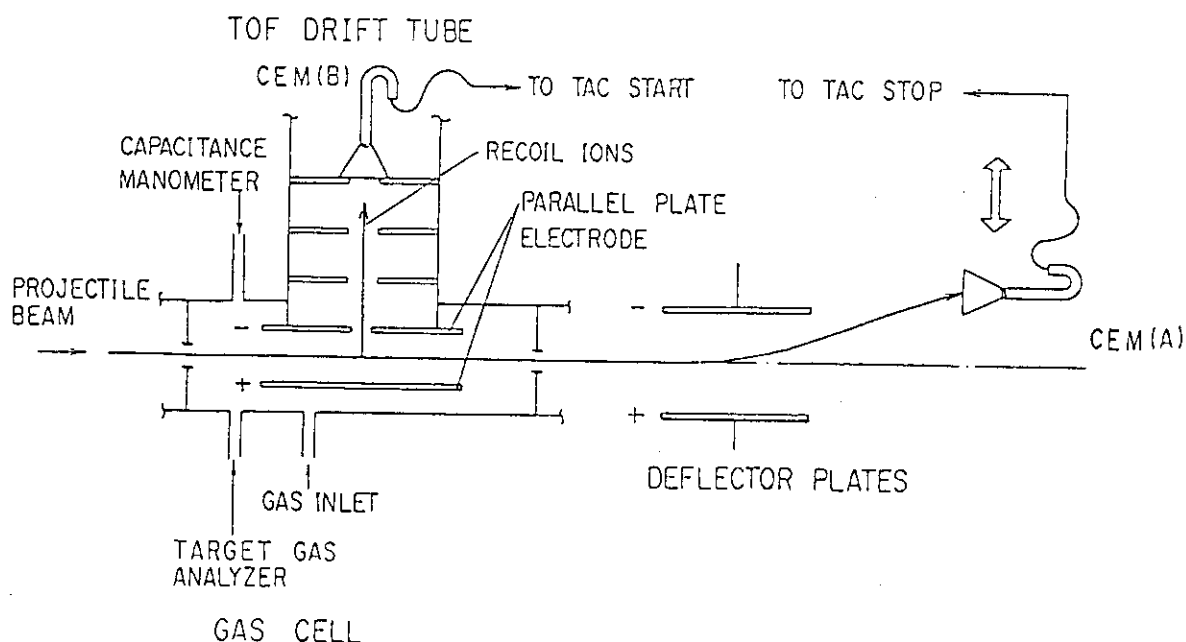
Fig. 1   A schematic diagram of the experimental apparatus. Three chambers containing a gas cell, a TOF drift tube and deflector plates are independently evacuated. A TOF spectrum are measured by the coincidence method between a postcollision projectile detected by a CEM(A) and extracted recoil ions detected by a CEM(B).
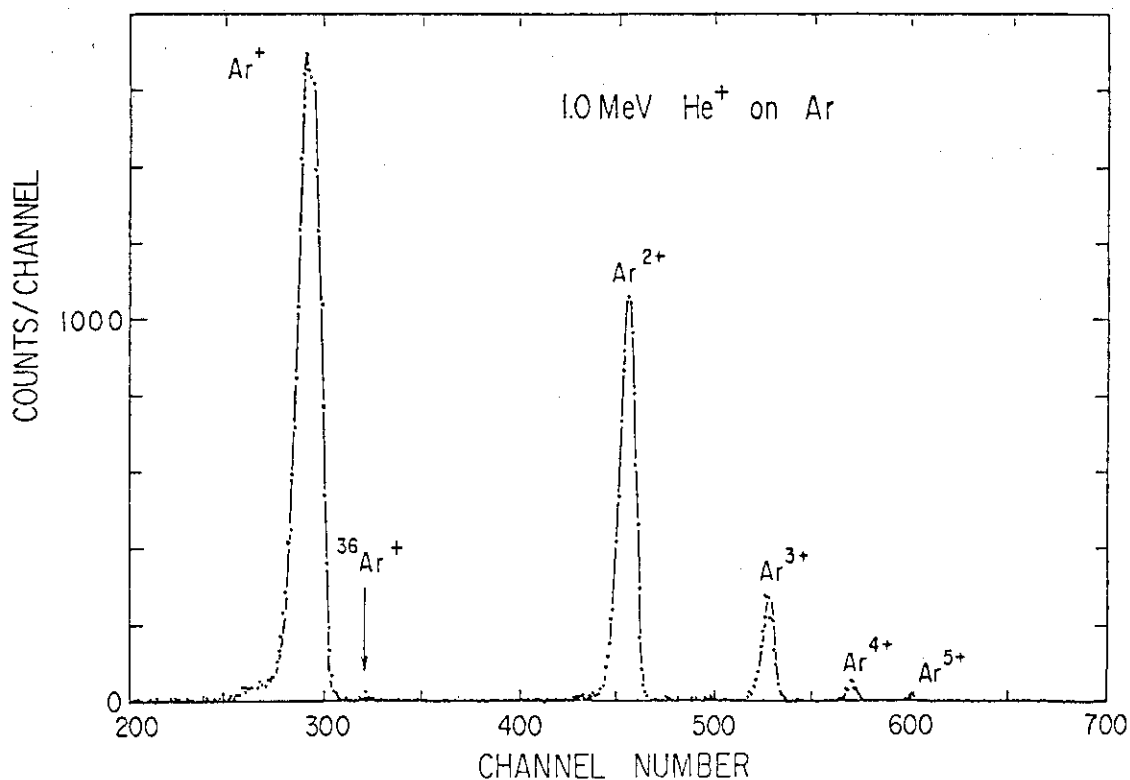
Fig. 2   A time-of-flight spectrum for multiple ionized Ar ions
produced by 1.0 MeV He[+] impact showing the distribution of
charge states.

References

1) M. Sataka, T. Shirai, A. Kikuchi and Y. Nakai: JAERI-M 9310 (1981).

2) E. H. Pedersen and L. Larsen: J. Phys. B 12 (1979) 4085.

3) T. J. Gray, C. L. Cocke and E. Justiniano: Phys. Rev. A 22 (1980) 849.

4) R. D. DuBois: Phys. Rev. A 52 (1984) 2348.

2.2 RADIATIVE ELECTRON CAPTURE IN HEAVY ION AND He COLLISIONS

Kiyoshi KAWATSURA, Masao SATAKA, Yasuaki SUGIZAKI,

Hiroshi NARAMOTO, Yohta NAKAI, Akio OOTUKA[*],

Ken-ichiro KOMAKI[*], Fuminori FUJIMOTO[*] and Kunio OZAWA[**]

Department of Physics, JAERI, [*]College of Arts and

Sciences, University of Tokyo, [**]Energy Research

Laboratory, Hitachi Ltd.

Introduction

Radiative electron capture (REC) in fast ion-atom collisions was first observed by Schnopper et al.[1] Since then, many investigations of REC processes have been reported. Most of the experimental data were taken by using solid or thick gas target. The experiments should be carried out under single collision conditions to compare with theoretical calculations. This work was done in order to extend our data under single collision conditions[2] to higher energies and different projectiles.

Experimental

The JAERI tandem accelerator provided F, Si, S and Cl ions at 2-5 MeV/amu. Using the post stripper (C foil, 15 $\mu g/cm^2$), the 0- and 1-electron ions were incident on He gas target. The REC and projectile K x-ray spectra were taken with a HORIBA Si(Li) x-ray detector at $90°$ to the beam direction. The energy resolution of the Si(Li) detector system was about 170 eV for Mn K_α x rays.

Results and discussion

Figure 1 and 2 show the x-ray spectra for Cl^{16+} and Cl^{17+} ion incident on a He gas target at an energy of 140 MeV. The centroid energies and widths of the REC x rays are given as[3]

$$\hbar\omega = \varepsilon_f - \varepsilon_i + (1/2)mv_0^2 = \varepsilon_f - \varepsilon_i + (m/M)E_0 \qquad (1)$$

$$\Gamma_{REC}(FWHM) = 2.04 (T_0 T_i)^{1/2}. \qquad (2)$$

Here $\hbar\omega$ is the REC x-ray energy, ε_i and ε_f the binding energies of electron in the initial and final states, E_0 is the energy of the incident projectile ion, v_0 the projectile velocity, m and M electron and projectile masses. T_0 is $(1/2)mv_0^2$ and T_i the kinetic energy averaged of

the target electron. The observed centroid energies of the REC x-ray spectra for F and Cl ions are shown in Figs. 3 and 4 as a function of the projectile energy. The calculated values for the REC centroid energy are also shown in Figs 3 and 4. The experimental results are, generally speaking, in good agreement with the calculated ones. The observed widths for He target atom are also shown in Fig. 5 as a function of the projectile velocity with the results of Kienle et al.[4], Sohval et al.[5], Kawatsura et al.[2] and Kambara et al.[6] The present results are in agreement with the calculated ones. More detailed discussion will be presented in the separate paper.[7]

References

1) H.W. Schnopper, H.D. Betz, J.P. Delvaille, K. Kalata, A.R. Sohval, K.W. Jones and H.E. Wegner: Phys. Rev. Lett. 29 (1972) 898.

2) K. Kawatsura, H. Tawara and P. Richard: IEEE Trans. Nucl. Sci. NS-28 (1981) 1053; H. Tawara, P. Richard and K. Kawatsura: Phys. Rev. A 26 (1982) 154.

3) M. Kleber and D.H. Jakubassa: Nucl. Phys. A 252 (1975) 152.

4) P. Kienle, M. Kleber, B. Povh, R.M. Diamond, F.S. Stephens, E. Grosse, M.R. Maier and D. Proetel: Phys. Rev. Lett. 31 (1973) 1099.

5) A.R. Sohval, J.P. Delvaille, K. Kalata, K. Kirby-Docken and H.W. Schnopper: J. Phys. B 9 (1976) L25.

6) T. Kambara, Y. Awaya, A. Hitachi, M. Kase, I. Kohno and T. Tonuma: J. Phys. B 15 (1982) 3759.

7) K. Kawatsura, A. Ootuka, M. Sataka, K. Komaki, H. Naramoto, K. Ozawa, Y. Nakai and F. Fujimoto: Nucl. Instrum. & Methods A (to be published).
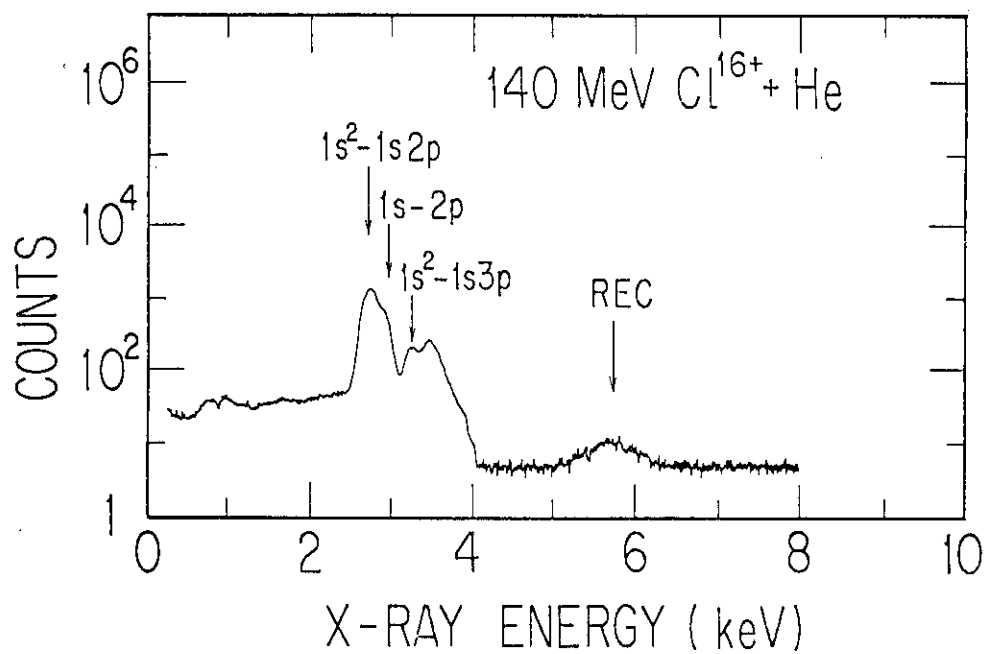
Fig. 1   The Cl and REC x-ray spectra for 140 MeV
          Cl^{16+} ion incident on He gas target.
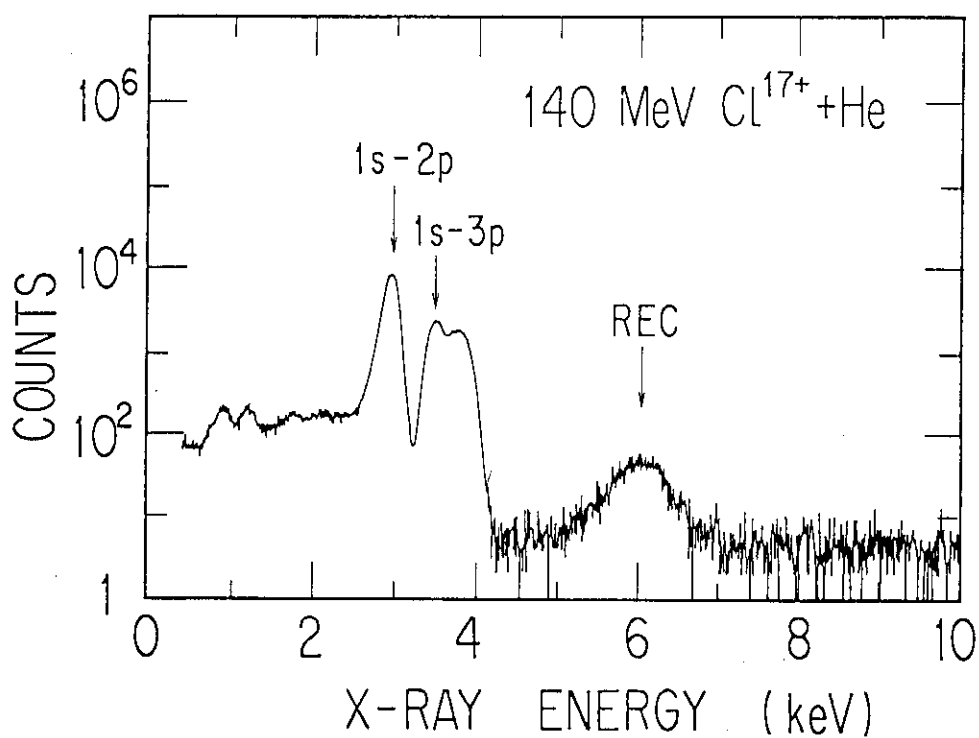
Fig. 2   The Cl and REC x-ray spectra for 140 MeV
          Cl^{17+} ion incident on He gas target.
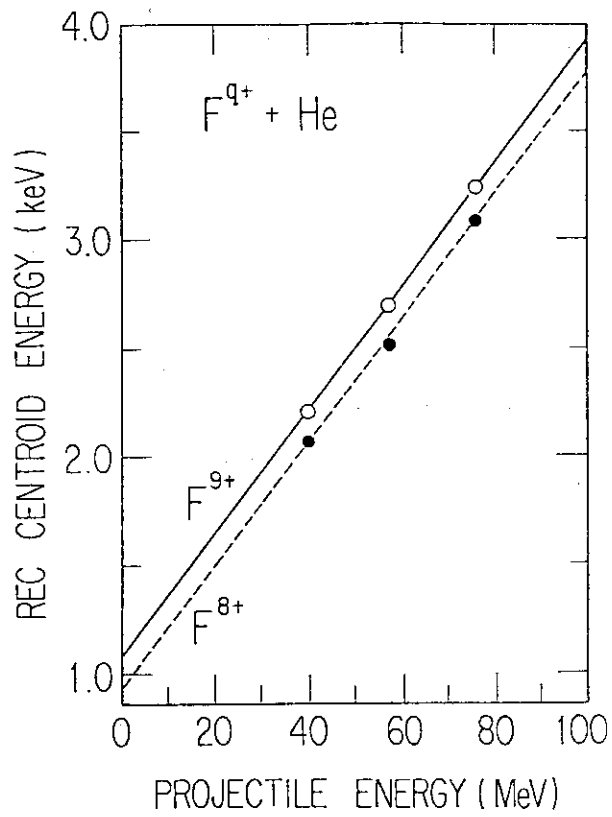
Fig. 3   The centroid energy
of the REC x rays.
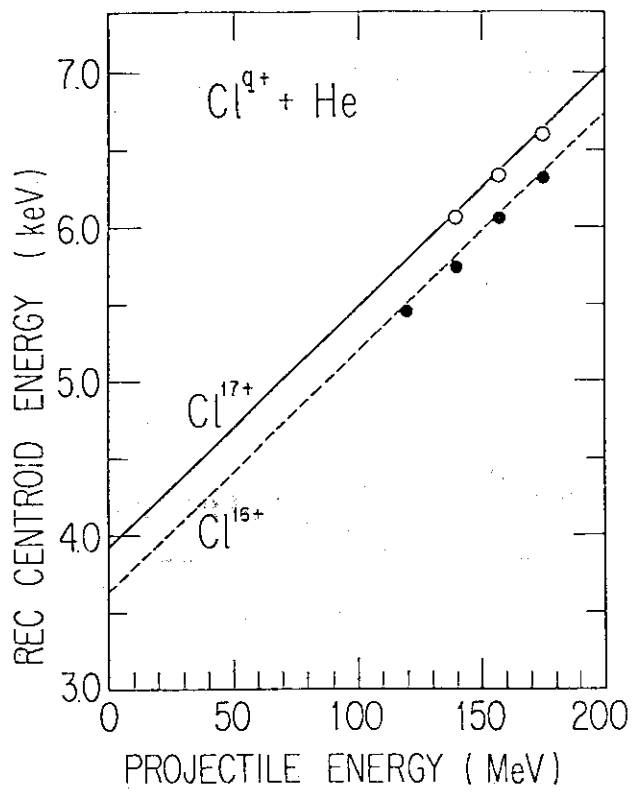
Fig. 4   The centroid energy
of the REC x rays.
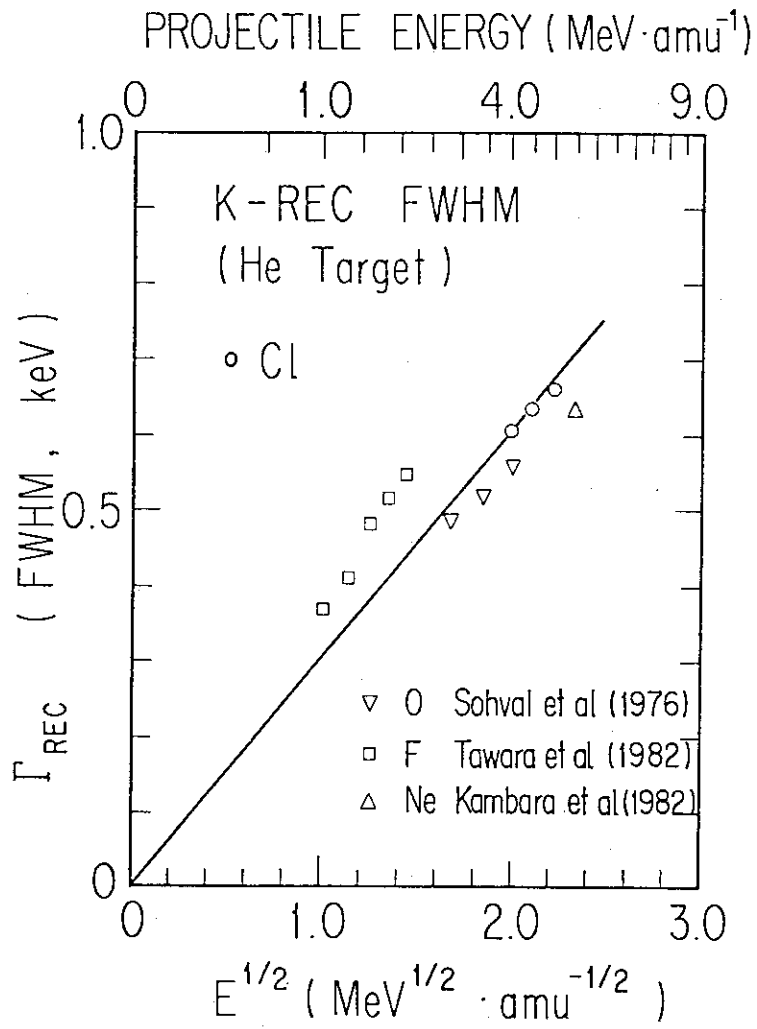
Fig. 5 The width of the REC x rays with the results of other works.

2.3   X-RAY EMISSION FROM FOIL-EXCITED CHLORINE BEAMS

Kiyoshi KAWATSURA, Masao SATAKA, Yasuaki SUGIZAKI,

Hiroshi NARAMOTO, Yohta NAKAI, Ken-ichiro KOMAKI[*],

Akio OOTUKA[*], Fuminori FUJIMOTO[*] and Kunio OZAWA[**]

Department of Physics, JAERI, [*]College of Arts and

Sciences, University of Tokyo, [**]Energy Research

Laboratory, Hitachi Ltd.

Introduction

The precise measurements of the transition energies and lifetimes of highly ionized heavy ions can provide an information of the relativistic effects and quantum-electrodynamics.   Forbidden decays in few-electron systems for the low Z atoms show too small rate to be observable.   They, however, become observable at the higher Z atoms.

In this paper we present the results of measurements of the Cl K x-ray transition energies obtained by the Bragg crystal spectrometer,[1] and the state lifetimes for the metastable states in helium-like and lithium-like chlorine obtained by the Doppler-tuned x-ray spectrometer(DTS).[2]

Experimental

The transition energies of the Cl K x-ray spectra were measured using a 12.7 cm, curved crystal spectrometer which was shown in Fig. 1.   The Cl K x rays were analyzed with a Si(111) crystal, 2d spacing of 6.27 Å.   The detail of this spectrometer has been described elsewhere.[1]   The lifetime measurement was performed using the Doppler-tuned x-ray spectrometer(DTS) similar to that described by Cocke et al.[3]   The DTS was set in the multipurpose scattering chamber which was also shown in Fig. 1.   In order to obtain Cl K x-ray spectra, we have used 120 MeV Cl ions as the incident projectiles, a 15 $\mu g/cm^2$ carbon foil as an exciter of the projectile beams and a 50 μm poly-vinylidenchloride film (Saran) as an absorber.

Results and discussion

High resolution spectroscopy is of great use to give a direct information of the transition energies at the x-ray region.   The K x-ray spectrum of the 120 MeV Cl ions incident on a 15 $\mu g/cm^2$ carbon foil is shown in Fig. 2.   The spectrum was obtained with the Bragg crystal

spectrometer. It involves most of the Cl K x rays ranging from four-electron (beryllium-like) to one-electron (hydrogen-like) ions. It is confirmed that the lines due to the transitions in the helium-like and lithium-like ions are sufficiently strong. This spectrum also reveals lines from multiply excited states. Our measurement is in good agreement with the similar measurement for 105 MeV Cl ions incident on an Al target by Richard et al.[4]

Another high resolution study of x-ray emission from the foil-excited beams was performed using a Doppler-tuned spectrometer (DTS) similar to that described by Cocke et al.[3] A typical DTS spectrum from 120 MeV chlorine beams is shown in Fig. 3. In upper of the figure the integral spectrum is shown as a function of the detector angle. A differential spectrum is shown at the bottom part of the figure. This measurement was done to make sure the position of steps due to the lines from Cl XVI $(1s2p)\ ^3P_2$ and Cl XV $(1s2s2p)\ ^4P_{5/2}$ in the DTS spectrum. The $^3P_2$ line (at 2778 eV) corresponds to the step at 77° and the $^4P_{5/2}$ line (at 2745 eV) cprresponds to that at 69°. Using the DTS we have measured the lifetimes of the $(1s2p)\ ^3P_2$ and $(1s2s2p)\ ^4P_{5/2}$ states in the helium-like and lithium-like chlorine at the energy of 120 MeV, respectively. Decay curves for these states were taken by measuring the x-ray yields on either side of each step shown in Fig. 3 as a function of foil-detector distance. The decay curves obtained in this manner are shown in Fig. 4. The observed lifetimes are 1.54 ns for the $^3P_2$ state, and 0.87 ns for the $^4P_{5/2}$ state, respectively. The result for the $^4P_{5/2}$ state seems to be in good agreement with the measured results of 0.91 ns by Sellin et al.[5] and of 0.94 ns by Cocke et al.[3] On the other hand, the present result for the $^3P_2$ state is shorter than those of 1.86 ns measured by Cocke et al.[3] and of 1.88 ns calculated by Drake.[6] The better statistics measurement is now in progress. It is, therefore, expected that this discrepancy will be soon explained.

References

1) K. Kawatsura, M. Sataka, H. Naramoto, K. Ozawa, Y. Nakai, A. Ootuka, K. Komaki and F. Fujimoto: JAERI-M 86-112 (1986) 31.

2) K. Kawatsura, M. Sataka, A. Ootuka, K. Komaki, H. Naramoto, K. Ozawa, Y. Nakai and F. Fujimoto: Nucl. Instrum. & Methods A (to be published).

3) C.L. Cocke, B. Curnutte, J.R. Macdonald and R. Randall: Phys. Rev. A 9 (1974) 57.

4) P. Richard, C.F. Moore, D.L. Matthews and F. Hopkins: Bull. Am. Phys. Soc. 19 (1974) 570.

5) I.A. Sellin, D.L. Pegg, P.M. Griffin and W.W. Smith, Phys. Rev. Lett. 28 (1972) 1229.

6) G.W.F. Drake: Astrophys. J. 158 (1969) 1199.

JAERI TANDEM ACCELERATOR (H-2 LINE)
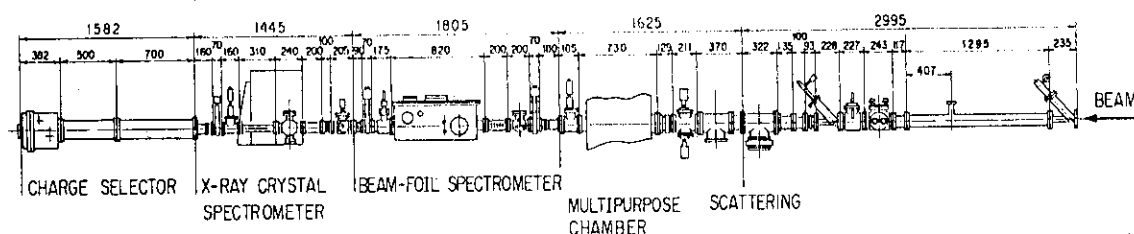
Fig. 1   Schematics of an exprimental set-up for atomic physics research at JAERI tandem accelerator.   The unit in figure is mm.
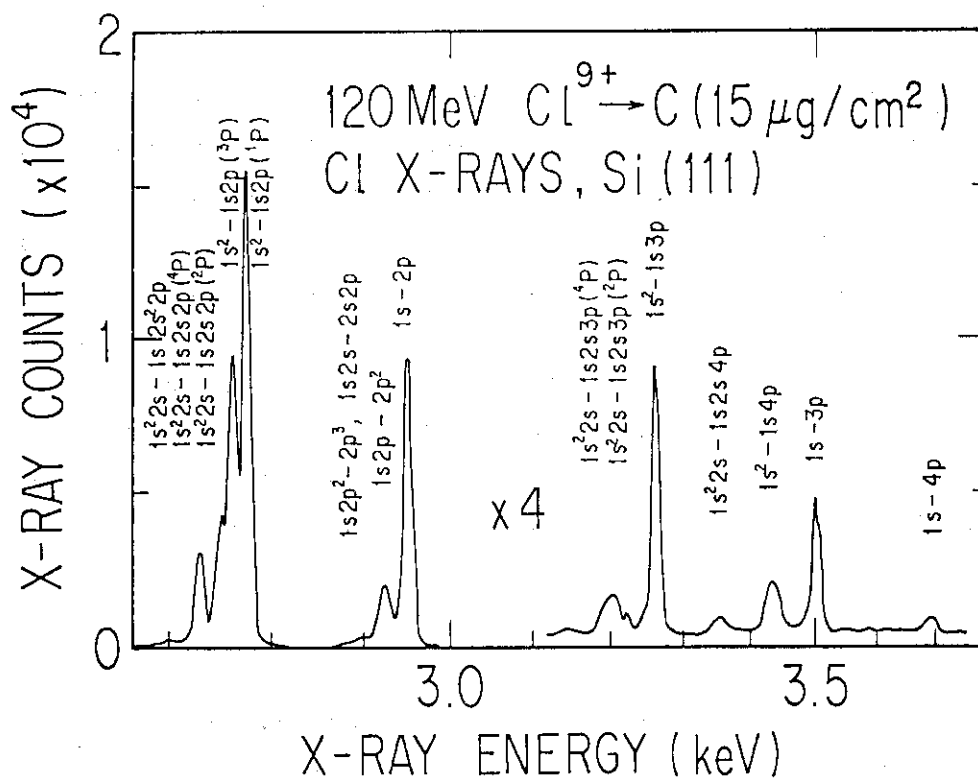
Fig. 2   High resolution Cl K x-ray spectrum resulting from 120 MeV Cl^{9+} ions incident on a carbon foil target.   This spectrum was obtained with a curved crystal spectrometer with a Si(111) analyzing crystal.

INTEGRAL DTS SPECTRUM
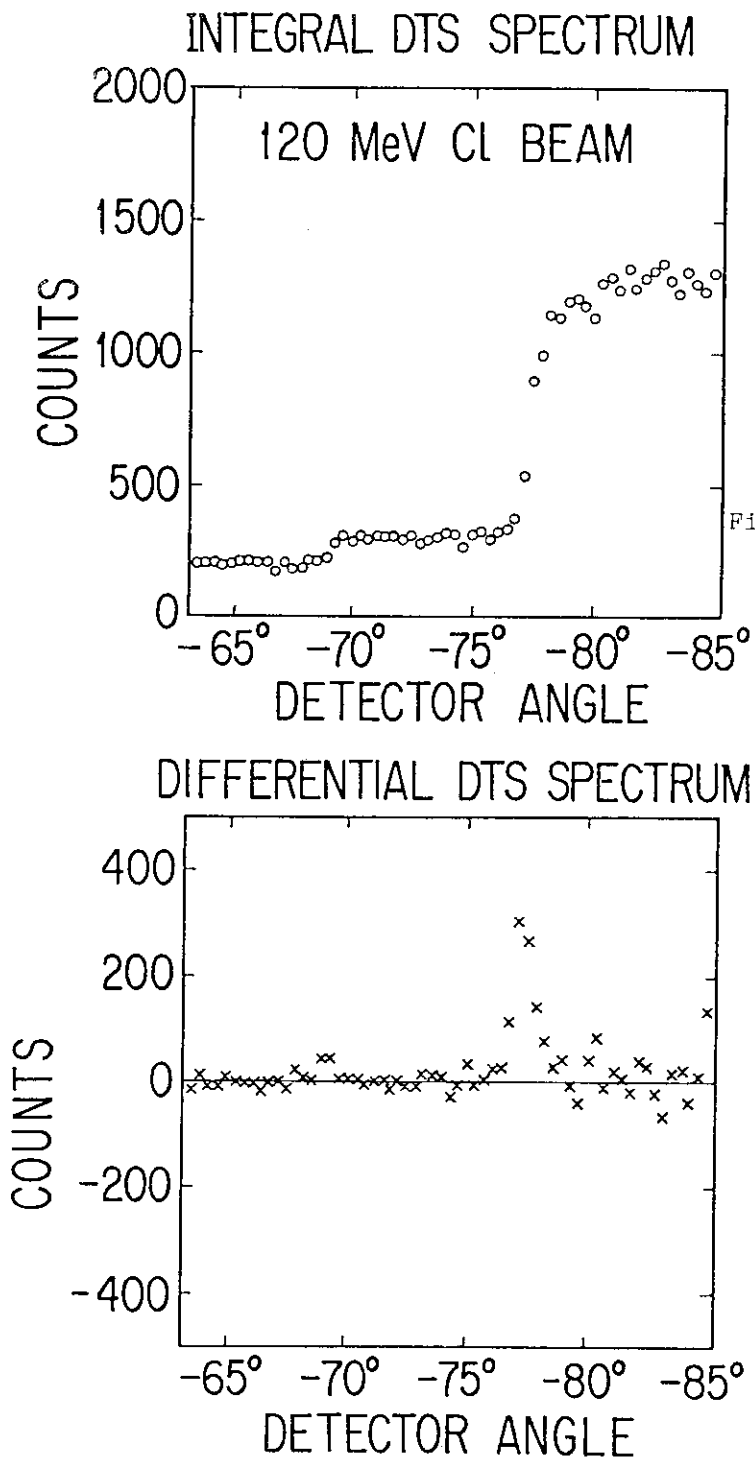
Fig. 3 Typical spectrum resulting from 120 MeV Cl ions taken with the Doppler-tuned spectrometer. The integral spectrum (upper) and its differential one (bottom).

DIFFERENTIAL DTS SPECTRUM
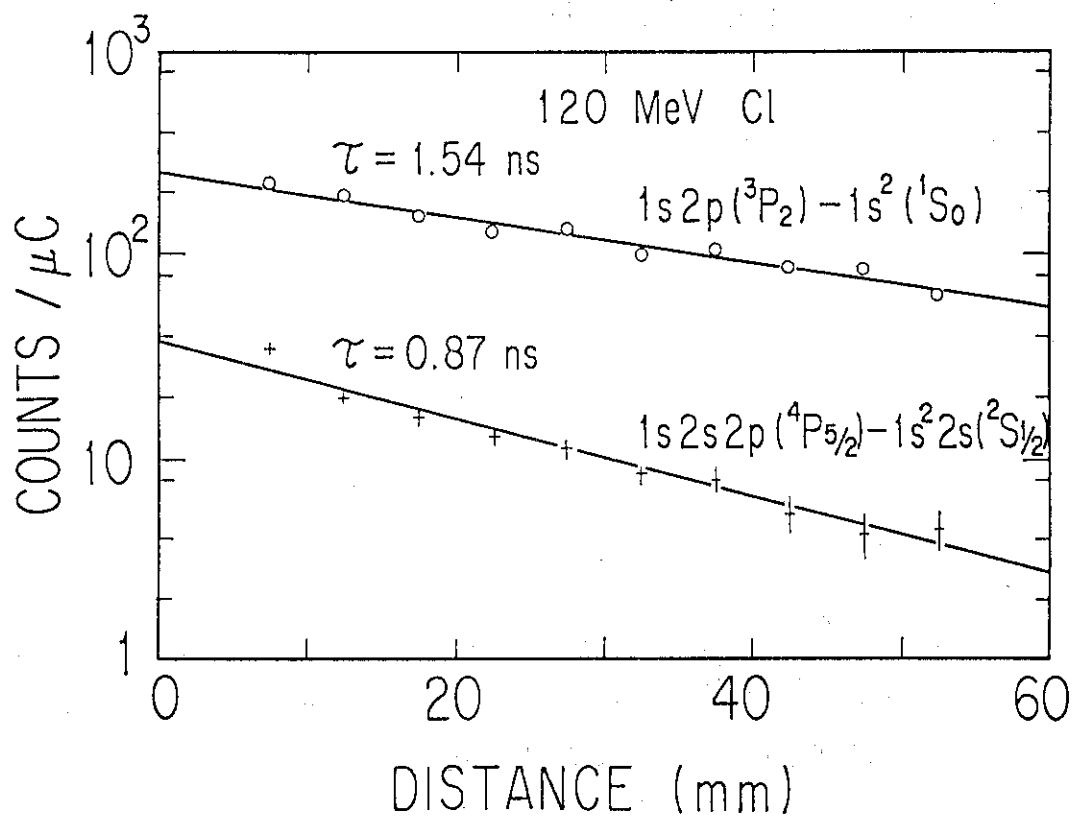
Fig. 4   Intensity decay curves taken with the DTS.

2.4   MOLECULAR EFFECT OF Al Kα SATELLITE X-RAY YIELDS

FROM A THIN Al TARGET FOR H^+ AND H_2^+ IONS IMPACT

Akio OOTUKA[*], Kiyoshi KAWATSURA, Ken-ichiro KOMAKI, Fuminori
FUJIMOTO[*], Noriyuki KOUCHI[**] and Hiromi SHIBATA[**]

Department of Physics, JAERI, [*]College of Arts and
Sciences, University of Tokyo, [**]Research Center for
Nuclear Sciences & Technology, University of Tokyo

Introduction

Inner-shell excitation produced by light ion impact is approximately
proportional to the square of the ion charge (Z^2).   Hence, the cluster
ions might be expected to show the same effect of enhancement in x-ray or
Auger electron production as they do in their energy loss processes.
Lurio et al.[1] have measured Al Kα x-ray yields from thin Al targets
(123 Å and 370 Å) for H^+ and H_2^+ ions at the energy of 1.0 MeV/amu.   They
found that the KL^1/KL^0 ratio by the clustered protons is slightly smaller
than that by the protons.

In the previous work, we have reported on the observations of spectra
of the O and Al Kα x rays from thin aluminum oxide films with the
thickness of 100 Å and 300 Å for H^+ and H_2^+ ions (0.8 - 0.95 MeV/amu)
impact by a Bragg crystal spectrometer.[2]   We found that the intensity of
the KL^1 line for H_2^+ ions is larger than that for H^+ ions and this
enhancement decreases with increasing of the target thickness.   This
result in the aluminum oxide case is on the contrary to the result in the
case of pure aluminum obtained by Lurio et al.[1]

In this report, we present the measurements of Al Kα x-ray spectra
from thin aluminum targets (100 - 500 Å) for H^+ and H_2^+ ions (0.8 - 1.5
MeV/amu).   In order to study the molecular effect, the intensity ratios
of the KL^1 line to the KL^0 one, $I(KL^1)/I(KL^0)$, for H^+ and H_2^+ ions with the
same velocity are compared.

Experimental

The thin aluminum films were deposited on thick silicon or iron
substrates by evaporation technique.   Beams of H^+ and H_2^+ ions were
obtained from the 2 MV Van de Graaff (VdG) accelerator of JAERI at an
energy of 0.8 MeV/amu and from the 3.75 MV VdG accelerator at HIT facility

of University of Tokyo at higher energies up to 1.5 MeV/amu. The details of the experimental arrangement have been already described in the previous papers.[2,3]

Results and discussion

In Fig. 1 are shown the observed spectra of Al K_α satellite x rays from a thin aluminum target of 100 Å thickness for 0.8 MeV/amu H^+ and H_2^+ ions, where the intensity of each line in the spectra normalized by the integrated intensity of the KL^0 line. We can see that the intensity of the KL^1 line for H_2^+ ions is higher than that for H^+ ions. The intensity ratios, $I(KL^1)/I(KL^0)$, were obtained from the peak area of the Gaussian distribution best fitted for each peak. The results are shown in Fig. 2, where δ is defined as $\delta = R_s(H_2)/R_s(H) - 1$ and $R_s(H_2)$ and $R_s(H)$ are the intensity ratios, $I(KL^1)/I(KL^0)$, for H_2^+ and H^+ ions with the same velocity, respectively. It is found that the enhancement of the intensity of the KL^1 line by H_2^+ ion beams is on the contrary to result obtained by Lurio et al.[1]

Basbas and Ritchie[4] have theoretically discussed the vicinage effects in the inner-shell ionization and estimated value of δ as a function of the internuclear distance, R. By using the expression of the internuclear distance given by Brandt and Ritchie[5], we estimated the value of δ for Al atoms in a 100 Å film for 0.8 MeV/amu H_2^+ ion bombardment. The calculated value is 0.04, which is only in qualitative agreement with the experimental one. The quantitative analysis on the experimental results is now in progress.

References

1) A. Lurio, H.H. Andersen and L.C. Feldman: Phys. Rev. A17 (1978) 90.

2) A. Ootuka, F. Fujimoto, K. Komaki, K. Kawatsura, K. Ozawa and M. Terasawa: Phys. Lett. A97 (1983) 191.

3) K. Ozawa, K. Kawatsura, F. Fujimoto and M. Terasawa: Nucl. Instrum. & Methods 132 (1976) 517.

4) G. Basbas and R.H. Ritchie: Phys. Rev. A25 (1982) 1943.

5) W. Brandt and R.H. Ritchie: Nucl. Instrum. & Methods 132 (1976) 43.
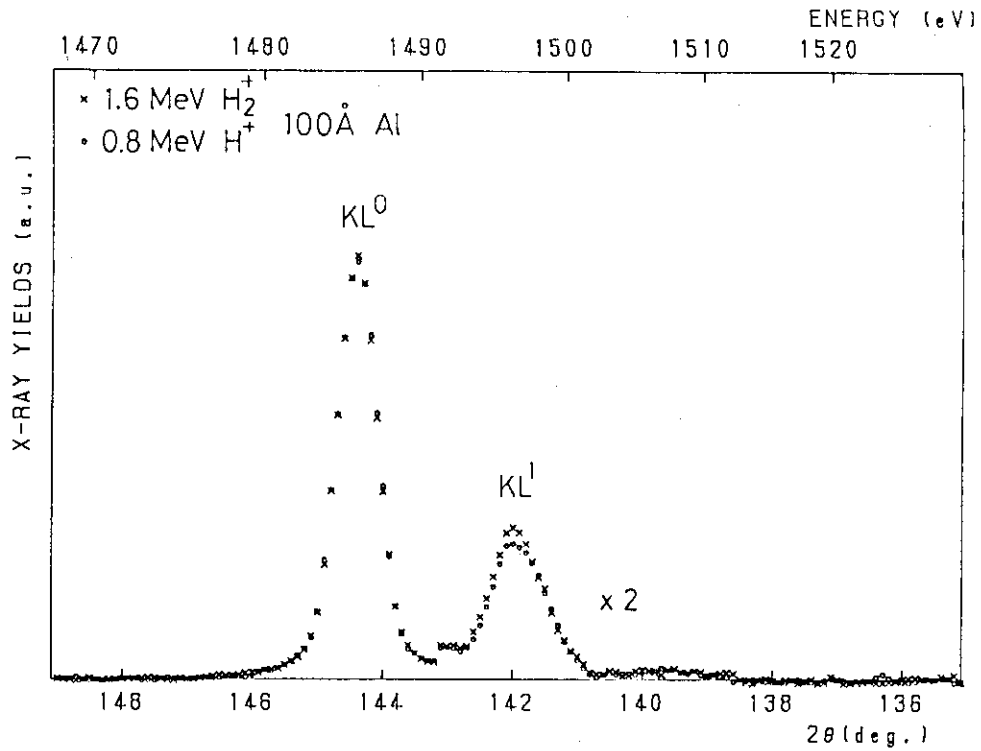
Fig. 1   Al Kα x-ray spectra for 0.8 MeV/amu
H⁺ and H₂⁺ ion bombardments.
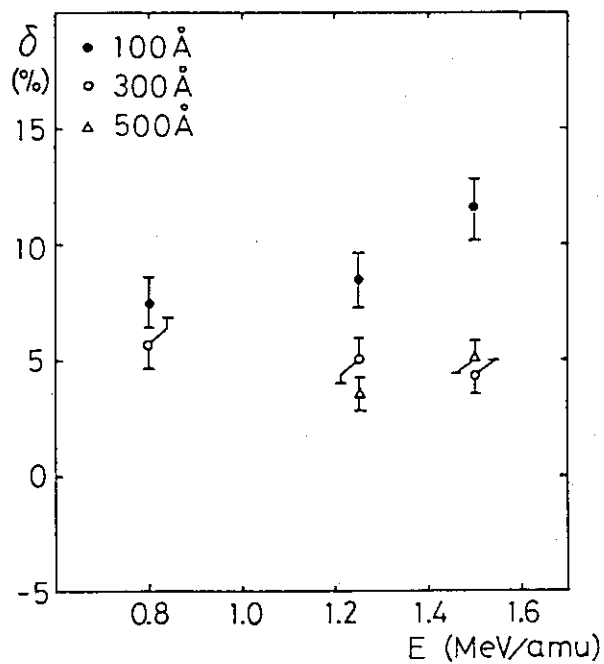
Fig. 2   Molecular effect for Al Kα x-ray
production cross sections.

2.5   BEAM-FOIL SPECTRA OF CHLORINE IONS IN HIGH ENERGY
REGION (IV)

Masao SATAKA, Kiyoshi KAWATSURA, Hiroshi NARAMOTO,
Yasuaki SUGIZAKI, Yohta NAKAI, Akio OOTUKA[*],
Ken-ichiro KOMAKI[*], Fuminori FUJIMOTO[*], Kunio OZAWA[**],
and Keishi ISHII[***]

Department of Physics, Japan Atomic Energy Research
Institute, [*] College of Arts and Sciences, University of
Tokyo, [**] Energy Research Laboratory, Hitachi Ltd.,
[***] Faculty of Engineering, Kyoto University

Beam-foil investigations of highly ionized chlorine have been
performing in the wavelength region 30 - 470 Å at the JAERI tandem
accelerator. The ion beam energy is varied from 80 to 150 MeV. The beam-
foil studies of Cl ions at an energy as high as a several ten MeV have
been reported thus far by two groups[1-3]. As the ion beam energy in the
present work is the highest among all, the spectrum mainly consists of
lines with line multiplet belonging to higher charge states than Cl XII.

Experimental apparatus has been described in detail in reference 4).
The apparatus is standard one using a 2.2 m grazing incidence spectrometer
mounted at $90°$ to the ion beam direction.

We have reported identification of the spectrum between 170 and 260
Å. Most of lines were identified as 2s-2p transitions[4]. Two lines were
newly classified as n=4-5 transitions in Cl XIV and Cl XV. Bashkin and
Martinson observed many new lines originated from the hydrogenic
transitions in the foil-excited Cl spectrum[4]. Hallin et al. extended the
ionization states to Cl XIV, using the ion beam energy up to 42 MeV[1],
followed by Bashkin et al.[5] and Bhardwaj et al.[6]. We have further
extended the observation to the shorter wavelength region with use of a
hundred MeV ion beams. In Fig. 1, the measured spectrum between 75 and 175
Å is shown with the theoretically generated spectrum. The strong peaks are
identified with the hydrogen-like transitions of n=3-4 and n=4-6 in Cl XV
and transitions of n=3-4, n=4-5 and n=4-6 in Cl XVI. The theoretical
spectrum has been generated based on calculation of term energies using

the polarization formula[7] and the charge state distribution of the Cl ions after passing through the carbon foil. The peak width reflects the experimental resolution. Further discussion will be given in reference (8).

Strong lines in the spectrum between 230 Å and 470 Å are identified with the lines of 2s-2p transitions belonging to Cl XIII - Cl XV and the lines of hydrogen-like transitions belonging to Cl XIV - Cl XVI. We have measured the intensity decay curves of lines attributed to $\Delta n=0$ transitions belonging to Cl XIV - Cl XV. We are analyzing these intensity decay curves by non-linear least square method[9].

In table 1 we list the some results of measured lifetimes with lifetimes measured by Ishii et al.[2] and Forester et al.[3]. The wavelengths and transitions cited in table 1 are taken from the table in ref.(10). The measured lifetimes for lines at 384.0 and 415.6 Å, belonging to the Cl XV resonance doublet, have been measured more precisely than previous measurement[4]. The lifetime of 2p $^2P_{3/2}$ of Cl XV is 0.76±0.01 nsec. The lifetimes is in excellent agreement with the result of Forester et al.[3]. But the measured lifetimes are slightly larger than the theoretical results of Martin and Wiese[11] (0.74 nsec), Armstrong et al.[12] (0.69 nsec) and Cheng et al.[13] (0.72 nsec). The measured lifetimes for 2p^2 $^3P_2$ based on 286.3 Å and 276.1 Å should be essentially same and the resultant lifetimes are in good agreement each other.

References

(1) R. Hallin, J. Lindskog, A. Marelius, J. Pihl and R. Sjödin: Physica Scripta 8(1973)209.

(2) K. Ishii, E. Alvalez, R. Hallin, J. Lindskog, A. Marelius, J. Pihl, R. Sjödin, B. Denne, L. Engström, S. Huldt and I. Martinson: Physica Scripta 18(1978)57.

(3) J. P. Forester, D. J. Pegg, P. M. Griffin, G. D. Alton, S. B. Elston, H. C. Haydon, R. S. Vane and J. J. Wright: Phys. Rev. A18(1978)1476.

(4) M. Sataka, K. Ozawa, K. Kawatsura, H. Yamaguchi, K. Ishii, T. Kitahara, K. Masai, A. Ootuka, K. Komaki, F. Fujimoto: JAERI-M 85-125 (1985)65.

(5) S. Bashkin, J. Bromander, J. A. Leavitt and I. Martinson: Physica Scripta 9(1973)285.

(6) S. N. Bhardwaj, H. G. Berry and T. Mossberg: Physica Scripta 9(1974)331.

(7) B. Edlén: in Handbuch der Physik, edited by S.Flügge (Springer-Verlag, Berlin, 1964), Vol.27,p.80.

(8) K. Ishii, M. Sataka, K. Kawatsura, Y. Nakai, K. Ozawa, K. Komaki, A. Ootuka : in preparation

(9) D. J. G. Irwin and A. E. Livingston: Computer Phys. Comm. 7(1974)95.

(10) R. L. Kelly: Atomic and Ionic Spectrum Lines below 2000 Angstroms, ORNL-5922(1982).

(11) G. A. Martin and W. L. Wiese: J. Phys. Chem. Ref. Data 5(1976)537; G. A. Martin and W. L. Wiese: Phys. Rev. A14(1976)699.

(12) L. Armstrong Jr. and W. R. Fielder: Phys. Rev. A14(1976)1114.

(13) K. T. Cheng, Y. -K. Kim and J. P. Desclaux: Atomic Data and Nuclear Data Tables 24(1979)111.

Table 1　Radiative lifetimes for $\Delta n = 0$ transitions in Cl XIV - Cl XV.

ION	WAVELENGTH ($\overset{\circ}{A}$)	TRANSITION		LIFETIME (nsec)		
				Present	Forester[a]	Ishii[b]
XIV	458.4	$2s2p\ {}^1P_1$	$- 2p^2\ {}^1D_2$	0.63	0.60	0.54
XV	415.5	$2s\ {}^2S_{1/2}$	$- 2p\ {}^2P_{1/2}$	1.04	0.95	1.0
XV	384.0	$2s\ {}^2S_{1/2}$	$- 2p\ {}^2P_{3/2}$	0.76	0.76	0.71
XIV	290.5	$2s2p\ {}^3P_1$	$- 2p^2\ {}^3P_0$	0.16		
XIV	286.3	$2s2p\ {}^3P_2$	$- 2p^2\ {}^3P_2$	0.16	0.16	
XIV	284.3	$2s2p\ {}^3P_1$	$- 2p^2\ {}^3P_1$	0.16		
XIV	276.1	$2s2p\ {}^3P_1$	$- 2p^2\ {}^3P_2$	0.16		
XIV	237.7	$2s^2\ {}^1S_0$	$- 2s2p\ {}^1P_1$	0.14	0.15	

a: Forester et al. (3).

b: Ishii et al. (2).
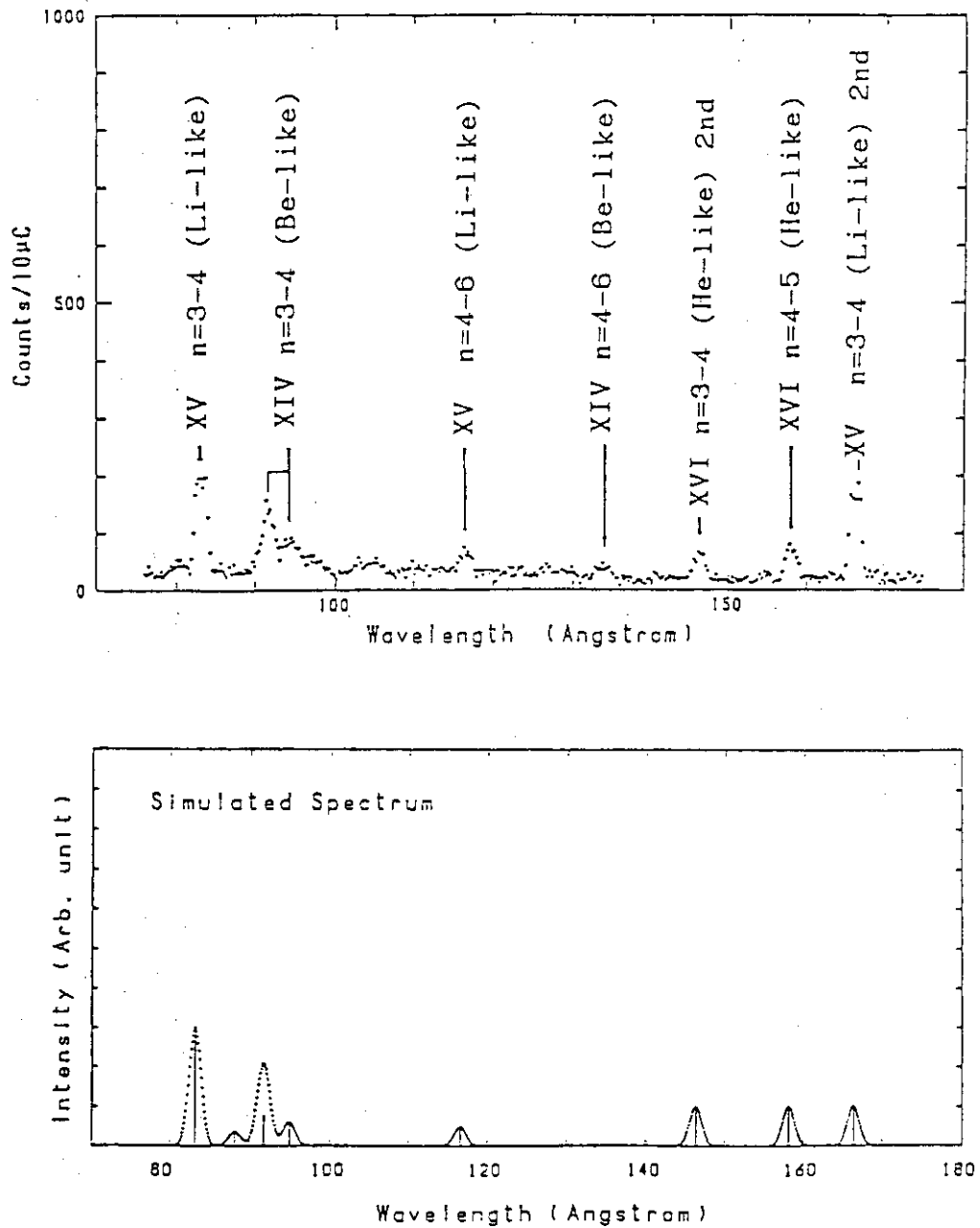
Fig.1 A portion of spectrum between 75 and 175 Å at 120 MeV (upper).
Simulated spectrum is also shown, where an appropriate excitation model
is assumed (lower).

2.6   ELASTIC RECOIL DETECTION ANALYSIS WITH HIGH
       ENERGY HEAVY IONS

Hiroshi   NARAMOTO,   Kiyoshi   KAWATSURA,   Masao
SATAKA, Yasuaki SUGIZAKI, Yohta NAKAI, Kunio
OZAWA*, Sadae YAMAGUCHI** and Yutaka FUJINO**

Department   of   Physics,   Japan   Atomic   Energy
Research Institute,*Energy Institute of Hitachi
, **Faculty of Engineering, Tohoku University

1.Introduction

       Ion beam analysis with a few MeV ions has been shown to
be an effective way to determine the atomic composition and
impurity concentrations in the near surface regions of solids
(1). Among the relevant species, heavier elements are easy to
analyse with a standard ion backscattering technique. On the
contrary,   the   detection   technique   of   lighter   elements   are
limited   because   of   smaller   cross sections   for   the   elastic
scattering   between   incident   ions   and   light   impurities. Many
low energy nuclear reactions(2) can be used to analyse several
of these elements. However,the use of more than one reaction
is often needed to profile many elements and, in some cases,
the energy overlap of various reaction products makes the use
of nuclear reaction analysis difficult.

       Light elements such as hydrogen, hydrogen isotopes, heli-
um, carbon and nitrogen coexist in the structural materials of
energy devices and sometimes play a critical and complex role.
The use of high energy heavy ions as the incident ions makes
it possible to detect these light elements simultaneously(3).

       The present report is concerned with the development of
elastic recoil detection analysis(ERDA) using 35 MeV^{35}Cl^{4+}ions.
The rather preliminary results are shown with an application
of ERDA analysis of ion irradiation damage in LiF crystal.

2.Experimental procedure

       For the development of ERDA technique, it is necessary to
prepare the various kinds of standard specimens which have the

localised distribtion in the near surface region and the known concentration of light elements. These specimens were made through the implantation of H, D, He, He, C, N,and O ions with the energies ranging from 10's to 100's keV.

The measurements of the elastic recoil spectra was carried out using 35 MeV $^{35}Cl^{4+}$ ions from JAERI tandem accelerator and "Ion Beam Analysis Chamber" which allows for independent selection of range filters and angular positioning of two detectors for ERDA and RBS measurements. Chlorine ions with the spot size of 0.6 mm were incident to the target and beam current was typically 10 pnA. Elastic recoils were detected in a 100 μm surface barrier Si detector with a slit of 2 mm in width, placed at a distance of 180 mm from the specimen. The incident angle to the specimen was 15 and the detection angle was 30°. Mylar foil with 12.3 μm was chosen finally to stop the incident chlorine ions only. The obtained yield and the leading edge were calibrated using bulky standard specimens, which have the uniform distribution along the depth.

3.Results and discussion

In ERDA analysis, the energy of recoils is proportional to that of incident ions, and the selectivity of elements is given by the variation of this proportional constant. This constant depends on the mass of recoils and the detection angle. The value of this constant is small for very big mass difference between incident chlorine ions and light elements in target. However, employing an absorber changes its feature drastically. In Fig.1, a dotted curve describes this property for recoils ejected from the surface with the detection angle of 30°. A calculated curve(a solid line) is shown for a comparison. As the absorber foil is chosen so as to stop the scattered chlorine ions, the energy of the recoils goes through a maximum. The energy and mass at this maximum depend on the detection angle and the absorber thickness for given incident ions.

Fig.2 shows the energy spectra of recoils from a Si sample containing the small amounts of H, D, C, N and O. Deuterium atoms were introduced by the implantation with the energy

of 15 keV to the dose of 3 x 10^{17}/cm . Detection of recoils was made at the angle of 25° and 30° for the energy spectra of Fig.2(a) and (b), respectively. It is clear that $^{35}Cl^{4+}$ at 35 MeV gives a wide range of outgoing energies and it is a better choice for the simultaneous analysis of some light elements. It is also recognised that the recoil energies depend strongly upon the detection angle and the calibration of the energies under the exactly same condition is unavoidable using a standard sample.

Fig.3 shows the energy spectrum of recoiled carbons and hydrogens from a diamond single crystal which was supplied by Sumitomo Denki Kogyo Co. This was chosen for the energy calibration of carbons because crystalline system gives the definite number density of carbon atoms and the clear leading edge which corresponds to the crystal surface, as shown in this figure. The spectrum feature is analogous to RBS spectrum reflecting the uniform distribution of carbons along the depth. A hump at the low enegy side comes from hydrogens of adsorbed water at the diamond surface. This yield is rather small compared with any other specimen if the special treatment is not made.

As an application of ERDA analysis, the ion irradiation damage of LiF was tried. In Fig.4, (a) and (b) show the energy spectra of recoiled lithium and fluorine atoms before and after 35 MeV $^{35}Cl^{4+}$ bombardment. (a) gives a simple spectrum which is characterized by the two steps at the high and low energy side. The components from lithium isotopes are not separated in the present system. With increasing the dose of chlorine ions,the leading edge of fluorine becomes diffuse, and after the irradiation of 6 x 10^{16} ions, lithium atoms in the surface region are lost and some of them recoiled into inner part of the specimen form a hump at the lower energy side. It is difficult to expect for any other light elements to form a hump at this energy region. The heavy irradiation also influences the distribution of lithium atoms as can be seen at the high energy region of this figure.

Through the present study, it becomes clear that detection angle and the acceptance angle of detector are the key

factors. The further efforts are needed for acquiring the crystallographic information by ERDA technique.

References
1) For example: J. W. Mayer and E. Rimini,ed.(Ion Beam Hand= book for Material Analysis, Academic Press, Inc., New York, San Francisco, London,1977).
2) For example: G. Deconninck(Introduction to Radioanalytical Physics, Elsevier Scientific Publishing Company, New, Amsterdam, Oxford, York,1978).
3) C. Moreau, E. J. Knystautas, R. S. Timsit and R. Groleau: Nucl. Inst. and Meth. in Phys. Research 218(1983)111.
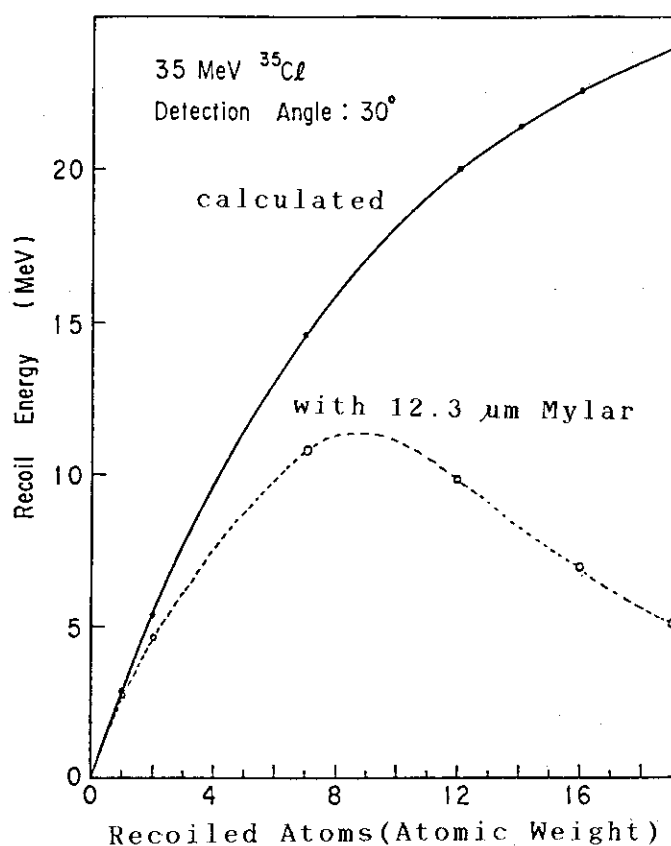
Fig. 1 Energy of recoils using 35 MeV $^{35}Cl^{4+}$ions. A solid line describes the calculated data without absorber, and dotted data were obtained from the energy analysis of recoils when 12.3 μm Mylar was employed as an absorber.
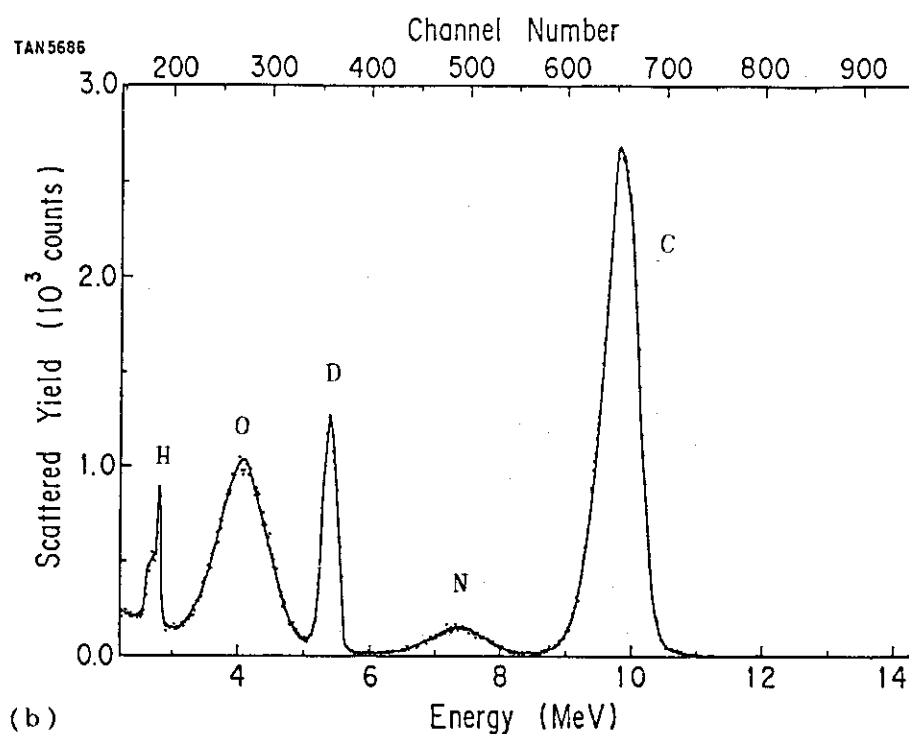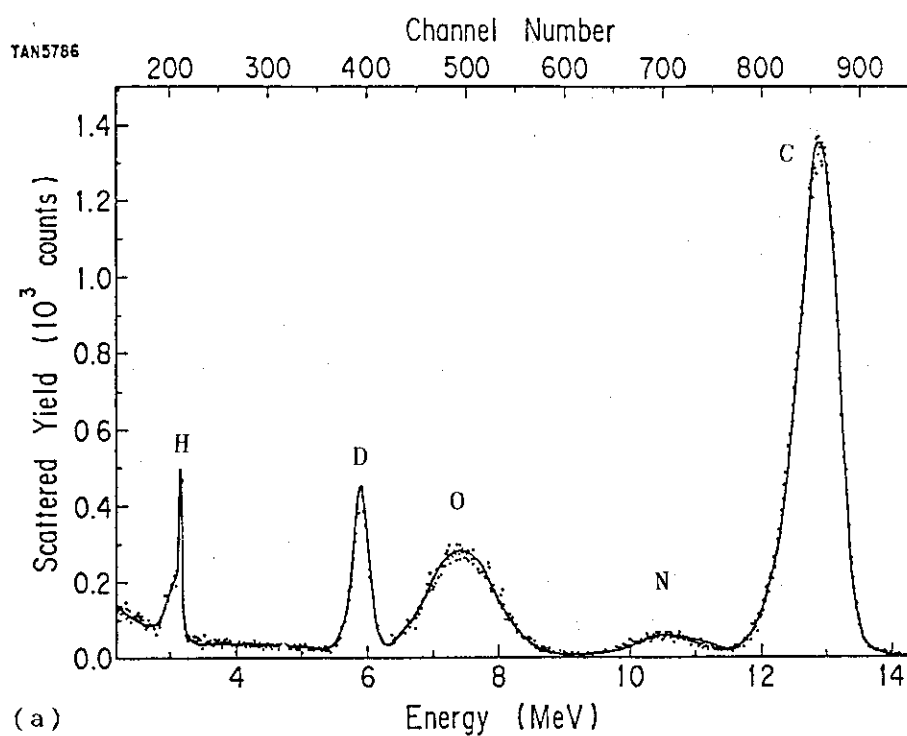
Fig. 2 Energy spectra of recoils from Si standard specimen containing the small amounts of H, D, C, N and O. The incident angle of $^{35}Cl^{4+}$ is 15°. The detection angles are 25° and 30° for (a) and (b), respectively.
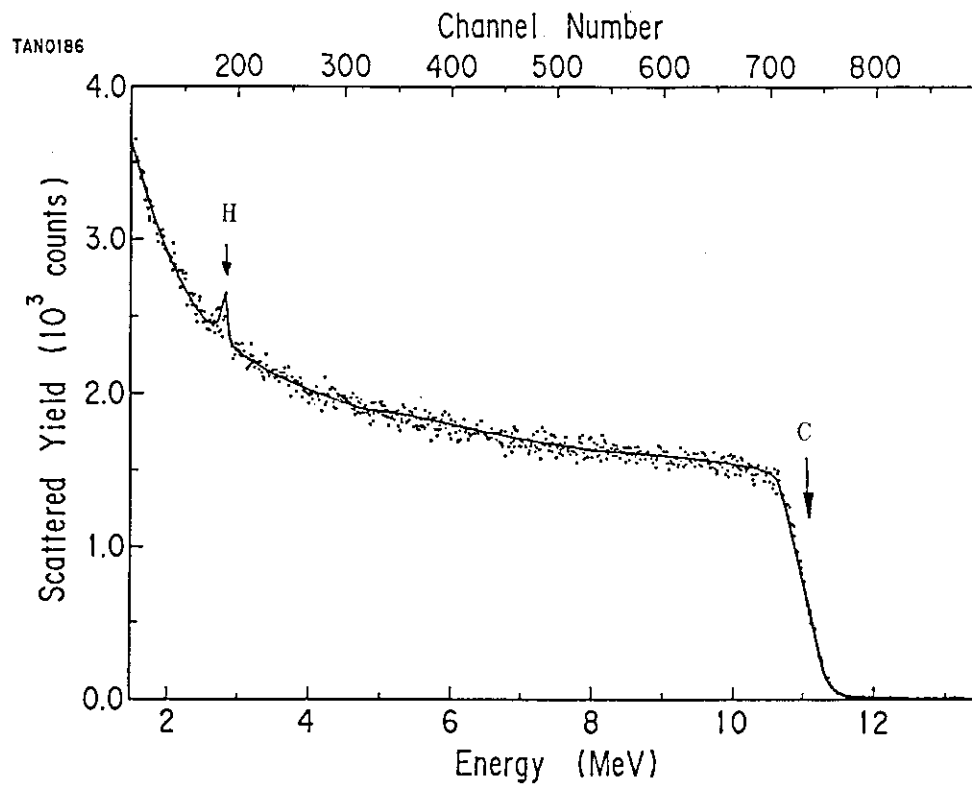
Fig. 3   Energy spectrum of recoiled carbons and
hydroges from a diamond single crystal. The
main contribution is from carbons and that
from hydrogens form a hump at the lower energy
side.
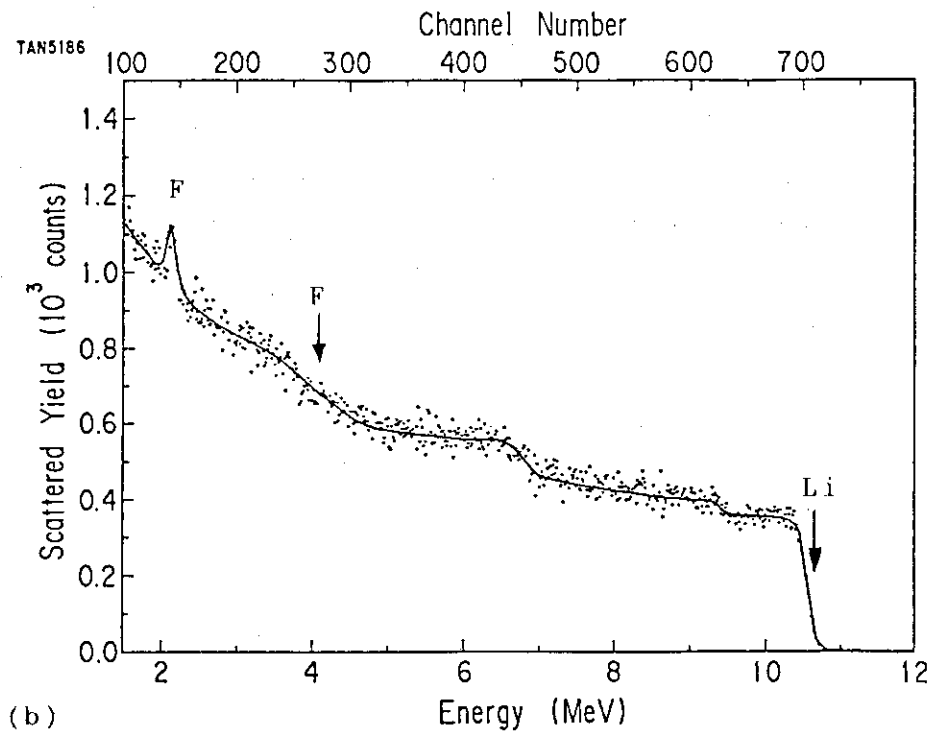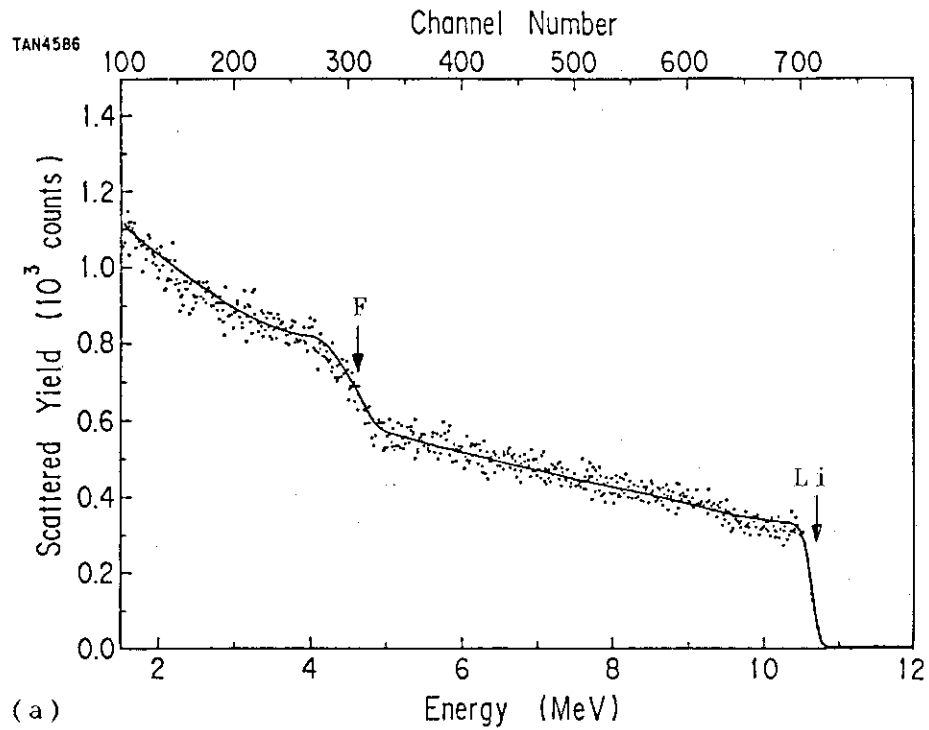
Fig. 4 Energy spectra of recoils from LiF crystal when bombarded with 35 MeV $^{35}Cl^{4+}$ ions. (a) is the spectrum before irradiation, and (b)after irradiation. The same ions were used for the analysis and the irradiation.

2.7 MOLECULAR ION BEAM EFFECTS IN THE RADIOLYSIS OF POTASSIUM NITRATE

Takeshi SOGA, Katsutoshi FURUKAWA and Shin-ichi OHNO

Department of Chemistry

1. Introduction

In chemical reactions induced by high-energy particles, both elastic collisions resulting in atomic displacements and inelastic collisions leading to electronic excitations have been considered as possible driving force. In our recent studies[1,2,3], we found that inelastic collision is about five times more efficient than elastic one for the decomposition of the solid potassium nitrate (KNO_3).[2,4] The following mechanism explains our previous results.

$$NO_3^- \xrightarrow{} NO_3^{-*} \longrightarrow NO_2^- + O \qquad (1)$$

$$(NO_2^- , NO_2^{-*}) + O \longrightarrow NO_3^- \qquad (2)$$

$$NO_3^- + O \longrightarrow NO_2^- + O_2 \qquad (3)$$
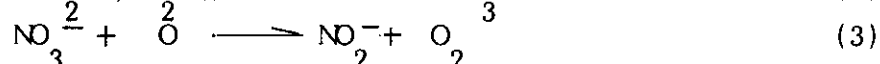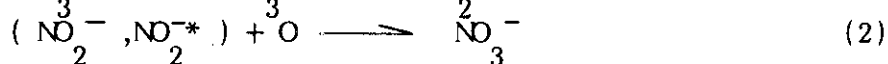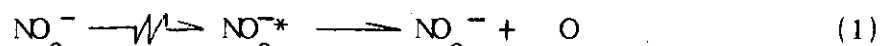
The present study has been carried out based on the following assumptions. When a molecular ion passes through a solid target, the energy loss per incident molecular ion should be equal to the sum of the energy loss of the atomic constituents of that ion. Therefore, the nitrite yield per 1 MeV H_2^+ ion may be equal to the twice of the yield per 0.5 MeV H^+, unless the molecular effects exist. The molecular-ion beam effects have been observed in ion-sputtering studies[5] and generally interpreted as due to "thermal spike" or dence collision cascades produced in the solid traversed by energetic ions.

2. Experimental

Polycrystalline potassium nitrate (Koso Chemical Co., Inc, analytical grade) was pressed into a disk of 10-mm diameter (2-mm thickness) and fixed onto the sample holder with clamps. It was irradiated at room temperature in vacuum (10^{-6} mmHg) with ions. Beans of 30 keV D^+, 60 keV D_2^+, 90 keV D_3^+, 0.5 MeV H^+ and 1.0 MeV H_2^+ were produced and focuced through an aperture of 6-mm onto the sample. The current density of the ion beam was

measured by Farady cup. The number of nitrite ion was determined spectrophotometrically.

3. Results and discussions

The amounts of nitrite ion vs. the number of the incident atoms are shown in Fig. 1 and Fig. 2 and Table 1. in each curves an initially rapid rate of formation fall off approaching a constant value or "saturation value". It is seen that (i) there is no molecular effects in initial stage of the reaction, namely the linearity between the yield and the energy deposited exist, but that (ii) in later stage of the reaction the molecular beam effect may appear. The formar may be understood if only a certain portion of the energy is effective in the forword reactions (1) and (3). Thus we may conclude that "thermal spike" of the ion tracks may not enhance the reaction in the initial stage. However, the molecular-beam effects observed in "saturation value" may be due to the "thermal spike" which might accelerate the NO_3^--reforming reaction (2).
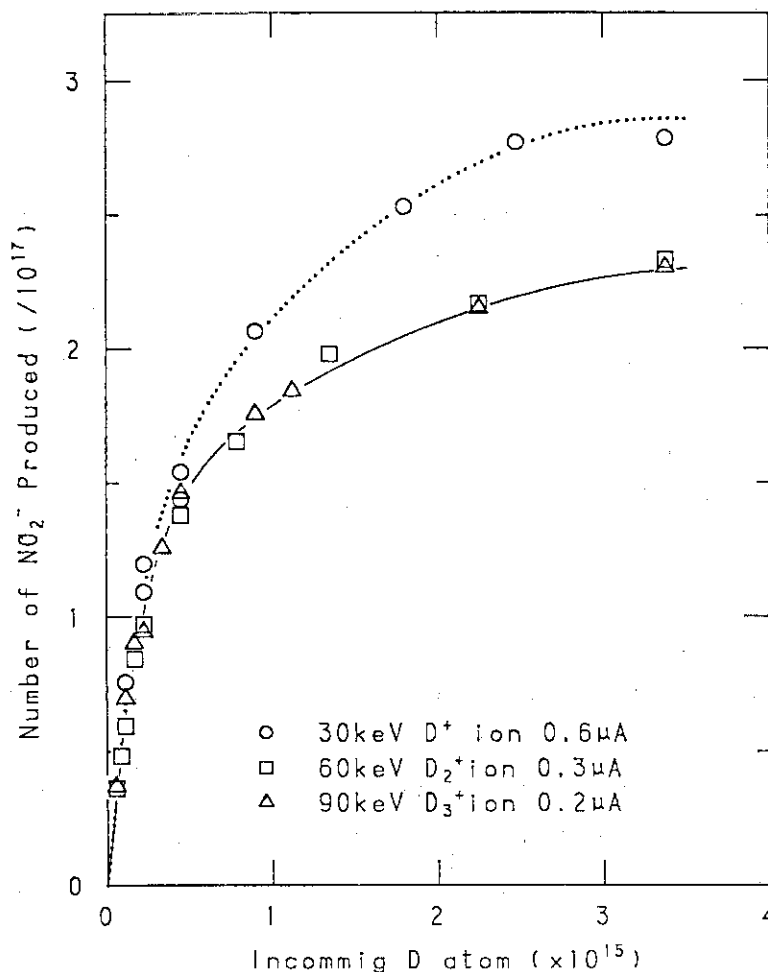
Fig. 1 Measured nitrite yield in solid potassium nitrate for 30-keV D^+ (0.6 uA),60-keV D_2^+ (0.3 uA) and 90-keV D_3^+ (0.2 uA) ion bombardment.
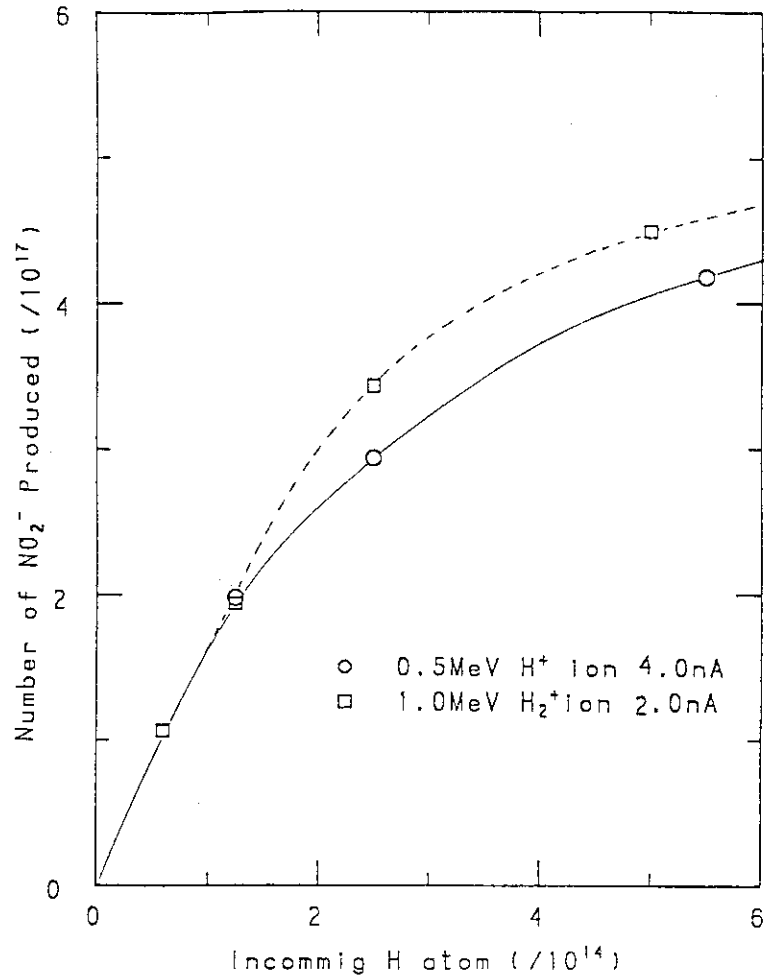
Fig. 2   Measured nitrite yield in solid potassium
nitrate for 0.5-MeV H⁺ (4.0 nA) and 1.0-MeV H_2^+(2.0 nA)
ion bombardment.

Table 1   Initial yield and "saturation yield" of NO_2^- from KNO_3^-.

Ion	Energy (keV)	Ion current (μA)	Initial yield per incident ion	G-value initial	saturation
D^+	30	0.6	766	2.45	2.25
D_2^+	60	0.3	1480	2.45	1.85
D_3^+	90	0.2	2220	2.45	1.85
	(MeV)	(nA)			
H^+	0.5	4.0	16960	3.39	3.13
H_2^+	1.0	2.0	33900	3.39	2.90

4. References

1) S. Ohno, K. Furukawa and T. Soga, Bull. Chem. Soc. Jpn.,<u>59</u>, 1947 (1986).

2) T. Soga, K. Furukawa and S. Ohno, Proc. 52nd Ann. Conf. Chem. Soc. Jpn., <u>1</u>, p.322 (1986).

3) T. Soga, K. Furukawa and S. Ohno, JAERI-M 86-112, p.100 (1986).

4) R. J. Batra and A. N. Garg, Radionchem. Radioanal. Lett.,<u>54</u>,177 (1982).

5) H. H. Andersen and H. l. Bay, J. Appl. Phys.,<u>46</u>, 2416 (1982).

2.8   CONSTRUCTION OF AN APPARATUS FOR STUDY OF HEAVY-ION
       INDUCED   CHEMICAL REACTIONS

Katsutoshi FURUKAWA, Shin-ichi OHNO, Yoshihide KOMAKI,
Takeshi SOGA, Shigemi FURUNO, Kiyoshi KAWATSURA*,
Yohta NAKAI*, Kunio OZAWA**, Kazuhiko IZUI, Teikichi SASAKI,
Kiichi HOUJYOU, Yuji BABA, Yasumasa IKEZOE***,
Nobutake SUZUKI***, Hideki NANBA***, Seiichi TAGAWA****,
Noriyuki KOUCHI**** and Hiromi SHIBATA****

Department of Chemistry, *Department of Physics,
***Department of Research, JAERI. **Energy Research
Laboratory, Hitachi Ltd. ****Nuclear Engineering Research
Laboratory, University of Tokyo

1. Introduction

   To study chemical reactions induced by energetic multiply-charged ions,
we proposed the installation of a special apparatus for this purpose at one
of the beam lines of the Tandem accelerator. We discussed the problem from
various   aspects,   e.g.,   research   philosophy,   possible   and available
experimental methods, design considerations of the experimental set-ups,
and so on. The results of the discussion were already presented elsewhere.[1]
Fortunately, our proposal was granted and we could start our research
project in this year. The apparatus has now been constructed. The first test
beam was introduced into the apparatus in March 1987.

   Below are described objectives of the research, designs of the
apparatus, and the results of the pumping test as well as the beam transport
test.

2. Objectives of the Research

   i). Microdosimetry in gases.

   ii). High-resolution mass analysis of the products formed in the sample
        during the bombardment with energetic multiply-charged heavy ions.

   iii). Fabrication of heavy-ion track-etched filter membranes.

   Objective i) is to get informations on the spatial distribution of the
energy deposition around the heavy-ion path in a solid. Radial distances of

1 nm from the ion path in the solid would correspond to distances of ~ 150 mm in a gas at a pressure of 10^{-4} Torr. By measuring ionization currents produced in a small volume in the gas as a function of distance from a narrow ion beam, we can investigate the structure of a heavy-ion track in matter.[2]

Objective ii) comes from our expectation that multiply-charged ion impact will produce highly excited states of a molecule which in turn decomposes into fragments with high charge states and/or large kinetic energy.

Objective iii) is a continuation of the work described in a previous paper.[3]

3. Design of the Apparatus

A schematic view of the whole apparatus is shown in Fig.1. This is connected to the H4 beam line in the H -1 room. The ion beam from the Tandem accelerator comes from the left side of the figure, and passes through a fast acting valve and a pumped vacuum stage, which avoids gas contamination of the beam line system, and enters the target chamber designated as through a 20-mm diameter diaphragm. In the middle of this chamber is placed an externally rotatable disk holding 10 samples to be irradiated. The chamber has a beam-profile monitor and a Faraday cup to measure current intensities

The second chamber (Ⅱ) is for several measurements during the bombardment. It is already equipped with a high-resolution quadrapole mass spectrometer (C-50, Extranuclear Lab., Co.) with an energy analysis unit. These are to analyze the mass/charge ratio and the kinetic energy of the fragments emitting from the sample traversed by a heavy-ion beam. The beam diameter is adjustable to 1 or 5 mm through an aperture which is located between Ⅰ - and Ⅱ -chambers.

The beam will further passes through a differentially pumped vacuum stage (designated as Ⅲ -chamber), which contains a beam collimation system, and finally enters a cylindrical chamber(Ⅳ) which is destined to the use for microdosimetry. The beam-collimation system consists of a set of apertures (0.1 and 0.3 mm diameter) movable in three dimensions through remote controller.

In Ⅳ -chamber the pressure of the gas is adjustable from 10^{-4} to 10^{2} Torr. The gas pressure is measured with a Baratron capacitance manometer and a steady gas flow is maintained with an aid of automatically controlled

variable leak valve. At the end of the IV-chamber is placed a current monitor which is in effect a Faraday cup or an electron-channel multiplier.

4. Pumping Test

Turbomolecular pumps are used to evacuate whole the system. The pressures at each chambers after 30-min and 24-hr operation, respectively, are shown in Fig.1. The pressures were also read when the air was introduced in the IV-chamber at atmospheric pressure. From the data given in Fig.1, one can see that the differentially pumping system is quite satisfactory.

5. Beam Transport Test

The first beam introduced through the chambers was that of $^{127}I^{6+}$ at the energy of 1 MeV/amu. The current intensity at II-chamber was 1.5μA. However, we could not conduct the beam to the IV-chamber, probably owing to the wrong alignment of the apparatus with respect to the beam line axis of the accelerator. The second try was with a beam of $^{16}O^{6+}$ at 5 MeV/amu and with enlarged apertures ; slit diameter 5 mm instead of 1 mm at the location between I and II, and slit diameter 0.2 mm instead of 0.1 mm at III-chamber. Then, the beam was observed to reach the end of IV-chamber. We have verified this by counting ions incident on a 5×5 mm² metal electrode from which electrons emitted and were amplified by a channeltron. The counting rate was $\sim 10^5$ cps. We expect to get better alignment of the apparatus before we start experiments on microdosimetry and mass analysis of the products.

Reference
1) Study Group for Ion-beam Induced Chemical Reactions:JEARI-M 85-164(1985).
2) S.Ohno:UTNL-R-0197 (1986) pp. 44-46.
3) Y.Komaki ,S.Ohno, H.Ohtsu, H.Itoh, T.Seguchi and M.Iwasaki:Nucle.Tracks Radiat.Meas.11(1986) 99.
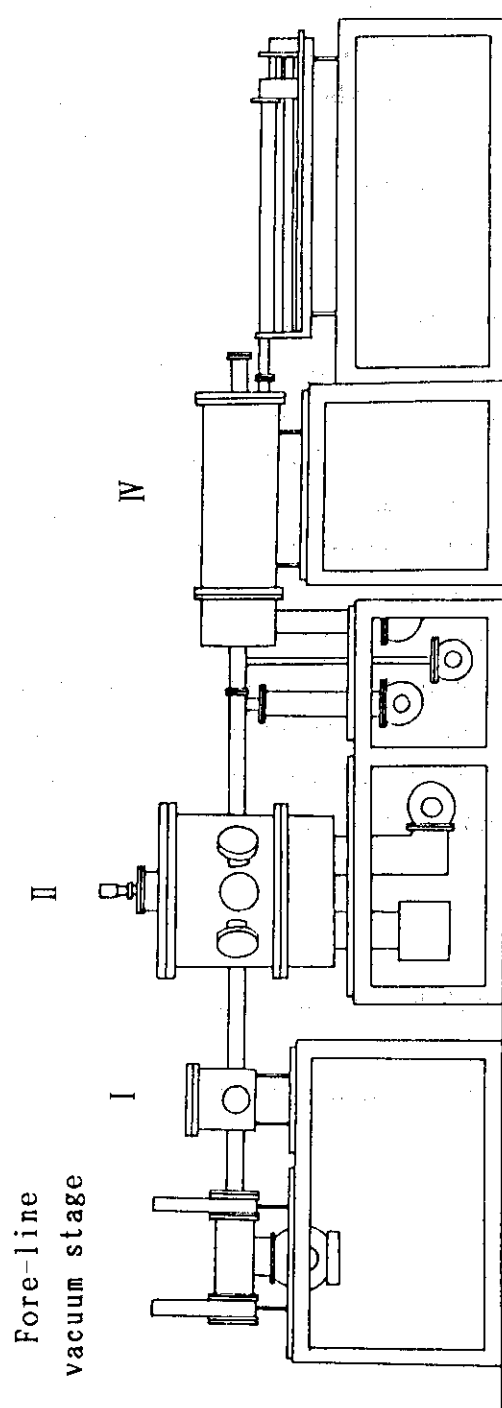
	Fore-line vacuum stage	I chamber	II chamber	IV chamber	IV chamber
The pressure after 30 min	1.1×10^{-6}	1.6×10^{-6}	1.9×10^{-6}	1.1×10^{-6}	
The pressure after 24 hr	3.9×10^{-9}	1.3×10^{-8}	2.0×10^{-8}	1.6×10^{-8}	
During differential pumping	3.9×10^{-9}	1.3×10^{-8}	2.0×10^{-8}	760	

(Torr)

Fore-line
vacuum stage

Fig.1 A Schematic View of the Whole Apparatus

- 63 ~ (64) -

Ⅲ RADIATION EFFECTS IN MATERIALS

3.1   A STUDY OF X-RAY DIFFRACTION ON HEAVY ION IRRADIATED LiF
      AND GaP CRYSTALS

Hiroshi MAETA, Katsuii HARUNA[*], Kazutosi OHASHI[*],
Takuro KOIKE[*] and Fumihisa ONO[**]

Department of Physics, JAERI, [*]Faculty of Engineering,
Tamagawa University, [**]College of Liberal Arts and
Sciences, Okayama University

1. Introduction

An energitic heavy ion incident on a metal produces a high local
concentration of vacancy - interstitial pair. At ambirnt temperatures,
these defects will make clusters which are primary form of structual
damage. Depending on the nature of the irradiation ions, the defect
configuration can very from ramdomly distributed vacancy interstitial pair,
densely populated with vacancies and interstitials.

In the present paper, we report the effects on changes of the   lattice
parameters in LiF and GaP by heavy ion irradiation. Furthermore, to study
the structure of the defects after heavy ion irradiation, the measurements
of the diffuse scattering for Si and InP were carried out   at room
temperature (RT).

2. Experimental Procedures

Single crystal LiF specimens of about 10 x 20 mm^2 and 1.8 mm in
thickness were used. GaP specimens were prepared in thin rectangular plates
of single crystal with area of 3x10 mm^2 and thickness of 0.3 mm.   The LiF
specimens were bombarded with 165 Mev Cl^{+10} ion to 10^{13} ion/cm^2 at R.T and
GaP specimens were irradated with 120 Mev Cl^{+10} ion to 10^{14} ion/cm^2 at
about liquid nitrogen temperature, then they were warmed up to RT . X-ray
measrements werc carried out at RT.   By using a CuKɑ beam through a fine
slit of 0.2 mm in width, the measurements of the lattice prameter were
carried out by the Bond method in which two counter were placed
symmetrically. The diffuse scattering measurements were also carried out at
RT using the monochromatized $CuK\alpha_1$ radiation and a solid state detector(
pure Ge).

3. Results and Discussion

Main results of this work are as follows :

1) Remarkable changes of diffraction profiles in LiF specimens which have appeared main peak with two peaks after heavy ion irradiation were found as shown in Fig. 1. The aditional peaks are located on the lower angle side of the Bragg peaks which come from the substrate region. They are due to the volume expansions in the irradiated regions where defects make to increase the lattice parameter in the these regions.

2) Very large values of increased lattice parameters $\Delta a / a_0 = 0.1$ by the irradiation were obtained.

On the LiF specimens we have found the Bragg peaks together with two peaks on lower side of the main peaks after haevy ion irradiation. The relative positions of the peaks show volume expansion of the damaged regions, respectively. Relative lattice parameters corresponding to these regions are obtained using the following formular,

$$\Delta a/a_0 = - 1/ tg \theta_{Bragg} \times \Delta\theta,$$

we find an expansion of $\Delta a/a_0 = 8 \times 10^{-4}$ for the region near the surface and $\Delta a/a_0 = 2.4 \times 10^{-3}$ for the heavily damaged region. These two peaks come from the irradiated regions where the defects have expaned the lattice parameters. A schematic drawing of the results is shown in Fig 2.

For GaP specimen it is very surprising that the relative changes of the lattice parameter after the heavy ion irradiation increase up to $\Delta a/a_0 = 0.1$. It is as much as that of InP specimen ($\Delta a/a_0 = 0.07$) after heavy ion irradiation reported previously [1].

The heavy ion irradiation introduces very much larger volume variation than light particles, for example, proton as found by Geist et al. to be $\Delta a/a_0 = 0.06$ for 4×10^{17} p cm^{-2} [2]. Therefore, it will be expected to produce larger number of the defects than that of the light ion. For the case of GaP specimen, we estimated the concentration of the induced defects by Cl^{+10} bombardments to be about 0.2 % from a calculation using by the E-DEP-1 code, where we assume that the defects do not move and recovery. The experimental conditions and results are also summarized in table 1, comparising with the results of InP and Si specimens [1].

The results of the diffuse scattering of InP and Si specimens after the irradiations show that these profiles are very sharp and there is not

very much change for the half width of the Bragg profiles. The facts suggest that the defects may be not so complicated. The large changes of the lattice parameter may be attributed to long range effects of point like lattice defects. Most of the defects may be interstitial clusters and/or small dislocation loops.

A more detailed analysis of the present results and experiments, are currently in progress and will be published elsewhere.

References

[1] H. Maeta, K. Haruna, K. Ohashi, T. Koike and F. Ono, JAERI TANDEM, LINAC & V.D.G. Annual Report 1985, p 45.

[2] V. Geist, C. Ascheron, R. Flagmeyer, H.J. Ullrich and D. Stephan, Radait. Eff. 54, 105 (1981)

[3] Point Defects in Solid, ed. by I.H. Crawhold and L.M. Slifkin, p.96.

Table 1

Increase of the lattice parameters of GaP, InP and Si single crystals irradiated by Cl^{+10} at liquid nitrogen temperature. The measurements were carried out at RT. The results of InP and Si after the irradiation are shown, as to compare with that of GaP.

specimens	ion	energy	range	Threshold Energy Td [3]	dpa	increase of lattice parameter $\Delta a/a_0$
GaP	Cl	120 MeV	22 μm	9.0 eV	0.20	0.10
InP	Cl	120 MeV	20 μm	7.5 eV	0.35	0.069
Si	Cl	120 MeV	32 μm	20.0 eV	0.06	0.019

Specimen
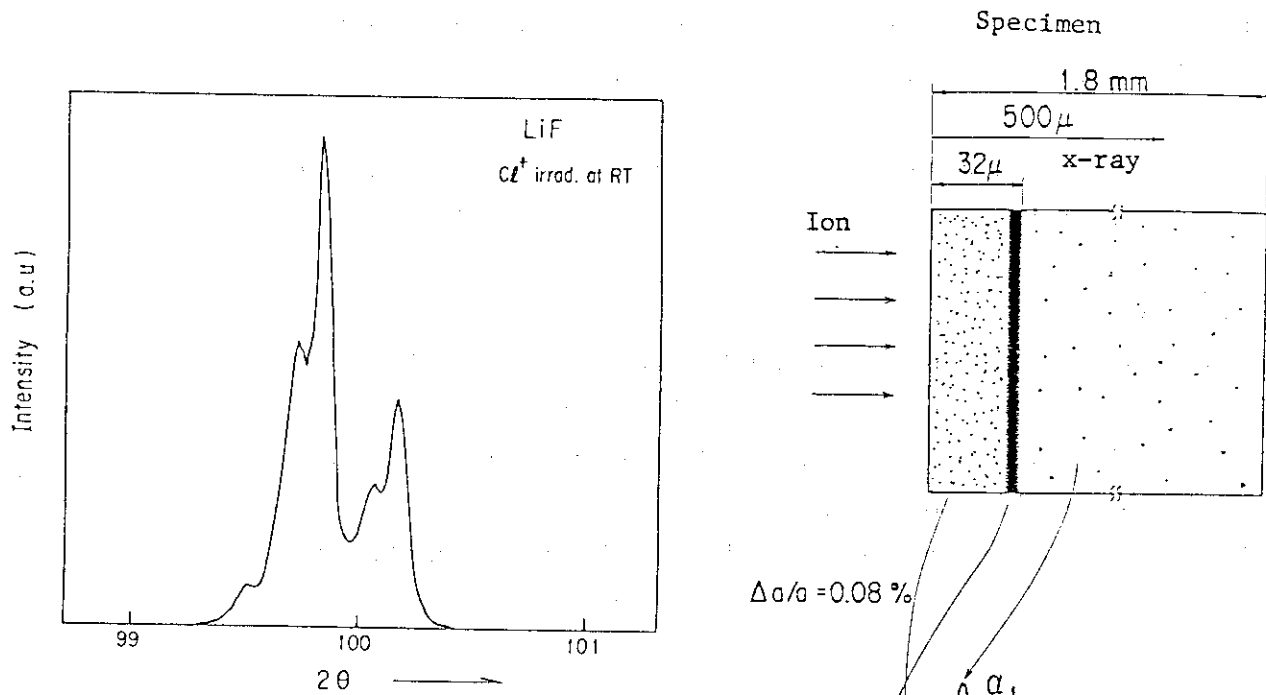
Fig. 1 X-ray profile of LiF
crystal after irradiation with
165MeV Cl^{+10} ion to 10^{13}
ion cm^{-2} at RT.
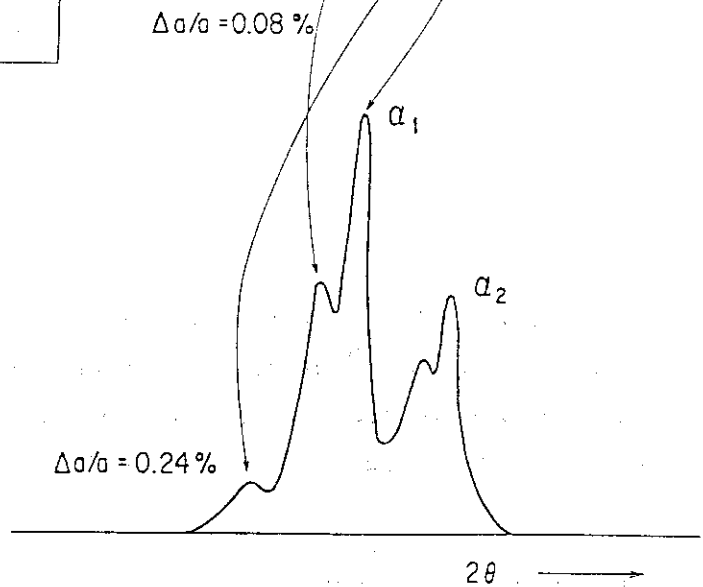
Fig. 2 A schematic drawing of x-ray profile on heavy ion irradiated
LiF crystal.

3.2   DAMAGE DISTRIBUTION OF HEAVY-ION IRRADIATION IN METALS
STUDIED BY ELECTRICAL RESISTIVITY MEASUREMENT

Saburo TAKAMURA, Kiyotomo NAKATA*, Mamoru KOBIYAMA** and
Takeo ARUGA***

Department of Physics, JAERI, * Hitachi Research Laboratory
Hitachi Ltd., ** Faculty of Engineering,Ibaraki University,
*** Department of Fuels and Materials, JAERI

§ 1. Introduction

The heavy-ion irradiations are widely employed for the simulation of
neutron irradiation in fusion and fission reactors. The radiation damage
by ions has a strong gradient of defects with the highly damaged region in
the direction of depth of a sample. The precise depth distribution of
damage is required for the irradiation experiment by ions.

In order to obtain the damage distribution by ion irradiation,
theoretical calculations are applied, and two computer codes are currently
used; one is the EDEP-1 code of analytical method[1], and the other is the
TRIM code of Monte Carlo simulation[2]. However, few experiments to
determine the damage profile have been performed[3][4], and the comparison
of experiment with theory is rather limited.

In this study, C, Cl and Br ions at energies of 90-160 MeV are
irradiated to multi-foil samples composed of pure metals at low
temperature. The depth profile in the samples is obtained from a change
in electrical resistivity of each foil. The experimental depth profiles
are compared with the theoretical predictions by the modified EDEP-1 and
TRIM codes.

§ 2. Experimental procedure

Foils used in this study were pure Al(99.7 %), Fe(99.85 %), Ni(99.95
%), Cu(99.97 %), Ag(99.97 %) and Ta(99.9 %) with 1-50 μm in thickness,
which were supplied by Goodfellow Metals Ltd.. Ratio of the resistivity
at 4.2 K to that at room temperature(RRR) was about 10 in the foils. The
foil thickness was determined precisely by a weighting method for the
foils of 20×20 mm²; the accuracy of the weighting was ± 0.5 μg. More
than ten foils cut to about 2 mm width were piled up on a sample holder to
be perpendicullar to the direction of ion beam, and about ten foils with 1
μm thick were set around the damage peak.

A schematic cross sectional view of a low-temperature ion-irradiation

cryostat is shown in Fig. 1. The samples were set on five faces of the sample holder in the shape of hexagonal pillar in the cryostat. The samples were cooled below 10 K before ion irradiation. The sample holder could be rotated by using the sample rotation system, and the five samples were irradiated successively. After the irradiation, the sample holder with samples was dropped into the transporting liquid He vessel connected to the cryostat without warming. The ions used in the irradiation were 90 MeV C, 150 MeV Cl and 160 MeV Br.

The irradiated samples were removed from the sample holder, and thin copper lead wires were pressed at the ends of each   foil in liquid N_2 for electrical resistivity measurement. The electrical resistivity was measured in liquid He by the conventional four-probe potentiometric method.

Fig. 1 Schematic cross sectional view of a low-temperature ion-irradiation cryostat.

In order to know the resistivity change caused by the radiation-produced defects, the irradiated foils were isochronally annealed for 300 s from 100 to 220 K by using an annealing copper box with electrical heater in the cryostat for electrical resistivity measurement. The annealing temperatures were controlled within an accuracy of ± 0.5 K.

§ 3. Results and Discussion

The damage distribution in metals, such as peak depth and half-value width, is changed with thermal migration of irradiation-produced defects and an interaction between the defects and implanted ions. However, the damage peak obtained in this work is not altered by the defect migration because no defects diffuse between the foils.

The damage distribution with ion irradiation is also estimated by the theoretical calculations. The calculations take generally no account of the effect of thermal diffusion of the defects and implanted ions. Therefore, the results in this study give an exact comparison with the
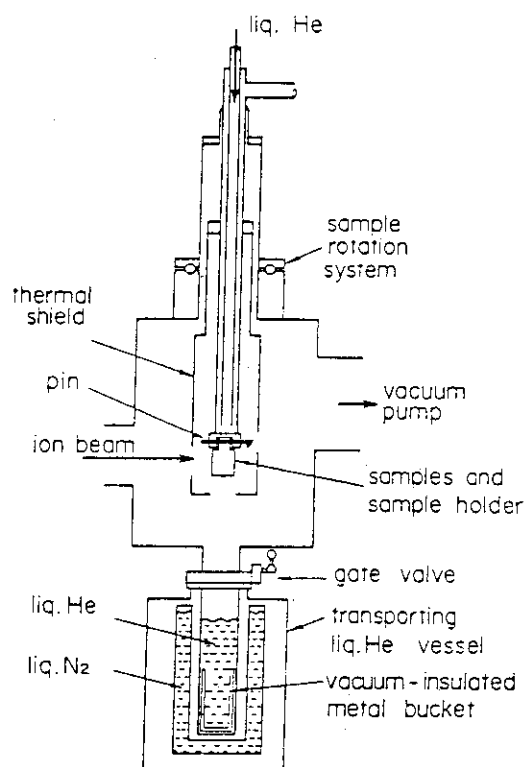
caluculated values. Fig. 2 shows the experimental damage profiles compared with the calculated ones by the modified EDEP-1, EDEP-81, and
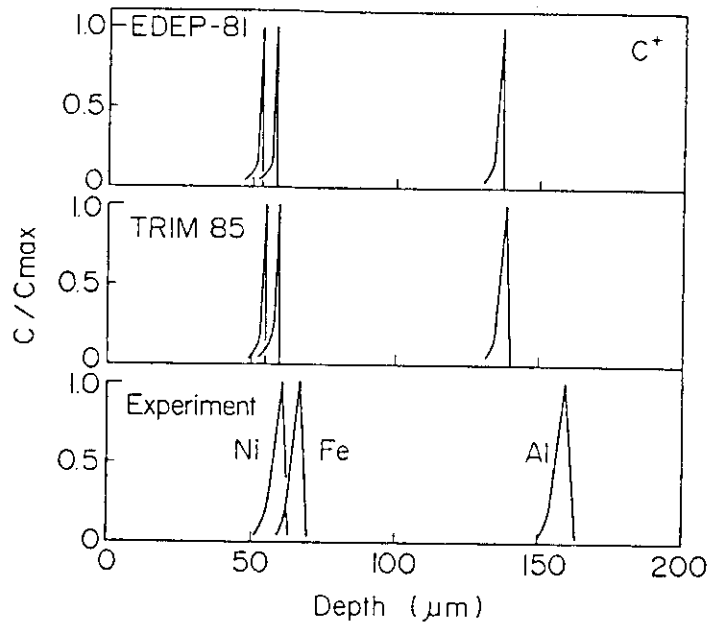
Fig. 2 The comparison between the experimenal damage profiles and calculated ones by EDEP-81 and TRIM 85 codes for Al, Fe and Ni irradiated with C ions at 90 MeV. Vertical axis means a ratio of resistivity or dpa at a depth to their maximum values.
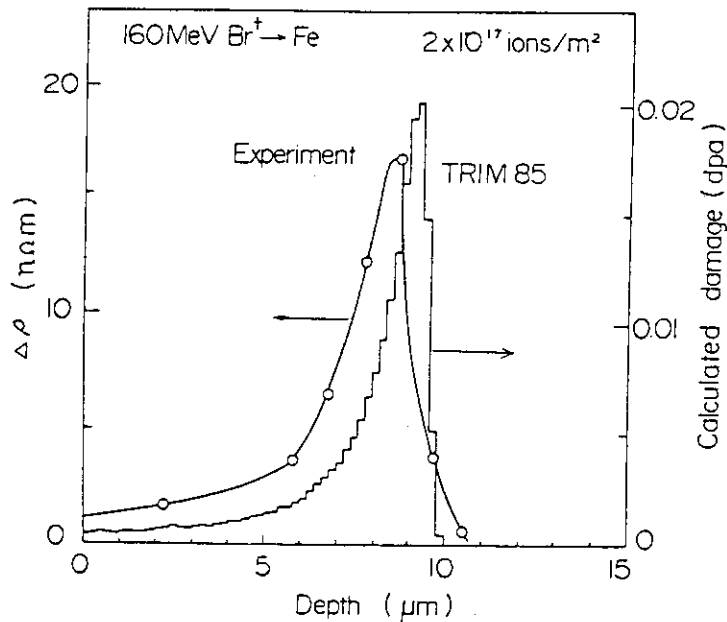
Fig. 3 The comparison between the experimental damage profile and TRIM 85 calculated one for Fe irradiated with Br ions at 160 MeV.

TRIM 85 codes for Al, Fe and Ni irradiated with C ions at 90 MeV. The depth of damage peak and half-value width calculated by the codes are smaller than that of experimental value in the samples. The comparison between the experimental and calculated damage profiles is shown in Fig. 3 for Fe irradiated with 160 MeV Br ions. In this case, the experimental damage profile is similar to the calculated one by the TRIM 85 code, although the peak depth calculated is slightly larger.

The difference between the calculated damage peak depth, Rcal, and experimental one, Rex, in the samples irradiated with C, Cl and Br ions is shown in Fig. 4 against the atomic number of metals. In the irradiation with C ions, the experimental depths of damage peak are about 15 % larger than the calculated ones for the metals with small atomic number, such as Al, Fe, Ni and Cu, and show a good agreement with the calculated depths for Ag and Ta. On the other hand, the results in the Cl ion irradiation indicate a good agreement between the damage peak depths obtained by the experiment and calculation using the EDEP-81 code, while the experimental value in Ag is slightly smaller than the calculated one.
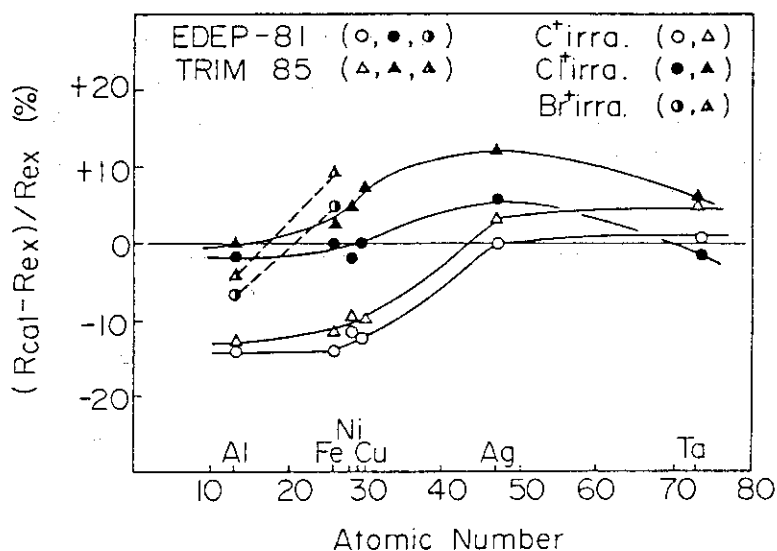
Fig. 4 The difference in percent between the calculated damage peak depth, Rcal, and experimental one, Rex, in the samples irradiated with C, Cl and Br ions as a function of the atomic number of samples.

References

1) I.Manning and G.P.Mueller, Comp. Phys. Comm. 7 (1974) 85.

2) J.P.Biersack and L.G.Haggmark, Nucl. Instr. and Meth. 174 (1980) 257.

3) T.S.Noggle, B.R.Appleton, J.M.Williams, O.S.Oen, T.Iwata and G.W.Vogl, J. Nucl. Mater. 125 (1984) 330.

4) S.Hamada, T.Sawai and K.Shiraishi, J. Nucl. Mater. 133&134 (1985) 370.

3.3 THE EFFECT OF HIGH DENSITY ELECTRON EXCITATION AND ELECTRON-PHONON INTERACTION ON THE DEFECT PRODUCTION IN NICKEL IRRADIATED WITH 100 MeV HEAVY IONS

Akihiro IWASE[*], Shigemi SASAKI[*], Tadao IWATA[*] and Takeshi NIHIRA[**]

[*] Department of Physics, Japan Atomic Energy Research Institute, [**] Faculty of Engineering, Ibaraki University

Introduction

In our previous paper, we reported that the anomalous reduction of the stage I recovery was observed in Ni irradiated with ∼100 MeV heavy ions and that this anomaly was strongly related to the high density electron excitation by energetic heavy ions and the following energy transfer from electrons to lattice through the strong electron-phonon coupling.[1] The transferred energies from electrons to lattice cause the local temperature increase along the ion beam path and annihilate the stage I interstitials. This effect is also expected to appear in the defect production process during irradiation. In this paper, we report the effect of the high density electron excitation and the electron-phonon interaction on the defect production and the defect saturation behavior in Ni.

Experimental procedure

The nickel foils about 2500 A thick were irradiated with 84 MeV ^{12}C, 115 MeV ^{19}F, 120 MeV ^{28}Si, 120 MeV ^{35}Cl, 100 MeV ^{81}Br and 100 MeV ^{127}I ions from the JAERI tandem accelerator at $\lesssim$ 10 K and the irradiation induced electrical resistivity $\Delta\rho$ was measured as a function of ion fluence ϕ. From the measurement, we can determine the damage energy which is necessary to produce a given concentration of defects in Ni and the effective recombination volume for each irradiation. The damage energy can be estimated from the theoretical defect production cross section and the ion fluence. The results were compared with those for low energy (0.5-1.8 MeV) ion irradiations[2].

Result and Discussion

Figures 1(a) and 1(b) show the damage energy which is necessary to produce the defect concentration of about 830 atomic ppm(this

concentration corresponds to the resistivity change of 500 nΩcm) in the specimen for each irradiation as a function of PKA median energy $T_{1/2}$ and as a function of electronic stopping power S_e, respectively. For comparison, the results for the low energy ion irradiation are also shown[2]. Figures 2(a) and 2(b) show the recombination volume for each irradiation as a function of $T_{1/2}$ and S_e, respectively. As can be seen in these figures, the damage energy and the recombination volume for high energy heavy ion irradiations are much larger than for low energy ion-irradiations as compared at the same $T_{1/2}$, and monotonically increase with increasing the electronic stopping power.

The present results can be explained as follows;
During irradiation, the annihilations of the stage I interstitials occur. The annihilations cause a substantial decrease of the defect production rate, and the damage energy necessary to produce the same concentration of defects increases with increasing the annihilation of the stage I interstitials. The newly injected ions cause a local temperature increase along the ion path, and annihilate the already produced defects. This process leads to the increase of recombination volume effectively.

The fact that the increases of the damage energy and the recombination volume are strongly related to the electronic stopping power shows that the annihilations of the defects originate from the high density electron excitations in Ni.

References

1) A. Iwase, S. Sasaki, T. Iwata and T. Nihira; Phys. Rev. Lett. 58, 2450 (1987).
2) A. Iwase, S. Sasaki, T. Iwata and T. Nihira; J. Nucl. Mater. 141-143, 786 (1986).
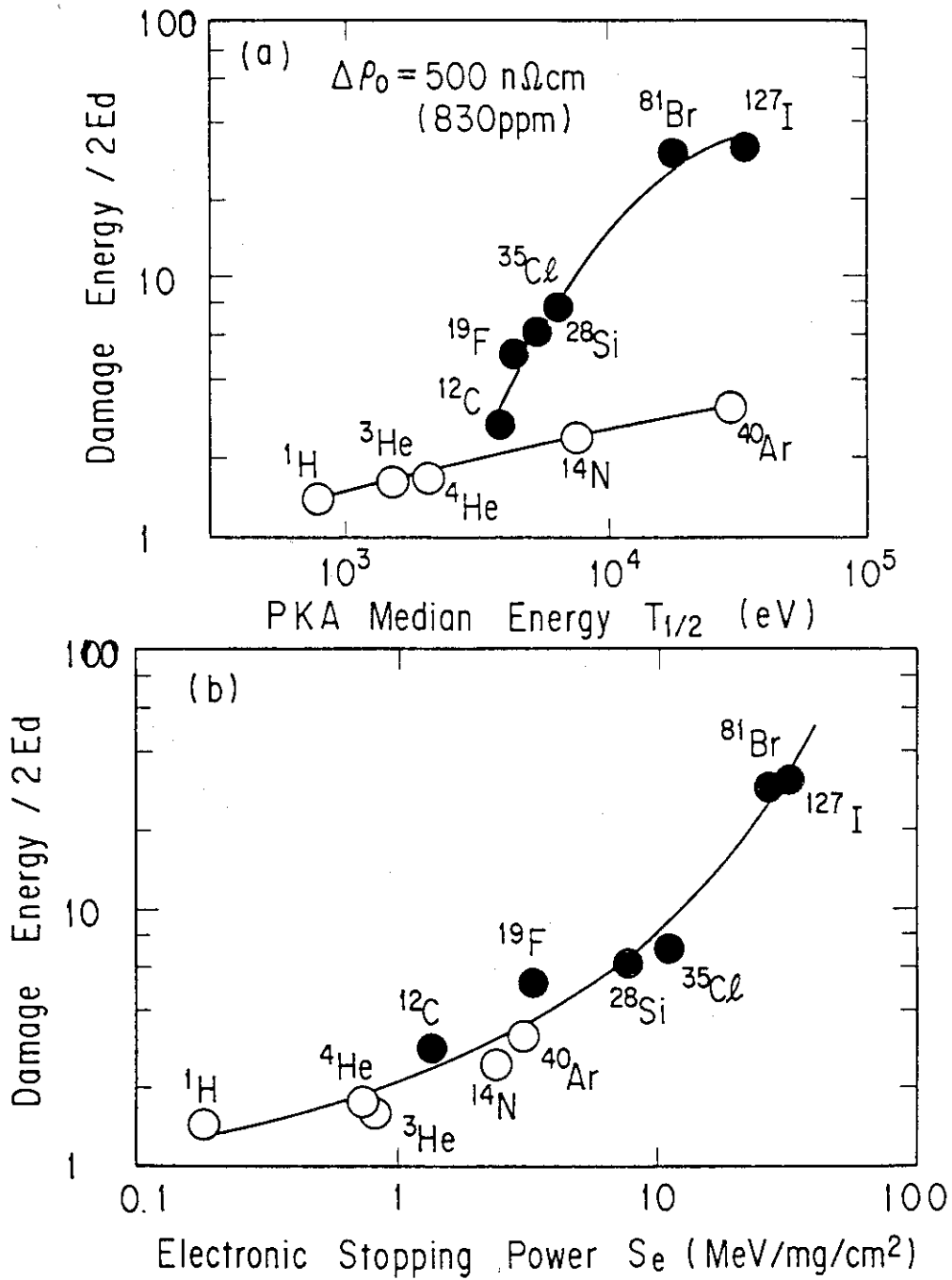
Fig.1 Damage energy which is necessary to produce the defect concentration
of 830 atomic ppm in the specimen as a function of PKA median energy
$T_{1/2}$(a), and as a function of electronic stopping power S_e(b).
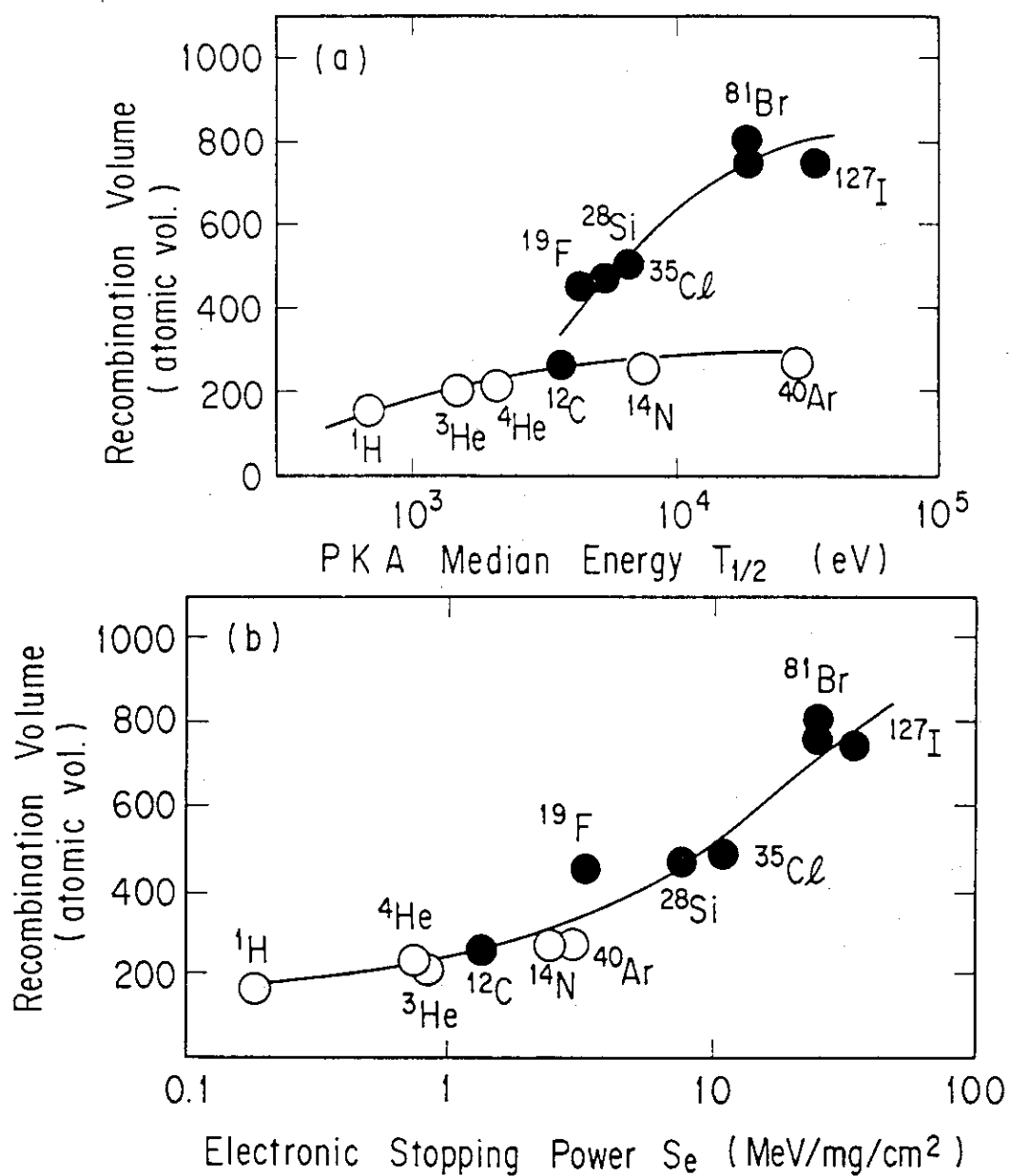
Fig.2 Recombination volume as a function of $T_{1/2}$(a) and S_e(b).

3.4 CASCADE DAMAGE IN MOLYBDENUM BY HIGH ENERGY HEAVY ION IRRADIATION

Shigemi SASAKI, Akihiro IWASE and Tadao IWATA

Department of Physics, Japan Atomic Energy Research Institute

Introduction

The presence of displacement cascades due to high energy primary knock-on atoms (PKA) is one of the most important features of damage structure evolution in metals during the irradiation with high energy particles such as neutrons and heavy-ions in contrtast with the case of electron irradiation. The displacement cascades of knock-on atoms introduce not only isolated Frenkel pairs but also point defect clusters simultaneously. The nature and the number of defect clusters depend on the energy and mass of irradiating particles.

Recently, microstructural changes in metals by irradiations with relatively low energy (10-100keV) of heavy ions have been studied for the comparison between experiments and calculations about damage production by PKA.[1] On the contrary, the observations of defect structures introduced by high energy (>MeV) heavy ion irradiations have not been performed extensively, though these irradiations, useful for simulating fusion neutron damage, introduce high energy PKA having energy greater than 100keV.

In this paper, the development of defect structure in molybdenum has been examined by using an electron microscope in order to understand the mechanism of defect cluster formation under high energy heavy-ion irradiations at vacancy immobile low temperatures.

Experimental procedure

A pure molybdenum rod supplied by Johnson Matthey Chemicals Ltd. was sliced to disks about the thickness of 250 μm. These disks were annealed in a vacuum of 10^{-9} Torr at a temperature about 1800℃. The disks were punched out to smaller disks of 3 mm diameter and were electropolished into wedge shaped specimens suitable for the observation in a transmission electron microscope. The irradiations on the polished specimens with high energy heavy ions were carried out with the JAERI

tandem accelerator in vacuum of 10^{-8} Torr at a temperature around 150 K. The irradiating ions were 84MeV $^{12}C^{5+}$, 150MeV $^{35}Cl^{9+}$, 100MeV $^{81}Br^{6+}$ and 120MeV $^{127}I^{7+}$.

The defect structures introduced by the irradiations were examined at room temperatures with an electron microscope JEM-2000FX operated at 200 kV.

Results

The observations showed that the ion irradiations introduced small defect clusters in the specimens. From the shape of image contrast, these clusters seemed to be dislocation loops of sizes less than 100Å

In Fig. 1, the areal number densities of defect clusters in the wedge shaped specimens were plotted against the foil thicknesses. The volume number density of defect clusters in each specimen was determined from the gradient of each line of thickness dependence. The volume number density of defect clusters against the fluence for each ion irradiation is plotted in Figs. 2-5. These figures show that the number of defect clusters increases linearly with the fluence. These results in this experiment are summarized in Fig. 6.
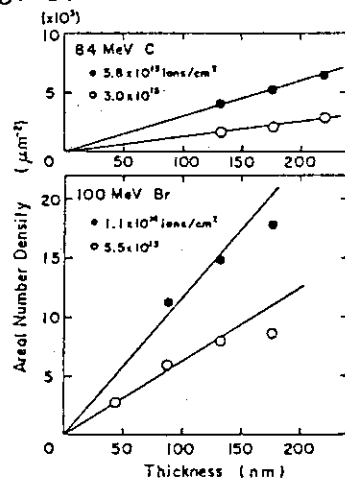
Fig. 1
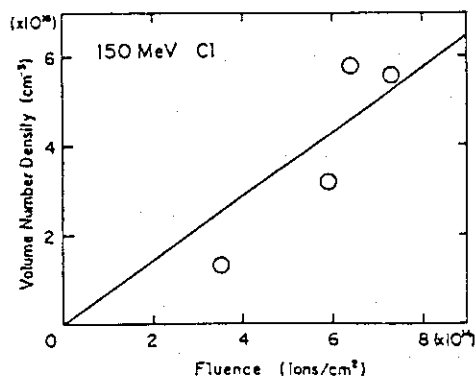
Fig. 2

Fig. 3
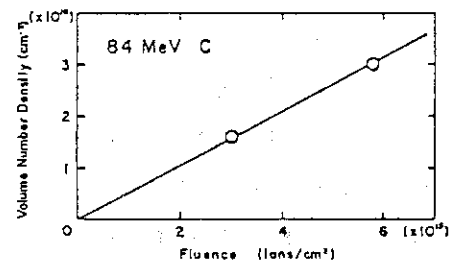
Fig. 4
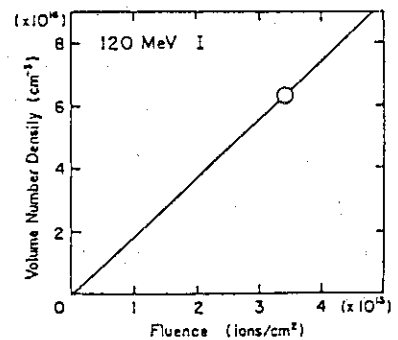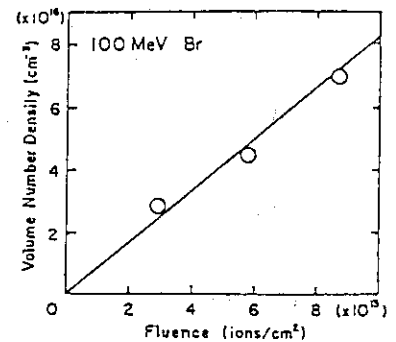
Fig. 5
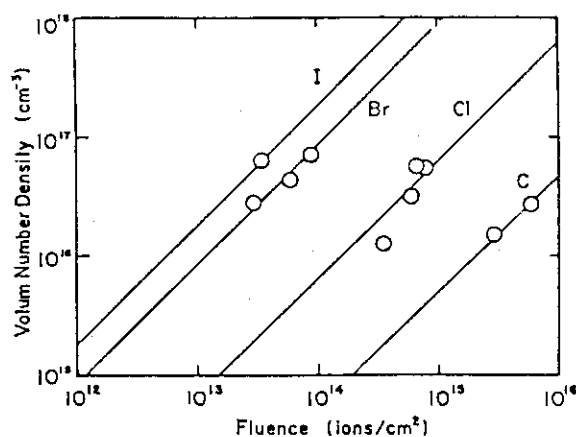
Fig. 6

Discussion

It is known in the case of electron irradiation that small inter-stitial type dislocation loops are introduced at vacancy-immobile low temperatures, and that the nucleation of interstitial loops ceased at the very beginning of irradiation and no increase of number density is observed.[2]

On the contrary, we observed linear increase of the number density of defect clusters against the ion fluence. This linear increase is quite similar to that observed in 14 MeV neutron irradiated copper.[3] According to Yoshida et al., more than half of defect clusters introduced by 14 MeV neutron irradiation were stacking fault tetrahedra. In the present experiment, however, were observed no stacking fault tetrahedra but small dislocation loops. Although the speciesof defect cluster in our case is different from in ref. 3, the essential mechanism for cluster formation seems to be the same. That is, every single cascade having energy greater than some threshold seems to offer a nucleus of defect cluster, otherwise the linear increase of number density of the clusters against fluence cannot be explained.

From the data of the present experiment, the cross section of the visible defect cluster production σ_p can be calculated by dividing the number density of defect cluster by the fluence. In addition, the threshold energy of defect cluster production can be easily calculated by assuming that the collision process is the Rutherford scattering. Each of the calculated value for each irradiation

Table I

	σ_p (cm^2)	E_d
84 MeV C	8.3×10^{-23}	74 keV
150 MeV Cl	1.2×10^{-21}	69 keV
100 MeV Br	1.3×10^{-20}	90 keV
120 MeV I	3.0×10^{-20}	110 keV

is listed in Table I.

Summary and Conclusions

(1)Pure molybdenum specimens were irradiated with high energy heavy ions by using the JAERI-tandem accelerator. The dependence of the defect cluster formation against the fluence for each ion irradiation was examined.

(2)In every irradiation, the defect clusters introduced were small (<100Å) dislocation loops. The number density of dislocation loops increased linearly with the fluence.

(3)The threshold energy for the formation of dislocation loop was calculated as 70-110 keV, i.e. only the PKA which recoiled more than several hundreds atoms supplied a nucleus of a dislocation loop.

Acknowledgments

References

1)B. L. Eyre and C. A. English : Proc. Int. Conf. on Point Defects and Defect Interactions in Metals, Kyoto, 1981 (Tokyo Univ. Press, Tokyo, 1982) p.799.

2)M. Kiritani : Proc. Int. Conf. on Fundamental Aspects of Radiation Damage in Metals, Gatlinburg, (1975), USERDA, Vol. II, p.695.

3)N. Yoshida, Y. Akashi, K. Kitajima and M. Kiritani : J. Nucl. Mater. 133&134 (1985) 405.

3.5   X-RAY TOPOGRAPHIC STUDY OF Si SINGLE CRYSTALS
       IRRADIATED WITH ENERGETIC HEAVY IONS (5)

Hiroshi TOMIMITSU

Department of Physics, JAERI

1.Introduction

The lattice imperfection within the Si single cryatls induced by ion=
bombardments has been studied by the conventional X-ray diffraction topo-
graphy(XDT). For the case of the irradiation with rather **heavy ions**, it
has been revealed as following[1,2,3];
1) The heavy lattice strains concentrate at the boundaries of the
   irradiated- and non-irradiated regions separated by the mask material.
2) The specimen crystal is often deformed macroscopically as a whole.
3) Characteristic and systematic fringes are observed within   the
   irradiated area.

Only the **effect** (1) mentioned above can be, on the other hand,
observed in the case of the irradiation with **lighter ions**.

In order to confirm the results mentioned above, further measurements
were made also in this fiscal year with several kinds of irradiation
conditions. The present report briefly summarizes the results of the XDT-
observation on those heavy-ion-irradiated Si single crystals.

2. Experimental

2.1 Ion Irradiations

Every irradiation was carried out with the tandem accelerator of this
institute, during the irradiation period the specimen being kept at the
LNT. Each irradiation conditions, together with ion species, energies
and dose, are listed in the tables bellow.

2.2 XDT-Observation

XDT-observation was carried out with the conventional Lang's method,
with a fine focus X-ray generator. Several reflections such as 004, 008;
111, 333; 220, 440 parallel, vertical and sianting to the specimen surface,
were used, mainly by Mo-Kαl radiation.

3. Results

3.1 Dependence of Irradiation Effects on Projectile Masses

The results together with the irradiation conditions are summarized in Table 1. The effects of the projectile mass are clearly seen in the Table.

Table 1   Summary of the XDT-Observation for Each Irradiation Conditions
(Without Beam-Scanning)

	Ions	Energy (MeV)	Dose (ions/cm^2)	Margin.Strain	Results[**] Deform.	Fringe
	$^{10}B^{4+}$	58	0.3×10^{13}	No	No	No
	$^{10}B^{4+}$	66	6	Yes	No	No
	$^{11}B^{3+}$	70	1	Yes	No	No
	$^{12}C^{5+}$	100	5	Yes	No	No
	$^{12}C^{5+}$	100	43	Yes	No	No
	$^{16}O^{7+}$	120	7	Yes	No	No
*	$^{19}F^{6+}$	60	2	Yes	No	No
	$^{28}Si^{8+}$	150	1	Yes	No	No
*	$^{28}Si^{9+}$	165	1	Yes	Yes	No
*	$^{32}S^{7+}$	50	0.1	Yes	Yes	Yes
*	$^{32}S^{8+}$	100	1	Yes	Yes	Yes
	$^{32}S^{10+}$	165	1	Yes	Yes	Yes
	$^{35}Cl^{9+}$	150	6	Yes	Yes	Yes
	$^{35}Cl^{10+}$	150	4, 8	Yes	Yes	Yes
	$^{58}Ni^{9+}$	165	0.5	Yes	Yes	Yes
	$^{80}Br^{6+}$	90	10	Yes	Yes	Yes
	$^{197}Au^{13+}$	169	1	Yes	Yes	Yes

* Those are examined in the fiscal year 1986.

** The visibility was compared on the topographs taken with 333, 004 and 220 reflections.

3.2 Effect of Beam Scanning on the Fringe Patterns in XDT

As for the origin of the interference fringe, Bonse, Hart and Schwuttke have attributed it to the inhomogeneity of the cross-sectional distribution of the projectile ions[4]. In order to confirm this assumption, the present author investigated the specimen crystals irradiated with homogeneous- and inhomogeneous beam distribution. The homogeneous irradiation was realized by the beam-scanning in the horizontal direction .

The results are summarized in Table 2. The interference fringe could not be observed in the case of homogeneous irradiation, and consequently the assumption mentioned above was apparently proved.

Table 2   Effect of the Beam Scanning on the Fringe Pattern

	Ions	Energy (MeV)	Dose ions/cm^2	Scanning Yes/ No	Fringe** Yes/No
	$^{32}S^{9+}$	150	29×10^{14}	Yes	No
	$^{32}S^{10+}$	165	1	No	Yes
	$^{35}Cl^{8+}$	120	52	Yes	No
*	$^{35}Cl^{8+}$	140	1	Yes	No
	$^{35}Cl^{9+}$	150	6	No	Yes
	$^{35}Cl^{10+}$	150	4, 8	No	Yes
	$^{58}Ni^{9+}$	165	0.5	No	Yes
	$^{58}Ni^{11+}$	192	3	Yes	No
*	$^{80}Br^{6+}$	90	10	No	Yes
*	$^{80}Br^{10+}$	120	3	Yes	No
	$^{197}Au^{13+}$	169	1	No	Yes
	$^{197}Au^{13+}$	210	1	Yes	No

* Those are examined in the fiscal year 1986.

** The visibility was compared on the topographs taken by 333 reflection.

3.3 Effect of Ion Energy on the Fringe Pattern in XDT

It was investigated how the visibility of the interference fringe changed with the ion energy, i.e. the range value, in the case of $^{19}F^{n+}$, $^{28}Si^{n+}$ and $^{32}S^{n+}$ ions with several energies.

The experimental conditions and the results are summarized in Table 3 together with the range values. Further investigation is now in progress.

Table 3 Effect of Ion Energy on Fringe Pattern

	Ions	Energy (MeV)	Dose (ions/cm^2)	Range[**] (µm)	Fringe[***] Yes/No
*	$^{19}F^{6+}$	60	2×10^{14}	37	Yes
*	$^{19}F^{7+}$	120	3	93	No
*	$^{28}Si^{8+}$	100	4	35	Yes
*	$^{28}Si^{9+}$	150	1	58	Yes
	$^{32}S^{7+}$	50	2	15	Yes
	$^{32}S^{8+}$	100	18	29	Yes
	$^{32}S^{10+}$	165	1	52	Yes

* Those are examined in the fiscal year 1986.

** The values were interpolated from the table in Ref.5.

*** The visibility was compared on the topographs taken by 333 reflection.

Acknowledgement

References

1) H.Tomimitsu: Jpn.J.Appl.Phys. 22 (1983) L674.

2) H.Tomimitsu: JAERI-M 84-129 (1984) pp.47.

3) H.Tomimitsu, Y.Kazumata and E.Sakai: JAERI-M 85-104 (1985) pp.93.

4) U.Bonse, M.Hart and G.H.Schwuttke: Phys.Stat.Solidi 33 (1969) 361.

5) U.Littmark and J.F.Ziegler: Handbook of Range Distributions for Energetic Ions in All Elements (Pergamon Press, N.Y., 1980).

3.6   MICROSTRUCTURE AND MECHANICAL PROPERTIES OF
      He IRRADIATED Fe-Cr-Mn ALLOY

T. Sawai, K. Miyahara*, Y. Hosoi* and A. Hishinuma

Department of Fuels and Materials Research,   JAERI,   *Faculty
of Engineering, Nagoya University

INTRODUCTION

Austenitic   Fe-Cr-Mn alloys are regarded as a potential alternative   to
the   traditional Fe-Cr-Ni stainless steel for fusion application because   of
their   substantially   lower residual radioactivity compared to that for   the
standard   Ni-containing austenitic stainless steel.   Our knowledge   on   the
behavior   of   such alloys under irradiation environment   is,   however,   not
sufficient,   especially   in   the   area of mechanical   propertiy   degradation
induced   by He generated.

Ion   accelerators are extensively applied to the   intended   irradiation
experiments   for its advantage to introduce displacement damage   accompanied
with   controlled   amount of impurity element implanted.   For   standard   316
SS[1],   the   foil   tensile   test showed the loss of ductility caused   by   He
irradiation   and the microstructural evolution affected by deposited   helium
was examined with cross-section method[2].

In this study,   austenitic Fe-Cr-Mn alloy is irradiated with 30 MeV He-
ion   and foil tensile test and microstructural observation are performed for
the investigation of helium embrittlement.

EXPERIMENT

A Fe-12%Cr-30%Mn alloy, whose chemical composition is given in table 1,
was solution-annealed at 1373 K for 3.6×10^3 s,   followed by rapid   cooling
in water.   The grain size resulted was about 20 um.   Then plates of 100 um
thickness   was obtained by mechanical polishing and the surface for   irradi-
ation   was finished with diamond paste.   Disks of 3 mm diameter for   trans-
mission   electron microscope (TEM) and tensile specimens of TN type [3] were
punched-out from these plates.   30 MeV He irradiation was performed in   the
cyclotron   of   University of Tokyo, with the beam current of 2 uA/cm^2.   A
sheet   of stainless steel foil of 100 um thickness and 0 to 4 sheets   of   Al
foils   of   7   um thickness was inserted into the beam pass as   the   energy

absorber, and the calculations of projected ranges based on the reported results[1] and stopping powers[4] show that this irradiation condition makes region of 20 um width uniformly He-implanted around the midst of the specimen thickness. Irradiation dose was 3.3×10^{17} and 2.1×10^{17} cm^{-2}, and the concentration of injected He are estimated to be 2700 and 1800 appm, respectively. Further experimental procedure is described elsewhere[1].

Table 1   Chemical composition of specimen

C	Si	Mn	P	S	Cr	W	N	O	Fe
<0.003	0.011	29.72	<0.003	0.013	0.013	<0.01	0.0016	0.011	Bal.

RESULTS AND DISCUSSIONS

The results of tensile tests indicates that the ductility of this Fe-Cr-Mn alloy is affected by He irradiation. Total elongation of irraiated and control specimens is given in Fig. 1, which shows the total elongation of the specimens decrease with He irradiation. This result is similar to that obtained with standard 316 SS[1]. Ultimate tensile strength and 0.2% proof strength are both reduced by He irradiation, which do no coincide with the results for standard 316 SS.

Scanning Electron Microscopy(SEM) observation of fractured specimen showed that the intergranular brittle fracture surface was very little both for 1800 and 2700 appm He deposited specimen, which was the typical fracture mode for standard 316 SS irradiated with similar condition. Some area of 1800 appm He deposited specimen showed clear transgranular fracture surface. These result is quite different from that for standard 316 SS[1].

The mean diameter of He bubbles observed in TEM was almost 2000 A and this value is larger than that of standard 316 SS irradiated at similar condition, 300 A. This microstructural difference may be caused by the difference in the behavior of injected He. Either the carbon concentration or the alloy structure itself may be due to this difference but further analysis requires more experimental data.

The large size of bubbles are considered to have reduced the strength of He-irradiated Fe-Cr-Mn alloy, and this is also supported by the results of Vickers hardness test. The hardness value of irradiated region is 51 and

that of He through and unirradiated region is 107. Too large bubbles have made the material porous and affected its mechanical properties.

CONCLUSION

The results obtained on the He embrittlement of the Fe-Cr-Mn alloy using ion irradiation is summarized as follows,

1. Ductility and strength(ultimate strength, 0.2% proof strength and micro Vickers hardness) of this alloy is reduced by He irradiation.

2. The microstructure of Fe-Cr-Mn irradiated with He is characterized with its large size of bubbles, and this can affects the mechanical property of this material.

REFERENCES

1) N. Igata et al.:J. Nucl. Mat. 141-143(1986)543.

2) S. Hamada:J. At. Eng. Soc. J. 28(1986)1165.

3) A. Okada et al.:J. Nucl. Mat. 133-134(1985)321.

4) J. F. Ziegler:"Helium Stopping Powers and Ranges in All Elemental Matter" (Pergamon Press, New York, 1977)
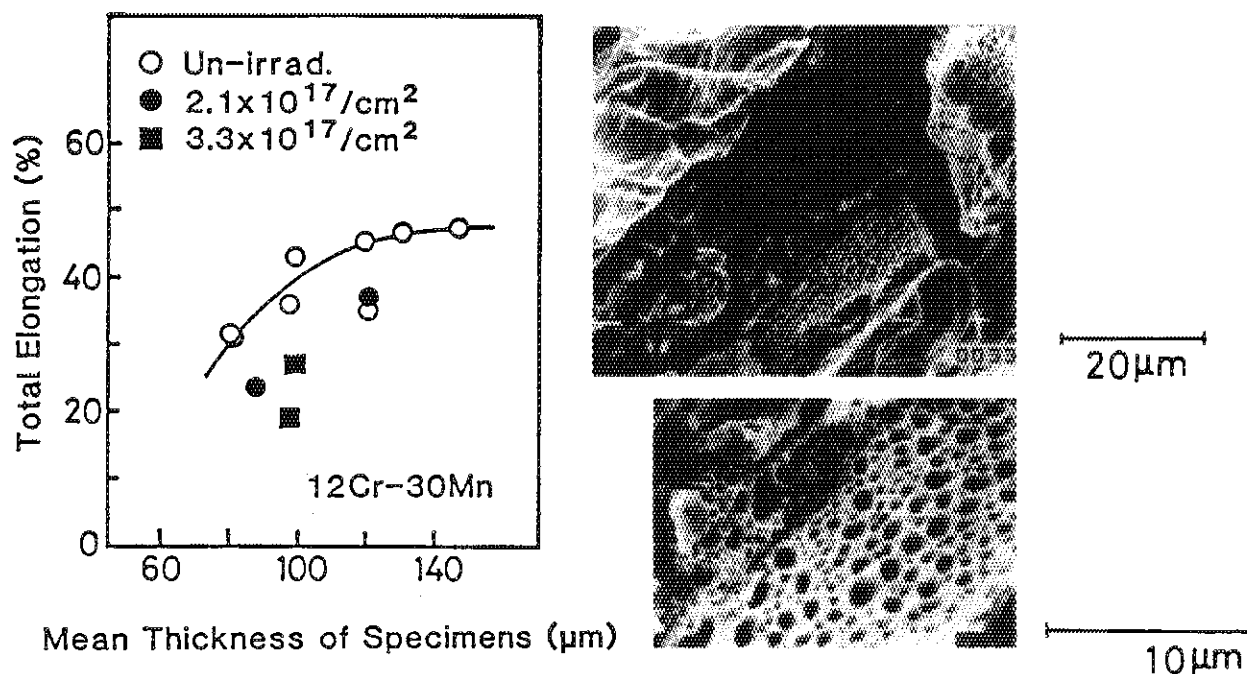
Fig. 1 Irradiation effect on total elongation in tensile test.

Fig. 2 SEM image of fractured specimen injected with He up to 1800 appm.

3.7 MICROSTRUCTURAL EVOLUTION IN HE-PREINJECTED STAINLESS STEEL IRRADIATED WITH ELECTRONS

Takeo ARUGA, Yoshio KATANO and Kensuke SHIRAISHI*

Department of Fuels and Materials Research, *Radioisotope and Nuclear Engineering School, JAERI

Helium has an extremely small solubility in metals and it tends to precipitate in bubbles when it is introduced by direct impingement of energetic helium particles from plasma or through (n,alpha) reactions in structural wall components of fusion reactors. These bubbles are known to deteriorate the mechanical properties such as swelling and embrittlement. A full understanding of the influence of helium on the microstructural evolution has therefore been required. On the other hand, it has been reported that helium atoms can alleviate the void swelling under electron-irradiation after preinjection of helium to 0.1 or 1.0 at % in the steel at 1023 K [1]. In this study, microstructural evolution during electron irradiation in the stainless steel preinjected with helium at room temperature was examined using a transmission electron microscope.

Type 316 stainless steel sheets of 0.2 mm thick with 4x8 mm^2 were solution-annealed for 1 h at 1373 K in a vacuum of 3 x 10^{-4} Pa followed by a rapid cooling to the room temperature. After cleaning the the surface by electropolishment, the samples were irradiated with 0.5 MeV He-ions at ambient temperature to a dose of 1.1 x 10^{20} He/m^2 using a Van de Graaff accelerator, with a current density of 50 mA/m^2. The injection produced a peak concentration of helium of 0.6 at % and displacement damage of 0.2 dpa at peak. The calculation from a modified E-DEP-1 [2] code shows that the injected helium is distributed in the range of 0.7 to 1.2 μm from the specimen surface. The disc specimens of 3 mm in diameter were punched out from the He-injected sample and were electropolished carefully so as to remove the front surface of the specimen by 0.7 μm. Then the specimens were back-thinned to perforation. The electron irradiation was made at 823 K with a JEM-1000D high voltage electron microscope at 1 MV. The irradiation flux measured with a Faraday cage was 3.8 x 10^{23} e/m^2 s, which corresponds to a damage rate of 1.7 x 10^{-3} dpa/s. The irradiation was

continued for 3.5 h up to a dose of 15 dpa. The foil thickness of the observed area was estimated to be about 0.5 μm by counting the number of equal thickness fringes from the foil edge. The microstructural change during electron irradiation at 823 K was continuously observed.

The typical change in microstructures of the sample under electron irradiation is shown in Fig. 1. In the as-He-irradiated condition, no definite changes in microstructure were discernible, except for the blurred texture in contrasts, which was not seen in the solution-annealed sample. On raising the temperature to 823 K before starting electron irradiation, defect clusters in black-dot contrasts with an average size of 5 nm appeared in a high density of $1.5 \times 10^{21}/m^3$. When the electron irradiation was made, the density of the defect clusters decreased exponentially with increases in electron dose, while the average size increased gradually, as presented in Fig. 2. At doses of 3 to 5 dpa, it is revealed by the grown clusters that these black-dot contrasts are due to small faulted loops of interstitial type in nature. The loops were seen to grow to be 30 nm in average at doses around 8 dpa and some loops were observed to grow with unfaulting into loops as large as 80 nm , as shown in Fig 1 and 2.

It should be noted that no dislocation networks developed and also that no visible cavities were discernible in the sample up to 10 dpa irradiation. These facts of remarkable retardation of dislocation development and suppression of cavity formation in the sample preinjected with helium to 0.6 at % under electron irradiation at 823 K are in a distinguished contrast to those generally observed in the sample without helium pre-injection; in which at doses from 5 to 10 dpa, highly tangled dislocation networks evolve and swelling becomes appreciable to be about 1 % by cavities with 30 nm in an avearge size[1]

It may be assumed that in the as-He-irradiated sample, injected helium atoms would form submicroscopic helium-point defect complexes in so a high density with the point defects produced by helium injection. When the internal pressure of the helium containing complexes increases to exceed a limit of the surface tension pressure on the rise of the temperature, the complexes may punch out the dislocation loops to gain vacancies, as has been already reported [3]. Then, the defect clusters or loops appeared at 823 K before the electron irradiation in the present sample may be mostly

formed during loop punching. Under the electron irradiation at 823 K, these complexes or loops may act as the recombination sites of the electron-irradiation produced point defects. Such a high density of the formation for these helium containing complexes and loops may enhance the recombination of the point defects to the extent that the supersaturation rate of vacancy would be reduced enough to inhibit cavity formation. Neither appreciable growth of loops nor dislocation development would take place due to little supply of the interstitials under the electron irradiadiation , as was observed in the present sample.

It should be noted from the present results that presence of thousands of appm helium atoms in the steel in the early stage of irradiation may suppress the microstructural development under the irradiation at temperatures where vacancies are mobile enough.

References

1) K. Shiraishi and Y. Katano: In Situ Experiments with HVEM (Osaka Univ., 1986) pp.251-254.

2) T. Aruga: JAERI-M 83-226 (1984) 1.

3) J. H. Evans, A. Van Veen and L. M. Caspers: Radat. Eff. 78 (1983) 105.

As   0 dpa   0.5 dpa   5.5 dpa   11 dpa
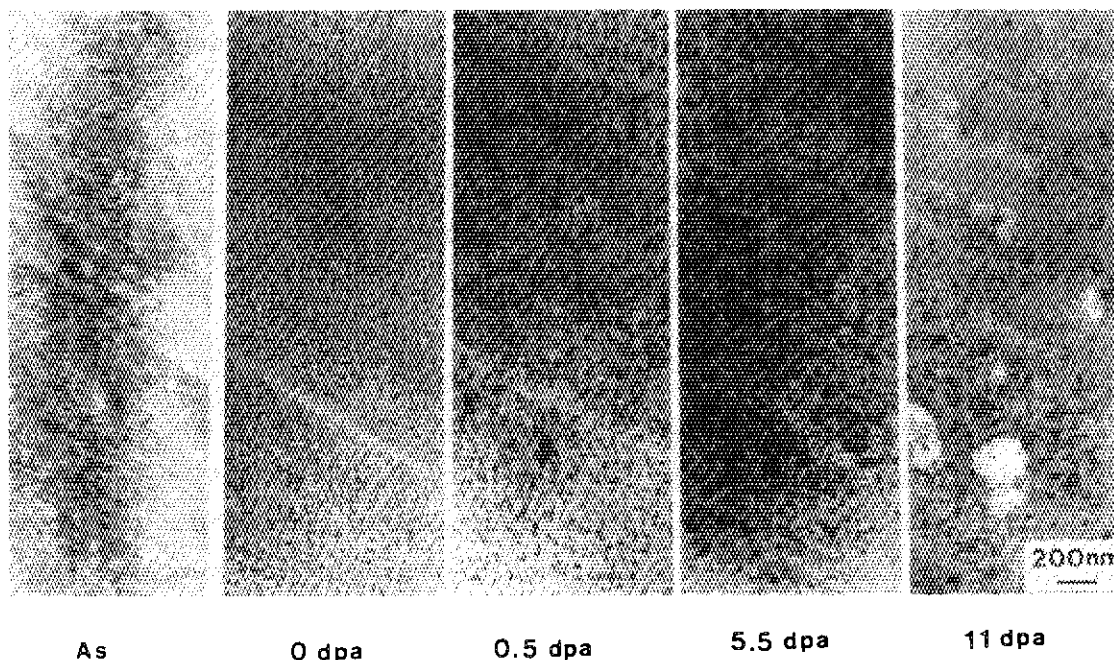
Fig. 1 The electron dose dependence of microstructures produced at 823 K in Type 316 stainless steel preinjected with 0.5 MeV He-ions at RT to a dose of 1.1×10^{20} He/m^2.
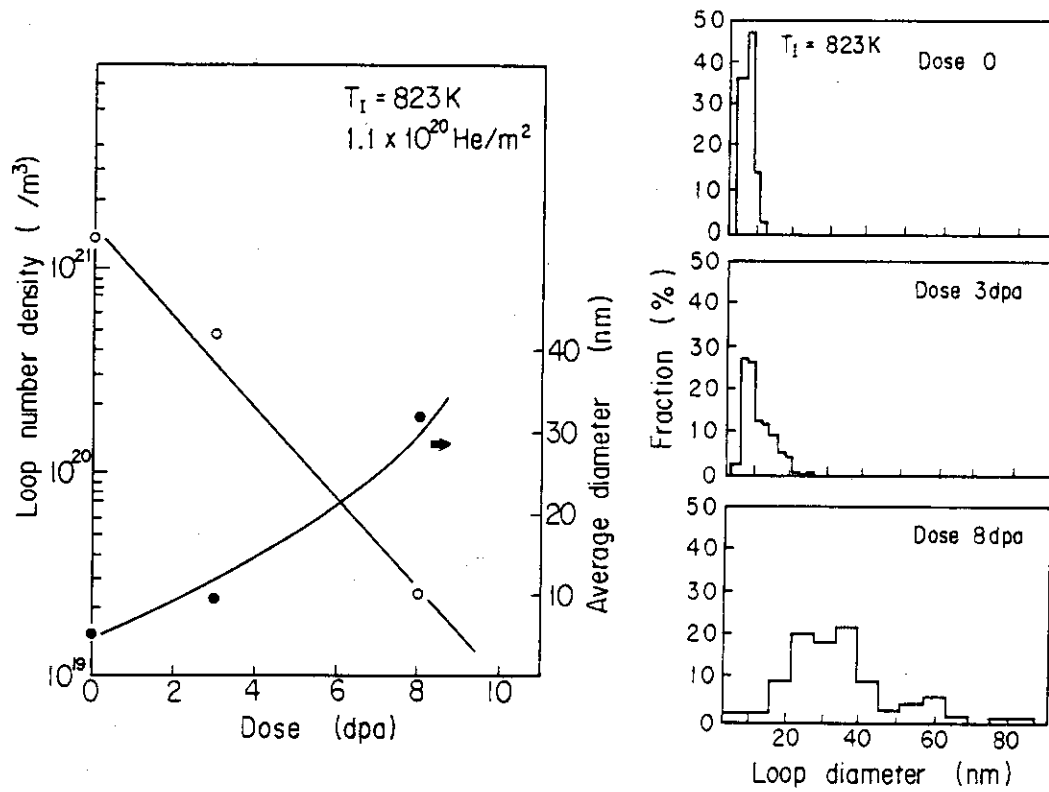
Fig. 2 The electron dose dependence of the number density and the average diameter for loops in the electron-irradiated Type 316 stainless steel preinjected with 0.5 MeV He-ions at RT to a dose of 1.1 x 10^{20}He/m^2.

3.8 ION CONDUCTIVITY CHANGE OF Li$_2$O BY OXYGEN ION IRRADIATION

Kenji NODA, Yoshinobu ISHII, Hisayuki MATSUI[*],
Satoshi SUZUKI[*], Mikio HORIKI[*], Naomi OBATA[*]
and Hitoshi WATANABE

Department of Fuels and Materials Research, JAERI,
[*]Faculty of Engineering, Nagoya University

1. Introduction

In lithium oxide (Li$_2$O) as a solid tritium breeder material of fusion reactors, a huge number of irradiation defects will be introduced during operation of the fusion reactors. These defects will not only induce swelling but also have a large influence on migration of tritium and helium as well as of lithium and oxygen atoms composing Li$_2$O.

Ion conductivity of Li$_2$O depends on impurities and lattice defects including the irradiation defects, and also reflects migration behavior (diffusion) of ions composing Li$_2$O. Recently, the ion conductivity of non-irradiated Li$_2$O was investigated, and it was found that there was a close relationship between diffusivity of lithium ions and that of tritium[1,2]. So, the irradiation effect on the migration behavior of tritium and lithium ions can be studied by measuring the ion conductivity change due to the irradiation.

In the present study, the ion conductivity of a Li$_2$O single crystal specimen irradiated with oxygen ions was measured to clarify the correlation between diffusivities of tritium as well as lithium ions and the irradiation defects.

2. Experimental

The specimen used was a thin plate of Li$_2$O single crystal (about 7 mm in length, 8 mm in width and 0.3 mm in thickness). The specimen was annealed at 1270 K for 10 h in a vacuum better than 1×10^{-3} Pa to eliminate OH$^-$ ions or LiOH in/on the specimen. The specimen was irradiated using the Tandem accelerator by oxygen ions with energy of 120 MeV. The ion conductivity was measured "in-situ" in an irradiation vacuum chamber with the two-terminal ac method using YHP Model 4192 A or 4194 A impedance analyzer after

interrupting sometimes the successive irradiation. The total oxygen ion fluence of 3.5x10^{19} ions/m^2 was attained.

After the irradiation, the recovery behavior of the ion conductivity was investigated by isochronal annealing experiments. The specimen irradiated was heated for 90 min. at each annealing temperature from 520 to 570 K.

3. Results and discussion

Prior to the irradiation, the conductivity of specimen was measured in the temperature range from 411 to 519 K in the irradiation vacuum chamber. The temperature dependence of the conductivity was essentially similar to those extrapolated from the data that were measured for non-irradiated Li$_2$O in the temperature range from 570 to 1420 K by Ohno et al.[1], although the values obtained in this study were slightly smaller than those extrapolated.

Fig. 1 shows the ion conductivity at 489 K as a function of measurement time for each measurement at various fluences (7.1x10^{18}, 2.5x10^{19} and 3.5x10^{19} ions/m^2) together with that before the irradiation. Each measurement was started when the specimen temperature of 489 K was attained. The conductivities at each fluence and also before the irradiation decreased with the measurement time and then the constant values of conductivities were attained

Fig. 1 Ion conductivity versus measurement time for various ion fluences.

after 10^4 s. This decrease with measurement time was assumed to be due to desorption of water or OH$^-$ ions near the surface of specimen, which arose from adsorption of water vapor in vacuum at temperatures lower than the measuring temperature (489 K) before the irradiation or during the irradiation. Such adsorption-desorption behavior of water near the surface of Li$_2$O in vacuum was confirmed by an experiment in which behavior of water

or hydrogen near the surface of Li_2O single crystal specimen in vacuum at various temperatures was studied with elastic recoil detection method using 2.0 MeV helium ions[3]. Consequently, the constant values for each measurement can be regarded as the ion conductivity of the specimen.

In Fig. 2 the ion conductivity of the Li_2O single crystal specimen at 489 K is shown versus the oxygen ion fluence. The conductivity decreased with the fluence in the examined fluence range (up to 3.5×10^{19} ions/m^2). This suggests that diffusivity of lithium ions is decreased by the irradiation. If the diffusion of lithium ions is closely related to that of tritium, it can be said that the diffusivity of tritium is decreased by the irradiation, i.e., introduction of irradiation defects.

The recovery behavior of the ion conductivity was observed by measuring at 489 K after each annealing, and it is shown in Fig. 3. The decrease of conductivity due to the irradiation was completely recovered in the temperature range from 520 to 570 K. This recovery temperature range is similar to that of the F^+ centers which are predominant irradiation defects in Li_2O[4,5].
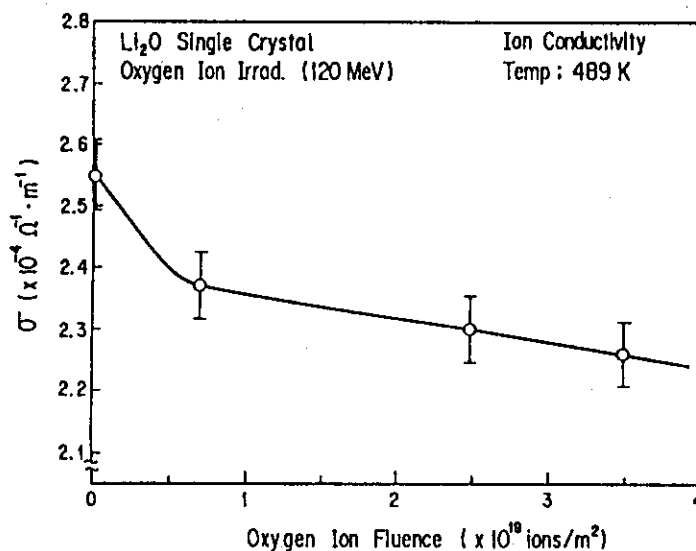
Fig. 2 Ion conductivity versus ion fluence.
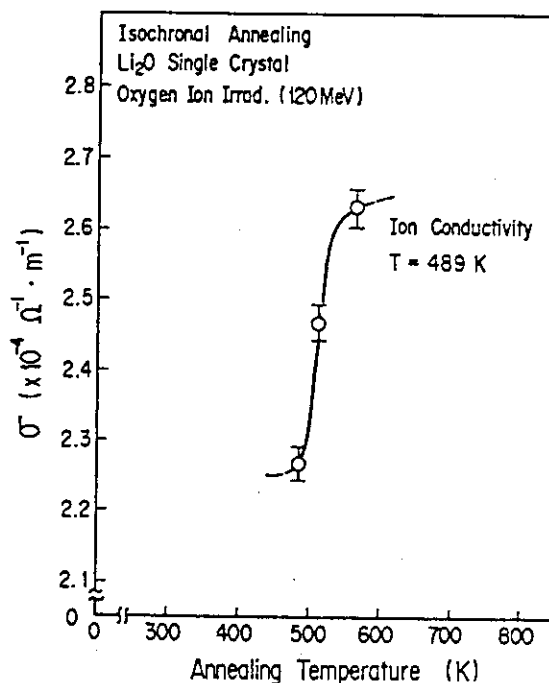
Fig. 3 Recovery behavior of ion conductivity.

The ion conductivity of Li_2O reflects migration behavior of lithium ions (i.e., mobility and concentration of lithium ion vacancies), since the diffusivity of lithium ions is much larger than that of oxygen ions. The lithium ion vacancies have negative charge, while the F^+ centers have positive charge. Therefore, the lithium ion vacancies are electrostatically attracted by the F^+ centers. The F^+ centers are immobile below their recovery temperature. Consequently, the decrease of ion conductivity (the decrease of diffusivity of lithium ion) can be attributed to the decrease of mobility of lithium ion vacancies due to retardation by the F^+ centers or the decrease of the number of mobile lithium ion vacancies due to trapping by the F^+ centers. However, the above-mentioned result is preliminary, and further investigations are required to clarify the irradiation effect on diffusivity of lithium ions or tritium and the mechanism of the irradiation effect.

References

1) H. Ohno, S. Konishi, K. Noda, H. Takeshita, H. Yoshida and H. Watanabe: J. Nucl. Mater. 118 (1983) 242.
2) H. Ohno, S. Konishi, T. Nagasaki, T. Kurasawa, H. Katsuta and H. Watanabe: J. Nucl. Mater. 133-134 (1985) 181.
3) L. M. Howe, J. A. Sawicki, K. Noda and M. H. Rainville: private communication.
4) K. Noda, K. Uchida, T. Tanifuji and S. Nasu: Phys. Rev. B 24 (1981) 3736.
5) K. Noda, Y. Ishii, H. Matsui and H. Watanabe: Radiat. Eff. 97 (1986) 297.

3.9 VOLUME CHANGE OF LITHIUM OXIDE BY OXYGEN
ION IRRADIATION

Yoshinobu ISHII, Kenji NODA and Hitoshi WATANABE

Department of Fuels and Materials Research, JAERI

1. Introduction

As well known, many kinds of defects are introduced in materials by irradiation. The defects of irradiated lithium oxide, especially F^+ center and lithium colloid were studied with ESR or optical absorption methods[1-3]. However, the nature of other defects has not been clear yet. When lattice defects are created in a crystal, the volume increases usually. The volume change measurements by using the photoelastic technique were carried out for LiF by D.A.Wiegand and R.Smoluchoweski[4]. This method has a high sensitivity and is very useful to understand the all of the defects introduced by irradiation.

In this paper, some preliminary results of the volume change measurements for the Li_2O using the photoelastic technique are shown as the first step of these experiments.

2. Experimental

Specimens were cut in rectangular shape from lithium oxide single crystals. The dimensions and orientations are shown in Fig.1(a). These were annealed at 1000 °C for 10 hours in high vacuum (1 x 10^{-3} Pa) to remove the stress induced by cutting and to eliminate LiOH or Li_2CO_3 from the surface. After this treatment the specimen was mounted on a polarimeter which was equipped in a high vacuum chamber. Only the half part of the specimen was irradiated with oxygen ions (120 MeV) by the tandem type accelerator at JAERI. By such irradiation the irradiated part expands, but the unirradiated part remains unchanged. Consequently, a strain field is introduced into the specimen as shown in Fig.1(a). The strain was measured by using a polarimeter.

The polarimeter consists of a light source(He-Ne laser), a polarizer, quarter wave plates, an analyser, photo-detectors and slits as shown in Fig.1(b). The light beam passing through a chopper is splitted into two beams using the half mirror. One of those is directly led to a detector
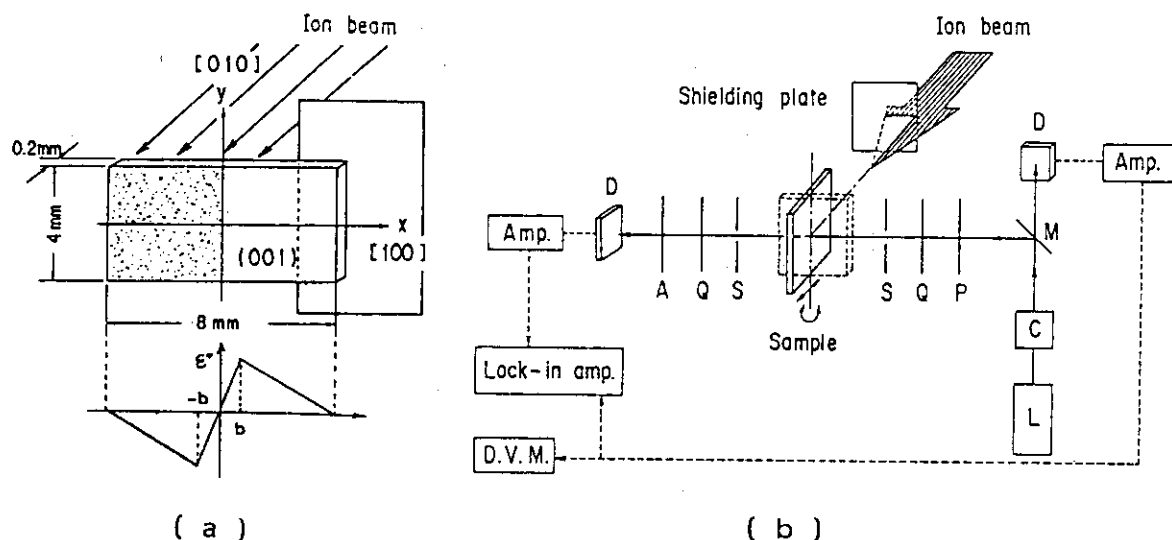
Fig. 1 Schematic illustration of the specimen and ploarimeter. L:light source, C:chopper, M:half mirror, P:polariser, Q:quarter wave plate, S:slit, A:analyser, D:photo-detector.

to measure the intensity of the light source, while the other is led to specimen through a polarizer, a quarter wave plate and a slit. The light after passing the strain field in the specimen is optically rotated, and the rotated angle is related to the magnitude of the strain. This light is led to an analyser after passing a quarter wave plate. The intensity of the light transmitting the analyser is given by

$$I = I_0 \sin^2(\theta/2) \ ,$$

where I_0 is the intensity of the incident light beam, and θ is the rotated angle.

The measurements of the volume change of a specimen were intermittently carried out after interrupting the irradiation. The total oxygen ion fluence was 8.2×10^{19} ions/m^2. All measurements were carried out at room temperature.

3. Results and discussion

The strain profiles of irradiated Li_2O are shown in Fig.2 as a function of the distance from the boundary between the irradiated and the unirradiated parts. Longitudinal axis indicates rotated angle which is proportional to the induced strain. Solid and open circles indicate the data for the fluences of 0.8×10^{19} and 8.2×10^{19} ions/m^2, respectively. These two strain profiles are similar in shapes. In the unirradiated

part, the rotated angle increases rapidly with the distance from the boundary and has a maximum value at $x \doteq 1mm$, then it decreases gradually toward the specimen edge. The strain profile has a symmetry with the origin of Fig.2. In these experiments, bomberded ions stopped at the depth of 0.1mm from the surface of the specimen. The number of defects such as F^+ centers which were introduced by the irradiation is very larger than the number of bomberded ions in the examined fluence range as described in our paper[1]. It is, therefore, considered that the measured strain profile was predominantly induced by irradiation defects. The fractional volume change of the specimen ($\Delta V/V$) is given by[4]

$$\frac{\Delta V}{V} = \frac{3C_{11}}{2C_{12} + C_{11}} \cdot \frac{2\theta}{180 \cdot d} \cdot \frac{\lambda}{C_\lambda} \cdot \frac{1}{1-2b/\ell} \text{ ,}$$

where C_{11}, C_{12} are elastic constants, C_λ the photoelastic constant, λ the wave length of the light, ℓ the length of the specimen, b the distance from the boundary to the position of the maximum strain , θ the maximum rotation angle in degree. In this experiment, the projected range was taken as d at the first approximation. The elastic constants were determined by the sound-wave velocity measurement of the Li_2O single crystal. The values of C_{11} and C_{12} are 197 GPa and 30.6 GPa, respectively. The photoelastic constant was deduced for measurement of
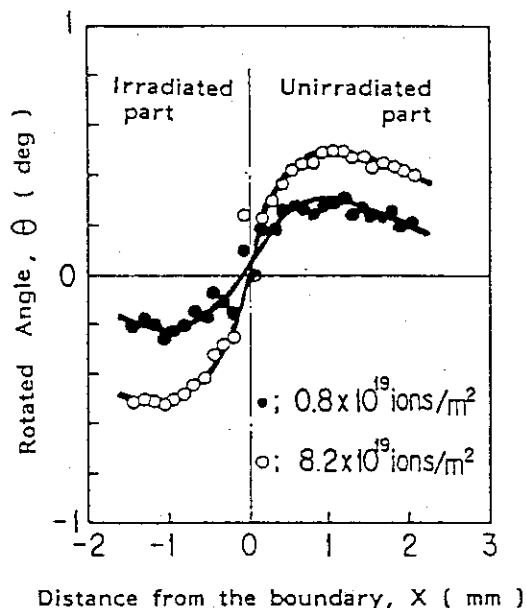
Fig. 2 Strain profile as a function of the distance from the boundary. Solid and open circles are the data of 0.8×10^{19} and 8.2×10^{19} ions/m^2, respectively.
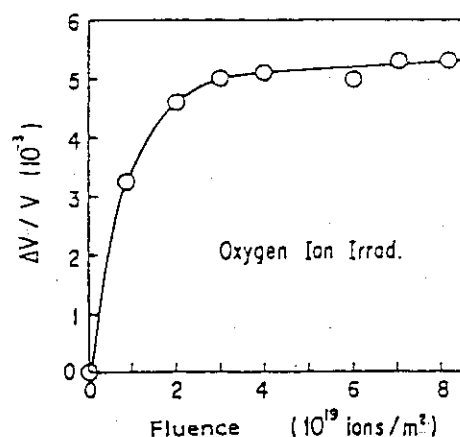
Fig. 3 Fluence dependence of the fractional volume change.

the optical rotation of Li_2O single crystal compressed by dead weights. The value of the photoelastic constant is 0.021. The fluence dependence of the fractional volume change of Li_2O is shown in Fig.3. The fractional volume change increases rapidly with the ion fluence up to 3 x 10^{19} ions/m^2. Above this value it increases very slowly.

The recovery behavior of the fractional volume change is shown in Fig.4 as a function of the annealing temperature. Two stages appeared in examined temperature range i.e., one was in the temperature range from 200 °C to 400°C, the other was above 400 °C. It is known by our ESR and optical absorption experiments that the F^+ centers and the lithium colloid recover at the temperature range from 200 °C to 400°C and from 400°C to 500 °C , respectively[1,2]. From these facts, it is understood that the first stage in these experiments is related with annihilation of F^+ centers and the second stage is probably related with the lithium colloid.

In this study, the volume change due to irradiation was preliminarily tried being evaluated using the oxygen ion irradiation. The improvement of the evaluations will be done using lithium ion irradiation, in which uniform volume expansions in the direction of the depth of the specimen occur because of its penetrating the specimen.
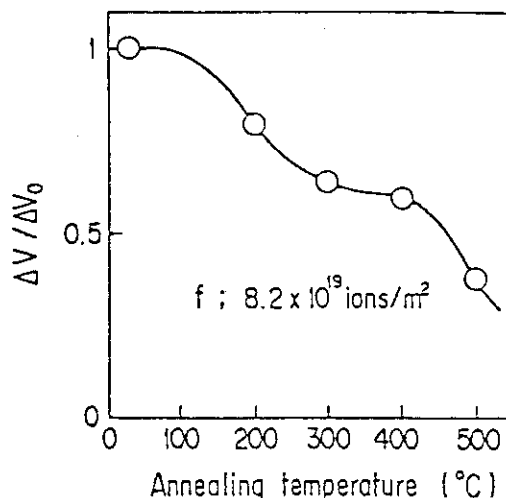
Fig. 4 Isochronal annealing of irradiated specimen. Annealing time is 60 minutes. ΔV_0 is a increased volume of the specimen irradiated up to 8.2×10^{19} ions/m^2.

References

1) K.Noda, T.Tanifuji, Y.Ishii, H.Matsui, N.Masaki, S.Nasu and H.Watanabe: J. Nuci. Mater. 122&123 (1984) 908

2) K.Noda, K.Uchida, T.Tanifuji, and S.Nasu : J. Nucl. Mater. 91 (1980) 234

3) K.Noda, Y.Ishii, H.Matsui and H.Watanabe: Radiat. Eff. 97 (1986) 297

4) D.A.Wiegand and R.Smoluchoeski: Phys. Rev. 116 (1959) 1069

3.10 IRRADIATION DAMAGE OF ION-IRRADIATED Si_3N_4

Kenji NODA, Yoshinobu ISHII, Kotaro KURODA[*],

Hiroyasu SAKA[*], Katsuhiro SASAKI[*], Michitaka SAKURAI[*],

Toru IMURA[*] and Hitoshi WATANABE

Department of Fuels and Materials Research, JAERI,

[*]Faculty of Engineering, Nagoya University

Refractory low-Z ceramic materials as plasma facing materials for fusion reactors are necessary for decreasing influences of plasma contamination due to the materials of the first wall. Such materials will be subjected to not only surface erosion but also irradiation damage due to 14 MeV neutrons. Characteristic feature of the irradiation damage in fusion reactor irradiation conditions is to accompany generation of helium gas due to nuclear reactions between the component atoms and high energetic neutrons. The helium gas has a large influence on the irradiation dimension stability characteristics such as swelling through formation of bubbles as well as displacement damage due to energetic neutrons. So, investigations of the effects of displacement per atom (dpa) and generated (or implanted) gas on the irradiation damage are required to evaluate the irradiation resistance performance of the ceramic materials under fusion reactor conditions. In this study, analysis of implanted Ar gas in the microstructures of Ar ion irradiated Si_3N_4 and electron microscopic observation of irradiation damage structure in sectional specimens of He ion irradiated Si_3N_4 along the incident ion beam were preliminarily conducted by using scanning transmission electron microscope (STEM) equipped with energy dispersive X-ray analyzer (EDX) to establish techniques for the above mentioned investigations.

The specimens used were sintered β-Si_3N_4 including 8%-Y_2O_3 as a binder. The specimens were irradiated by Ar ions with an energy of 400 kV or He ions with an energy of 1.2 MeV. Before (in case of Ar gas analyses)or after (in case of sectional specimens)the irradiations the sintered Si_3N_4 was thinned by ion beam milling, to make the specimens for STEM observation. STEM observation and analyses were carried out using JEOL 2000 FX.

Fig. 1(a) shows an electron micrograph of a sintered Si_3N_4 irradiated

to 2.2×10^{21} ions/m^2 by Ar ions. As described in the previous works[1-3], a β-Si$_3$N$_4$ grain (denoted by A) was partly transformed into amorphous state by the irradiation, while other phase containing Y (denoted by B) which was precipitated among the Si$_3$N$_4$ grains was entirely changed into amorphous state. EDX spectra of the Si$_3$N$_4$ grain and the Y-containing phase are shown in Fig.1 (b) and Fig. 1 (c), respectively. As shown in these figures, Ar was detected in both the Si$_3$N$_4$ grain and Y-containing phase.

Fig. 2 (a) and Fig. 2 (b) show electron micrographs of the sectional Si$_3$N$_4$ specimens irradiated to 6.9×10^{21} ions/m^2 by He ions with an energy of 1.2 MeV. Cavities (indicated by white arrows) which are considered to consist of many voids[1,3] in Y-containing phases are found in the regions at the depth of 1 to 2 μm from the surface (the surface corresponds to the edges of electron micrographs in Fig 2 (a) and Fig. 2 (b).).

In electron microscopy of the sectional specimens along the incident ion beam the irradiation damage structures at various ratios between dpa and introduced gas content can be observed simultaneously. So, this method is very useful to study correlation among the irradiation damage, dpa and the introduced gas. The investigations of such correlation will be conducted by combining the electron microscopy of the sectional specimens and analysis of the introduced gas.

References

1) K. Noda, Y. Ishii, K. Kuroda, H. Saka, Y. Nakata, M. Arita, T. Imura and H. Watanabe: JAERI-M 85-104, p.122-123.

2) K. Noda, Y. Ishii, K. Kuroda, H. Saka, M. Arita, M. Hashimoto, T. Imura and H. Watanabe: JAERI-M 86-112, p.94-97.

3) K. Kuroda, K. Noda, Y. Ishii, H. Saka, T. Imura and H. Watanabe: Proc. 11th Int. Cong. on Electron Microscopy, Kyoto, 1986, p.1305-1306.
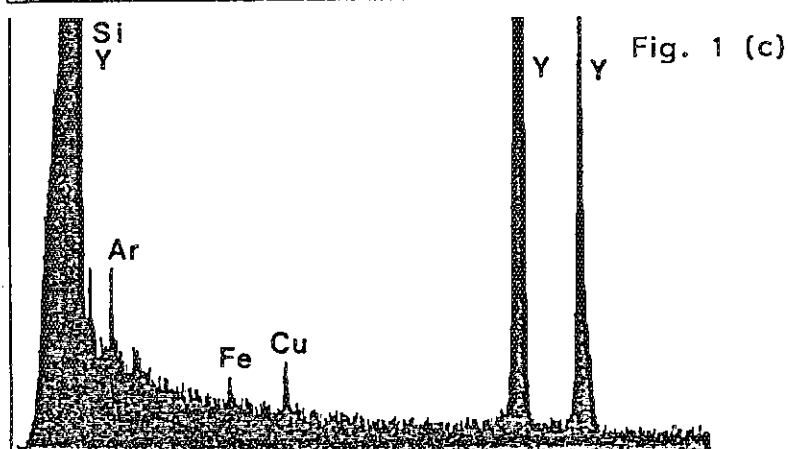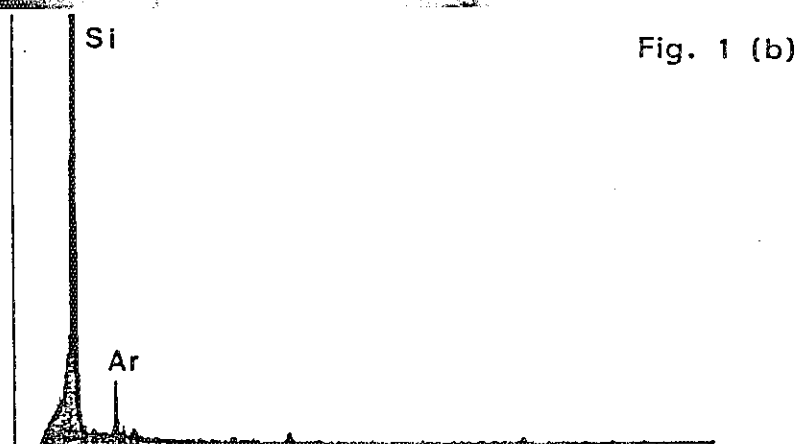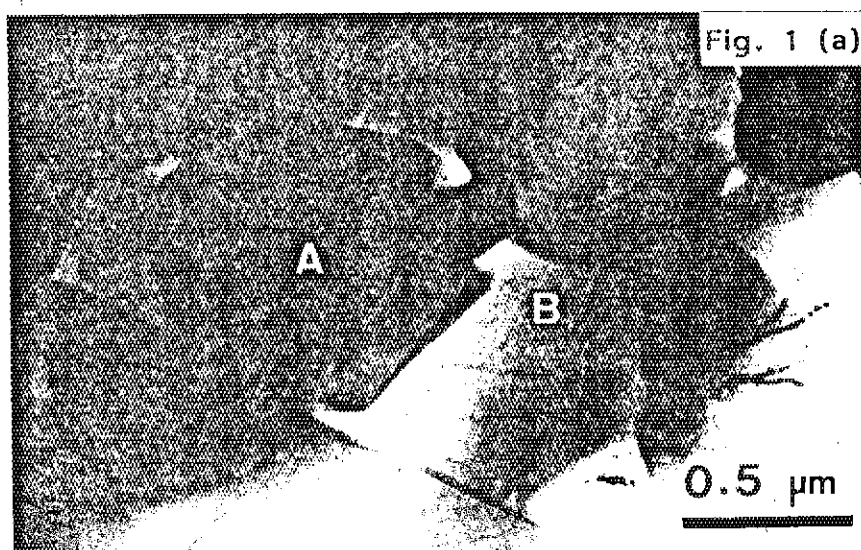
Fig. 1 An electron micrograph of a sintered Si_3N_4 irradiated by Ar ions (Fig. 1 (a)), EDX spectra obtained from the $\beta-Si_3N_4$ grain denoted by A (Fig. 1 (b)) and the Y-containing phase denoted by B (Fig. 1 (c)).

(a)   (b)
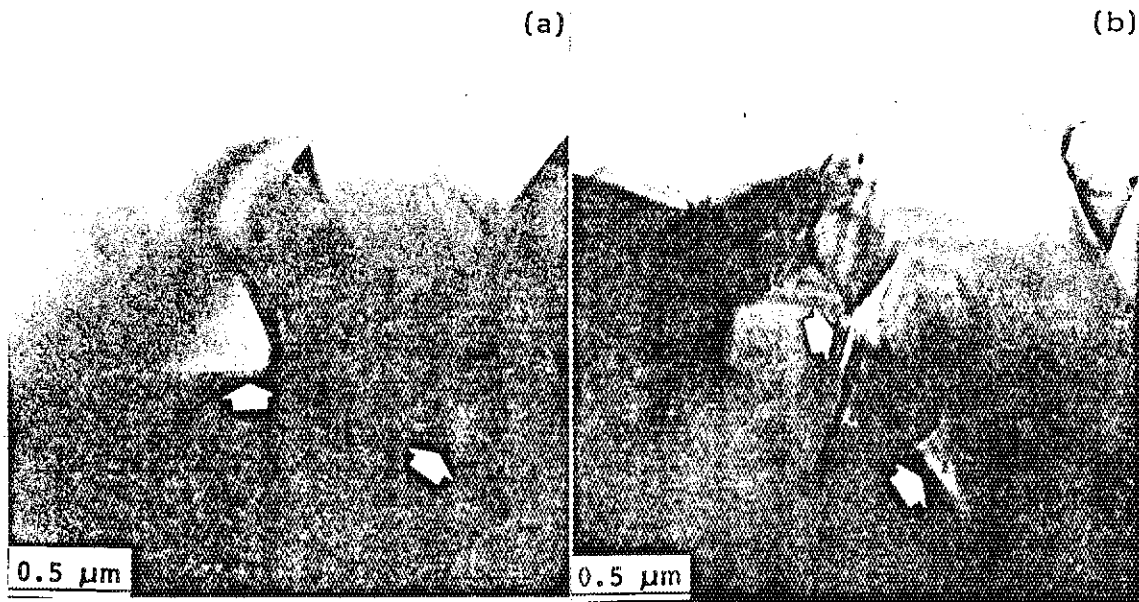
Fig. 2 Electron micrographs of the sectional Si$_3$N$_4$ specimens irradiated
by He ions.

3.11   DAMAGE STRUCTURE IN Al$_2$O$_3$ SINGLE CRYSTAL IRRADIATED WITH He-IONS

Yoshio KATANO, Hideo OHNO, Takeo ARUGA and Hiroshi KATSUTA

Department of Fuels and Materials Research, JAERI

Alumina is a prime candidate material for near-first wall components such as insulators and RF windows of future fusion reactors because of its generally good structural, electrical and dielectrical properties.
Although much work has been done for understanding radiation effects of alumina by fission neutron irradiation[1] , the structural stability of alumina containing a large amount of helium has not yet been well studied. Helium is calculated to be produced in alumina by 500 appm per 1 MW.year/m² via (n,alpha) reaction with fusion neutrons[2]. Therefore, it is of practical importance to have knowledges on the behavior of helium in alumina and the influences on microstructural development. In the present work, damage structures of single crystal alumina irradiated with energetic helium ions were investigated.

Single crystal alumina (α - Al$_2$O$_3$) were irradiated with 0.4 MeV He-ions up to a dose of 1x10²⁰ He/m² at temperatures of 1023 to 1223 K using a Van de Graaff accelerator in JAERI. The injection of helium to a peak concentration of 4 x 10³ appm produces a displacement damage of 0.5 dpa at peak. The front surface was removed about 0.8 μm by ion thinning and irradiated samples were back-thinned to an electron-transparency. The radiation-produced microstructure was examined with an electron microscope operating at 200 KV.

Microstructures produced in alumina samples irradiated with He-ions at temperatures of 1023 to 1223 K are shown in Fig. 1, compared with that in non-irradiated sample. The microstructures in the irradiatios at tempera-tures of 1023 to 1223 K were characterized by the high density defect clusters of 4 x 10²² /m³ with the size of 7 nm on average. In the sample irradiated at 1223 K, several defect clusters were grown to be dislocation loops of some 10 nm on prismatic {10$\bar{1}$0} planes. These dislocation loops were all revealed to be pure edge type and interstitial in character.

Therefore, the defect clusters observed in the iradiations at these temperatures may presumably be mostly small dislocation loops formed by aggregation of radiation-produced interstitials. The temperature dependence of the density and the average size for the defect clusters or loops are presented in Fig. 2 , along with the fractional distributions of the loop sizes. It is noted that in the range of these temperatures the defect cluster formation is almost independent of the irradiation temperature. Fine cavities smaller than 2 nm were observed in a fairly high density in the sample irradiated at 1223 K, although not clearly resolved; whereas no cavities were discernible in the irradiation below 1123 K.

In the sample annealed for 1 h at 1223 K after the irradiation at 1023 K, conspicuous cavities were formed in the high density of $5 \times 10^{22}/m^3$ with an average size of 7 nm, as shown in Fig. 3. The cavity size was seemed to be larger for the region of the depth around the ion-range in the sample as observed by using a stereo-microscopy technique. In addition, the considerable coalescence of cavities occurred at the same region into large cavity channels of 300 nm long and 30 nm in diameter at maxima. The resultant swelling was estimated to be 1.2 %. The annealing also grew the dislocation loops to an average size of 70 nm. Moreover, the spherical precipitates of 5 nm in average size were formed at the depth beyond the ion-range in relatively a high density of $1.2 \times 10^{22}/m^3$.

It is revealed that helium bubbles were hardly formed in the alumina injected below 1123 K with helium to 4×10^3 appm. The precipitates observed in the annealed sample are believed to be Al metal colloids from the morphology as discribed in the literatures; the Al metal colloid is reported to form in an electron-irradiated alumina[3], both non-injected and pre-injected with helium, and to disappear on annealing at the higher temperatures than Al melting point. The precipitates in the present sample were formed during annealing at 1223 K, e.g. , much higher than the Al melting point. The fact indicates that the Al metal precipitates were formed and are stabilized under the strong influence of highly injected helium atoms and radiation-induced defect clusters such as cavities and loops.

References

1) F. W. Clinard,Jr., G. F. Hurley and L. W. Hobbs: J. Nucl. Mater. 108 & 109 (1982) 655.

2) G. P. Pelles: J. Nucl. Mater. 122 &123 (1984) 1338.

3) T. Shikama and G. P. Pelles: Philos. Mag. A 47 (1983) 369.
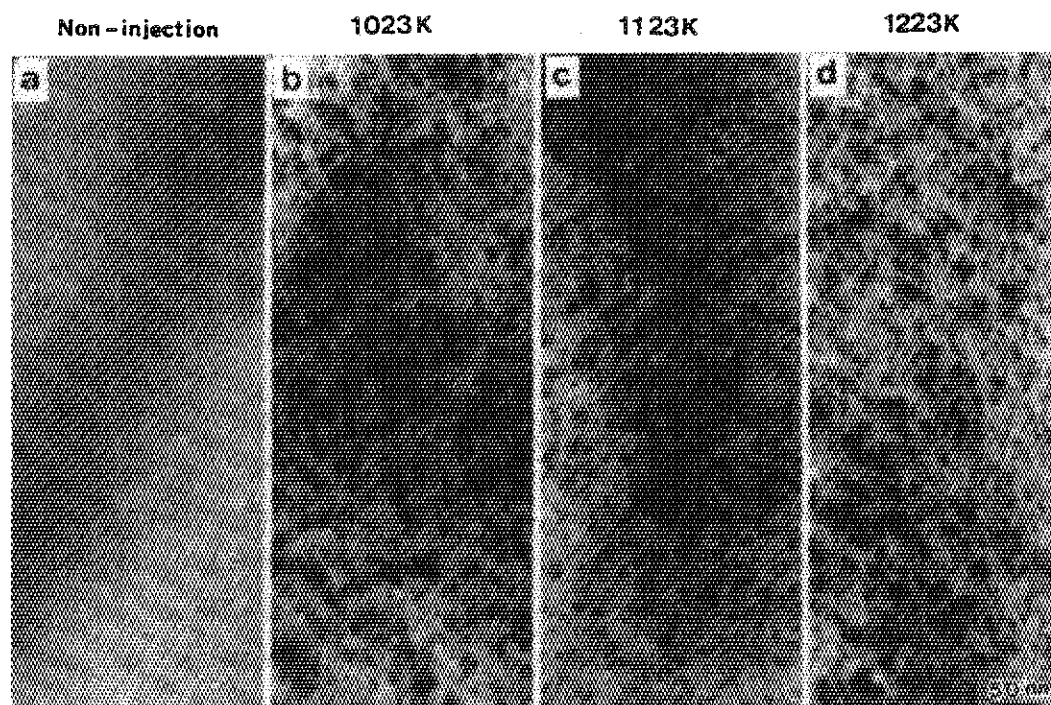
Fig. 1 Microstructures produced in single crystal alumina irradi-
ated with 0.4 MeV He-ions at 1023 to 1223 K.
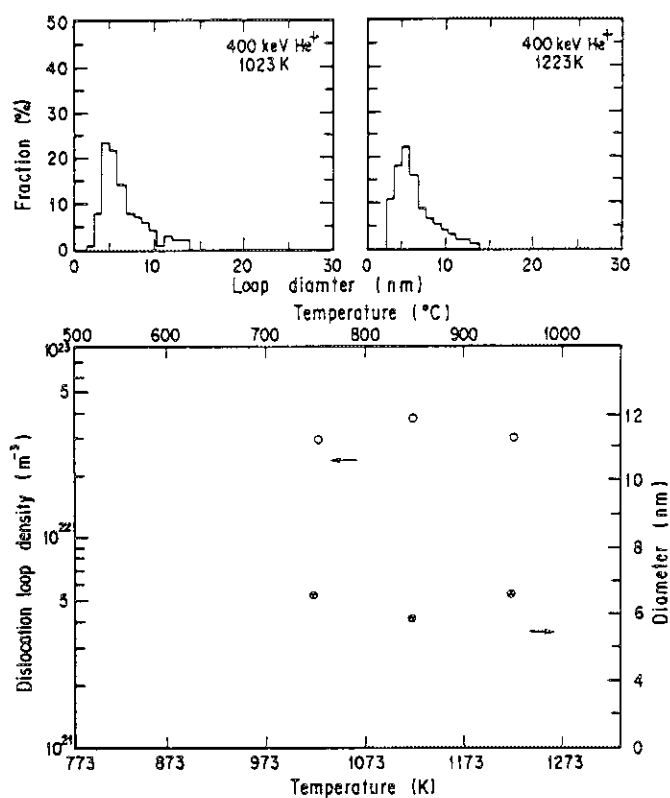
Fig. 2 Temperature dependence
of the density and the average
size for the loops produced in
single crystal alumina irradi-
ated with 0.4 MeV He-ions up
to a dose of 1 x 10^{20} He/m^2,
and the loop size distributions
at 1023 and 1223 K.
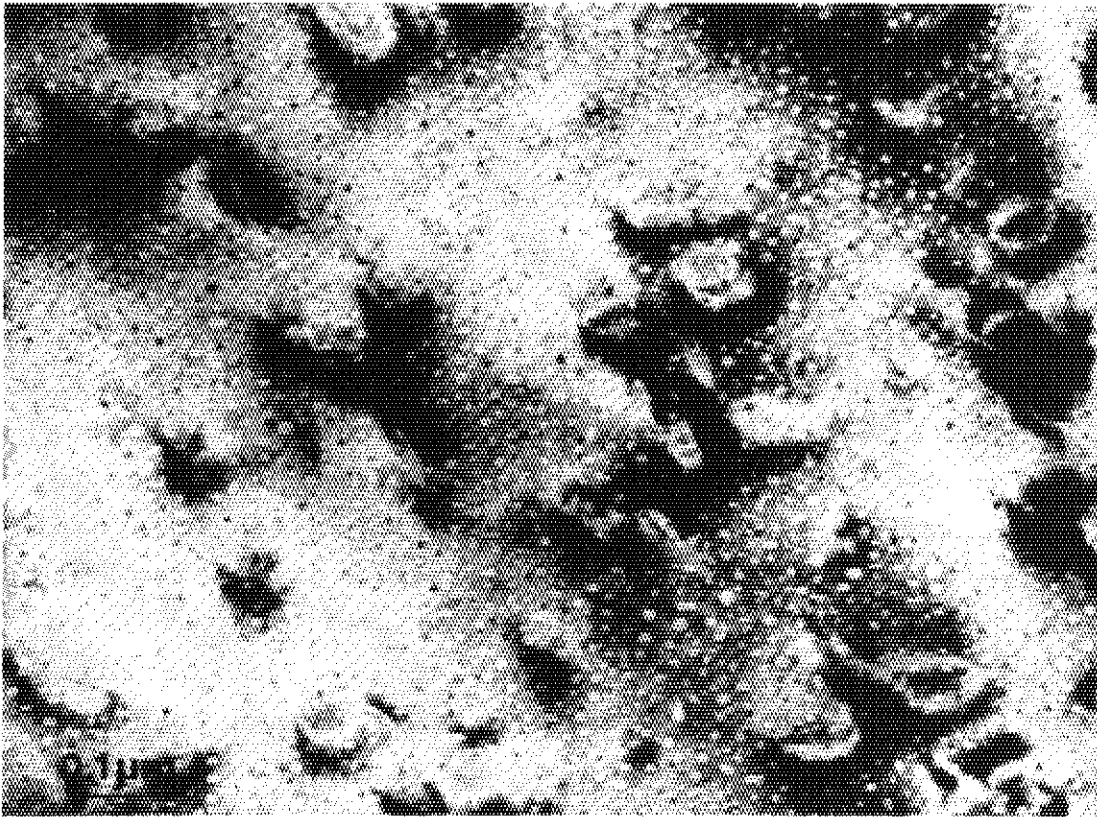
Fig. 3 Damage structure produced in single crystal alumina annealed
for 1 h at 1223 K after 0.4 MeV He-ion irradiation at 1023 K to a dose
of 1 x 10^{20} He/m^2.

3.12 MICRO-RAMAN SCATTERING OF IRRADIATED SiC

Yukio KAZUMATA and Hiroshi NARAMOTO

Department of Physics, JAERI.

1.Introduction

Polytypizm in SiC offers abundant information about lattice vibration from light scattering. Raman scattering experiments have been done for a variety of polytype crystals of SiC $(1 \sim 4)$. These experiments by Raman scattering by themselves could determine the phonon dispersion curves in the large zone scheme of SiC without any information from neutron scattering. On the basis of these experiments, a few authors reported the influence of lattice defects induced by irradiation on the lattice vibration $(5 \sim 7)$. Irradiation effects were found in the deterioration of Raman spectrum, in the Si-H stretch vibration on H^+ implantation, in the vibration of a C=C bond forming a split <100> interstitial and so on. These experiments were carried out by a so-called conventional spectrometer in which laser beam illuminating samples spreads out about $2 \sim 3$ mm in a diameter. In micro-Raman scattering, however, the diameter of laser beam can be set down to 1 μm through an optical microscope.

In this paper, micro-Raman scattering is applied to study the lattice disorder of irradiated samples. Three characteristic experiments are described; firstly Raman scattering from micro-single crystals dispersing in a polycrystal, next the reduction of the intensities of Raman lines from optical phonons in the lateral direction to the path of a projectile by ion bombardment, finally the detorioration of Raman lines along the path of a projectile.

2.Experimental procedures

Micro-Raman scattering was carried out with the Raman spectrometer, NR-1000 , equiped with a microscope, manufactured by Japan spectroscopic Co., Ltd. The samples used in this experiment were a 6H SiC single crystal offered

from National Institute for Research in Inorganic Materials
and a polycrystal containing ∝ and β phases, synthesized by
CVD method by Toshiba Co. A tandem accelerator was used for
ion bombardments. The samples were kept at about 80 K in the
vacuum of 10^{-8} mmHg during irradiation.

3.Results and Discussion

The result of micro-Raman scattering for the polycrystal
is shown in Fig.1. In the sample, micro-single crystals are
dispersed in a variety of sizes and shapes. The largest size
of the micro crystal is about 200 μm and two distinct shapes
are observed, which are hexagonal and rectangular,
respectively. The mixture of α and β phases indicates itself
the presence of two distinct shapes at least in a superficial
feature because the α and β phase have a hexagonal and a cubic
structure, respectively. The former structure shows the same
Raman spectrum as observed in a 6H SiC single crystal
expectedly. After ion bombardments, Raman lines reduce their
intensities, particularly the lines at 769 and 788 cm^{-1}. The
reduction of the intensities means an increase of disorder in
the lattice vibration by ion bombardments.

The distribution of lattice distortion with ion
bombardments was examined in the lateral direction to the
path of a projectile. As shown in Fig.2, no significant
change of the Raman lines was observed at 2 μm away from the
boundary between the irradiated and the unirradiated area,
while at the boundary the intensities of the lines diminish,
and then at the irradiated area they are heavily destroyed as
expected. This result shows that the lattice distortion
induced by irradiation is restricted in a very narrow region.

Finally the deterioration of the Raman lines along the
path of a projectile is shown in Fig.3 for 100 MeV C^{5+} ion
bombardments. The projected range of the ions is estimated to
be 140 μm from the Table in the reference (8). The maximum
reduction of the intensity is observed just at the point of
the range. The effect of the ion bombardments extends 160 μm
beyond the range and the effect can be clearly seen even at
the surface as well.

References

(1) W.J.Choyke: Radiation Effects in Semiconductors,1976 (The Institute of Physics, Bristol and London. ed by N.B. Urli and J.W. Corbett) p58.

(2) D.W.Feldman, J.H.Parker,Jr., w.J.Choyke and L.Patrik: Phys. Rev. 170 (1968) 698.

(3) D.W.Feldman, J.H.Parker,Jr., w.J.Choyke and L.Patrik: Phys. Rev. 173 (1968) 787.

(4) D.Olego and M. Cardona: Phys. Rev. 25B (1982) 1151.

(5) Y.Kazumata, H.Naramoto, N.Masaki and A.Kikuchi: To be published in Report of the 2nd Joint Seminar on A.P., S.S.P. & M.S.

(6) D.M.Gruen, R.Varma and R.B. Wright: J. Chem. Phys. 64 (1976) 5000.

(7) L.A. Rahn, P.J. Colwell and W.J. Choyke: Proc. 3rd Int. Conf. on Light Scattering in Solids. ed by M. Blkanski, R.C.C. Leit and S.P.S.Porto (Paris: Flammarion) 1976, p607.

(8) J.F. Ziegler: Handbook of Stopping Cross-section for Energetic Ions in All Elements, Vols 3 and 4. Pergamon Press, New York (1980).

Fig.1 Micro-Raman scattering for micro-single crystals dispersed in a poycrystal. The micro-single crystals have hexagonal or rectangular shapes.

Application of micro-Raman scattering.

D-sample

(1) Hexegonal shape micro-crystol, before irradiation

(2) After the irradiation of 1.0 MeV P^+ to a dose of 1×10^{16} P^+/cm^2

(3) Rectangular shape miero-crystol before irradiation

(4) After the irradiation of 1.0 MeV P^+ to a dose of 1×10^{16} P^+/cm^2

WAVE NUMBER (cm^{-1})

Fig.2 Reduction of the intensities of Raman lines for the lateral direction to the pass of the projectile, 120 MeV F^{7+} ions.

Application of micro-Raman scattering Irradiation by 120 MeV F^{7+}: 4.2×10^{14} parti/cm^2

A - sample

(1) At unirradiated part.

969   790   769
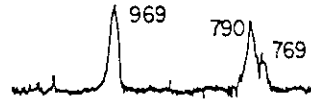
(2) At 2 μm off the boundary (unirrad part.)
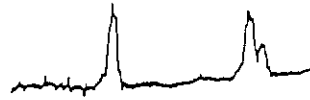
(3) At the boundary between unirradiated and irradiated part.

(4) At irradiated part.

1100   700

WAVE NUMBER (cm^{-1})

Laser beam

c-plane

100 MeV C^{3+} ions

Depth from the surface (μm)

200

180

160

140

120

100

80

60

1000 950 900 850 800 750 700

WAVE NUMBER (cm^{-1})

Fig.3 Change of the intensities of Raman lines along the pass of the projectile, 100 MeV C^{+5} ions. The projected range of the ion is estimated to be 140   m.

3.13 FREE RADICALS IN POLYVINYLIDENE FLUORIDE IRRADIATED BY
HEAVY IONS.

Yoshihide KOMAKI, Saburo TAKAMURA, Norio MORISHITA,[**] and
Naohiro HAYAKAWA[**].

Department of Chemistry,[*] Department of Physics, and[**] Takasaki
Radiation Research Establishment, Japan Atomic Energy Re-
search Institute.

Recently, we have attempted to identify free radicals which may be
formed in polyvinylidene fluoride (PVDF) by heavy ion irradiation, but
unfortunately such radicals could not be detected, primarily because of
the increase in temperature after irradiation.

This work was undertaken to re-examine this problem under low tem-
perature irradiations and subsequent low temperature measurements of ESR
spectra.

The 100 μm thick PVDF films were irradiated by two kinds of ions,
$^{35}Cl^{9+}$(150 MeV) and $^{12}C^{5+}$(90 MeV) at 5-6°K, respectively.

After etching in the 10N NaOH solution at 85°C, the perforated etched
tracks of ions, ^{35}Cl, ^{58}Ni, and ^{115}In of 150 MeV energy were clearly ob-
served in PVDF, but no tracks of ions by ^{12}C and ^{16}O were observed.

It has been reported that the etched tracks are formed in Lexan
(polycarbonate) and Daicel(cellulose nitrate) with bombardments of heavier
ions above He ion and proton.

We have detected free radicals in PVDF irradiated by two kinds of
ions,$^{35}Cl^{9+}$ and $^{12}C^{5+}$ at a low temperature and measured the amounts of
the radicals.

Figure 1 shows the radical spectra measured at 77°K after irradia-
tion by γ-ray of ^{60}Co of 1 Mrad at 77°K (a), the Cl^{9+}ion (b) and the
Cl^{9+}ion of higher dose at 5-6°K (c), and after keeping each specimen in
air at room temperature (d).

The spectra of (a) and (b) resemble each other and show hyperfine
structure with wide line width and complicated overlap. With increase
in temperature, the overlap signal separates clearly and 12 lines are
counted for (a), but the (b) remains complicated.

In γ-irradiation, three kinds of radicals like alkyl and conjugated

double bond radicals, are assigned.

At higher fluence of heavy ions, carbon-like radicals, which indicates sharp repeated signals like carbon structure and no longer polymeric radicals, occurrs. But at intermediate fluence a single large signal reveals near the center as shown in (c).

In contact with air, all of radicals convert to peroxy radicals as shown in (d), which shows asymmetrical feature.

The signal of (c) seems to be characteristic of irradiation by the heavy ion alone and remains after increase in temperature. This results from the lone pair electrons in conjugated double bonds of PVDF.

Figure 2 shows radicals formed by C^{5+} irradiation of PVDF. Amount of radicals is small and radicals diminish quickly after increasing temperature up to the room temperature.

The life times of radicals of (b) and (c) in Fig.1 and in Fig.2 are shown in Fig.3.

Fig.1 ESR spectra st 77°K of PVDF films irradiated by (a) γ-ray (b) the Cl^{9+}ion, (c) the Cl^{9+}ion of higher dose, and (d) specimen of peroxy radical at 25°C.

It is found from this figure that the life times of radicals by the C^{5+}irradiation are shorter than those by the Cl^{9+}ion and of the conjugated double bonds.

Figure 4 shows the relation of the formation of radicals in PVDF by the bombardments of $Cl^{9+}$and $C^{5+}$with the irradiation dose.

The amounts of radicals formed by the Cl^{9+}irradiation show to be several times as much as that by the $C^{5+}$and to increase

Fig.2 ESR spectra at 77°K and 25°C of PVDF irradiated by the C^{5+} ion.

linearly up to some dose. However, further increasing the irradiation dose to very high dose, polymer radicals formed decrease reversely to zero. The PVDF polymer is found to carbonize at the dose of 6×10^{-6} C.
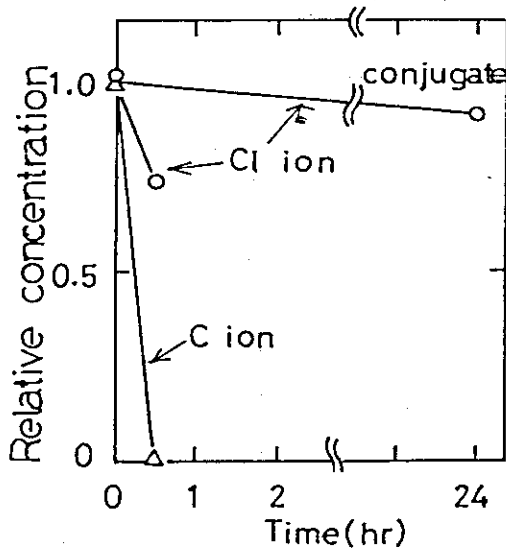
Fig.3 Life times of radicals in PVDF irradiated by the Cl ion and the C ion.
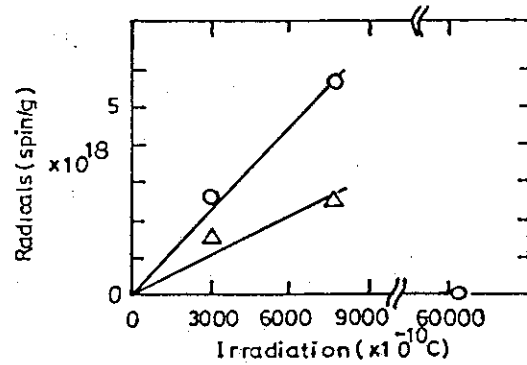
Fig.4 Variation of concentration of radicals in PVDF irradiated by the Cl ion and the C ion.

Table 1 Concentration of radicals in PVDF versus radiation doses, by Cl^{9+} and C^{5+} irradiations.

Ion and Energy (MeV)	Irradiation					
	3000 $(\times 10^{-10}$ C)			7600 $(\times 10^{-10}$ C)		
	Particles cm^{-2}	Radicals		Particles cm^{-2}	Radicals	
		spin/g	spin/particle		spin/g	spin/particle
Cl^{9+} (150)	4×10^{10}	2.6×10^{18}	6.5×10^{7}	8×10^{10}	5.7×10^{18}	7.1×10^{7}
C^{5+} (90)	9×10^{10}	1.3×10^{18}	1.4×10^{7}	2×10^{11}	2.5×10^{18}	1.3×10^{7}

The characteristic differences of radical formations by the Cl and C ion irradiations are briefly summarized as follows:

1) Amounts of radicals by the C ions are small.

2) Life time of radicals by C ions is shorter.

3) Irradiation by the C ion leaves little peroxy radicals.

The authors believe firmly that these results are useful in understading the formation process of the etched tracks in PVDF.

References

1) Y.Komaki, S.Ohno, N.Morishita, and T.Seguchi: JAERI-M-85-104,p87(1984).

2) A.Chambaudet and J.Roncin:Solid State Nucl.Track.Detect,11th,(1981),p51.

3.14 MEASUREMENTS OF INDUCED RADIOACTIVITIES IN SILICON AND GERMANIUM IRRADIATED WITH HIGH-ENERGY HEAVY IONS

Eiji Sakai

Department of Reactor Engineering, JAERI

Semiconductor detectors are known to be sensitive to radiation damage which may be annealed by heating at an elevated temperature. In high-energy heavy-ion detection with semiconductor detectors, nuclear reactions in the semiconductor materials themselves are expected to introduce radioactive nuclides which increase background counting rates of the detectors during and after the irradiation. These radioactive nuclides can not be removed by heating and the only method to remove them is etching. The production of radioactive nuclides is also important in manufacturing doped layers buried deep into semiconductor materials by the ion implantation since the radioactive nuclides may result in noisy devices and also the nuclides as well as their daughters may change the type of the materials.

In order to evaluate the amount of background counting rate increase in semiconductor heavy-ion detectors, we started measuring the induced radioactivities in Si and Ge after the irradiation with various high-energy heavy ions. Gamma-ray spectra from irradiated Si and Ge wafers were measured using a high-purity germanium spectrometer to determine the induced gamma-ray-emitting nuclides, their radioactivities, their numbers of atoms at the end of the irradiation and the numbers of atoms per incident heavy-ion. Some of the results were already published[1,2].

In this fiscal year(1986), irradiations with 20 MeV/30 MeV/40 MeV $^{10}B^{3+}/3+/4+$, 80 MeV $^{16}O^{6+}$, 60 MeV $^{19}F^{6+}$, 100 MeV $^{28}Si^{8+}$ and 190 MeV $^{58}Ni^{12+}$ were made and some of the results are summarized in Table 1.

References

1) Eiji Sakai: IEEE Trans. Nucl. Sci., NS-31(1984)316-319.

2) Eiji Sakai: IEEE Trans. Nucl. Sci., NS-33(1986)651-654.

Table 1   Residual gamma-ray-emitting nuclides induced in Si and Ge irradiated with heavy ions, their radioactivities at the end of irradiation, corresponding numbers of atoms, numbers of atoms per incident ion, resultant stable daughter nuclides and the calculated threshold energies for compound nucleus formation

* 2.88×10^{14}

Heavy ions (Range)	Number of particles	Irradiated material	Residual nuclide	Radioactivity(nCi)	Number of atoms	Number of atoms per particle	Stable daughter nuclide	Threshold energy(MeV)
20 MeV $^{10}B^{3+}$ (11.2 μm)	4.15E14 /3.14cm²	Si	Sc-44m(2.442d)	3.44	3.87E7	9.73E-7	Ca-44	17.03
			Sc-44(3.927h)				Ca-44	
20 MeV $^{10}B^{3+}$ (8.6 μm)	3.73E14 /1.77cm²	Ge	None					27.20
30 MeV $^{10}B^{3+}$ (45.2 μm)	2.88E14* /1.77cm²	Si	Be-7(53.29d)	0.51	1.24E8	4.33E-7	Li-7	17.03
			Na-24(14.659h)	2.30	6.48E6	2.65E-8	Mg-24	
30 MeV $^{10}B^{3+}$ (30.0 μm)	2.95E14 /2.14cm²	Ge	Ge-69(1.627d)	1.89	1.42E7	5.02E-8	Ga-69	27.20
			As-71(2.70d)	2.79	3.47E7	1.21E-7	Ga-71	
			As-72(1.083d)	4.96	2.47E7	2.21E-7	Ge-72	
			As-73(80.30d)	0.81	2.98E8	1.01E-6	Ge-73	
			As-74(17.78d)	0.56	4.62E7	1.58E-7	Ge-74,Se-74	
			Br-76(16.2h)	19.6	6.11E7	2.28E-7	Se-76	
			Br-77(2.3765d)	27.1	2.97E8	1.03E-6	Se-77	
			Kr-79(1.460d)	56.1	3.78E8	1.32E-6	Br-79	
40 MeV $^{10}B^{4+}$ (66.8 μm)	2.25E13 /1.77cm²	Si	Be-7(53.29d)	0.09	2.14E7	9.5 E-7	Li-7	17.03
40 MeV $^{10}B^{4+}$ (45.0 μm)	2.29E13 /2.00cm²	Ge	Ge-69(1.627d)	0.84	6.34E6	2.80E-7	Ga-69	27.20
			As-71(2.70d)	2.0	2.55E7	1.12E-6	Ga-71	
			As-72(1.083d)	3.87	1.93E7	8.56E-7	Ge-72	
			As-74(17.78d)	0.24	1.98E7	8.68E-7	Ge-74,Se-74	
			Br-76(16.2h)	29	9.13E7	4.08E-6	Se-76	
			Br-77(2.3765d)	18.9	2.07E8	9.11E-6	Se-77	
			Kr-79(1.460d)	40.3	2.72E8	1.20E-5	Br-79	
			Rb-83(86.2d)	0.09	3.44E7	1.51E-6	Kr-83	
70 MeV $^{10}B^{4+}$ (155 μm)	8.13E13 /0.77cm²	Si	Be-7(53.29d)	3.83	9.43E8	1.16E-5	Li-7	17.03
			Na-22(2.602y)	0.094	4.12E8	5.07E-6	Ne-22	
70 MeV $^{10}B^{4+}$ (97.2 μm)	7.49E14 /3.14cm²	Ge	Ga-67(78.3h)	23.2	3.49E8	4.77E-7	Zn-67	27.20
			As-71(2.70d)	418	4.90E9	6.74E-6	Ga-71	
			Se-72→As-72(1.083d)					
			As-73(80.30h)	42.9	1.82E10	2.43E-5	Ge-73	
			As-74(17.78d)	65.6	5.38E9	7.22E-6	Ge-74,Se-74	
			Se-72(8.40d)	32.2	1.25E9	1.67E-6	Ge-72	
			Se-75(118.45d)	42.7	2.33E10	3.11E-5	As-75	
			Br-77(2.3765d)	2810	3.08E10	4.11E-5	Se-77	
			Kr-79(1.460d)	3420	2.31E10	3.24E-5	Br-79	
			Rb-83(86.2d)	2.9	1.17E9	1.56E-6	Kr-83	

3.15   LOW-TEMPERATURE ELECTRON IRRADIATION CRYOSTAT

Teruo KATO, Mituo WATANABE, Akihiro IWASE and Tadao IWATA

Department of Physics, JAERI

In this note we describe a cryostat for the electron irradiations to solids at low temperatures below 10 K.

Electron irradiations can produce a small scale of displacements in solids and then displaced atoms exist as isolated defects if frozen at low temperatures. On the other hand, ion irradiations can produce relatively a large scale of atomic displacements where displaced atoms tend to form defect clusters. Therefore, both irradiations are complementary to each other in the study of defect productions in solids. Low temperature are necessary to freeze irradiation-produced defects in the nascent states.

The JAERI Electron Linear Accelerator is used as the source of electrons. It can supply mono-energetic electrons with continuously variable energies between 50 and 190 MeV.

Figure 1 is a schematic drawing of the cryostat. The cooling of the samples is performed by directly immersing the samples in a stream of liquid helium. Liquid helium is provided through the liquid helium transfer system from the outside of a concrete radiation-shielding wall 3 m thick as shown in Fig. 2.

In order to simulate the heat evolution during irradiations, the cooling ability of the system was tested by supplying the electric power to samples.   Figure 3 shows the change in sample temperature as a function of the supplied power. If the electron beams of 60 MeV and 1 micro-A are irradiated to a Cu sample 2mm thick, the heat evolution is about 5 W and the temperature of the sample will be kept near 8 K. Liquid helium of about 10 litters is needed for this cooling.

After the irradiations, by using a double-walled bucket[1] with liquid helium in it, samples are taken out from this cryostat and are transferred without warmup to the other measuring cryostats to study the physical property changes. Such a simple property as the electrical resistivity can be measured in situ during irradiations.

Reference

1) H. Meta, T. Kato and S. Okuda: J. Phys. E,8(1975)577.
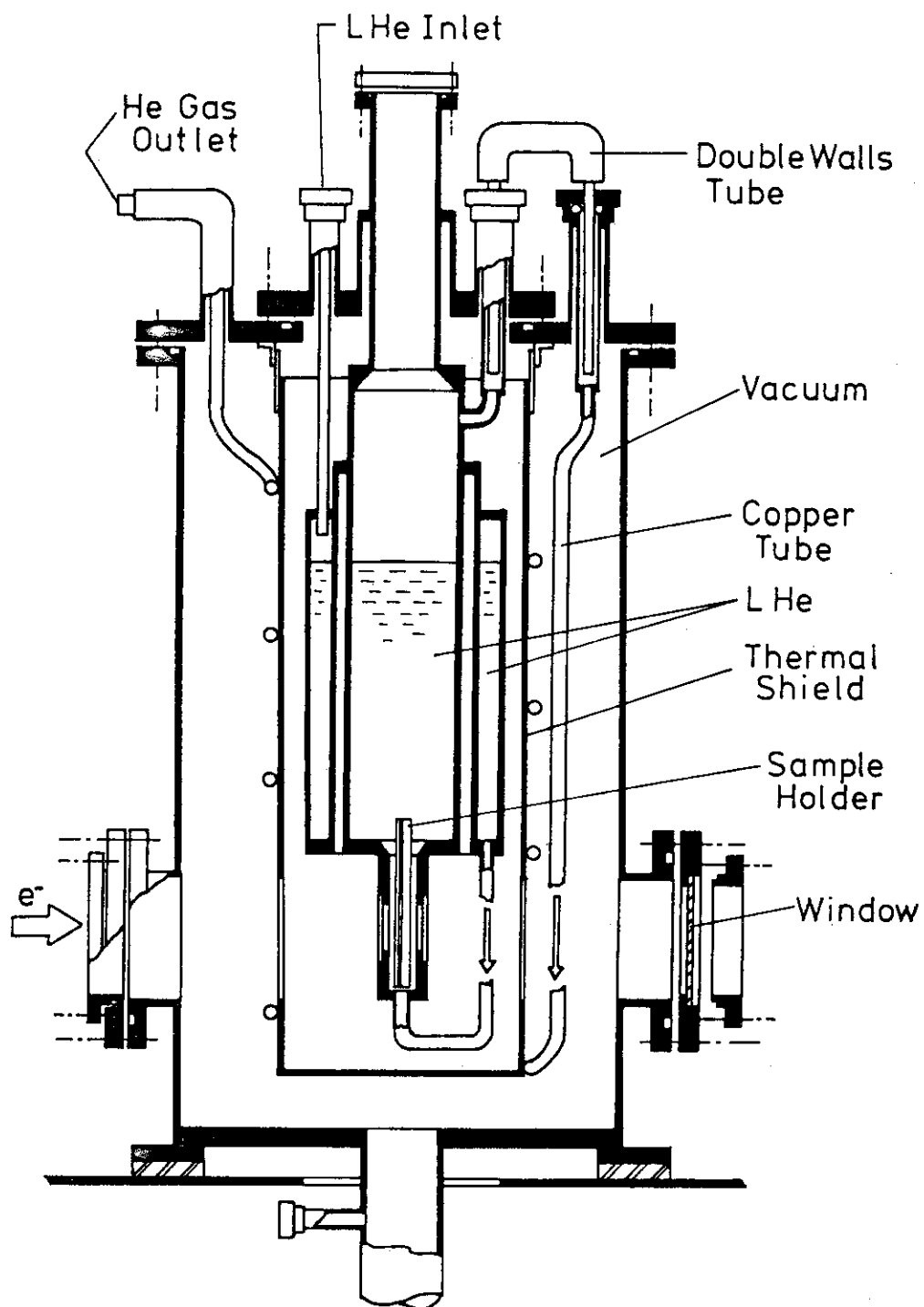
Fig.1 Shematic drawing of the liquid helium cryostat
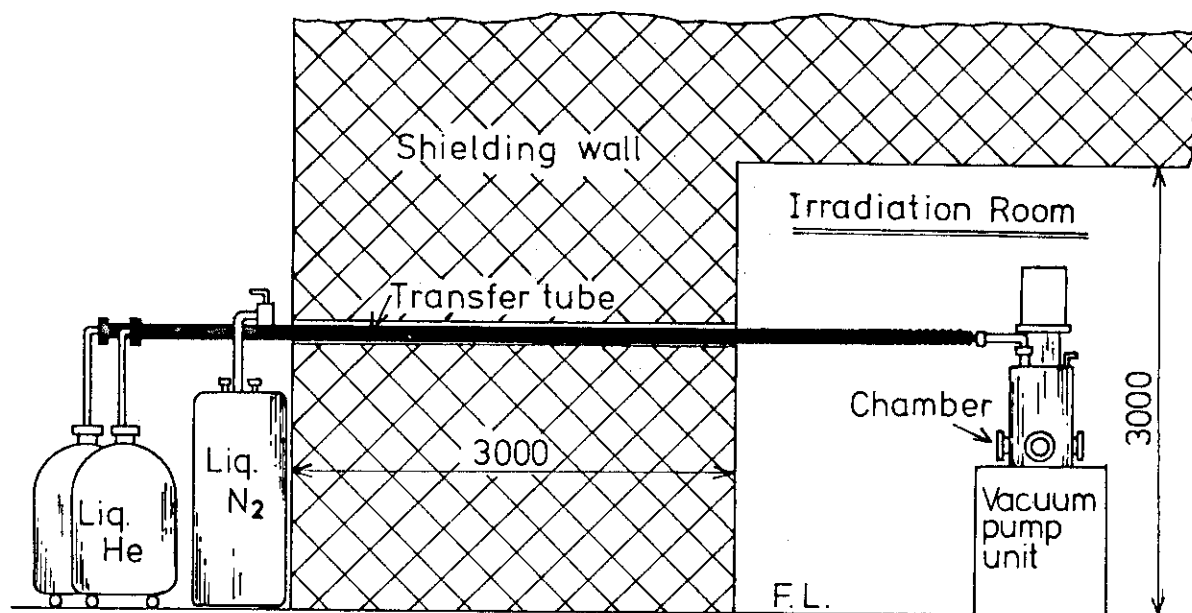
Fig.2 Schematic drawing of the liquid helium circuit
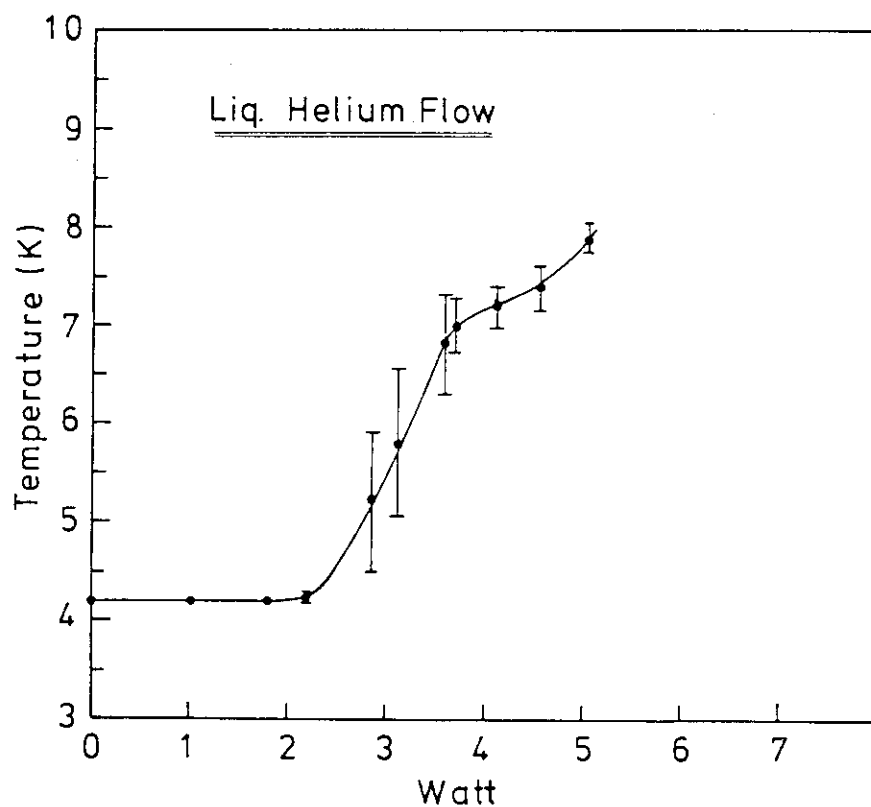
Fig.3 Change in the sample temperature as function of heat supplied

Scientific Meetings

Kato,T., Watanabe,M., Iwata,T.
Cryostat for Electron Irradiation at Liquid Helium
Temperature (I)
34th Meeting of the Cryogenic Association of Japan
in Osaka (November,20-22,1985)

Kato,T., Watanabe,M., Iwase,A., Iwata,T.
Cryostat for Electron Irradiation at Liquid Helium
Temperature (II)
36th Meeting of the Cryogenic Association of Japan
in Yokohama (November,19-21,1986)

Ⅳ NUCLEAR CHEMISTRY

4.1   DECAY PROPERTY OF ^{245}Cf

Nobuo SHINOHARA, Masaaki MAGARA, Shigekazu USUDA,

Shin-ichi ICHIKAWA, Toshio SUZUKI, Hideki IIMURA,

Yoshii KOBAYASHI, Tadashi YAMAMOTO, Yuichiro NAGAME[*],

Yuichi HATSUKAWA[**], Takayoshi HORIGUCHI[***],

Seiichi SHIBATA[****] and Ichiro FUJIWARA[*****]

Department of Chemistry, [*]Department of Radioisotopes, JAERI,
[**]Department of Chemistry, Tokyo Metropolitan University,
[***]Department of Physics, Hiroshima University,
[****]Institute for Nuclear Study, University of Tokyo and
[*****]School of Economics, Otemon Gakuin University

Introduction

     Californium-245 was produced in 1950 as the first isotope of 98th
element by the reaction of ^{242}Cm$(\alpha,n)^{245}$Cf[1].   Chetham-Strode et al. have
reported that the ^{245}Cf nuclide decays by both orbital electron capture,
EC, and alpha-particle emission, α, with branchings of about 70% for EC
and 30% for α decay[2].   The alpha-particle energies measured by Kusch
et al.[3] were 7.137 MeV, 7.084 MeV, 7.036 MeV, 6.983 MeV and 6.886 MeV,
but intensity of each alpha-ray has not been determined yet.

     In order to study the decay characteristics of ^{245}Cf more in details,
^{245}Cf was produced by the ^{238}U$(^{12}$C,5n$)^{245}$Cf reaction and the decay was
studied by radiochemical methods.   This article describes the half-life,
the branching ratio of α/EC and the intensities of the alpha-rays of ^{245}Cf.

Experimental

     Thin targets of ^{238}U (99.98%) were prepared by an electrodeposition
method to measure the excitation function of ^{245}Cf and thick targets (natu-
ral uranium) were made by sedimentation method using acetone.   Backings
of the targets were aluminum foils of 7 μm and the thickness of the targets
were 0.7-0.9 mgU/cm^2 for the thin and 3-7 mgU/cm^2 for the thick targets.
Irradiations with ^{12}C ions were performed at the JAERI tandem Van de Graaff
accelerator and the average beam intensity was 160 particle nA.   After
irradiation of the target for 3 hours, the produced californium nuclides
were separated rapidly by anion-exchange methods[4].   The alpha-rays of

^{245}Cf were measured with a silicon surface barrier detector. The branching ratio of α/EC was determined by measuring gamma-rays of ^{245}Bk which was formed by EC decay of ^{245}Cf.

Results

The excitation function of the formation of ^{245}Cf measured in the energy range 60-90 MeV was well agreed with that determined by Sikkeland et al.[5]. Figure 1 shows an alpha-ray spectrum of the californium fraction after chemical separation. Five peaks were observed in the spectrum and their energies were in good agreement with the results previously reported[2]. The relative intensities of alpha-rays were determined by analysing the spectra obtained, and the results are given in Table 1. Half-life was determined to be 46.4±0.3 minutes that is slightly larger than the reported value of 43.6±0.8 minutes[6]. Branching ratio of α/EC obtained in this work was 0.56±0.04 (α=36% and EC=64%).

Further experiments are in progress in order to clarify the decay scheme of ^{245}Cf.

References

1) S. G. Thompson et al.: Phys. Rev. 80 (1950) 790.

2) A. Chetham-Strode et al.: Phys. Rev. 102 (1956) 747.

3) W. Kusch et al.: JINR-E6-3992 (1968).

4) S. Usuda et al.: J. Radioanal. Nucl. Chem. 111 (1987) 477, 111 (1987) 399, 115 (1987) in press.

5) T. Sikkeland et al.: Phys. Rev. 169 (1968) 1000.

6) P. R. Fields et al.: Phys. Lett. 24B (1967) 340.
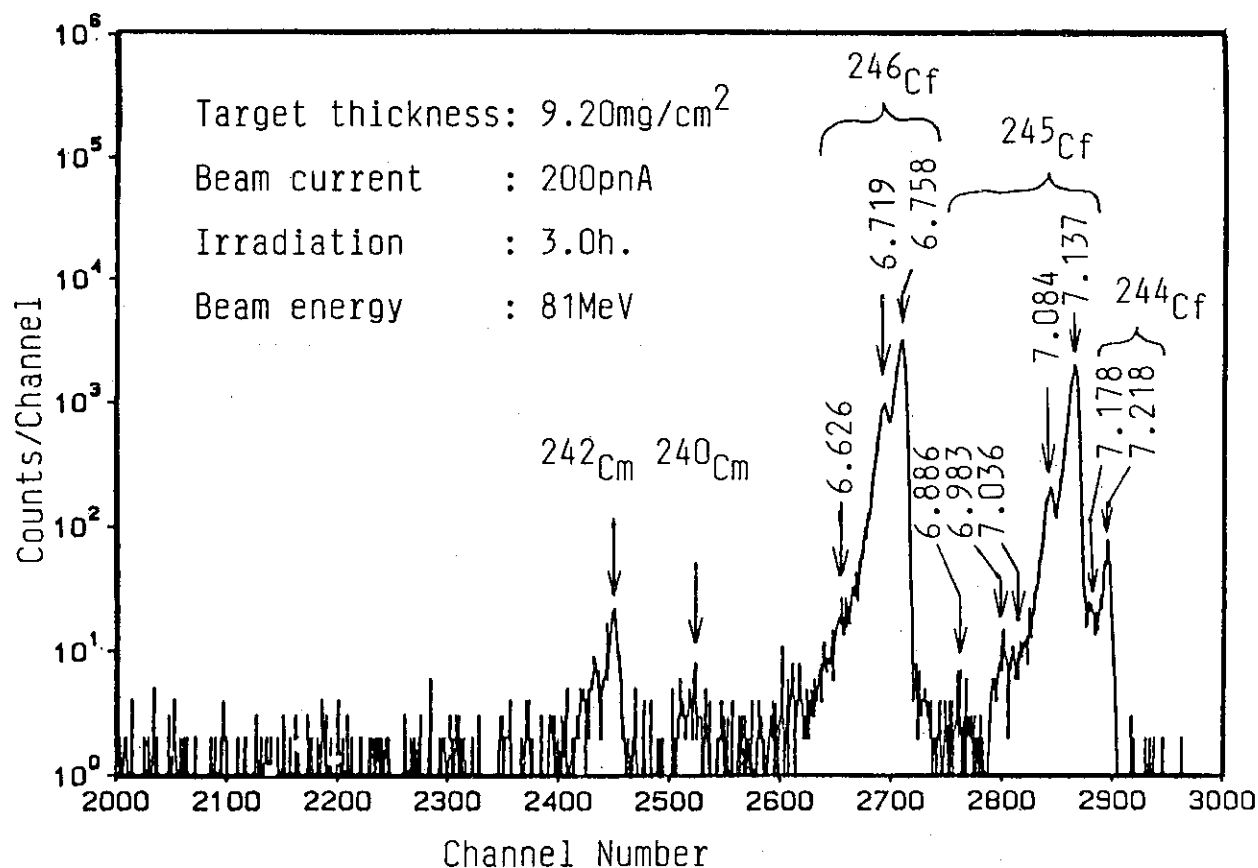
Fig. 1 Alpha-ray spectrum of the californium fraction separated by the ion-exchange method. Numerals in the figure stand for the alpha-ray energy (MeV).

Table 1 Decay property of ^{245}Cf.

	this work	references[2,3,6]
half-life	46.4 ± 0.3 min.	43.6 ± 0.8 min.
alpha-ray energy (relative intensity)	7.137 MeV (91.3%)	7.137 MeV
	7.084 MeV (7.8%)	7.084 MeV
	7.036 MeV (0.4%)	7.036 MeV
	6.983 MeV (0.4%)	6.983 MeV
	6.886 MeV (–)	6.886 MeV
α/EC	0.56 ± 0.04 (α 36%, EC 64%)	0.43 (α 30%, EC 70%)

4.2 A HELIUM-JET RECOIL-TRANSPORT SYSTEM
FOR STUDIES OF SHORT-LIVED ACTINIDE NUCLIDES

Nobuo SHINOHARA, Masaaki MAGARA, Shigekazu USUDA,

Shin-ichi ICHIKAWA, Toshio SUZUKI, Hideki IIMURA,

Yoshii KOBAYASHI, Tadashi YAMAMOTO, Yuichiro NAGAME [*],

Yuichi HATSUKAWA [**], Akihiko YOKOYAMA [***],

Takayoshi HORIGUCHI [****], Masanori WAKASUGI [****],

Seiichi SHIBATA [*****] and Ichiro FUJIWARA [******]

Department of Chemistry, [*] Department of Radioisotopes, JAERI,
[**] Department of Chemistry, Tokyo Metropolitan University,
[***] Department of Chemistry, Osaka University,
[****] Department of Physics, Hiroshima University,
[*****] Institute for Nuclear Study, University of Tokyo and
[******] School of Economics, Otemon Gakuin University

The helium-jet recoil-transport (abbreviated to HJRT) method has proven
to be a valuable means of transporting recoil nuclei from target position
to an area of low background radiation within a few seconds[1,2] and can
be applied to a continuous chemical separation system. We are developing
an on-line chemical separation system which consists of a HJRT system,
a continuous multistage solvent extraction system (Short-lived Isotope
Studied by AKUFVE technique, SISAK)[3], and a rapid ion-exchange system
in order to study the short-lived actinide nuclides. The purposes of
this paper are to report on our preliminary experiments of the HJRT system.

Figure 1 shows the principal arrangement of the HJRT system. The
principle is the following: The nuclei produced by a heavy-ion reaction
are thermalized through collision with helium atoms and attached to aerosol
particles in the gas. By using vacuum pump the aerosol particles are
extracted through a Teflon capillary (2mm diameter and 30m long) into a
tape transport system and here blown to the collection tape where the nuclei
produced are concentrated to a spot of a few mm diameter. After collection
for an appropriate time, the tape is transferred to a detector position
where the alpha and gamma activities are measured with SSD and Ge detectors.

In off-line experiments, optimum conditions for the aerosol generator
were investigated by using spontaneous fission products of a ^{252}Cf source

as tracers to determine the size and quantity of aerosol and the flow rate of helium gas. For evaluation of the transport efficiencies, the activities of the fission products from the ^{252}Cf source and of ^{239}Np from a ^{243}Am source were measured. Table 1 shows the maximum efficiencies obtained.

The HJRT system was also tested in on-line experiments, in which the nuclides, ^{190}Hg, ^{205}At and ^{129}Sb, were produced by the ^{181}Ta(^{14}N,5n)^{190}Hg, ^{197}Au(^{12}C,4n)^{205}At and ^{235}U(^{12}C,fission)^{129}Sb reactions, respectively, and transferred from the targets to the tape transport system. The maximum transport efficiencies estimated were also given in Table 1.

The maximum transport efficiencies for the fission products, ^{104}Tc, ^{141}Ba and ^{129}Sb, differ apparently from those of the evaporation residues, ^{190}Hg and ^{205}At, and the recoil nuclei from alpha decay, ^{239}Np, as shown in Table 1. These results can be explained from the difference of the recoil ranges between them. The structure of the recoil chamber was not adequate for the recoiling nuclei of short ranges. Improvement of the recoil chamber and development of SISAK system to be coupled with the HJRT system are in progress.

References

1) R. D. MacFarlane and W. C. McHarris: Nuclear Spectroscopy and Reactions, Vol.A (J. Cerny, Ed., Academic, New York, 1974) pp. 243-286.

2) K. Okano et al.: Nucl. Instrum. & Methods 186 (1981) 115.

3) P. O. Aronsson et al.: J. Inorg. Nucl. Chem. 36 (1974) 2397.
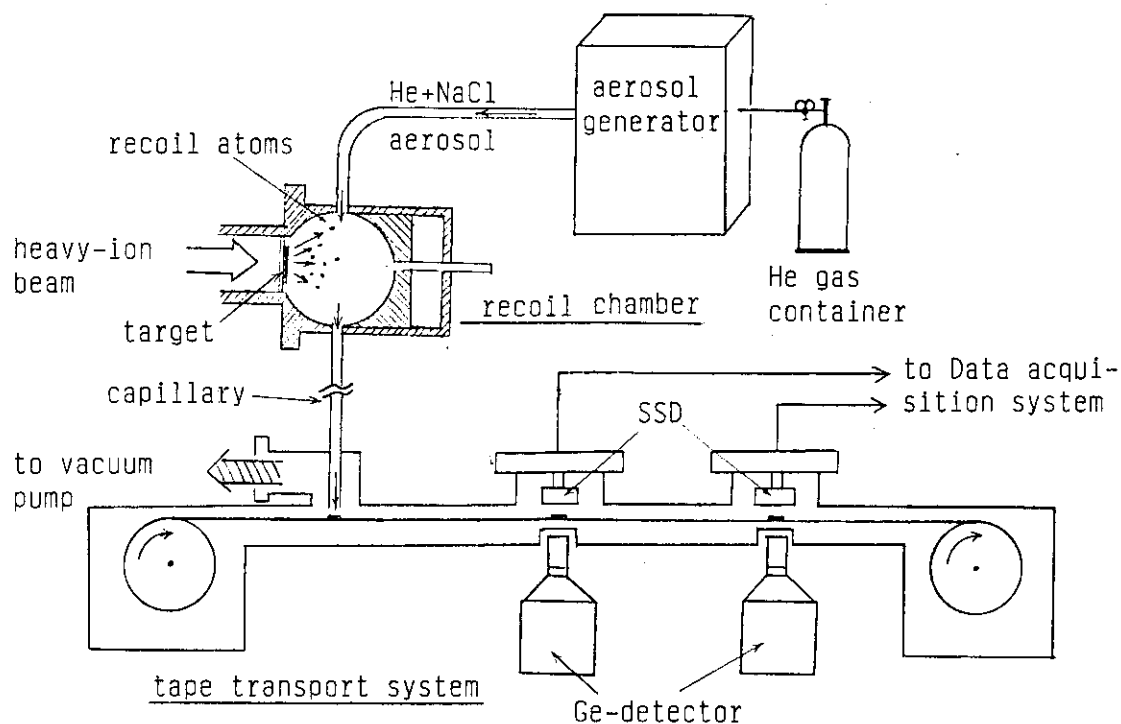
Fig. 1   Principal arrangement of the HJRT system.

Table 1   Maximum transport efficiency for the HJRT system.

Tracer	Source or Reaction	Range in He		Efficiency
^{104}Tc	^{252}Cf-spontaneous fission	2	mg/cm^2	65 %
^{141}Ba	^{252}Cf-spontaneous fission	2	mg/cm^2	60 %
^{239}Np	^{243}Am-alpha decay	0.003	mg/cm^2	5 %
^{129}Sb	^{235}U(^{12}C,fission)^{129}Sb	2	mg/cm^2	50 %
^{190}Hg	^{181}Ta(^{14}N,5n)^{190}Hg	0.2	mg/cm^2	10 %
^{205}At	^{197}Au(^{12}C,4n)^{205}At	0.2	mg/cm^2	10 %

4.3   ON-LINE MASS SEPARATION OF THE MONOXIDES IN THE LIGHT
       RARE-EARTH REGION

Shin-ichi ICHIKAWA, Toshiaki SEKINE[*], Masumi OSHIMA[**],
Naruto TAKAHASHI[***] and Hideki IIMURA

Department of Chemistry, [*]Department of Radioisotopes
and [**]Department of Physics, JAERI, [***]Faculty of
Science, Osaka University

1. Introduction

     To search for new isotopes in the rare-earth and investigate their
decay properties, we have studied mass separation of the monoxide ions
of the rare-earth elements produced by heavy-ion reactions and ionized
in a high-temperature surface ion source. The monoxides are favorably
ionized by surface ionization, since their ionization potentials are
lower than those of the metals by 0.3 to 0.7 eV.[1,2] Besides, elemental
selectivity of the rare-earths in increased in the surface ionization
of the monoxides MO, because the dissociation energy of MO into M + O
varies considerably from element to element.[3] With the elemental
selection in ionization prior to mass separation one may make unique A
and Z determination.

     The present paper describes the results obtained from off-line and
on-line experiments; the off-line experiments were carried out to
study the behaviour of the neibouring elements from caesium to euro-
pium except promethium, under the same ion-source conditions as
on-line. In the on-line experiment ^{124}La, ^{122}La and the new isotope,
^{121}La, were produced in the reaction ^{32}S + ^{nat}Mo and mass-separated as
lanthanum-monoxide (LaO^{+}) ions.

2. Off-Line Experiment

      1 mg of a starting material was deposited at the vaporizer
together with 1 mg of BaO acting as a mass marker. As starting
material, high-purity oxides were used in the case of the rare earths
from lanthanum to europium. The ion source loaded with samples was
heated to 1900 K and pumped until the pressure in the extraction cham-
ber lowered to approximately 1.5×10^{-4} Pa. The voltages for extraction
and acceleration were increased to 20 kV and 50 kV, respectively, and

the einzel lenses and the quadrupole doublet were adjusted so as to maximize the $^{138}Ba^+$ intensity. Then, measurement of the yields of M^+ and MO^+ ions was started. By tuning the magnetic field, the ion currents, $i(M^+)$ and $i(MO^+)$, were measured with a Faraday cup. The measurements were repeated at different temperatures between 1900 and 2730 K. The pressure in the extraction chamber, p, was also recorded.

The current ratios, $i(MO^+)/\{ i(MO^+) + i(M^+)\}$, obtained from the measurements at $P \doteq 1.5 \times 10^{-4}$ Pa and 6×10^{-5} Pa are plotted against the ion temperature in Fig.1. The values of barium and europium are not plotted since the values were less than 10^{-5}. The values of samarium at $P \doteq 6 \times 10^{-5}$ Pa are also out of the range; the maximum value was 10^{-3}. As seen in Fig.1, the $i(MO^+)/\{ i(MO^+) + i(M^+)\}$ values decrease with increasing temperature and atomic number and with decreasing pressure. Further, it is concluded that lanthanum and cerium behave in almost the same manner. Therefore, lanthanum and cerium are not separable from each other. They, however, can be separated from the neighbouring elements at the highest temperatures.

3. On-Line Separation of La Isotopes

A 4.1-mg/cm^2 thick target of Mo of natural isotopic composition was bombarded with a 140-MeV ^{32}S beam. The temperature of the ion source was set at 2400 K, pressure was 2×10^{-5} Pa. The mass-separated products were collected at an aluminum coated Mylar tape and transfered periodically to a detection port; the period for collection-counting was chosen to be suitable for a La isotope to be studied. The detection port was equipped with a Ge(HP) detector and a 2-mm thick plastic scintilator; the time spectra of β rays and the multispectra of singles and β-gated γ rays were obtained. A comparison between the yields of La^+ and LaO^+ was done for ^{124}La; that is, mass separation was performed at A=124 and 140. Additionally, $^{122}LaO^+$ and $^{121}LaO^+$ were mass-separated.

Figure 2 shows the γ ray spectra obtained at A=124 and 140. One can notice the γ lines associated with the decay of ^{124}La in the spectrum at A=140. Although, ^{124}Cs γ lines are observed in this spectrum, it is found from their time spectra that the radioactivity is due to the decay chain $^{124}La \rightarrow ^{124}Ba \rightarrow ^{124}Cs$. Comparing the two spectra in Fig.2, the ratios, $i(MO^+)/ \{i(MO^+) + i(M^+)\}$, are deduced to be $\gtrsim 0.93$ for ^{124}La and ≤ 0.001 for ^{124}Cs and ^{124}Ba.

In mass separation at A=138 and 137, the beams of $^{122}LaO^+$ and $^{121}LaO^+$, respectively, were also obtained; as reported in the subsequent paper[4], the new isotope ^{121}La was identified with a half-life of 8±2 sec.

In conclusion, we can claim that mass separation of the oxide ions workes efficiently in the pesent reaction systems.

Refereneces

1) E. G. Rauh and R. J. Ackermann, J. Chem. Phys. 60 (1974) 1396.

2) H. G. Staley and J. H. Norman, Int. J. Mass Spectrom. Ion Phys. 2 (1969) 35.

3) L. L. Ames, P. N. Walsh and D. White, J. Phys. Chem. 71 (1967) 2707

4) T. Sekine et al.: "Decay Spectroscopy of ^{130}Pr, ^{128}Pr, ^{124}La, ^{122}La and the new isototpe ^{121}La", a paper in the same volume.

5) J. Conrand, R. Pepow, E. Gross, H. Homeyer, E. Jasechke and J. P. Wurm, Nucl. Phys. A234 (1974) 154
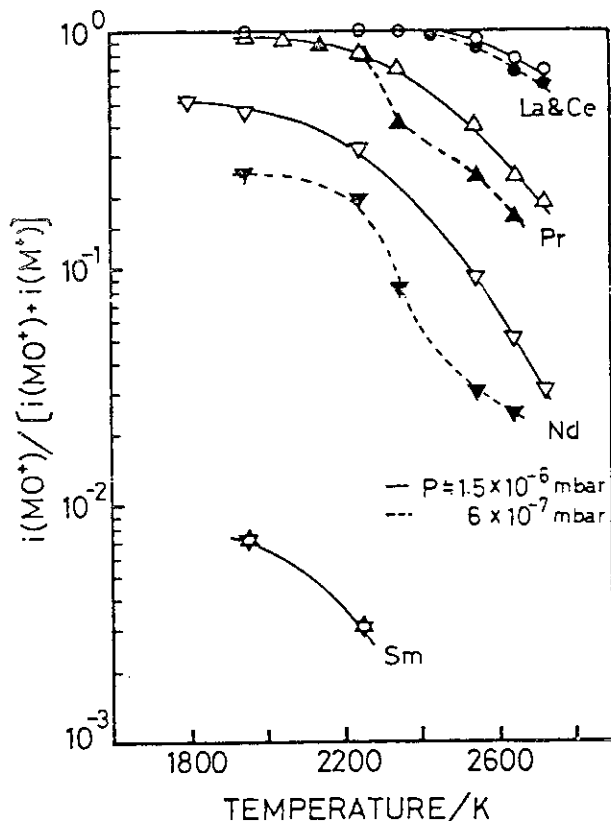
Fig. 1 Temperature dependence of $i(MO^+)/\{ i(MO^+) + i(M^+)\}$ under different pressures.
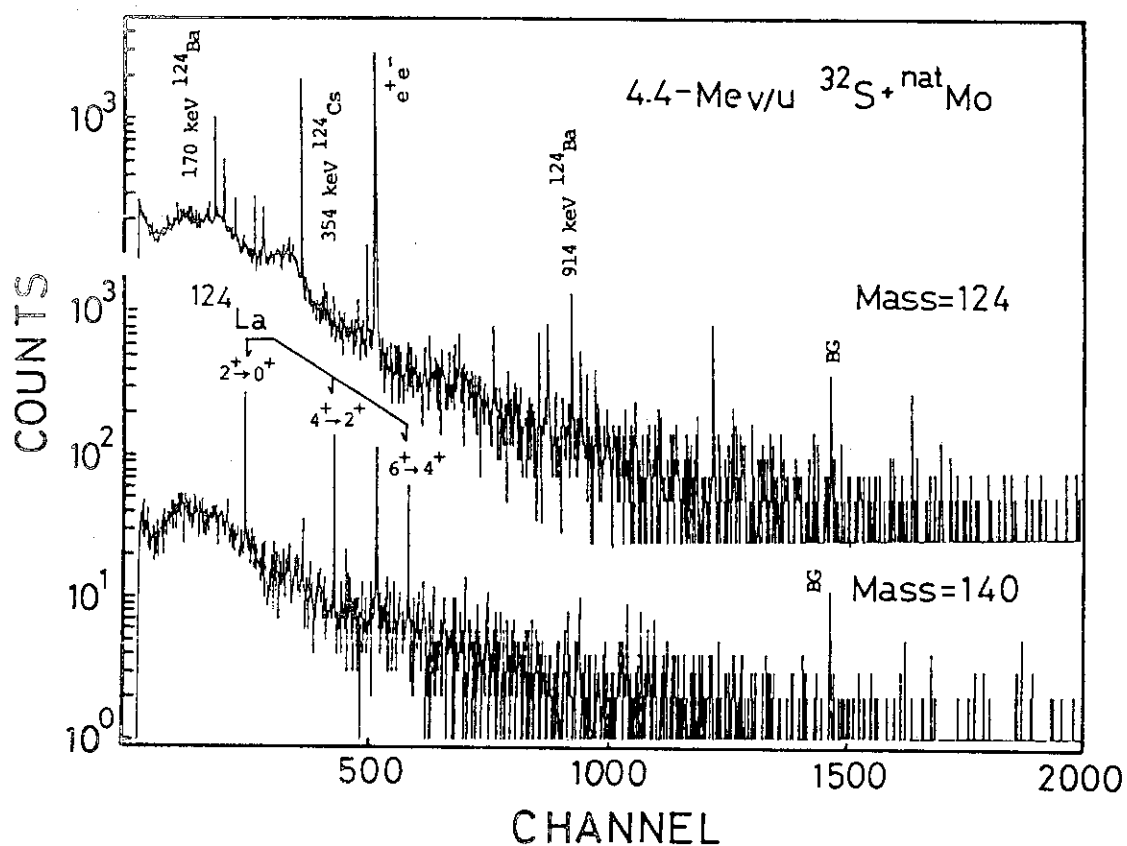
Fig. 2 γ-singles spectra obtained at mass 124 and 140.

Fusion-evaporation residues were produced in the reaction 4.4-MeV/u ^{32}S + ^{nat}Mo and ionized at a temperature of 2400 K. The γ lines enhanced at A=140 were assigned to ^{124}La.[5]

4.4   DECAY SPECTROSCOPY OF ^{130}Pr, ^{128}Pr, ^{124}La, ^{122}La AND
THE NEW ISOTOPE ^{121}La

Toshiaki SEKINE, Kentaro HATA, Yuichirou NAGAME,
Shin-ichi ICHIKAWA[*], Hideki IIMURA[*], Masumi OSHIMA[**],
Naruto TAKAHASHI[***] and Akihiko YOKOYAMA[***]

Department of Radioisotopes, [*]Department of Chemistry,
[**]Department of Physics, JAERI, [***]Faculty of Science,
Osaka University

Much progress has been made in exploring neutron deficient iso-
topes in the light rare-earth region by using heavy-ion reactions
and on-line mass separation. In this region very neutron deficient
isotopes were found by taking advantage of their β-delayed proton
emission; detailed β and γ spectroscopy is needed for these nuclei.

The present work is to study the decay properties of the
odd-odd nuclides of ^{130}Pr, ^{128}Pr, ^{124}La and ^{122}La, and to search for
the new isotope ^{121}La.

1. Experimental

A 4.1-mg/cm^2 thick Mo foil with natural isotopic abundances and
a 3.8-mg/cm^2 thick ^{103}Rh foil were bombarded with ^{32}S beams for pro-
duction of the Pr and the La isotopes, respectively. The beam ener-
gies and currents are summarized in Table 1. The reaction products
were ionized with a high temperature surface ion source. As reported
in another paper[1], the La isotopes were ionized at an ion
source-temperature of 2400 K as monoxide ions (LaO$^+$), and well
separated from their Cs and Ba isobars. On the other hand, the Pr
isotopes were ionized as metallic ions at 2700 K, being separated
from their Ce and La isobars.

The mass-separated products were implanted into an aluminized
Mylar tape in front of two Ge(Li) dectectors for γ-γ coincidence
measurement. After collecting for a preselected time period, the
activiy was transported within 1 sec into the counting position,
equipped with a 2 mm-thick plastic scintillator for β detection and

a Ge(HP) detector for γ detection. For each isotope studied, the collection-counting cycle was chosen to be approximately three times the reported or estimated half-life; within this cycle time eight or sixteen time-multiscaled γ-ray spectra were recorded together with a β time spectrum. Some 260 to 6500 cycles were combined to obtain the final sets of spectra for each isotope studied.

2. Results and Discussion

The averaged source intensities collected at the tape were determined with their β intensities. They are summarized in Table 1 together with the averaged primary beam currents.

Table 1   Beams, targets and mass-separated source intensities

Projectile	Energy (MeV)	Current (pnA)	Target	Product ion	Half-life	Source intensity (atom/sec)
$^{32}S^{+10}$	175	25	^{103}Rh	$^{130}Pr^{+}$	28 s	200
	200	12	^{103}Rh	$^{128}Pr^{+}$	3.0 s	2.5
$^{32}S^{+9}$	160	30	^{nat}Mo	$^{124}LaO^{+}$	29 s	280
				$^{122}LaO^{+}$	8.7 s	4.6
				$^{121}LaO^{+}$	8 s	0.2

From the mass-separated sources, we have obtained β-coincident γ-ray spectra for $A=$ 130, 128, 140($^{124}LaO^{+}$) and 138($^{122}LaO^{+}$), as shown in Fig.1; the spectrum for $A=$ 137($^{121}LaO^{+}$) is not shown since it had no meaningful γ lines. In the $A=140$ and 138 spectra one can notice the γ lines associated with the decays of ^{124}Cs and ^{122}Cs. Their activities are found from their time spectra to be mainly due to the successive decays $^{124}La\rightarrow^{124}Ba\rightarrow^{124}Cs$ and $^{122}La\rightarrow^{122}Ba\rightarrow^{122}Cs$. All the spectra in Fig.1 show prominent $2^{+}\rightarrow0^{+}$ and $4^{+}\rightarrow2^{+}$ transitions in their

daughter nuclei. In the decays of both ^{128}Pr and ^{122}La, no other transitions were observed. This means that their ground-state spins are possibly as small as 3. On the other hand, the ground-state spins of ^{130}Pr and ^{124}La must be higher, since in their daughter nuclei are populated such high spin states as 6^+ state for ^{130}Pr and 10^- state for ^{124}La. Construction of the decay schemes is in progress.

Fig.2 shows the β-time spectrum obtained at $A=137$. From the spectrum corrected for the background a half-life of 8 ± 2 sec was deduced. The possible sources for the β ray are restricted to ^{121}LaO$^+$ and ^{121}CeO$^+$, since the compound nuclei are $^{132-x}$Ce, and no fission reaction is expected to occur in the interaction between the ^{32}S beam and the ^{nat}Ta target, which was acting as a catcher. The possibility of ^{121}CeO$^+$ as a main source of the β ray, however, was eliminated because of its small cross section in the reaction ^{32}S+^{92}Mo that was predicted by ALICE code[2] to be 0.07 mb, compared with 8 mb for ^{121}La. In addition, the gross theory of β decay[3] supports ^{121}La rather than ^{121}Ce; it predicts the half-lives to be 5 sec for ^{121}La and to be 1 sec for ^{121}Ce. From these arguments, we have assigned the 8 ± 2 sec β ray to the new isotope ^{121}La.

References

1) S. Ichikawa, T.Sekine, M. Ohshima, N. Takahashi and H. Iimura: "On-Line Mass Separation of the Monoxide Ions in the Light Rare-Earth Region", paper in the same volume.

2) M. Blann and J. Bisplinghoff: COO-3494-27 (1975).

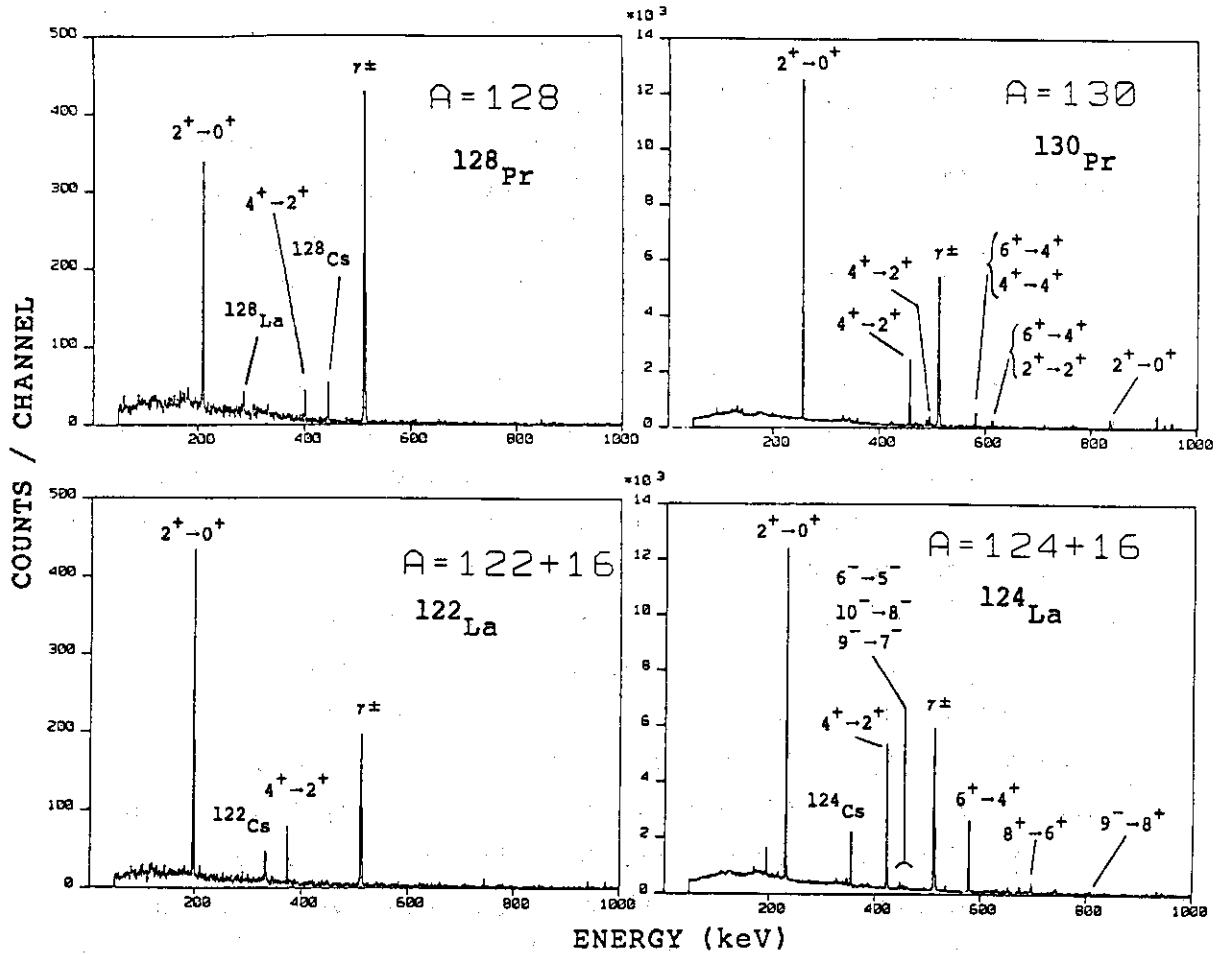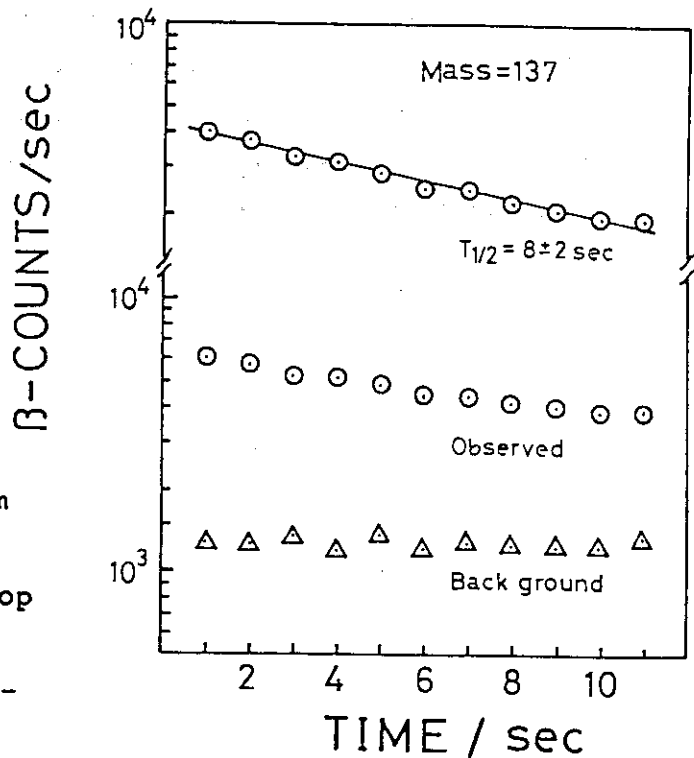3) K. Takahashi, M. Yamada and T. Kondoh: At. Nucl. Data Tables 12 (1973) 101.

Fig.1   β-coincident γ-ray spectra obtained at A=128 and 130 in the reaction ^{32}S + ^{103}Rh, and at A=138 and 140 in the reaction ^{32}S + ^{nat}Mo.

Fig.2   β time spectrum obtained at A=137 (^{121}LaO$^+$). At the top the spectrum corrected for the backgound is plotted.

4.5   PROTON INDUCED FISSION OF ACTINIDE ELEMENTS

Tsutomu OHTSUKI,   Keisuke SUEKI,   Yuichi HATSUKAWA,

Hiromichi NAKAHARA, Masaaki MAGARA[*], Nobuo SHINOHARA[*],

and Yuichiro NAGAME[**]

Department of Chemistry, Tokyo Metropolitan University

* Department of Chemistry, JAERI, ** Department   of

Radioisotopes, JAERI

Introduction

Since the discovery of fission nearly half a century ago, mass yield curves of various low energy fissions of actinides have been investigated by many workers. However, no theory has yet been successful in explaining the mass-division phenomena even partially.

Recently, we made a systematic study of mass yield data reported for thermal-neutron-induced fissions and spontaneous fissions and found that the full width at the half maximum height(FWHM) of the heavier asymmetric mass-yield peak increased slowly as the mass number of the fissioning nuclide(A_f) became larger. This trend can be qualitatively understood by the statistical argument of the increased number of freedom for mass division for the large fissioning mass.

But the smooth increasing trend of FWHM was found to decrease suddenly at around A_f=240, reaching minimum at A_f=245, and, then, to keep increasing again. This gap in FWHM around A_f=240-245 is clearly observed for thermal-neutron-induced fissions but not for spontaneous fission due to no report on the spontaneous fissions of A_f<238 that have extremely long partial half lives. The sudden gap is hardly understood by the smooth trend of the liquid drop model and may reveal the importance of the shell effects of either the fissioning nuclide or of the final fragments, or of both, on the mass division.

The aim of the present study is to find if a similar gap can be observed in proton-induced fissions of actinides, namely, in fissions of higher excitation energy. In the past, mass yield curves were studied only for (^{232}Th+p)[1], (^{237}Np+p)[2], and (^{238}U+p)[3]. Therefore, in this work, we carried out the mass yield study of proton-induced fissions of ^{235}U, ^{242}Pu, ^{244}Pu, and ^{243}Am at the incident energy of 12 MeV.

Experimental procedure and data analysis

Enriched isotopes of ^{235}U, ^{242}Pu, ^{244}Pu and ^{243}Am were purified from fission products by anion exchange in HCl media, and then, from other actinides by the nitric acid-methanol cation exchange method. The isotopic composition of each target was as follows: ^{243}Am target - ^{243}Am 99.612%, ^{241}Am 0.107%, ^{244}Cm 0.281%; ^{242}Pu target - ^{242}Pu 99.849%; ^{244}Pu target - ^{244}Pu 97.89%, ^{239}Pu 0.03%, ^{240}Pu 0.68%, ^{241}Pu 0.07%, ^{242}Pu 1.33%.

After the purification steps, the acid was removed, and the target materials were dissolved in isopropyl alcohol for the electrodeposition on a 10 mg/cm^2 Al foil with the condition of 500 V, 2mA/cm^2 for 30 minutes under cooling by circulation of water. The efficiency of electrodeposition was over 80% for all these elements and the thickness of each target was estimated by α-spectrometry to be about 100 μg/cm^2. Each target was wrapped with a sheet of Al foil thick enough to stop all fission products.

The bombardment was performed at a tandem accelerator of Japan Atomic Energy Research Institute (JAERI) with the beam current of about 1 μA at the proton energy of 12 MeV.

After bombardment, the targets were left for about 30 minutes for cooling, and γ-ray activities were measured directly with a Ge(Li) detector equipped with a 4096 channel pulse height analyzer for the determination of cross section of fission products.

Results and Discussion

Mass yield curves were constructed from the observed cross section of each fission product. The cumulative yield for each isobaric chain was estimated with an assumption of a gaussian charge distribution with the most probable charge Z_p of the unchanged charge distribution model. The gaussian width parameter of 0.95 was used as suggested by J. A. McHugh et al.[4]. The constructed mass yield curves are shown in Fig. 1. All the mass yield curves are mostly asymmetric and similar to those of thermal-neutron induced and spontaneous fissions in the actinide elements. However, some details of these mass yield curves are different from each other. The ^{235}U+p fission give broad asymmetric peaks while ^{242}Pu+p and ^{244}Pu+p fissions result in sharper asymmetric peaks. Total fission cross sections are much large for the ^{242}Pu+p and ^{244}Pu+p systems than for the ^{235}U+p and ^{243}Am+p systems, that suggests larger Γ_f/Γ_n values for the former fission systems. Weighted means of peak masses of the asymmetric mass yield curves are shown in Fig. 2 together with literature values reported for other

fission systems. The mean mass of the heavier asymmetric products varies only slightly over the broad mass range of the fissioning nuclide A_f, whereas the mean mass of the lighter products increases substantially with increasing A_f. A similar tendency is also observed for thermal-neutron induced fissions and spontaneous fissions.

The FWHM of the asymmetric mass yield peaks observed in this work are shown with filled squares in Fig. 3 as a function of the fissioning mass A_f. Also shown are FWHM values estimated from mass yield curves reported previously for thermal-neutron induced fissions (open circle), spontaneous fissions (open triangles) and for proton-induced fissions (open squares). The sudden decrease of the FWHM for A_f=240-245 observed in the thermal-neutron induced fissions is also clearly seen in the proton-induced fissions investigated in this work. It has to be pointed out, however, that in (^{235}U+p), (see Fig. 1), and similarly in (^{232}Th+p), (^{237}Np+p), and (^{238}U+p), the yields of symmetric mass divisions which are known to show quite different incident-energy dependence are so large that they may have caused an erroneous estimation of the FWHM values for these fission systems. The effect of symmetric mass divisions on the estimation of the FWHM of the asymmetric mass yield peak will be investigated in future by observing incident energy dependence . Sudden decrease of the FWHM observed in this work suggests that the influence of shell effects on final mass divisions is still persistent in the fission of a compound nucleus with the initial excitation energy of 16-17MeV.

Reference

1) H. Kudo, H. Muramatsu, H. Nakahara, K. Miyano, and I. Kohno, Phys. Rev. C25, 3011 (1982).

2) to be published.

3) to be published.

4) J. A. McHugh and M. C. Michel, Phys. Rev. 172, 1160 (1968).
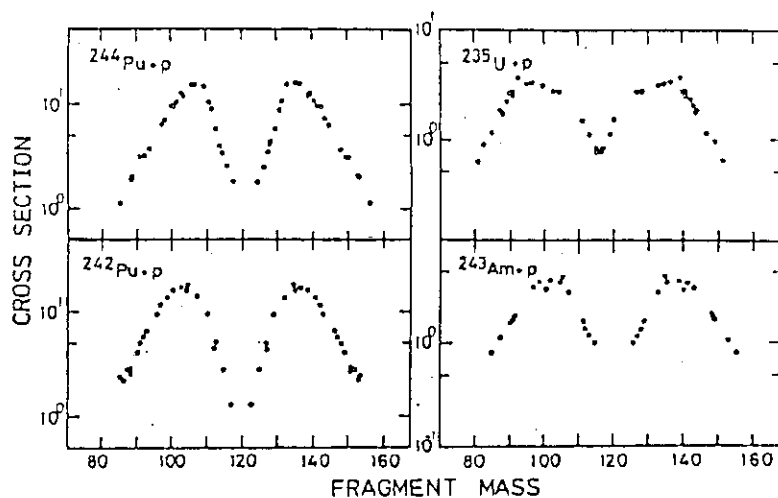
Fig. 1
Mass yield curves of
proton induced fissions
of ^{244}Pu, ^{242}Pu, ^{235}U
and ^{243}Am

Fig. 2
The weighted mean mass
number of asymmetric
mass yield peaks
observed for the proton
fission of a fissioning
nuclide A_f at the
excitation energy of
16-17 MeV
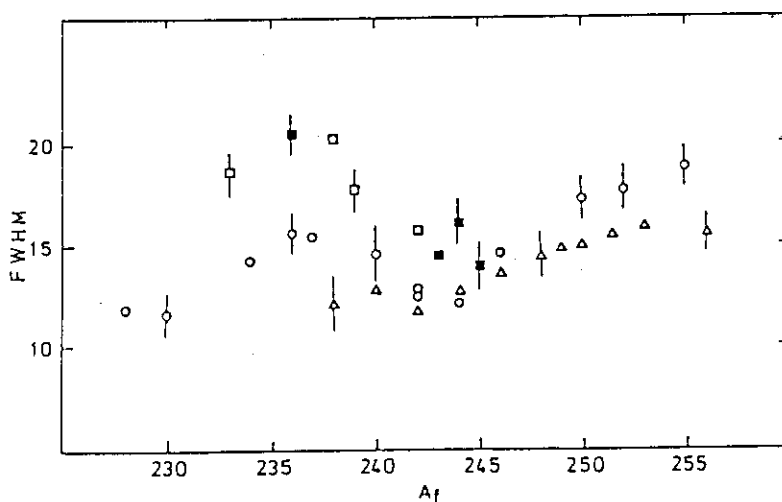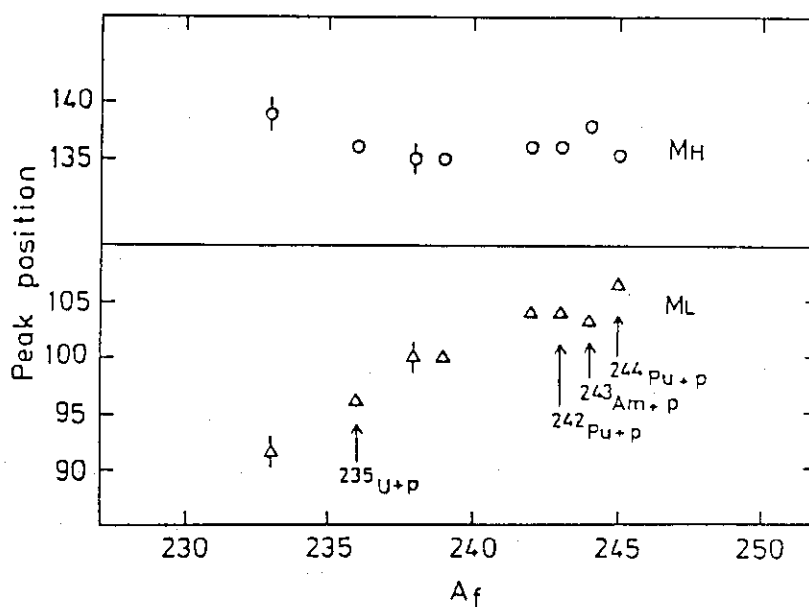
Fig. 3
The FWHM of asymmetric
mass yield peaks in
various fissioning sys-
tems plotted as a func-
tion of fissioning
nuclide A_f. O ,thermal
-neutron induced fission
□ ,proton induced fission
reported in the past; ■ ,
observed in this work
△ , spontaneous fission.

4.6 STATISTICAL DECAY OF THE ^{105}Ag COMPOUND NUCLEUS

Yuichiro NAGAME, Akihiko YOKOYAMA[***], Yuichi HATSUKAWA[****], Masaaki MAGARA[*], Hiromitsu MATSUOKA, Kentaro HATA, Shin-ichi ICHIKAWA[*], Toshiaki SEKINE, Sumiko BABA and Kazumi IDENO[**]

Department of Radioisotopes, [*]Department of Chemistry and [**]Department of Physics, JAERI, [***]Department of Chemistry, Osaka University, [****]Department of Chemistry, Tokyo Metropolitan University

There are some characteristic features on decay properties of a highly excited compound nucleus at a high angular momentum in the relatively light or medium mass region($A \lesssim 100$): i) formation of evaporation residues following multi-nucleon emissions including charged particles and ii) the possibility of symmetric fission[1,2] . With respect to the former, we have studied previously[3] the decay properties of the compound nucleus ^{105}Ag in the reactions of ^{37}Cl+^{68}Zn and ^{12}C+^{93}Nb. Isomeric yield ratios and recoil ranges were measured on the ^{99}Rh nuclei produced through (HI,α2n) and (HI,2p4n) channels. The present work is to extend the study to a broad range of products and to the fission process by using activation techniques as well as in-beam particle spectroscopy.

The ^{105}Ag(Z=47) compound nucleus was formed in the range of excitation energy (60MeV$\lesssim$E$_{CN}^{*}$$\lesssim$110MeV) from both the entrance channels. The ^{37}Cl and ^{12}C beams produced by the JAERI tandem accelerator were impinged on targets of ^{68}Zn($\sim$300μg/cm^2) and ^{93}Nb($\sim$3mg/cm^2), respectively.

The eighteen evaporation channels were measured by off-line γ-ray spectrometry and the products(Z=42-46) following multi-nucleon emissions were observed in both the reaction systems. The experimental excitation functions of the product nuclides were compared with those from statistical model calculations. The typical data of the products, ^{99}Pd(Z=46), ^{99m}Rh(Z=45) and ^{97}Ru(Z=44), are shown in Figs.1(a) to 1(c), respectively. The solid and dashed lines are the

calculated values by using ALICE code[4] which uses the Weisskopf-Ewing formalism in evaporation process, for the reactions of $^{37}Cl+^{68}Zn$ and $^{12}C+^{93}Nb$, respectively. The amount of the angular momentum removed by a particle emission is not followed rigorously in the calculation and, instead, it is assumed that each evaporated proton and neutron changes the angular momentum of a residual nucleus by $1\hbar$ and each alpha particle by $4\hbar$. As shown in Fig.1, the data of ^{97}Ru and ^{99m}Rh are relatively well reproduced by this calculation. On the other hand, it is not possible to get an agreement with this method in the production of ^{99}Pd. The detailed analysis of the data is in progress to investigate the angular momentum effects in exit channels by means of a Hauser-Feshbach code[5] which uses the more rigorous procedure for angular momentum coupling at each state of deexcitation.

The further experiment to study the symmetric fission and the complex fragment emission(mass-asymmetric decay) [6-8] is also under way using the gas ΔE-E counter telescopes.

References

1) S. Cohen et al.: Ann. Phys.(N.Y.), 82(1974)557.

2) H. J. Krappe et al.: Phys. Rev. C20(1979)992.

3) T. Sekine et al.: JAERI TANDEM, LINAC & V.D.G.,
   Ann. Rep. (1985)p.143

4) F. Plasil: ORNL/TM-6054(1977).

5) A. Gavron: Phys. Rev. C21(1980)230.

6) L. G. Moretto: Nucl. Phys. A247(1975)211.

7) L. G. Sobotka et al.: Phys. Rev. Lett. 51(1983)2187.

8) M. A. McMahan et al.: Phys. Rev. Lett. 54(1985)1995.
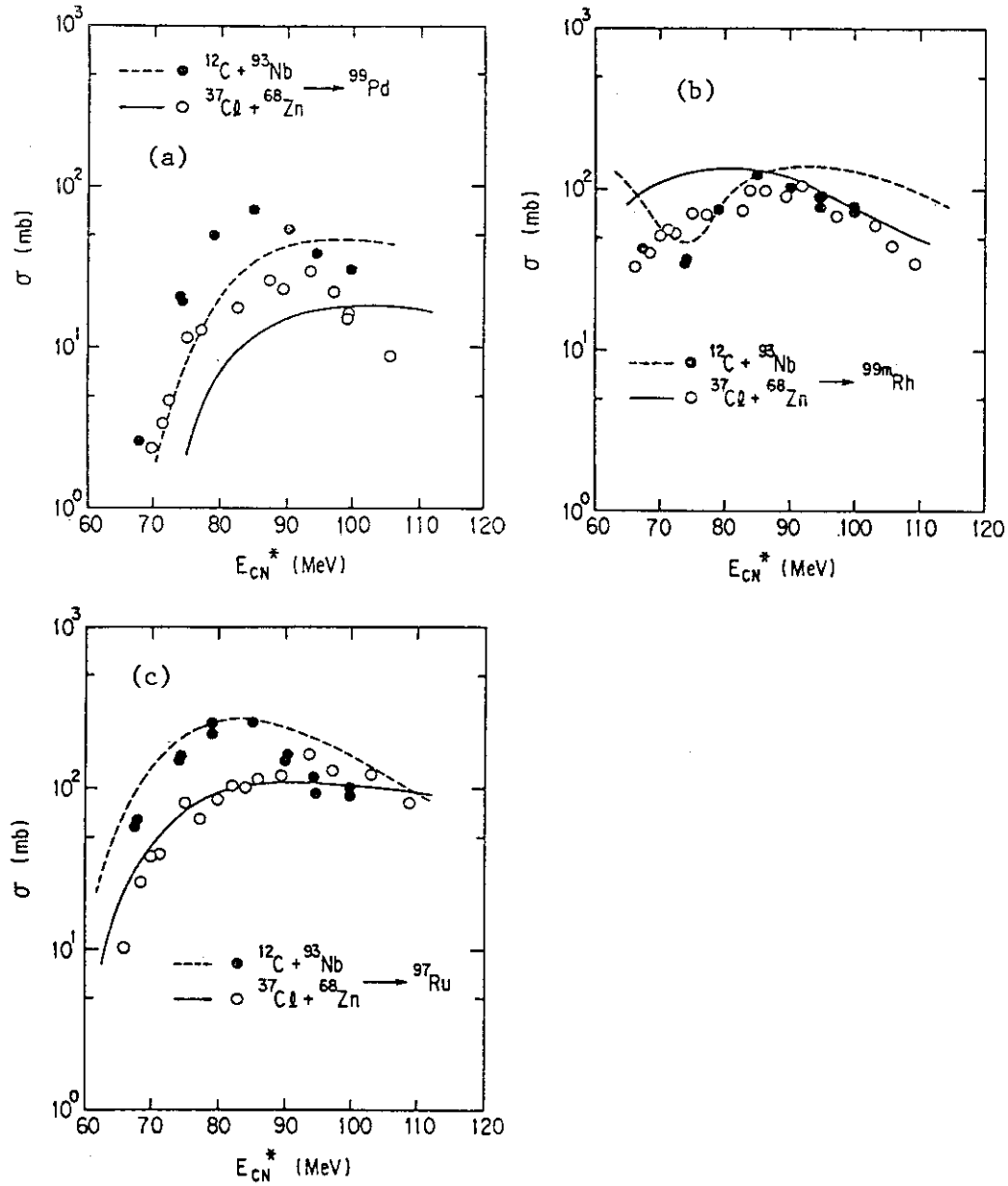
Fig.1 Comparison between experimental excitation functions and statistical model calculations by ALICE code[3] for the products (a) ^{99}Pd, (b) ^{99m}Rh and (c) ^{97}Ru.

4.7 MEASUREMENT OF FISSION FRAGMENT ISOTOPIC DISTRIBUTION BY ISOL

Sumiko BABA, Toshiaki SEKINE, Kentaro HATA, Yuichiro NAGAME, Shin-ichi ICHIKAWA[*], Hiroshi BABA[**], Naruto TAKAHASHI[**], Akihiko YOKOYAMA[**] and Ming-Jinn Duh[**]

Department of Radioisotopes, [*]Department of Chemistry, JAERI, [**]Faculty of Science, Osaka University

In recent years, the fission fragment yields in various nuclear systems have been measured with high accuracy by means of a mass spectrometer. An on-line mass spectrometer enables us to measure the independent yields of short-lived nuclides. It is hoped that the mass spectrometric results will help to clarify the mechanism of charge distribution in fission. Nevertheless, only a few experiments have been done by the on-line mass spectrometry on the heavy ion induced fission.[1] We attempted to collect the basic data for the purpose of measuring the fission fragment yields by the ISOL at JAERI. Though we have obtained the data on the behavior of several elements which are produced as evaporation residues in heavy ion reaction and implanted into the ionization source of the ISOL, there were no data measured on fission fragments.[2] At first we need to know the hold-up time of the fission fragments in an ionization source and the efficiency of transportation from target to collection tape.

A target was prepared by electrodeposition of 2.0 mg/cm^2 ^{238}U onto a 5 μm Ta foil. The target was bombarded with 100 MeV ^{12}C from the tandem accelerator at JAERI. The fission fragments were ionized in the surface ionization source. The ions were mass-separated in an analyzing magnet and finally deposited onto an aluminized tape. After the ions were collected during certain period the tape was moved to a counting position where a Ge detector was placed. On-line gamma and X-ray measurements were done. Two kinds of isotopes, ^{86m}Rb produced from ^{181}Ta + ^{12}C system and ^{136m}Cs from ^{238}U + ^{12}C, were used to measure the hold-up time in the ion source. We observed experimentally how the yield of a given isotope fall off with time after the ^{12}C beam

was switched off.

In this experiment the gamma-rays from the Cs isotopes of A = 130, 136 and 138 were observed. Furthermore, the IT gamma-ray (517 keV) from the ^{136m}Cs was measured and half-life of the isomer, $T_{1/2} = 17 \pm 2$ sec was obtained. This half-life agrees with that in literature.[3] In Fig.1 delay curves are shown for ^{86m}Rb and ^{136m}Cs. No contribution from the parent nuclide is considered in both isotopes since they are shielded nuclides. In Fig.1 the straight line defines an exponential $e^{-\mu t}$, where $\mu = \lambda^* + \lambda$, λ^* is delayed "decay constant" and λ is decay constant. An average delay time $t_{1/2} = 1/\lambda^*$ can be obtained by the analysis of the straight line. The delay times obtained for ^{86m}Rb and ^{136m}Cs are shown in Table 1 together with another experimental results[2] which were obtained for the isotopes produced by evaporation of particles from the compound nucleus. It is found that the delay time of isotopes originated in fission is longer than that of evaporation residues. A long delay time of fission fragments may be attributable to their large kinetic energies. This results show that the fission fragments of the half-life longer than a few second can be measured in the present system.

References

1) M. S. Simon, S. Haam, G. Audi, A. Coc, M. Epherre, P. Guimbal,
   A. C. Mueller, C. Thibault, T. Touchard and M. Langevin,
   Phys. Rev. C 26(1982) 2477.
2) S. Ichikawa, T. Sekine, M. Oshima, K. Hata, N. Shinohara and
   N. Takahashi, JAERI-M 86-112 (1986) 115.
3) H. L. Ravn, S. Sundell, L. Westgaard and E. Roeckl,
   J. Inorg. Nucl. Chem. 37(1975) 383.

Table 1   Average delay time $\bar{t}_d$ of alkali and alkali earth
elements in the surface ionization source

Element	Production	
	Fission *	Evaporation**
Rb (^{86m}Rb)	37 ± 5 sec	
Cs (^{136m}Cs)	9 ± 1 sec	
(^{122}Cs)		3 sec
Ba (^{122}Ba)		1 sec

*These values were obtained in this work

**These were quoted from reference (2)
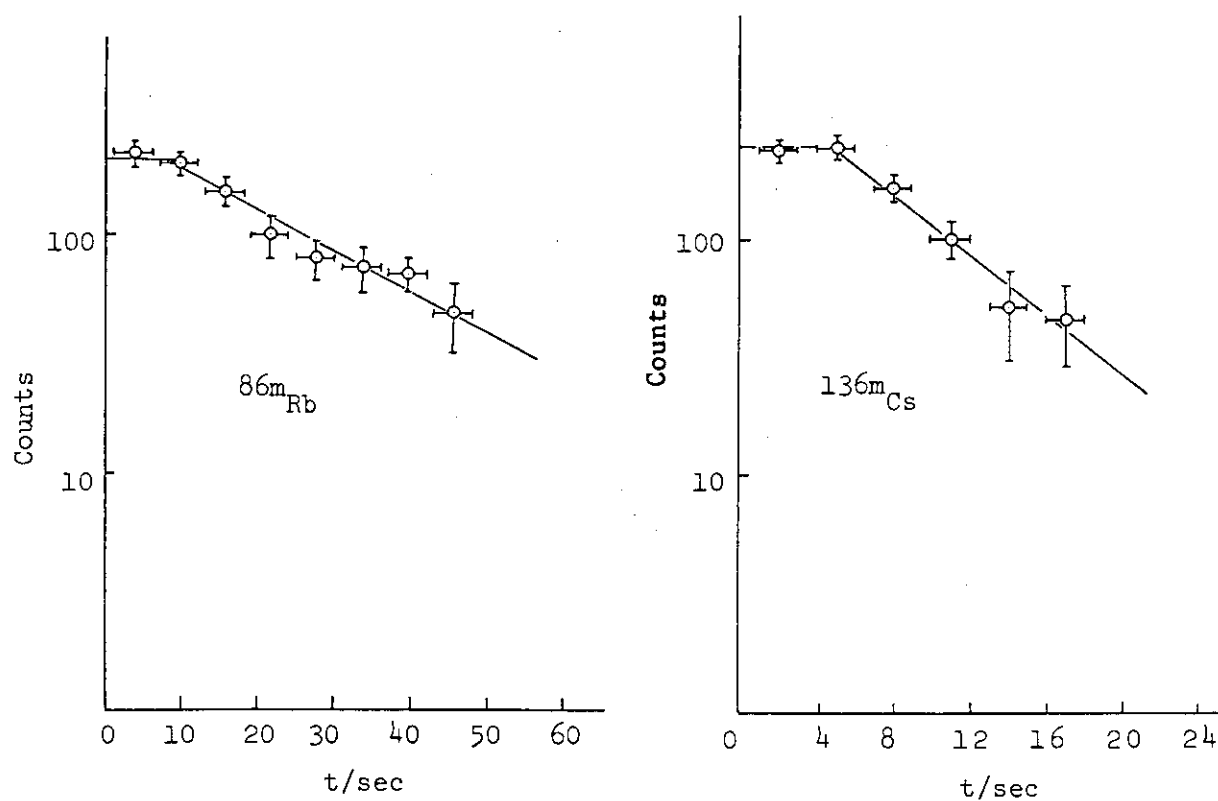
Fig. 1   Delay curves for ^{86m}Rb and ^{136m}Cs

4.8 NEUTRON TRANSFER REACTION IN THE SYSTEM ^{37}Cl + ^{103}Rh

Sumiko BABA, Kentaro HATA, Toshiaki SEKINE, Yuichiro
NAGAME and Akihiko YOKOYAMA

Department of Radioisotopes, JAERI

In nucleon transfer reactions induced by heavy ions, two characte-
ristic processes are observed: the deep-inelastic transfer (DIT) and
quasi-elastic transfer (QET) reactions. These two reactions differ
from one another in several features of process. One of them is degree
of dissipation of orbital angular momentum of reaction. This diffe-
rence is expected to result in products in different spin states. In
general it is considered that the dissipation in DIT reaction is larger
than that in QET reaction and that nuclei in higher spin states will
be preferably produed in DIT reaction.[1,2] To test the possibility of
discriminating between those two transfer reactions by observation of
behaviors of nuclear isomers, we carried out a radiochemical experi-
ment on the neutron transfer reaction in ^{103}Rh + ^{37}Cl system. This
reaction system was chosen because Rh products in neutron transfer
include some pairs of high and low spin isomers.

Formation cross sections and differential recoil ranges of Rh iso-
topes were measured. The mean energies of ^{37}Cl projectile in Rh
targets (0.5 mg/cm^2) were 166, 178 and 198 MeV. The formation cross
sections of Rh isotopes were determined with an experimental method
described in the previous report.[1] To obtain differential recoil
range, a stacked target consisting of a Rh foil and four Au catcher
foils(2mg/cm^2) was bombarded and radioactivity distributions for Rh
products in foils were measured.

The cross section ratios of high spin isomer to low spin isomer
are plotted in Fig.1. Only lower limits are given for ^{99}Rh, because
the yields of ^{99g}Rh (low spin) were less than the limit of detection.
As the figure shows, the yield of low spin isomers rapidly decreases,
compared to that of high spin isomers, as number of transferred

nucleons from the target nuclide increases. It suggests that the low spin isomers are produced chiefly in fewer nucleon transfer reactions. In Fig.2 distributions of some Rh isotopes in target and catcher foils are presented. The solid arrows indicate average recoil ranges. The broken arrows show calculated recoil ranges for a target-like nucleus elastically scattered by a grazing projectile. For the low spin-isomers, ^{102m}Rh(2-) and ^{101g}Rh(1/2-), observed average recoil ranges corresponded to the calculation. On the other hand, the high spin isomers had the shorter ranges, which may be due to emission angles more backward than those in grazing and/or due to kinetic energies less than those in elastic scatter. From the results shown in Fig.1 and Fig.2, it is concluded that high spin isomers are produced through deeper interactions between target and projectile than low spin isomers.

References

1) J. V. Kratz et al. : Nucl. Phys. A357 (1981) 437.

2) K. Hata et al. : JAERI-M 85-104(1985),p.135.

3) S. Baba et al. : JAERI-M 86-112(1986),p.113.
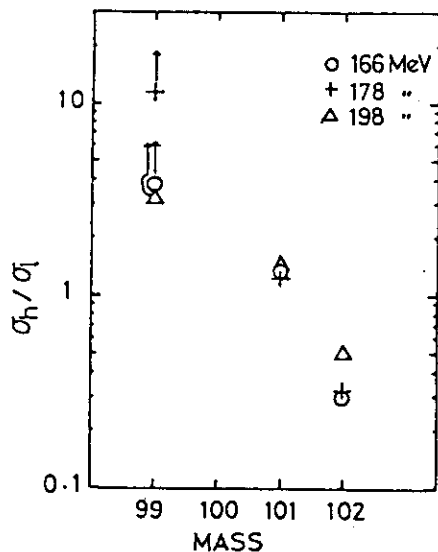
Fig.1 Isomer ratios of Rh isotopes
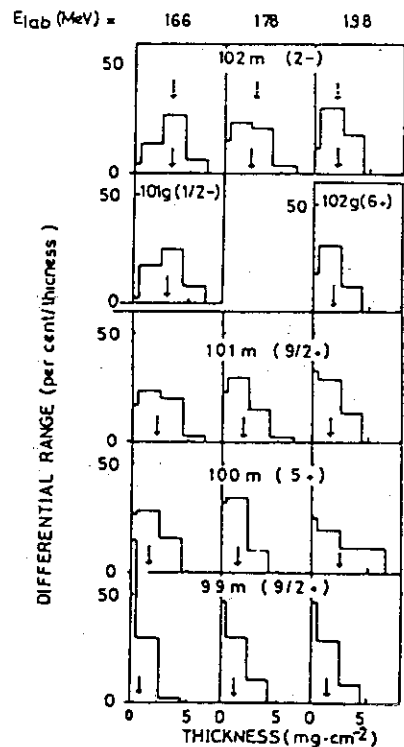
Fig.2 Differential recoil ranges for isomers of Rh isotopes

4.9   NUCLEON TRANSFER REACTION OF THE ^{16}O + ^{197}Au
      SYSTEM IN THE ENERGY REGION BELOW 10-MeV/u

Kentaro HATA, Yuichiro NAGAME, Toshiaki SEKINE,
Sumiko BABA, Sin-ichi ICHIKAWA[*], Akihiko
YOKOYAMA[**], Hiroshi BABA[**], Tadashi SAITO[**],
Atsushi SHINOHARA[**], Satoshi WAKAMATSU[**]

Department of Radioisotopes, [*]Department of
Chemistry, JAERI, [**]Faculty of Science, Osaka
University

Nucleon transfer reactions were studied on ^{197}Au with
6.6-MeV/u and 8.8-MeV/u ^{16}O ions and the results were analyzed
as a nuclear relaxation process. The relaxation process was
treated by a diffusion model[1] and a sum rule model[2]. Details
of experiments were described in our previous report[3].

Fig.1 shows the most probable value and width of the dis-
tribution of particle kinetic energy as a function of the
atomic number of emitted particle. In Fig. 1 the energy of
isotope with the maximum cross section of each element emitted
with the identical velocity of the projectile is given with
solid lines for the two incident energies; those are the upper
limit of energy for non-dissipative process. A dashed line
represents the exit Coulomb repulsion energy between two
touching spheres in the complete damping of the incident
kinetic energy; that corresponds to the lower limit of energy.
One has to note that the dissipation of kinetic energy is in-
complete in the case of larger atomic numbers or higher inci-
dent energies. In addition, the width of the kinetic energy
distribution increased with decreasing atomic number.

Figure 2 shows the isotopic cross sections observed in
the reaction with 8.8-MeV/u, and the N/Z ratio of isotope with
the maximum cross section of each element in comparison with
the N/Z ratio of composite system. The figure also shows that
equilibration of N/Z was not attained in the system. We plot
in Fig.3 the isotopic differential cross sections obtained at

27° in the laboratory system in the reaction of 8.8-MeV/u as a function of Q_{gg}. It is seen that isotopes Z = 2 to 7 obey the Q_{gg} systematics[4]. The slopes of straight lines drawn through the isotopic cross sections are very close to one another. The results in Fig. 3 may be interpreted as that the product nuclides are produced via a hot zone at the same nuclear temperature.

Fig.4 shows angle-integrated element distributions. The open circles give the experimental cross sections, and the solid lines and histograms represent the calculated cross sections by use of the diffusion model and those by the sum rule model, respectively. The sum rule model reproduced the experimental cross sections better than the diffusion model. It may be ascribed to a fact that the sum rule model takes into consideration the Q_{gg} dependence which is clearly observed in the isotope cross sections.

From the analysis described above, we conclude that the nucleon transfer reactions might occur rather in the partial equilibration than the diffusion process.

References

1) G. Wolschin and W. Nörenberg, Z. Phys. __A284__ (1978) 209; S. Agarwal, Z. Phys. __A297__ (1980) 41.

2) J. Wilczyński et al, Nucl. Phys. __A373__ (1982) 109.

3) K. Hata et al., JAERI TANDEM LINAC & V. D. G. Annual Report 1985, JAERI-M 86-112 (1985) p109.

4) V. V. Volkov, Phys. Rept. __44__ (1978) 93.

5) S. Wald et al., Phys. Rev. __C32__ (1985) 894.
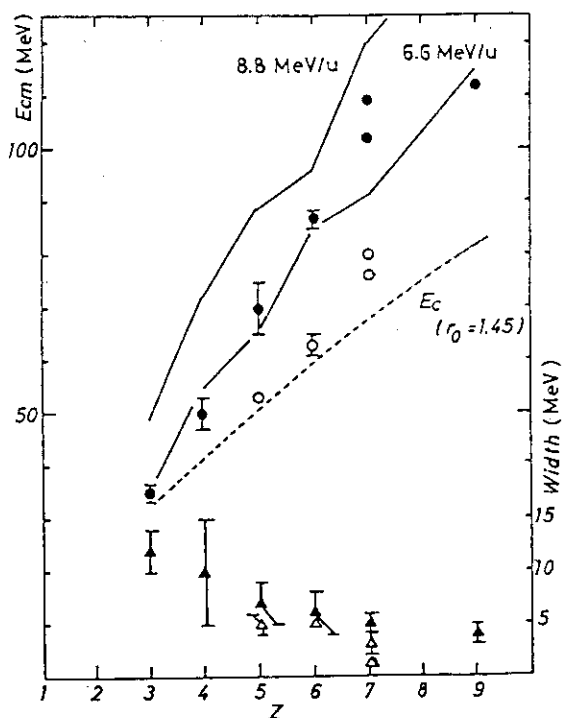
Fig. 1 Most probable value and width (FWHM) of the distribution of particle kinetic energy are plotted with circles and triangles, respectively. The open symbols represent experimental values for 6.6-MeV/u and the closed ones are those for 8.8-MeV/u. Explanation of lines is given in the text.
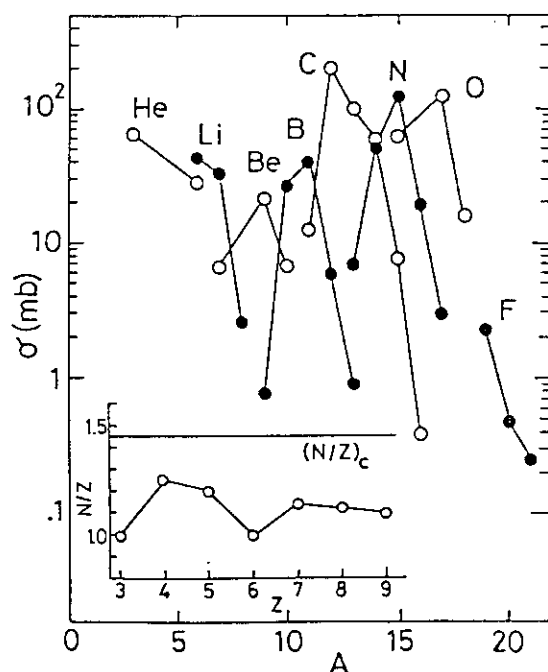
Fig. 2 Distribution of the isotope cross section and the N/Z ratio of isotope with the maximum cross section of each element in the 8.8-MeV/u $^{16}O+^{197}Au$ reaction.
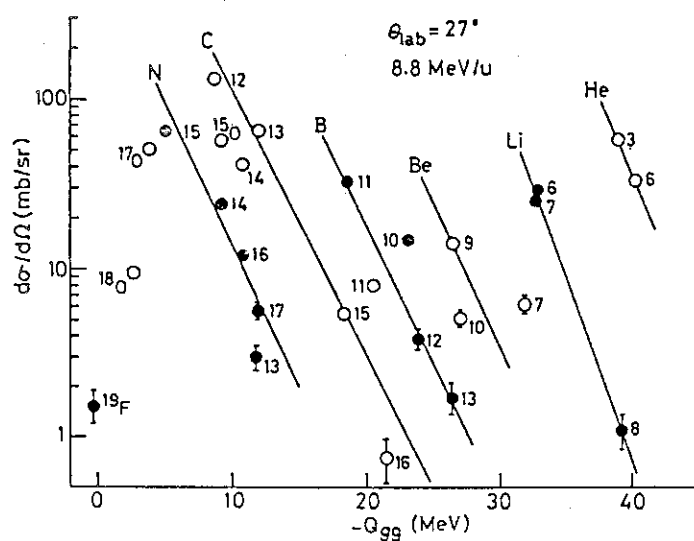
Fig. 3 Q_{gg} dependence
of isotope differential
cross sections in the
8.8-MeV/u $^{16}O + ^{197}Au$
reaction at 27° in lab.
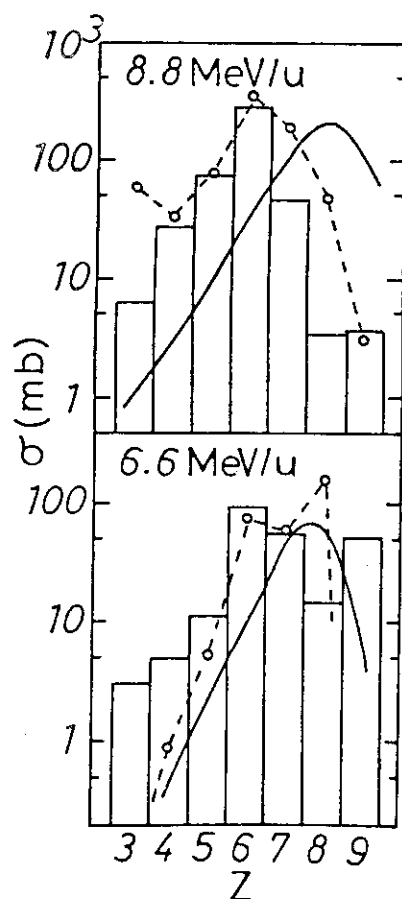
Fig. 4 Distributions of
elements in the reactions
of 8.8-MeV/u (top) and
6.6-MeV/u (bottom) $^{16}O + ^{197}Au$.

4.10   PREPARATION OF ^{211}Rn-^{211}At GENERATOR SYSTEM
       FROM ^{209}BI IRRADIATED WITH ^{14}N.

Hiromitsu MATSUOKA, Sumiko BABA, Kentaro HATA,
Yuichiro NAGAME, Takashi MORIYA, Mishiroku
IZUMO and Takami SORITA

Department of Radioisotopes, JAERI

A production method of an α-emitting astatine isotope ^{211}At   has been studied by using the ^{209}Bi(^{14}N,X)^{211}Rn-^{211}At reaction.   The formation cross-section and thick-target yield of ^{211}Rn were obtained in the previous work[1].

In this work, we tried to develop the ^{211}Rn-^{211}At generator system.   Thick targets of bismuth oxide were prepared as follows: About 1g of Bi_2O_3 powder was mixed with 0.5 ml ethylalcohol and prepared in a pellet of 15 mm in diameter and $\sim$ 500 mg/cm^2 thick under a pressure of 2 ton/cm^2.Then the pellet was heated to 800 ℃ to make sintered Bi_2O_3. Fig.1 shows a target assembly that consists of: (1) a Ti-foil window , (2) a water-cooled target holder acted as Faraday cup, and (3) the target fixed on the water-cooled taget holder with a collar ring. The face of the target was cooled by a flow of He gas at 1atm. Bombardments were performed at the JAERI tandem accelerator with an incident energy of 84Mev for 7 hours. The average beam current was monitored by a current integrator connected to a Fraday cup, being $\sim$ 100 enA.

After irradiation the target was heated to 900 ℃ in a quartz tube under a flow of He gas. Radon gas released from the target was passed through a silver wool trap which is used to remove other radiohalogen impurities formed in the target,and introduced to a charcoal(20-40 mesh) trap cooled with liquid-nitrogen.   After 14 hours, ^{211}At generated from decay of ^{211}Rn was extracted by dry distillation in a He carrier gas from the charcoal trap at 600 ℃ and transferred to a mixture of sodium hydroxide solution(100 mmol) and sodium sulphite solution (10 mmol). The radiochemical purity of ^{211}At

was determind by α - and X-ray spectrometry.

The overall radiochemical yield of ^{211}At was about 50 %, and no radiohalogen impurity in the solution was observed. Improvement of the distillation apparatus is in progress to increase the recovery of ^{211}At.

Reference

1) H.Matsuoka, S.Baba, K.Hata, Y.Nagame, T.Moriya, T.Moki, M.Izumo and T.Sorita : JAERI-M 86-112 (1986) 120.
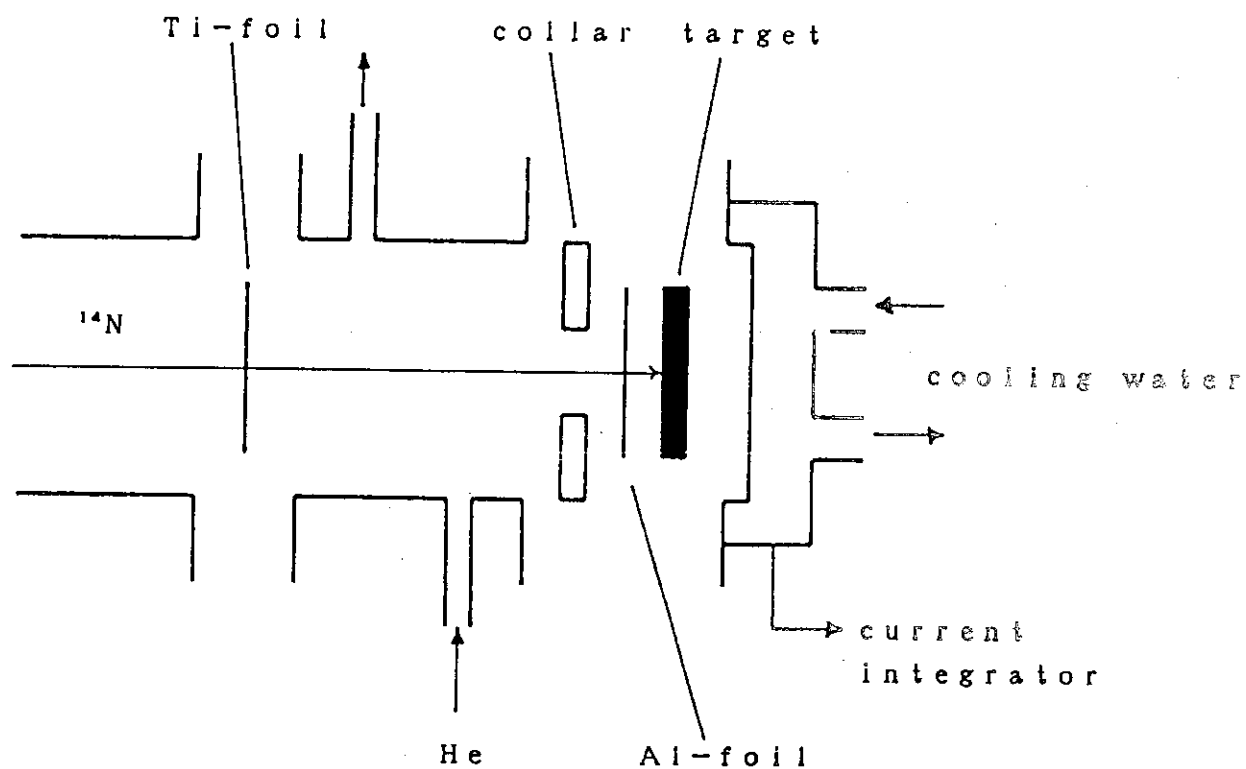
Fig. 1 Target assembly

Ⅴ　NUCLEAR　PHYSICS

5.1 TRANSFER CROSS SECTION FOR ^{16}O + ^{148,152}Sm NEAR THE COULOMB BARRIER

Yasuharu SUGIYAMA, Yoshiaki TOMITA, Hiroshi IKEZOE, Kazumi IDENO, Norihisa KATO[*], Tsuyoshi SUGIMITSU[*] and Hiroshi FUJITA[**]

Department of Physics, JAERI, [*]Department of Physics, Kyushu University, [**]Daiichi College of Pharmaceutical Sciences

The correlation between quasielastic reactions and the enhanced subbarrier fusion attracts much interest in heavy-ion reactions near the Coulomb barrier. In the quasielastic reaction cross sections measured for ^{28}Si+^{58,82}Ni, a strong isotope dependence has been observed[1]. The isotope dependence has been similar to the one of the subbarrier fusion cross sections[2]. Coupled-channels calculations have been carried out for Si+Ni fusion reactions[3]. A good overall agreement with the data has been obtained by including transfer cross sections whose magnitude is consistent with the experimental values.

In this report we describe results of the quasielastic reaction for the systems ^{16}O+^{148,152}Sm carried out at the JAERI tandem accelerator. The ^{16}O beam energy was 72 MeV which was about 10% higher than the Coulomb barrier. The energy spectra were measured with an energy resolution of ~200 keV by using the heavy-ion spectrograph[4] "ENMA". The entrance slit of the spectrograph had horizontal and vertical opennings of 6.9° which corresponded to a solid angle of 14.4 msr. Mass number, atomic number, Q value and atomic charge state q of reaction products were determined unambiguously from a measurement of the total energy E, energy loss δE and position Bρ. Six nuclei ^{17}O, ^{18}O, ^{15}N, ^{12}C, ^{13}C and ^{14}C were observed in addition to elastically scattered ^{16}O. Other reaction products could not be identified because of their small yields.

Energy spectra obtained at θ_{lab}=95° from the reactions ^{148}Sm(^{16}O,^{17}O)^{147}Sm, ^{148}Sm(^{16}O,^{15}N)^{149}Eu, ^{152}Sm(^{16}O,^{17}O)^{151}Sm and ^{152}Sm(^{16}O,^{15}N)^{153}Eu are shown in Fig.1. Angular
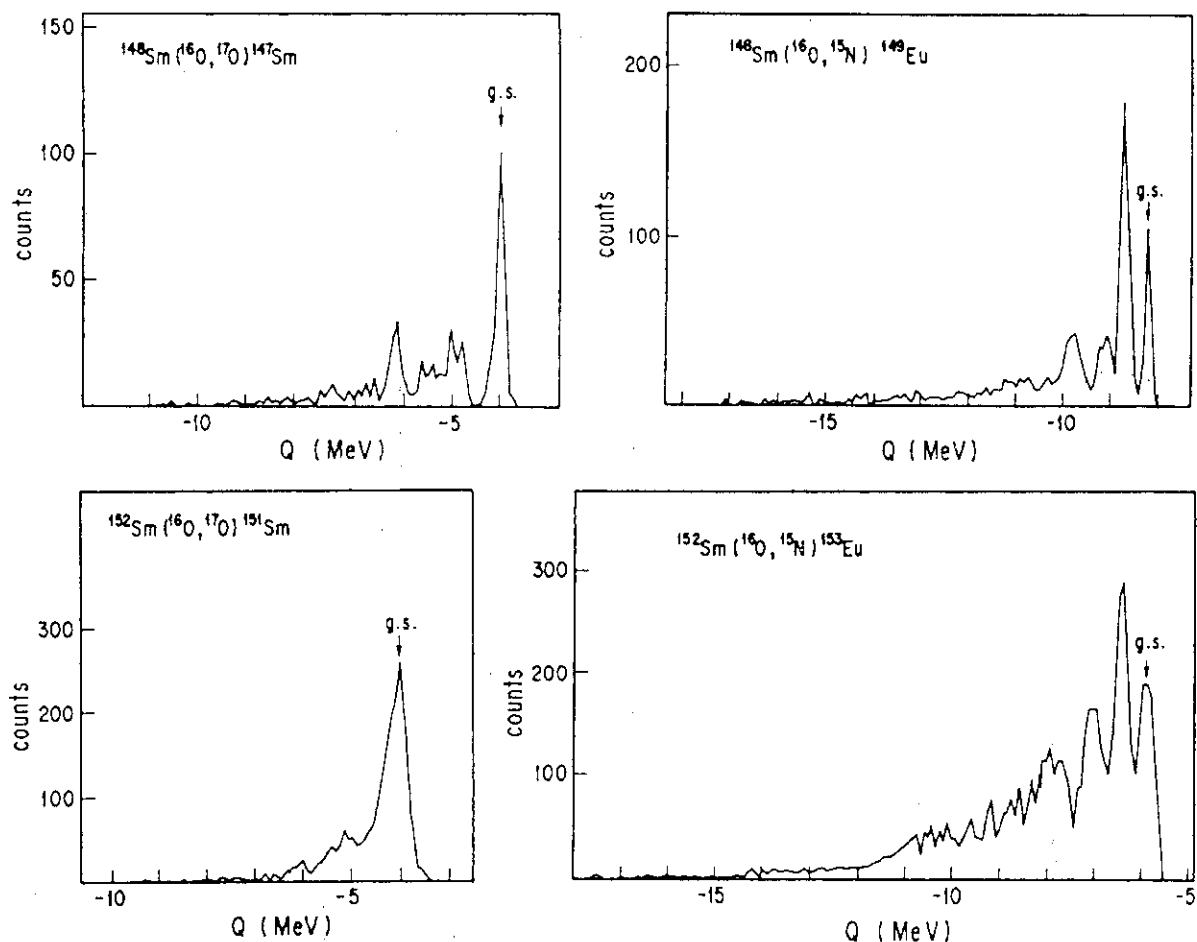
Fig.1 Spectra obtained from the (^{16}O,^{17}O) and (^{16}O,^{15}N) reactions on ^{148}Sm and ^{152}Sm at $\theta_{lab}=95°$.

distributions for these reactions are shown in Fig.2. In the reaction ^{148}Sm(^{16}O,^{17}O)^{147}Sm, the cross sections for the ground state transition (g.s.) and for energy-integrated excited state transitions (total) are plotted. In the reaction ^{152}Sm(^{16}O,^{17}O)^{151}Sm the angular distribution for the energy-integrated cross sections (total) is shown. Absolute values of the reaction cross sections were derived by normalizing the yields to those of the elastic scattering which were measured simultaneously. The absolute value of the elastic scattering cross sections was taken from the data by Weber et al.[5]

DWBA calculations for one-neutron pickup and one-proton transfer reactions were performed with the code Ptolemy. We used the optical potential parameters which were obtained through the coupled-channel analysis for the elastic scatter-ing[6]. For the spectroscopic factors we used the values

5.2 DETECTION OF THE ^{8}Be NUCLEUS FROM HEAVY ION REACTIONS

Kazumi IDENO, Yoshiaki TOMITA, Yasuharu SUGIYAMA,

Hiroshi IKEZOE, Susumu HANASHIMA and Yuichiro NAGAME*

Department of Physics, *Department of Radioisotopes, JAERI

In the heavy ion reactions fragments are generated with different excitations and spins so that it is not so easy to identify each fragment with definite quantities of these quantum numbers. For light unstable fragments, however, we can know their excitations and spins from the spacial and energy correlations of the decaying particles[1]. This is the case for the groundstate ^{8}Be nucleus, which decays into two alpha particles soon after ejected from the composite system. Since this nucleus is the simplest cluster of alpha particles, it will serve as a reference for the study of clustering effects in the complex heavy ion reactions.

For the detection of coincident alpha particles, we constructed a detector system in which two sets of two-dimensional position-sensitive detectors were installed at a close distance; drift chambers similar
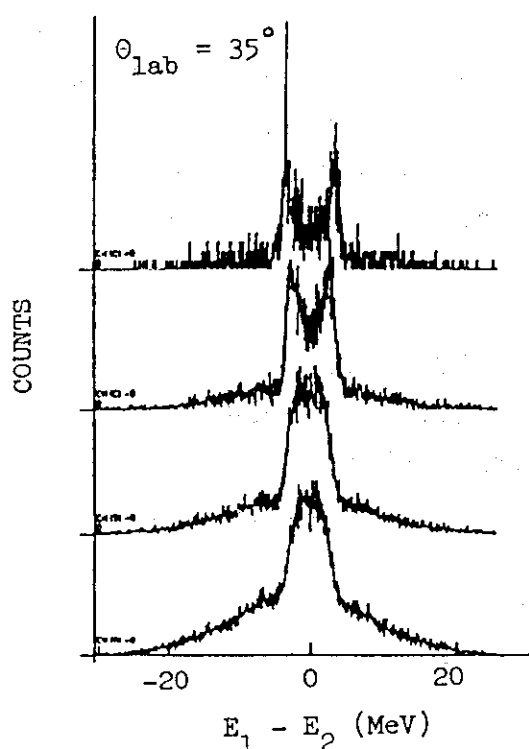
Fig. 1 Observed energy difference for the two coincident alpha particles for the system of ^{32}S + ^{64}Ni at 180 MeV. The average acceptance angle spanned between the two flying alpha particles varies from 3 to 11 degrees, correspondingly to the curves in the upper part of the figure to the lower ones.

to the one by Breskin et al.[2] were used as the ΔE counter and Si detectors with an area of 1600 mm^2 as the E counter. We operated the drift chambers with isobutane gas. We measured ^{8}Be fragments from the reaction of ^{32}S + ^{64}Ni, where the bombarding energy was 180 MeV. Fig. 1 shows the plot of the difference between the energies of two coincident alpha particles. It is seen that at Θ_{lab} = 35 degrees the two alpha particles decaying from the ^{8}Be groundstate fly into the cone with small angles. The yield of the groundstate ^{8}Be nucleus was measured to be as high as that of the ^{12}C nucleus. We are going to extend our measurement to a variety of 4N composite systems around A = 100.

References

1) S. Kubono: Preprint HMI-P 86/12 R (1986).

2) A. Breskin, I. Tserruya and N. Zwang: Nucl. Instr. and Methods 148 (1978) 275.

5.3 MASS DISTRIBUTIONS OF FISSION FRAGMENTS FROM THE ^{19}F- AND ^{32}S-INDUCED REACTIONS

Hiroshi IKEZOE, Naomoto SHIKAZONO, Yoshiaki TOMITA,
Yasuharu SUGIYAMA, Kazumi IDENO, Watalu YOKOTA,
Mitsuhiko OGIHARA[*], Hideaki FUJIWARA[*], S.C.JEONG[*],
S.M.Lee[*], and David J.HINDE[**]

Department of Physics, JAERI, [*]Tandem Accelerator center,
University of Tsukuba, [**]Research Center for Nuclear Physics,
Osaka University

Measurements have been made of the mass distributions of fission fragments from the ^{19}F- and ^{32}S-induced reactions. Targets of ^{154}Sm, ^{181}Ta, ^{197}Au, ^{208}Pb and ^{209}Bi were bombarded by ^{19}F ions with the beam energies from 100 to 161 MeV and by ^{32}S ions with the beam energies from 185 to 210 MeV. The product masses were determined by measuring the energies and the velocities of the fragments with a time-of-flight telescope[1]; the telescope consisted of a carbon-foil microchannel-plate detector for the start signal detection and a Si surface barrier detector for the stop signal detection.

The mass distributions for all fission reactions studied here showed a Gaussian-like shape centered at the half of the compound nucleus mass A_{CN} at low bombarding energies. As the bombarding energy increased, the mass centroids measured at the forward center-of-mass angles Θ_{CM} deviated gradually from the value of $A_{CN}/2$ for the ^{19}F-induced fission reactions. In Fig.1 we show the mass centroids for the ^{19}F + ^{197}Au reaction as a function of Θ_{CM} at various bombarding energies. At the higher energies the mass centroids obviously depend on the angle Θ_{CM}. This result contradicts the prediction of the complete fusion-fission reaction that the mass distribution of fission fragments is independent of Θ_{CM}.

Although the mass centroids for the ^{32}S-induced fission reactions agreed with the value of $A_{CN}/2$ and were independent of Θ_{CM}, the mass distributions showed asymmetric shapes as shown in Fig.2; at the forward angles the portion of light fragments tails in contrast to the symmetric mass distribution obtained at the more backward angles. This asymmetric component increases at the forward angles and deviates from the $1/\sin\Theta_{CM}$ angular dependence.

In order to confirm the present results, further measurements at the more backward angles are planned.
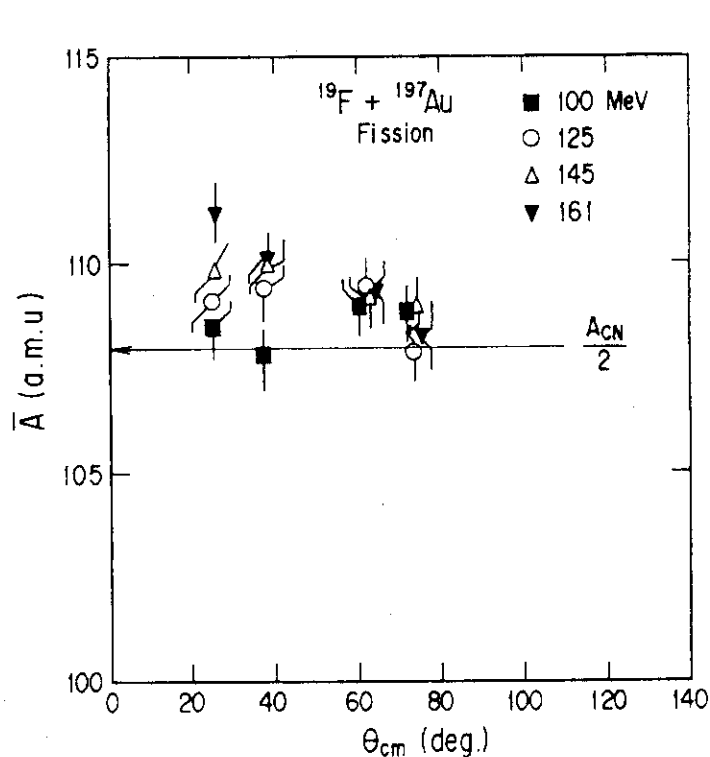
Fig.1 Mass centroids of the fission fragments as a function of center-of-mass scattering angle at various bombarding energies.
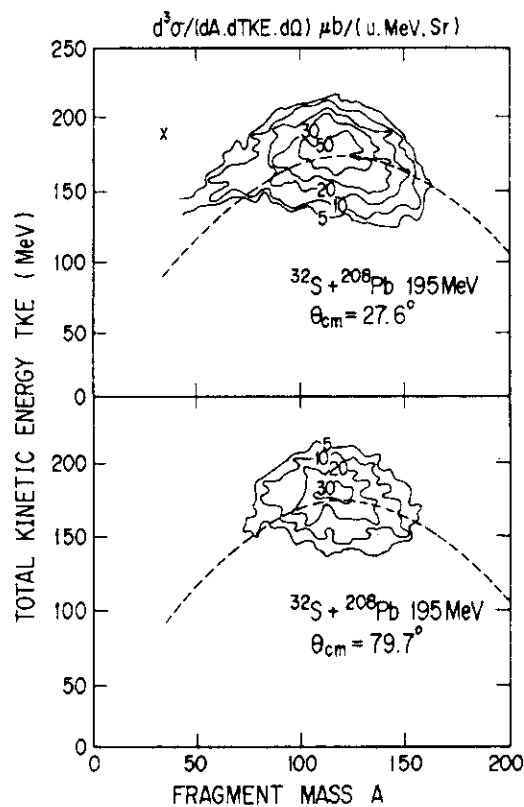
Fig.2 Contour plots of double-differential cross section as a function of total kinetic energy and fragment mass. The dotted lines are the Coulomb energies and elastic scattering is indicated by cross.

References

1) J. D. Bowman and R. H. Heffner: Nucl. Instrum. & Methods. 148 (1978) 503.

5.4 MULTIPLE COULOMB EXCITATION OF ^{161}Dy

Masumi OSHIMA, Eisuke MINEHARA, Shin-ichi ICHIKAWA,[*] Hideki
IIMURA,[*] Takashi INAMURA,[**] Akira HASHIZUME[**] and Hideshige
KUSAKARI[***]

Department of Physics, [*]Department of Chemistry, JAERI,
[**]RIKEN, Wako-shi, Saitama 351-01, [***]Faculty of Education,
Chiba University, Yayoi-cho, Chiba 260

It is well known that the Coriolis interaction causes a strong
perturbation for rotational bands of high-spin orbits. In fact large
signature dependence of B(M1) values has been observed in several odd-A
nuclei and this was interpreted as the rotational perturbation effect.[1-3]
Those works demonstrated that information on transition probabilities plays
a crucial role in understanding the rotational perturbation of the nuclear
system. Moreover, the theoretical works[1,2] indicate that the B(E2;I $\rightarrow$ I-1)
values are closely related to the deviation of nuclear shapes from axial
symmetry. In this connection, reliable data on the $\Delta I=1$ M1 and E2
transition probabilities are needed.

We have carried out a multiple-Coulomb excitation experiment on ^{161}Dy
with a 250-MeV ^{58}Ni beam to study the ground-state rotational band based on
a high-spin ($\nu i_{13/2}$) single-particle orbit. The heavy-ion beams were
provided by the JAERI tandem accelerator. γ-ray branchings and E2/M1 mixing
ratios were determined up to the $\frac{25+}{2}$ state by measuring the γ-ray angular
distributions and the γ-γ angular correlations. Nuclear lifetimes of the
levels up to spin $\frac{25}{2}$ have been measured by using the Doppler-shift recoil-
distance method. Preliminary results of this work have been reported in
Ref. 4.

Three types of reduced transition probabilities have been derived as
shown in figs. 1, 2 and 3. The experimental data for the levels up to spin
$\frac{9}{2}$ are cited from ref.[5]. The results are compared with a microscopic
calculation[6] assuming axially-symmetric shapes of the nucleus (solid
lines in the figures). The experimental B(E2;I $\rightarrow$ I-2) values show no
significant signature dependence. In contrast, the experimental B(M1;I $\rightarrow$ I-
1) values show an evident oscillation for I > $\frac{13}{2}$. The phase of the
oscillation supports interpretation of this phenomenon as the perturbation
effect of rotation[1-3]. The experimental results are well reproduced by
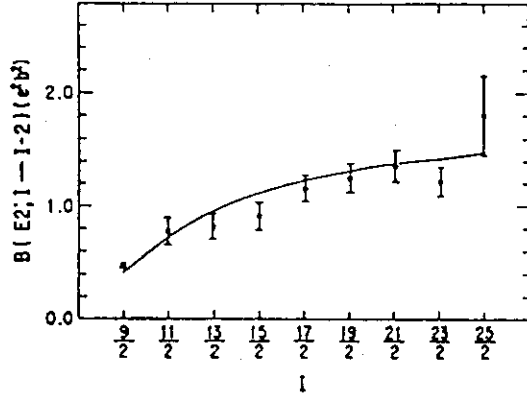
FIG. 1   The B(E2;I → I-2) values
for the ground-state rotational
band in ^{161}Dy.
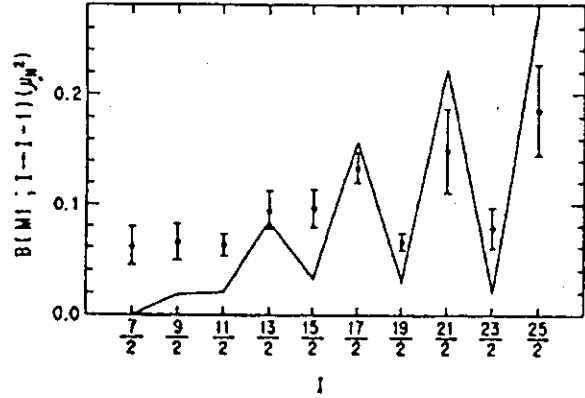
FIG. 2   The B(M1;I → I-1) values
for the ground-state rotational
band in ^{161}Dy.
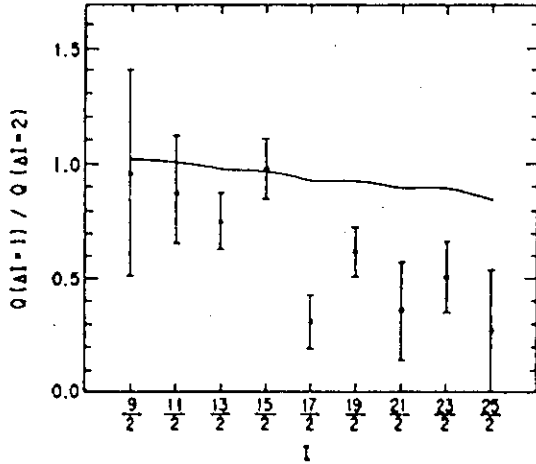
FIG. 3   The ratio of $\Delta I=1$
transition quadrupole moments to
those for $\Delta I=2$.

the microscopic calculation.

In Fig. 3 we present the ratios of the $\Delta I=1$ transition quadrupole moments to those for $\Delta I=2$, which are defined by

$$Q(\Delta I) = \{ \frac{16\pi}{5} B(E2;I \to I-\Delta I) \}^{1/2} / \langle I,2,K,0 \mid I-\Delta I,K \rangle ,$$

where $\langle I,2,K,0 \mid I-\Delta I,K \rangle$ is a Clebsch-Gordan coefficient. Because of no significant signature dependence of the $Q(\Delta I=2)$ or $B(E2;I \to I-2)$ values (see Fig. 1), the major feature in Fig. 3 is ascribed to the $Q(\Delta I=1)$. As shown in Fig. 3, the ratio $Q(\Delta I=1)/Q(\Delta I=2)$ decreases as the spin increases and is always smaller than unity. This trend is not well reproduced by the microscopic calculation. A triaxial-rotor-model calculation[7] has recently performed for a $\pi h_{11/2}$-orbit band with $|\gamma| \leq 15°$. The result shows a

gradual decrease of the B(E2;I → I-1) with the increase of the spin and is in a qualitative agreement with the present experiment. Quantitatively speaking, however, the experimental B(E2;I → I-1) decreases more rapidly than the calculation.

Another interesting feature in Fig. 3 is that the Q(ΔI=1) for ^{161}Dy seems to have a weak signature dependence with the phase opposite to that for the B(M1). According to the triaxial-rotor model[1] the signature dependence of the B(E2;I → I-1) indicates a non-axially-symmetric shape of the nucleus with (or without) the γ vibration. So the present data for the B(E2;I → I-1) provide information on the triaxiality of the nucleus. Theoretical investigation is in progress along this line.

References

[1] I.Hamamoto, Phys. Lett. 106B (1981) 281; Nucl. Phys. A421 (1984) 109c; I.Hamamoto and B.R. Mottelson, Phys. Lett. 132B (1983) 7.

[2] A.Ikeda, Nucl. Phys. A439 (1985) 317.

[3] K.Hara and S.Iwasaki, Nucl. Phys. A430 (1984) 175.

[4] T.Inamura et al., RIKEN Accel. Progr. Rep. 17 (1983) 26; ibid 19 (1985) 32; M.Oshima et al., JAERI-M Report 86-112 (1986) 129.

[5] R.G.Helmer, Nucl. Data Sheets 43 (1984) 1.

[6] S.Iwasaki, priv. comm.

[7] G.B.Hagemann et al., Nucl. Phys. A424 (1984) 365.

5.5 G-FACTORS OF THE SIDE BAND BASED ON THE 10_2^+ STATE IN ^{126}Ce

Tetsuro ISHII, Mitsuhiko ISHII,
Kenichi YANAGIDA*, Masao OGAWA*

Department of Physics, JAERI,
*Tokyo Institute of Technology, Yokohama

We previously investigated the nucleus ^{126}Ce and found a side band based on the 10^+ state as shown in fig.1. The present g-factor measurement aimed at seeing if this band consists of two quasi-protons (h 11/2)$^2_{10+}$ coupling with collective motion, as is the case for the 10^+ and 12^+ states in ^{138}Sm [1].

^{126}Ce levels were populated by the reaction ^{94}Mo(^{35}Cl,1p2n) with a 150 MeV ^{35}Cl beam from the JAERI tandem accelerator. 4 mg/cm^2 of Gd was evaporated on the ^{94}Mo target 3mg/cm^2 thick. The Gd layer was polarized at the temperature of liquid nitrogen in the applied magnetic field 300 oersted with the polarity, ↑ or ↓. The γ-rays were sorted by nuclide with the help of the Si-box [2]. The γ-ray angular distributions were observed by two Ge detectors placed at 45° to the beam direction. The intensity ratios I(↑)/I(↓) of the γ-rays involved are plotted in fig.2. All observed states in ^{126}Ce inherit negative precessions from some higher excited states which are subject to the transient magnetic field parallel to the applied one; the 4^+ and 2^+ states with long lifetimes suffer additional positive precessions in the static hyperfine field. The
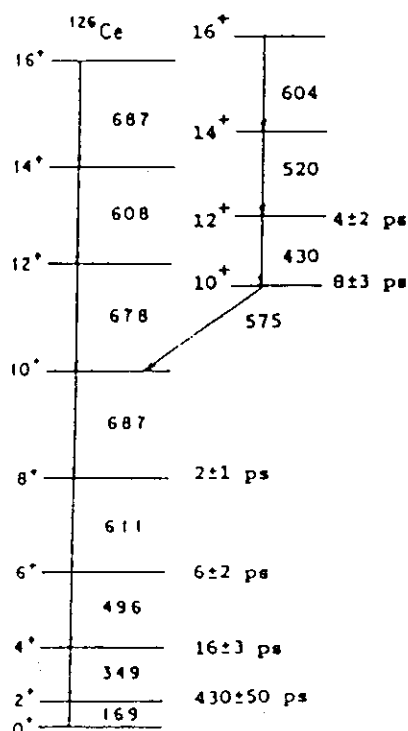
Fig.1 Level scheme of ^{126}Ce.
The half lifetimes are
given in units of ps.

entry states to the ground-state band precess by about -3° and so do the ones to the side band. Assuming a transient magnetic field strength of 20 MG and an effective transient time of 0.5 ps, the g-factors of those states are estimated to be about +0.75. This suggests the alligned coupling scheme between two quasi-protons and collective motion for the 10_2^+ state in the side band.
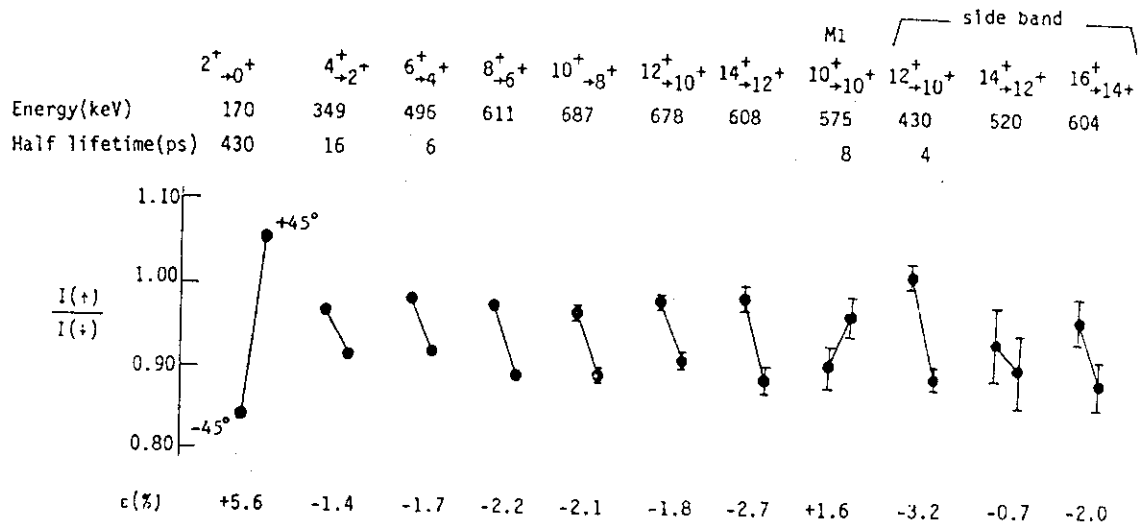
Fig.2 Intnsity ratios I(↑)/I(↓) of the γ-rays.
The left(right) point at each transition presents the ratio measured with the Ge detector placed at -45° (+45°) to the beam direction.
ε = (I(↑)-I(↓))/(I(↑)+I(↓)) × 100   at +45°

References

1) M.Ishii et al., Int. Nuclear Physics Conference, Harrogate U.K., 1986

2) M.Ishii et al., in Nuclei off the Line of Stability (ed. R. A. Meyer and D. S. Brenner, A.C.S., Washington D.C., 1986) ch. 75.

5.6   STUDY OF HYPERFINE INTERACTION

OF RARE-EARTH NUCLEI IN GD HOST

Tetsuro Ishii, Mitsuhiko Ishii,

Kenichi Yanagida* and Masao Ogawa*

Department of Physics, JAERI, *Tokyo

Institute of Technology, Yokohama

We have studied the hyperfine interaction of rare-earth nuclei in Gd host by the Integral Perturbed Angular Distribution method. Those nuclei were produced by the following reactions:

$$^{94}\text{Mo (150 MeV } ^{35}\text{Cl, 3p2n) } ^{124}\text{Ba,}$$
$$^{94}\text{Mo (150 MeV } ^{35}\text{Cl, 2p2n) } ^{125}\text{La,}$$
$$\text{and } ^{94}\text{Mo (150 MeV } ^{35}\text{Cl, 1p2n) } ^{126}\text{Ce;}$$
$$^{107}\text{Ag (165 MeV } ^{32}\text{S , p}\alpha\text{2n) } ^{132}\text{Nd,}$$
$$\text{and } ^{107}\text{Ag (150 MeV } ^{32}\text{S , 1p2n) } ^{136}\text{Sm.}$$
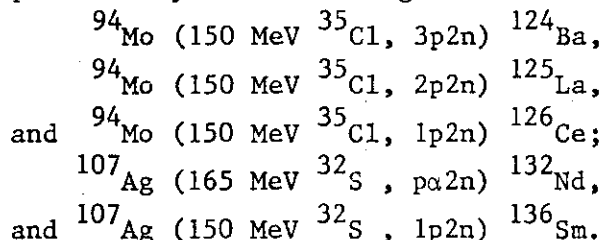
They recoiled out of the target and were implanted into the Gd backing which was polarized at the temperature of liquid nitrogen. The IPAD's of γ-rays were taken for the polarization of Gd host, up or down, with two Ge detectors placed at ±45°(±60°) to the beam direction. The Si-box [1] permitted identification of nuclides emitting γ-rays and simultaneous observation of their Larmor precessions as well. The angular distributions and the half-lives of all the γ-rays concerned except one had been measured in the previous experiments [2,3]; the $2^+ \rightarrow 0^+$ transition in ^{124}Ba was assumed to show the same angular distribution as the one in ^{126}Ce does; with the empirical formula for the E2 transition probability [4], its half-life was estimated from that of the 2^+ state in ^{126}Ce. g-factors of the 2^+ states in the even-even nuclei were taken as 0.35; that of the $15/2^+$ state in ^{125}La was estimated to be 1.1 on the assumption that it consists of a proton h11/2 coupling with collective motion. The experimental results are summarized together with some estimated values in table 1. It is noted that the hyperfine field of the rare-earth nuclei in Gd host is directed opposite to the field in Fe host and that its sign changes at atomic number Z=57 in both cases [5]. The field strengths obtained contain rather large errors, mainly due to estimation of the g-factors, but help our first guess in planning g-factor experiments.

Table 1　Hyperfine field of rare-earth nuclei in Gd host.
　　　　　Positive (negative) sign of the precession and the
　　　　　hyperfine field means that the precession axis and
　　　　　the field direction are parallel (antiparallel) to
　　　　　the applied magnetic field.

	states	Larmor precessions	g-factors (assumed)	half-lives (ps)	hyperfine field (kG)
^{124}Ba	2^+	− 0.2°(0.5)	0.35	120 (estimated)	+ 13 (30)
^{125}La	$(15/2^+)$	− 5.1°(1)	1.1	150(15)	+ 78 (20)
^{126}Ce	2^+	+12.0°(1)	0.35	430(50)	−200 (40)
^{132}Nd	2^+	+ 8.0°(1)	0.35	220(20)	−260 (50)
^{136}Sm	2^+	+10.0°(1)	0.35	130(10)	−550(100)

References

1) M. Ishii et al., Nuclei Off the LIne of Stability (ed. R. A. Meyer and D. S. Brenner, A. C. S., Washington D. C., 1986) ch. 75.

2) A. Makishima et al., Phys. Rev. C 34, 576(1986).

3) T. Ishii et al., Int. Nucl. Phys. Conf. Harrougate U. K., 1986.

4) L. Grodzins, Phys. Lett. 2(1962)88.

5) N. J. Stone, Nuclei Off the Line of Stability (ed. R. A. Meyer and D. S. Brenner, A. C. S., Washington D. C., 1986) ch. 53.

5.7   PRECESSION OF RARE-EARTH NUCLEI
      IN TA AFTER TRANSIT THROUGH GD

Tetsuro Ishii, Mitsuhiko Ishii,
Kenichi Yanagida* and Masao Ogawa*

Department of Physics, JAERI, *Tokyo
Institute of Technology, Yokohama

We have observed that nuclei ^{136}Sm and ^{132}Nd in the first 2^+ state anomalously precess in Ta after they transit through a magnitized Gd foil.

Very light rare-earth nuclei were produced by bombarding a ^{107}Ag target 1 mg/cm^2 thick with a 150 MeV ^{32}S beam. They recoiled from the target and took a flight in a vacuum; 70 % or more of ^{136}Sm nuclei stayed in the 4^+ (or 2^+) state and transitted through a cooled, polarized Gd layer 2 mg/cm^2 thick. Then they stopped in a Ta backing 2.4 mg/cm^2 thick. The parentage of in-beam γ-rays was identified by the use of the reaction channel filter "Si-box" [1]. The perturbed γ-ray angular distributions were observed for the applied magnetic field, up or down, with two Ge detectors placed at $\pm 45°$ to the beam direction. The ratios R of the γ-ray intensities I($\pm 45°$, u or d) were measured for the E2 transitions of interest; R = I($45°$, u)·I($-45°$, d)/I($45°$, d)·I($-45°$, u). The precession angles are closely related to the quantities (R-1). The present results are given in table 1 together with the half-lives of the excited states [2].

Table 1

	states & transitions(keV)		half-lives (ps)	g-factors (assumed)	recoill distances(mm)	R - 1 (%)
^{136}Sm	4^+,	432	9(2)	0.3	0.05	-1.7(1.0)
	2^+,	255	130(10)	0.3	0.18	-1.0(1.0)
					0.23	-0.0(1.0)
^{135}Pm	(15/2$^-$),	287	70(5)	1.1	0.05	-1.9(0.6)
^{132}Nd	2^+,	213	220(20)	0.3	0.23	+2.1(1.0)

In the present experiment we expected that the excited nuclei involved precessed in negative direction with respect to the applied magnetic field by the angles proportional to the magnitudes of their g-factors. This is because they are populated in a few tens of ps in the above fusion reaction and have the same transit time in the Gd layer. Against expectation the present results show that the nuclei in long-lived states precess negatively in Gd and positively in Ta. This fact suggests a possibility that both the transient and static hyperfine interactions act in the rare-earth atoms in Gd and relax in Ta with different time constants; the former is due to polarized electrons in their inner shells and the latter due to the magnetic 4f electrons under the Russell-Saunders coupling.

References

1) M. Ishii et al., Nuclei Off the Line of Stability (ed. R. A. Meyer and D. S. Brenner, A.C.S., Washington D.C., 1986) ch. 75.
2) A. Makishima et al., Phys. Rev. C $\underline{34}$, 576(1986).

5.8   A UNIFIED DESCRIPTION OF $K^{\pi}=0^{+}$ AND $K^{\pi}=0^{-}$ BANDS
      FROM OCTUPOLE VIBRATIONAL
      TO OCTUPOLE DEFORMED NUCLEI

Michiaki SUGITA and Takaharu OTSUKA*

Department   of   Physics,   JAERI,   *Department   of
Physics, University of Tokyo

The $K=0^{+}$ and $K=0^{-}$ bands in actinide nuclei are described
in   terms   of   a   boson   model   with s, p, d and f bosons which
represent bosons of 0^{+}, 1^{-}, 2^{+}, 3^{-}, respectively. This model is
based on a microscopic consideration in Ref. 1. The Hamiltonian
is   composed   of   single   particle   energies   and a boson-boson
interaction containing quadrupole-quadrupole, dipole-dipole and
octupole-octupole   interactions.   The   parameters   of   the
Hamiltonian   are   optimized   so as to reproduce main features of
those   nuclei.   The   number   of bosons is equated to the half of
the number of valence nucleons on the ^{208}Pb core.

    The   diagonalization   of   this   Hamiltonian   is   extremely
difficult,   and   probably   impossible   in practice. We use mean
field   approximation   where   the   axially-symmetric parity-mixed
intrinsic   state is introduced as $\Phi \propto$ ($s^{\dagger}+$ x $p_0^{\dagger}+$ y $d_0^{\dagger}+$ z $f_0^{\dagger}$)^{n}
$|0)$ with x, y and z being variational parameters. The parity is
mixed   since   the   quadrupole and octupole motions are coupled.
The   variation   with   respect   to   the amplitudes x, y and z is
carried   out   after   the projection of the angular momentum and
parity.   The   intrinsic state is therefore altered from state to
state for a fixed nucleus in principle.

    By   changing values of a few parameters of the Hamiltonian
as   smooth   functions   of   N and Z,   one can describe various
situations   of   actinide   nuclei   within   the same model. As an
example,   the Th isotopes are considered. The experimental[2] and
theoretical   excitation   energies   of the states of the $K=0^{+}$ and
$K=0^{-}$ bands   are   shown   in   Fig. 1. One finds a good agreement
between   experiment   and   theory,   particularly in the interplay
between   the   two   bands. Note that the functional dependence of

the above parameters are nearly linear on N (Z is constant). A typical pattern of the static octupole deformation can be observed around N=134-136, while the situation is like the octupole vibration around N=142. In fact, the octupole correlation is largest around N=134-136, whereas the quadrupole deformation evolves continuously as N increases.

The Energy Displacement and E1, E2 and E3 transitions are calculated and compared with experiment in Fig. 2 and 3. Here the Energy Displacement is defined by $\delta E_I = E(I) - \{ (I+1)E(I-1)+I\cdot E(I+1) \}/(2I+1)$. In this model we can reproduce these quantities with a few parameters.
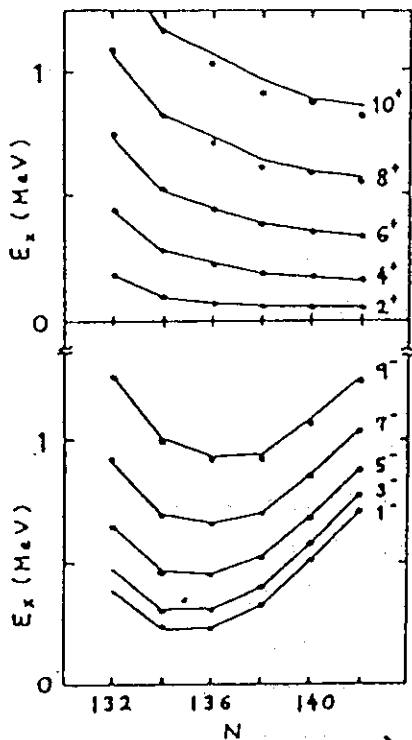
Fig. 1 Experimental[2] (points) and theoretical (lines) energy levels of lowest states of the Th isotopes.
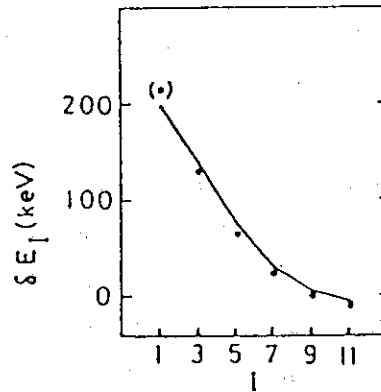
Fig. 2 Experimental (points) and theoretical (lines) Energy Displacement for ^{224}Th.
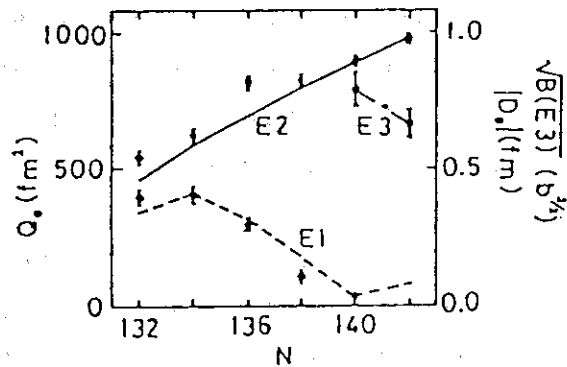
Fig. 3 Experimental (points) and theoretical (lines) moments for the Th isotopes.

References

1) T. Otsuka, Phys. Lett. 182B (1986) 256.

2) P. Schuler et al., Phys. Lett. 174B (1986) 241.

5.9 EQUIVALENCE BETWEEN γ-INSTABILITY AND TRIAXIALITY IN FINITE BOSON SYSTEMS

Michiaki SUGITA and *Takaharu OTSUKA

Department of Physics, JAERI, *Department of Physics, University of Tokyo

The O(6) limit[1] of the Interacting Boson Model has been known as a γ – unstable system. For instance, the O(6) ground state is obtained by the integration from $γ = 0°$ through $γ = 60°$ with equal weight[2]. On the other hand, its potential energy surface has a minimum at $γ=30°$[3]. Thus, the relation between the γ-unstable and triaxial pictures has been rather unclear.

To see this problem, we introduce an intrinsic state as
$$Ψ(β,γ) ∝ \{s^† + β [\cos(γ) d_0^† + \sin(γ) [d_2^† + d_{-2}^†]/\sqrt{2}] \}^N |0).$$
In the following, β is set equal to unity because of O(6). We calculate the probabilities to find various O(6) eigen states in the 0^+ state obtained by projecting this intrinsic state onto angular momentum 0. Fig. 1 shows the probabilities for $γ=30°$ as functions of the boson number N, where O(6) eigen states are classified in terms of the quantum number $ν_Δ$. The ground state has $ν_Δ=0$, while $ν_Δ=2$ and 4 states are excited states. Fig. 1 implies that the projected 0^+ state with $γ=30°$ has large overlap with the exact O(6) ground state. The overlap is indeed equal or close to 100 % for all realistic values of N, whereas it becomes quite small for N extremely large. The overlap becomes smaller also for $β≠1$ or $γ≠30°$. Since the O(6) ground state is always a γ-unstable state[2], the present result suggests that the γ-instability and triaxiality are equivalent in systems with finite number of bosons. This conclusion can be extended to the Ginocchio model, suggesting that bosons does not affect the above equivalence.

The energy levels of an O(6) Hamiltonian are calculated by the above $γ=30°$ intrinsic state. The mixing of the K quantum number is treated properly in the angular momentum projection. The obtained energies are compared with the exact O(6) result

for ^{196}Pt [taken from Ref. 1] in Fig. 2. One finds a good agreement between the two spectra. This good agreement indicates that the above equivalence remains in excited states to a great extent. For realistic N and energy region, the difference is indeed rather insignificant.
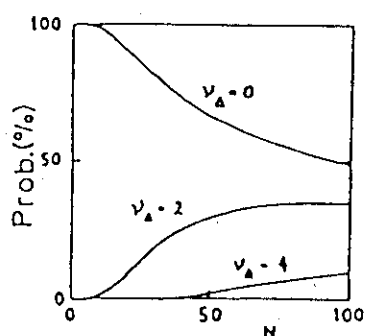
Fig. 1 Probabilities of various O(6) eigenstates in the projected 0^+ state with Y=30°.
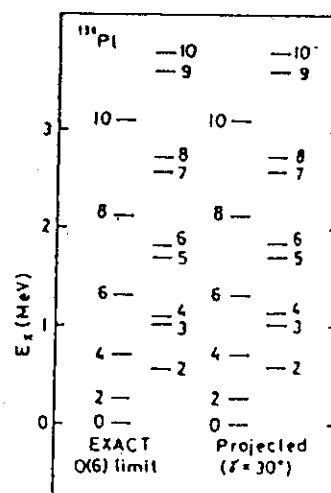
Fig. 2 O(6) and projected spectra for ^{196}Pt.

References

1) A. Arima and F. Iachello, Ann. Phys. (N.Y.) 123 (1979) 468.

2) J. N. Ginocchio and M. W. Kirson, Nucl. Phys. A350 (1980) 31.

3) J. Dobes, Phys. Lett. 158B (1985) 97.

5.10   EFFECT OF PROJECTILE AND TARGET DEFORMATION
IN SUBBARRIER FUSION REACTION

Akira IWAMOTO

Department of Physics, JAERI

We developed in ref.1, a semiclassical model of heavy-ion subbarrier fusion reactions in which a neck formation mechanism was explicitly taken into account.[1] This mechanism enables us to interpret systematically the enhancement of the subbarrier fusion cross section over the one-dimensional barrier penetration calculation. There were two systems, $^{74}Ge+^{74}Ge$ and $^{90}Zr+^{90}Zr$, however, for which we could not reproduce the data well. $^{90}Zr+^{90}Zr$ is the system which needs an extra push energy in the above barrier energy and thus it is no wonder that this influences the subbarrier cross section. More interesting is the case of $^{74}Ge+^{74}Ge$, where even with the neck formation mechanism, the calculation underestimates the cross section data. We will analyze the anomaly of this system below.

A characteristic of the $^{74}Ge+^{74}Ge$ system is the following. The nucleus ^{74}Ge is spherical in the ground state but it is very soft against deformation. On the other hand, the compound system ^{148}Gd lies in the mass region of nuclei which have the super-deformed band.[2] This band is thought to be originated from the shape isomeric state caused by the long range shell correction energy. Thus we investigate how the fusion barrier changes by inclusion of the shell effect.

The shell effect was calculated by the Strutinsky procedure for the neck-formed fusion barrier configuration. The barrier height was determined by the intrinsic energy of the barrier configuration minus the intrinsic energy of asymptotic two ^{74}Ge systems. The resultant barrier height changes little by inclusion of the shell energy. The situation changes ,however, as we allow the deformation of two ^{74}Ge. In the figure we show the fusion barrier height as a function of the deformation of two ^{74}Ge. (we assumed the same deformation for the projectile and the target) The dotted line is the Yukawa plus exponential model[3] calculation normalized at δ =0. (absolute barrier height at δ =0 is 115.3 MeV) Inclusion of deformation $\delta \sim 0.2$ lowers the barrier height by about 2.3 MeV. Addition of the shell energy to the dotted line results in total energy shown by the solid line. Due to large negative shell energy at large deformation, the barrier height is

lowered by 5.1 MeV at $\delta \sim 0.35$. This is related to the fact that an isolated ^{74}Ge has large negative shell energy at $\delta \sim 0.4$. At the barrier region, the macroscopic energy does not increase so rapidly as for the ground deformation energy of an isolated nucleus and thus the effect of large negative shell correction energy appears strongly in the total energy. This lowering of barrier height by about 5 MeV explains the discrepancy between the data and the calculation of Ref.1.
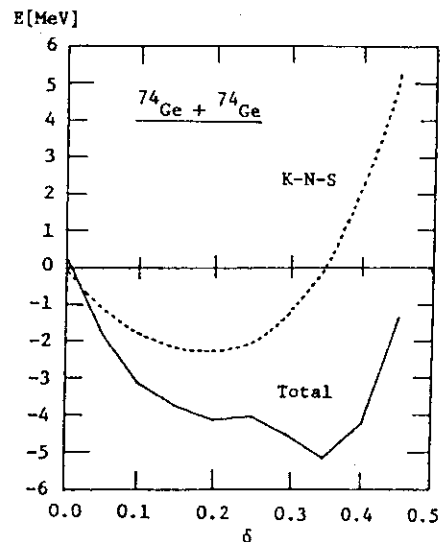
In summary, the model calculation including the shell correction energy together with the deformation of fusing heavy ions explains the anomalous enhancement of the subbarrier fusion of the ^{74}Ge+^{74}Ge system. Further relation between this effect and super-deformed band of compound nucleus is being pursued.

References

1) A. Iwamoto and K. Harada: Z. Phys. A326 (1987) 201.

2) P. J. Twin et al.: Phys. Rev. Lett. 57 (1986) 811.

   A. J. Kirwan et al.: Phys. Rev. Lett. 58 (1987) 467.

   E.M. Beck et al.: Phys. Rev. Lett. 58 (1987) 2182.

3) H. J. Krappe, J. R. Nix and A. J. Sierk: Phys. Rev. C20 (1979) 992.

5.11   WIDTH OF THE MASS DISTRIBUTION IN HEAVY-ION-INDUCED FUSION-FISSION REACTIONS

Akira IWAMOTO

Department of Physics, JAERI

Recently, the width of the mass distribution in heavy-ion-induced fusion-fission reactions has been measured systematically by using the JAERI Tandem accelerator.[1]   New data, together with the old one in light-ion-induced fission reactions[2], give the width as a function of the fissility parameter x of compound nuclei. The width shows a pronounced minimum near x = 0.7 and arouses theoretical interest. In fact several authors tried to reproduce the width curve by the use of an old type of liquid-drop formula for the restricted case of $\ell=0$, which is not good for heavy-ion-induced fission. The present calculation is a new attempt based on a generalized liquid drop formula[3] including the effect of finite angular momentum which plays an importantr role in heavy-ion-induced fission.

Let s stands for the mass of fission fragment, by s_0 a half mass of the compound mass and by E(s) the fission barrier height for the mass division s. We define the stiffness parameter q by

$$E(s) - E(s_0) = (1/2)q(s-s_0)^2 \ . \qquad (1)$$

Then the quantum statistical model predicts the mass distribution as a function of the temperature T and the mass parameter M for the fissioning motion.   For $kT \gg \hbar\sqrt{\frac{q}{M}}$, which is satisfied in the case of our interest, we obtain the relation,

$$\sigma_A^2 = kT/q \ , \qquad (2)$$

where σ_A^2 is the variance of the mass distribution. We calculate q by Eq.(1) and compare it with the experimental values of q obtained from the experimental values of σ_A^2 in terms of Eq.(2).

To calculate q by Eq.(1), we first introduce four shape parameters to specify the shape of the nuclei at conditional saddle. They are the center separation of two nuclei, the deformation of two nuclei, the neck parameter which fixes the shape of the neck part and the mass asymmetry s. For the

calculation of energy $E(s)$, we used the Yukawa plus exponential model, the parameters of which is taken from Ref.3. The mass parameter for fissioning motion is calculated by Werner-Wheeler method. The calculations have been done for the compound nuclei ^{148}Pm, ^{173}Lu, ^{186}Pt, ^{200}Pb, ^{216}Ra and ^{227}Am.

The present calculation of q differs from the previous one in Ref.4.. Our calculated q has maximum near $x = 0.65$ and decreases very slowly for $x \gtrsim 0.7$. On the other hand, in the calculation of Ref.4 q has a maximum at fissility $x \sim 0.6$ and decreases rapidly as x departs from 0.6. The first Businaro-Gallon point in our calculation appears at $x \sim 0.5$ but the second Businaro-Gallone point which was predicted in Ref.4 does not appear. As to the $\mathcal{l}$-dependence, q behaves as follows: For $x \lesssim 0.6$, q is larger for larger $\mathcal{l}$. As a consequence, Businaro-Gallon point for $\mathcal{l}=60$ is smaller than $x=0.4$. For $x \gtrsim 0.6$, $\mathcal{l}$-dependence is inverted and q becomes smaller for larger $\mathcal{l}$. This tendency is consistent with the result of Ref.1. The absolute value of q, as a whole, is a little smaller than the experimental data and the calculation of Ref.4.

In summary, our model predicts 20 to 100 % larger value of variance σ_A^2 compared with the experimental data. Change of σ_A^2 as a function of fissility is rather small compared with the experimental data and the calculation of Ref.4. With respect to these point, the present calculation is not satisfactory. As to the $\mathcal{l}$-dependence, however, we get a consistent result compared with the heavy-ion data.

References

1) H. Ikezoe et al.: this annual report.

2) Ye. N. Grazintsev et al.: Z. Phys. A323 (1986) 307.

3) P. Moller and J. R. Nix: Nucl. Phys. A361 (1981) 117.

4) M. Strutinsky: Sov. Phys. JETP 18 (1964) 1305.

Ⅵ NEUTRON PHYSICS

6.1 MEASUREMENT OF THE FAST NEUTRON SCATTERING CROSS SECTIONS OF ^{7}Li AT En = 11.0 AND 13.0 MeV

Satoshi CHIBA, Yoshimaro YAMANOUTI, Motoharu MIZUMOTO, Mikio HYAKUTAKE[*] and Shin IWASAKI[**]

Department of Physics, JAERI,, [*]Faculty of Engineering, Kyushu University, [**]Faculty of Engineering, Tohoku University

Introduction

Fast neutron cross sections below 14 MeV are very important for the development of D-T fusion reactor systems. Among them, those of ^{7}Li are of special importance, because ^{7}Li is the major tritium breeding material as well as ^{6}Li. The inelastic scattering to the 4.63-MeV state of ^{7}Li accounts for about half of the total ^{7}Li(n,n't)α reaction cross section. In spite of its importance, the cross section is not well confirmed between 7 and 13 MeV. The present experiments have been made to resolve the discrepancy of the 4.63-MeV level cross section of ^{7}Li reported by several authors.

Experimental Procedure and Data Reduction

The experiments were made at the JAERI 20-MV tandem accelerator facility. Pulsed deuteron beams were supplied from the in-terminal ion source, at a repetition rate of 2 MHz. They striked the target D_2 gas. The deuteron beams were accelerated up to 8.1 and 10.2 MeV to produce 11.0 and 13.0-MeV neutrons by the D(d,n)^{3}He reaction, respectively. The beam current was about 1.2 μA at Ed = 8.1 MeV and 6 μA at 10.2 MeV. The time spread of the beam was about 2.8 ns at FWHM.

The scattering sample was an enriched metal cylinder, 99.9% in ^{7}Li. It was contained in a 0.3-mm thick SUS container, 3.1cm in diameter and 4cm high, to protect it from oxygen in the air. An empty can of the same shape was also used to subtract backgrounds. These samples were loaned from Tohoku University. A polyethylene and a carbon scatterer, 1.1cm in dia. by 5cm in height, were also used to determine

the relative detection efficiency and absolute normalization by the
H(n,n) reaction. These samples were located at 12cm from the neutron
source.

The fast neutron time-of-flight spectrometer used was the same
described in a previous paper[1]. Secondary neutrons were detected at
angles between 20 and 140°. Bias level of the main detector system was
set to about 500keV proton equivalent. Two 5-cm dia. by 1.27-cm thick
NE213 scintillators were used as source neutron monitors.

In Fig. 1, a TOF spectrum
of the d-d source neutrons, at
Ed = 8.1 MeV, is displayed.
Besides the main peak at 490 ch.,
there is a prominent peak formed
by the C(d,n) or O(d,n) reaction
at 380ch. To subtract these
unwanted neutrons, measurements
without the target D_2 gas were
made at all of the angles.

The scattering yield
was obtained by subtracting
backgrounds measured by both of
the scatterer-out and gas-out runs.
Typical TOF spectrum, after
backgrounds have been subtracted,
is shown in Fig. 2. Since the
first 0.478-MeV level could not be
separated from the elastic peak,
two peaks associated with the
$^7Li(n,n_0+n_1)$ and $^7Li(n,n_2)$
(Q=-4.63 MeV) are assigned.
Yields of these peaks were deduced
finally by subtracting a linear
backgrounds below each peak. They
were converted to the absolute
values by comparing these yield
with those of H(n,n) reaction.
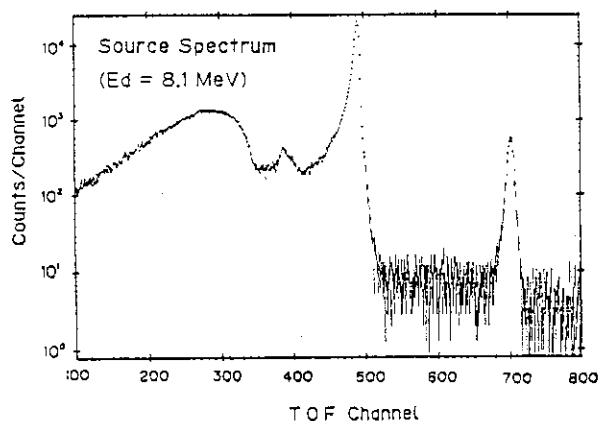
Fig. 1 Source neutron TOF
spectrum at Ed=8.1MeV
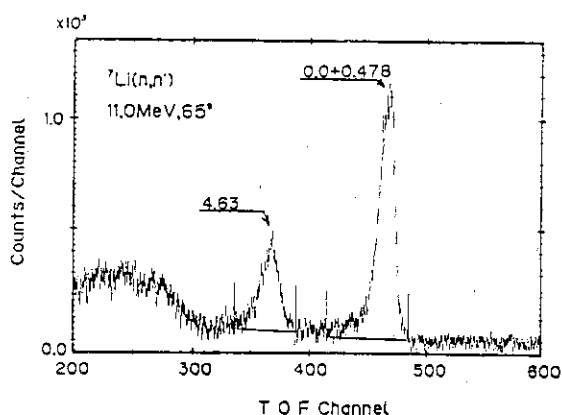
Fig.2 Typical TOF spectrum of
the scattered neutrons measured
at En = 11.0 MeV, 65°

The effects of flux attenuation, multiple scattering and ^{6}Li impurity were corrected by the monte-carlo method.

Results

Presently measured ^{7}Li(n,n_0+n_1) and ^{7}Li(n,n_2) reaction cross sections are shown in Figs. 3(a) and 3(b). The data of Hogue et al.[2] and evaluation in JENDL-3PR2[3] are also displayed. Dashed curves represent the Legendre fitting to the present data.
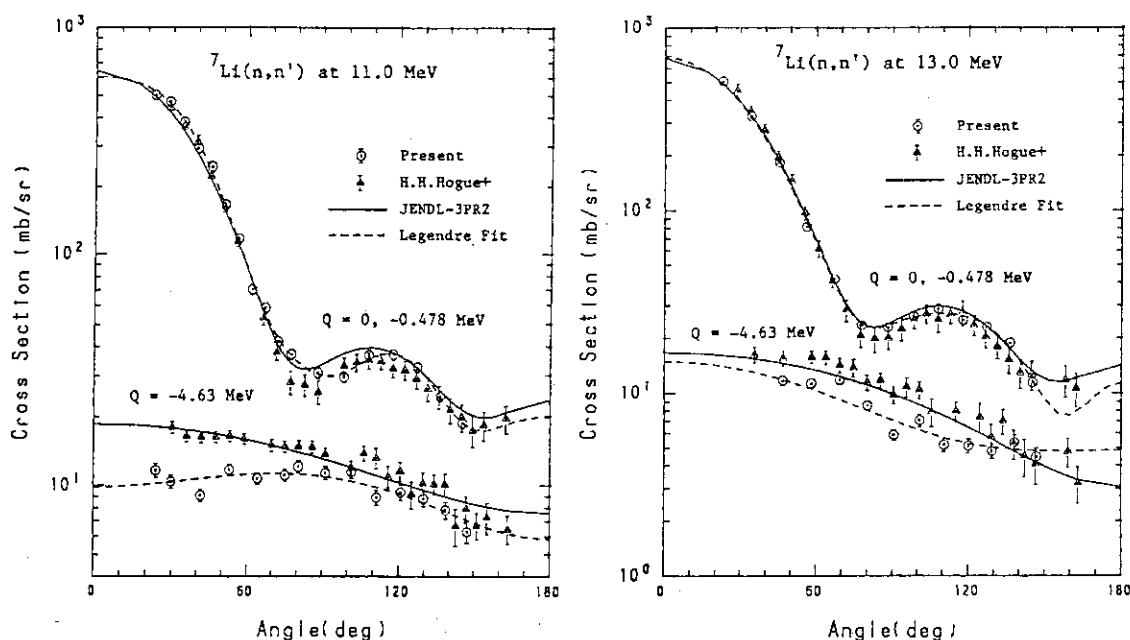
Fig. 3 Angular distributions of the ^{7}Li(n,n_0+n_1) and (n,n_2) reactions at En = (a) 11.0 MeV and (b) 13.0 MeV.

The presently measured angular distributions for the groud state plus the first 0.478-MeV level agree very well with those of Hogue et al. and JENDL-3PR2. Thus they seem to be well established in this energy range.

On the other hand, those for the 4.63-MeV level are significantly smaller than the data of Hogue et al. at forward angles. They are also lower than the JENDL-3PR2 data, which is evaluated based on the TUNL data at both energies. At backward angles, however, the present results agree with the data of Hogue et al. within the experimental errors.

In Fig. 4 shown are the angle integrated values of the ^{7}Li 4.63-MeV cross section. The present results are consistent with the data around 10-MeV[4,5,6] and 14-MeV[7] region. They are, however, considerably smaller than those measured at TUNL. A possible explanation of this disagreement is that because Hogue et al.

Fig.4 Angle-integrated cross section to the 4.63-MeV state of ^{7}Li

did not subtract backgrounds coming from the neutron source, i.e., C(d,n) or O(d,n) reactions, their values will tend to be higher. According to the present results, the data in JENDL-3PR2 are too large in the energy range below 14 MeV. Thus a re-evaluation of the JENDL-3PR2 data will be needed.

References

1. S. Chiba et al.: JAERI-M 87-025, 262 (1987).

2. H.H. Hogue et al.: Nucl. Sci. Eng. 69, 22 (1979).

3. S. Chiba: JAERI-M 86-029, 32 (1986).

4. P.W. Lisowski et al.: LA-8342(1980).

5. N.S. Birjukov et al.: Proc. Fourth All Union Conf. Neutron Physics, Kiev 1977, Vol.2, 27(1977).

6. J.A. Cookson et al.: Phys. Rev. A91, 273 (1967).

7. S. Chiba et al.: Jour. Nucl. Sci. Technol., 22, 771 (1985).

8. R. Bathcelor and J.H. Towle: Nucl. Phys., 47, 385 (1963).

9. A.H. Armstrong, et al.: ibid, 52, 505 (1964).

10. F. Merchez et al.: Nuclear Data for Reactors, Vol. 1, 393 (1967).

11. G. Ferch et al.: INDC(CCP)-221,L, 18 (1984).

6.2   CROSS SECTION MEASURMENT OF Pb(n,xn) REACTIUON AT 11 MeV

Shin IWASAKI[*], Kazusuke SUGIYAMA[*],

Satoshi CHIBA, Yoshimaro YAMANOUTI, Motoharu MIZUMOTO

and Mikio HYAKUTAKE[**]

Department of Physics, JAERI

[*]Faculty of Engineering, Tohoku University

[**]Faculty of Engineering, Kyushu University

Introduction

Lead is now considered as an important neutron multiplying material in the fusion reactor blanket.   In spite of the importance of its (n,2n) cross section, the present status of the accuracy of the cross section is far from the required one (3%) for the fusion reactor design.

In the past few years, several groups[1],[2] have been measured the secondary emission cross sections around 14MeV and provided reference spectra for the evaluation of the cross sections.   However, from the point of view of the cross section evaluations, some additional data are needed at different incident energies. We have investigated the feasibility of the cross section measurement for Pb(n,xn) using the JAERI tandem accelerator in the energy range of so called 'energy gap' (En= 7-14MeV) using the D+d neutron source.   In this energy range the source neutrons are accompanied by sizable continuous energy neutrons due to the break up process.   The break up component, whose maximum energy is about 5MeV, does not contribute to the (n,2n) reactions when the incident deuteron energy is 8MeV as in the present case, since the threshold of the Pb(n,2n) reaction is about 7MeV. Effects from the break up component on the low energy secondary neutron group can be corrected using a certain cross section set, and the (n,2n) neutron energy spectra can be estimated.

Experimentals

The source neutrons were produced by the D(d,n) rections in a gas target sealed in a cell. The taret cell was fabricated with stainless steel and had a thin entrance window of molybdenum metal and a gold end plate. In spite of the choosing such materials for the cell, the neutrons due to (d,n) reactions on these materials contaminated the source spectrum in addition to the break up component.

A scattering sample of the lead was a high purity metal cylinder of 5cm-height and 2cm-diameter, which was hung by a string at a distance of 13 cm from the center of the gas target cell. Scattered neutrons were observed by a 12.5 cm-diameter and 5cm thick NE213 scintillation detector which was located at 5m from the sample in the collimeter channel of the large neutron spectrometer. The threshold energy of the detector was about 0.3MeV.

The scattered neutron spectra were observed in five directions; at 30, 60, 90, 120, and 140degs. At each angle, the scattering runs were done in following six cases, which were the result of the combination of three source conditions, i.e., deuterium(D_2) gas-in, gas-out, and herium-3 gas-in, and two scattering sample's ones, i.e., in and out of the position. In both gas-in cases, the gas pressure was 1atm. From the data in the former four cases of the D_2 gas, we can deduce the contribution from the source itself, i.e., the monoenergetic 11MeV neutrons and the break up neutrons. From the latter herium-3 cases, we hoped to estimate the contribution from the break up neutrons because the ^{3}He+d reaction has similar reaction Q-value and produces only break up neutrons. The source neutron spectra from each target condition were observed in the 0 deg. direction.

Relative efficiencies of the main detector were determined by measuring neutron-hydrogen scattering from a forward angle to 75deg. These efficiency measurements covered the neutron energies from 10 MeV down to 0.4 MeV. The absolute cross sections of the lead sample were again determined by normalizing the results to the hydrogen scattering cross section as a standard.

Results

The measured source neutron spectra are presented in Figs.1 (a) and (b). As shown, the main peak due to the D(d,n) reaction has broad tail in the low energy side and the rather large low energy break up component follows it. From the figures, we concluded that the contribution of the break up neutrons from the D_2 gas can not be simulated by the He-3 gas target source because the Q-values are slightly different. However, it would give us an important information about the contribution from the low energy neutrons which overlapped on the neutron spectra from the Pb(n,2n) reaction.

In Fig. 2 (a) and (b), typical composite neutron spectra of the contributions from the 11MeV source neutrons and the break up neutrons are shown. Above 5MeV, the contributions come mainly from the former neutrons, and some discrete levels are identified. To the contrary, below 5MeV the contributions come from both neutrons. The shoulder component in the energy range from 2 to 4 MeV is considered to be due to the break up neutrons. At 30 deg., a rather big hump results from the forward peaking angular distribution of the elastic scattering for the neutrons of low incident energies.

If some reliable elastic and inelastic cross section set in these enegy range are used, the cross section data on the Pb(n,2n) reaction at 11MeV can be obtained. We now plan to use the EFF set by Gruppelaar[4], if available, and the JENDL-3T set by Mizumoto, JAERI, for the correction.

References

1) A. Takahashi et al., Oktavian Report, A-83-01 (1983) and A-87-01 (1987), Osaka University.

2) S. Iwasaki et al., Intnl. Conf. Nucl. Data for Basic and Applied Science, May 1985, Santa Fe, NM U.S.A.

3) S. Iwasaki et al., Progress Report FNL, NETU-38 p49 (1981).

4) H. Gruppelaar, IAEA Adv. Gr. Meet. on Nucl. Data for Fusion Reactor Tech., Dec. 1986, Dresden.
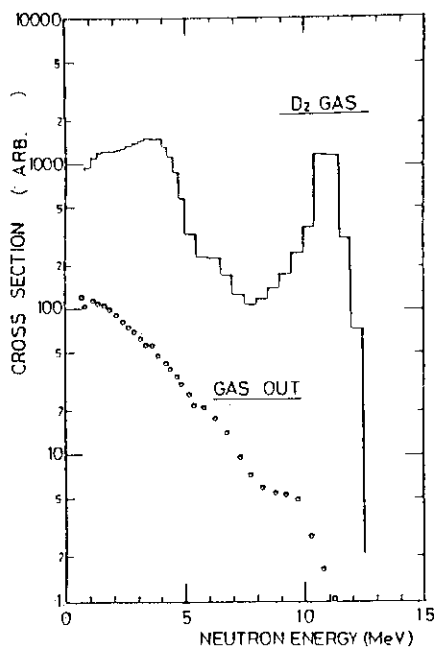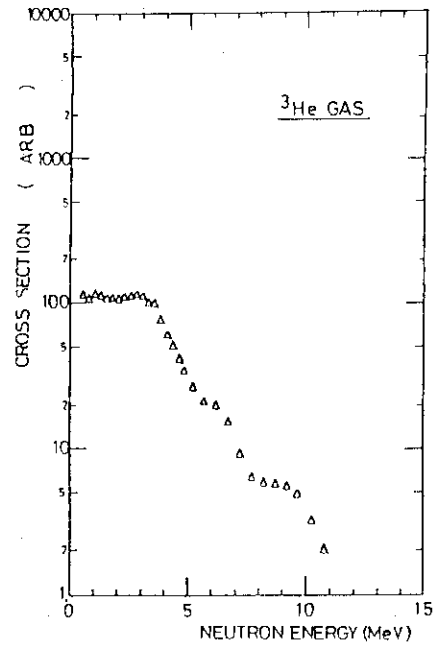
(a)   (b)

Fig. 1   Source neutron spectra for D_2 gas-in and out (a),

and ^{3}He gas-in (b).
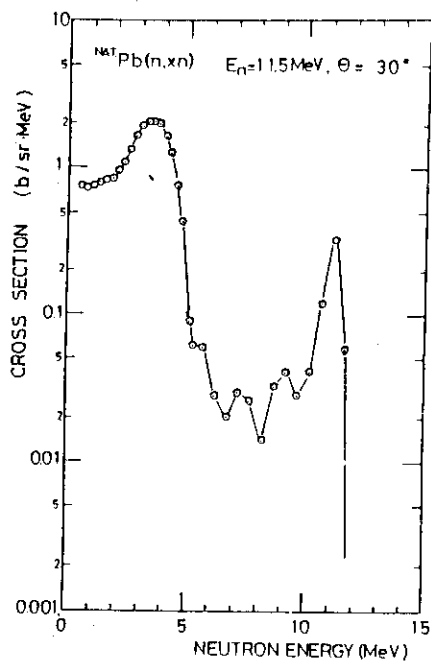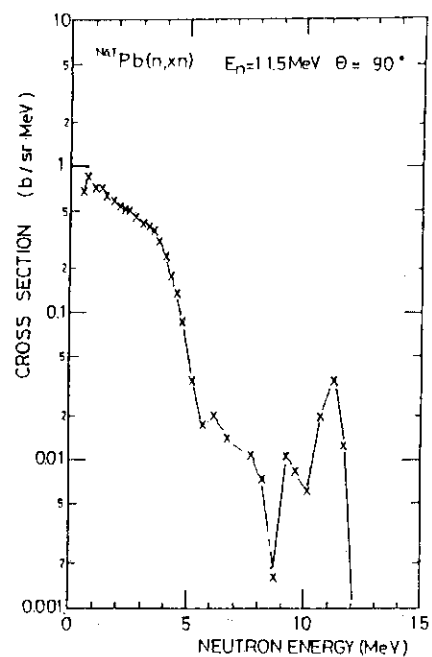
(a)   (b)

Fig. 2   Typical secondary neutron spectra for Pb(n,xn) reaction at 11 MeV.
30 deg. (a)   and 90 deg. (b)

6.3 NEUTRON RESONANCE PARAMETERS OF ^{121}Sb and ^{123}Sb

Makio OHKUBO

Department of Physics, JAERI

Abstract

Neutron transmission measurements have been carried out on natural antimony, and separated isotopes $^{121, 123}$Sb at the TOF facility of the JAERI linear accelerator. Resonance parameters of ^{121,123}Sb are deduced up to 5.3 keV. The s-wave strength function S_0, average level spacing D are obtained to be

^{121}Sb : S_0 = (0.24 $\pm$ 0.03)x10^{-4} for 188 levels below 5.3 keV

　　　　　D = 10.3 $\pm$ 0.5 eV　　　　below 0.6 keV,

^{123}Sb : S_0 =(0.25 $\pm$ 0.03)x10^{-4} for 202 levels below 5.3 keV

　　　　　D = 20 $\pm$ 1   eV　　　　below 1.3 keV,

1. Introduction

Though there are several sets of the neutron resonance data on antimony, [1~4] they are insufficient in the energy resolutions and in the accuracy for more detailed analysis of the resonance properties. A few years ago, we have made neutron transmission measurements on the separated isotopes of antimony at the 47-m TOF station of the JAERI linac, with the overall time resolution of $\sim$0.6 ns/m. The resonance parameters were obtained by analysing the transmission data with an area analysis program. Recently, we have deduced resonance parameters for both isotopes up to 5.3 keV.

2. Measurements and Analyses

Transmission measurements were carried out at a 47-m TOF stations of the JAERI electron linac. The electron beam was 120 MeV, peak current $\sim$3 A, the pulse width 25 ns and the repetition rate 600 pps. The pulsed neutrons traversed to the station through evacuated flight tube, and were detected with a ^{6}Li-glass neutron detector. A B$_4$C filter was inserted in the neutron beam to absorb slow neutrons. A ^{6}Li-glass neutron flux monitor

was placed upstream the sample and the detector. The transmission samples were exposed in the 35 mm diameter collimated neutron beam at the sample position which was separated ~1.5 m from detector with an evacuated flight tube.

The time between the electron beam pulse(start pulse) and the detector pulses(stop pulses) were analyzed with a 4096 channel time analyzer with a minimum channel width of 31.25 ns. Neutron pulses from the flux monitor were gated to count in the time region corresponding to the neutron energy from 0.3 to 1.1 keV. The accumulated data in the time analyzer were finally stored on a disk memory of a large computer FACOM M380 at the JAERI computing center, and the data processing were made through a remote terminal at the linac laboratory.

Natural antimony (^{121}Sb 57.25 %, ^{123}Sb 42.75 %) samples were metallic plates or powder. The separeted isotope samples of ^{121}Sb and ^{123}Sb were metallic powder, lent from the Oak Ridge National Laboratory isotope pool. Thicknesses of these samples were from 2 to 35 mm for natural antimony, and were from 2 to 10 mm for separated isotope samples.

The background in the time spectra were estimated from the counts at the saturated resonances of cobalt (132 eV), manganese(337 eV), aluminum(35 and 88 keV), and some of the saturated resonances of these samples. Energy scale of the TOF system was calibrated by the aluminum resonances at 5.9035 keV by adgusting the initial delay time of the analyzer. Transmission data of ^{121}Sb and ^{123}Sb were analyzed to deduce the neutron widths of the resonances by a modified single level Atta-Harvey area analysis program.

3. Results

Resonance parameters were determined for 188 levls of^{121}Sb and for 202 levels of ^{123}Sb up to 5.3 keV, assuming all the levels are s-wave levels.

Resonance parameters of ^{121}Sb from 2.5 keV to 5.3 keV, and of ^{123}Sb from 4.1 keV to 5.3 keV are newly determined. The plot of cumulative number of levels vs. neutron energy for ^{121}Sb is shown in Fig.1, and for ^{123}Sb in Fig.2, where cut-off in $g\Gamma_n^0$ are made as described in the previous work.[5] From these figures, average level spacing for mixed ensemble of s- and p-wave levels were deduced to be

^{121}Sb   D = 10.3 ± 0.5 eV   below 0.6 keV

^{123}Sb   D = 20 ± 1 eV   below 1.3 keV.

where the missing levels are small.   Cumulative values of $g\Gamma_n^0$ vs.
neutron energy for ^{121}Sb are shown in Fig.3, and for ^{123}Sb in Fig.4.
It seems that an undulation with a period of about 1 keV is superimposed on
the constant gradient slope.   However, the s-wave strength function S_0
were deduced to be

^{121}Sb S_0 = (0.24 ± 0.03) x 10^{-4} below 5.3 keV,

^{123}Sb S_0 = (0.25 ± 0.03) x 10^{-4} below 5.3 keV,

It is ascertained that the strength functions of both isotopes are nearly
the same value in a broad energy region in which sufficient averaging of
the local fluctuations are took place.   In consideration of the local
variations of the strength fucnctions, the present S_0 values are
consistent with the previous values within experimental errors.

References

1. S.F.Mughabghab, M.Divadeenam and N.E.Holden;"Neutron Cross Sections"
   VoL 1, Part A, Z=1-60, Academic Press(1981)

2. S.Wynchank, J.B.Garg, W.W.Havens,and J.Rainwater:Phys.Rev.166,1234(1968)

3. G.V. Muradyan, Yu.V.Adamchuk and Yu.G.Shchepkin: Yader.Fiz.8,852(1968):
   transl. Sov.J. Nucl.Phys. 8,495(1969)

4. M.Ohkubo,Y.Nakajima,A.Asami and T.Fuketa;J.Phys.Soc.Japan 33,1185(1975)

5. M.Ohkubo, M.Mizumoto and Y.Kawarasaki; J.Nucl.Sci.Technol. 21,254(1984)
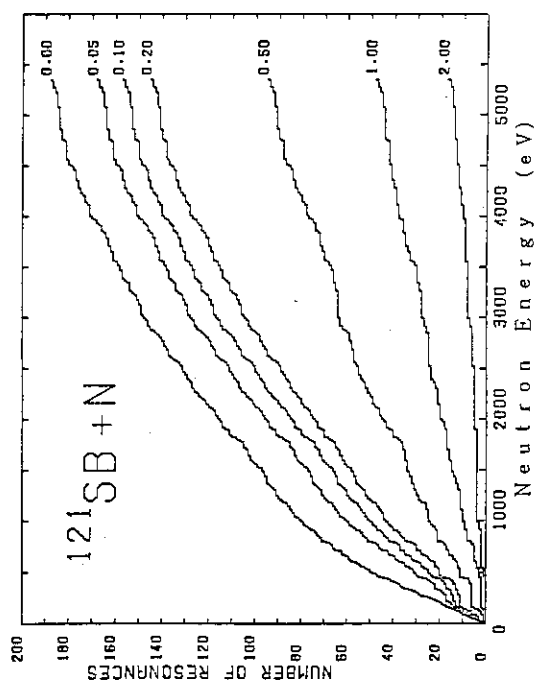
Fig. 1
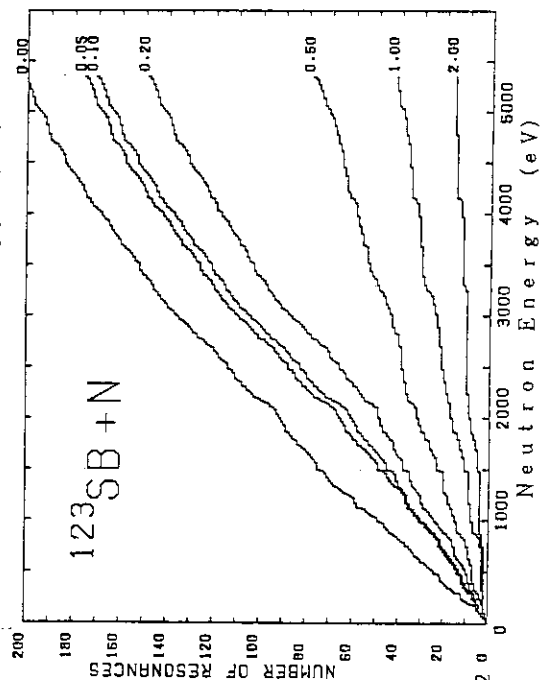
Fig. 2
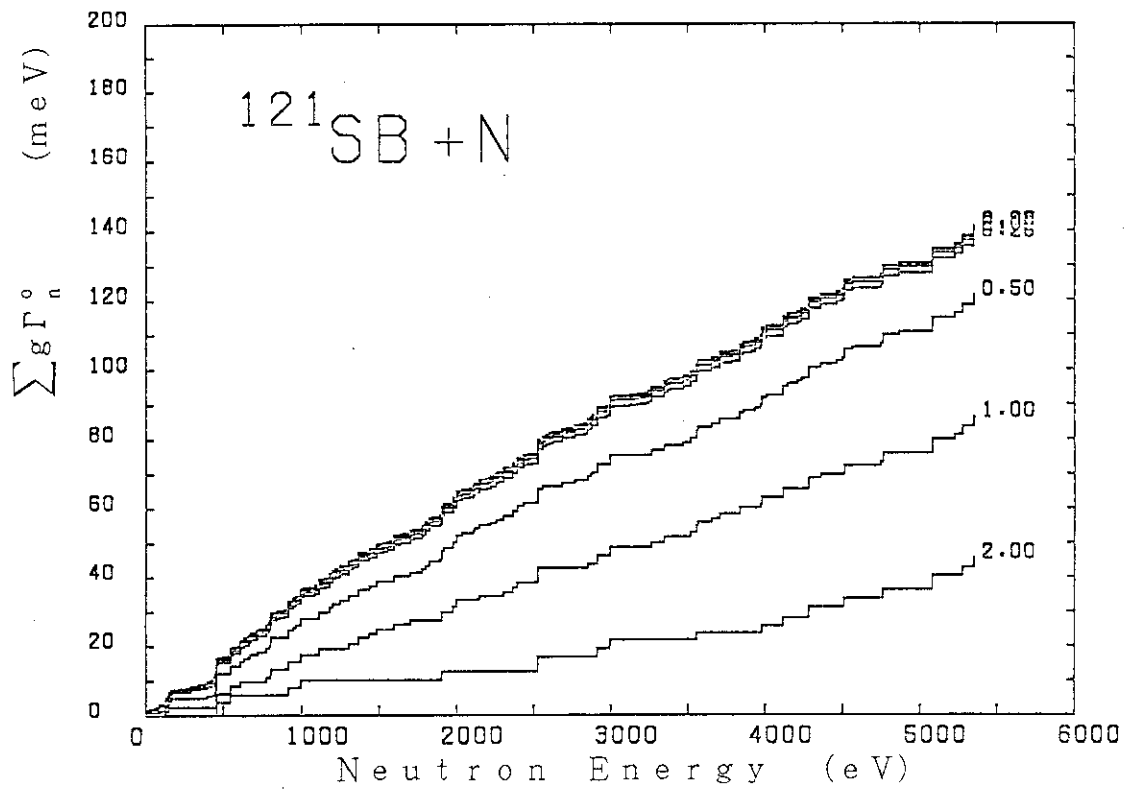
Fig. 3
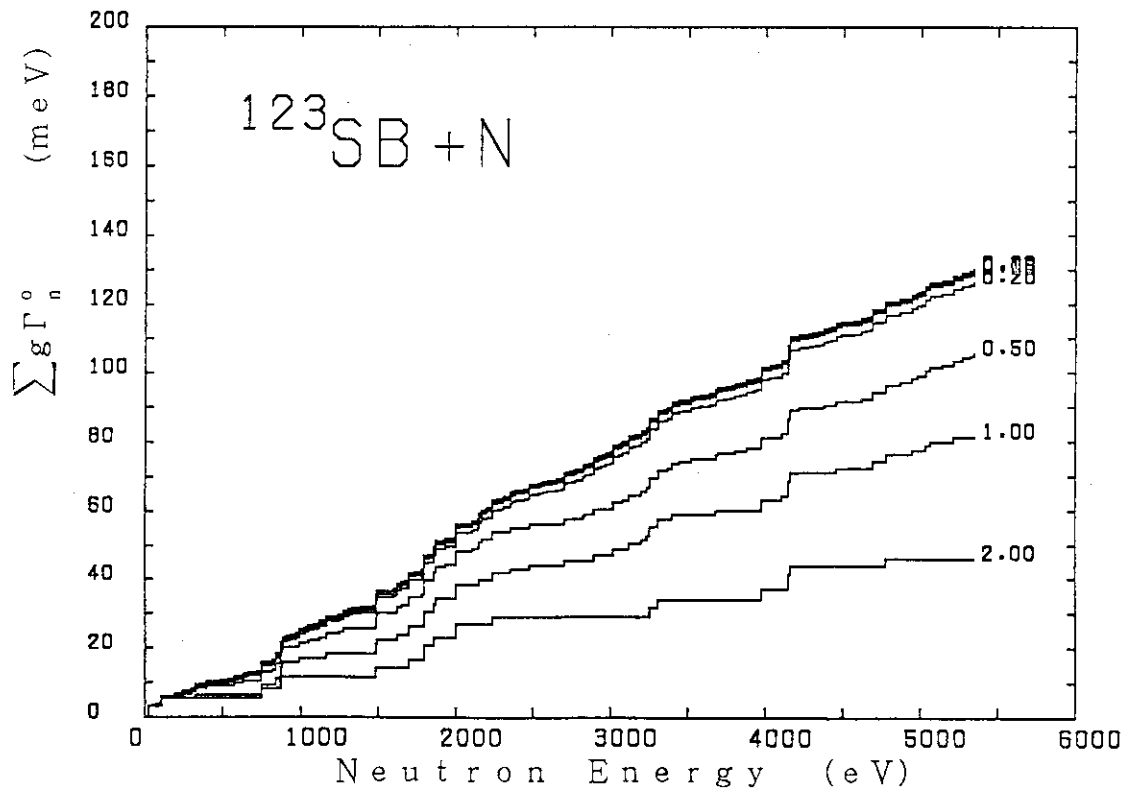
Fig.4

6.4   NEUTRON RESONANCE PARAMETERS OF ^{135}Ba, ^{137}Ba AND ^{138}Ba

Motoharu MIZUMOTO

Department of Physics, JAERI

Introduction

Transmission measurements for odd Barium isotopes, ^{135}Ba and ^{137}Ba were made previously in the neutron energy range below 2 keV[1,2]. The capture cross sections were measured at ORELA and capture areas were extracted for resonances from 2.7 to 12 keV[3,4]. For ^{138}Ba, the transmission was measured up to 200 keV[5] and the capture was measured to 36 keV[6]. The BNL-325[7] recommends parameters in the energy region up to 5.978 for ^{135}Ba, 34.64 keV for ^{137}Ba and 189 keV for ^{138}Ba.

However, there still exists the energy region where there are no previous data available from 1.5 to 2.7 keV. Furthermore, in the low energy region, the published data are old and not reliable, and above 2.7 keV neutron widths determined from capture data are also questionable. We have tried to determine resonance energies and neutron widths more accurately with high resolution transmission experiments.

Experiment

The experiments were carried out with the neutron time-of-flight spectrometer of the 120 MeV JAERI electron linear accelerator. Pulsed neutrons were produced in a laminated water-cooled Ta target and moderated by a 5 cm thick boron loaded polyethylene plate. The neutron target was shielded by a lead and copper shadow bar of 4 cm x 6 cm area and 60 cm long (in the beam direction) in order to reduce the direct gamma-flash. The linac was operated at 300 pps with electron pulse widths of 30 ns and a peak current of 3.5 A.

Samples enriched in ^{135}Ba, ^{137}Ba and ^{138}Ba were provided in the form of carbonate powder or nitrate powder from the Isotope Distribution Office of the Oak Ridge National Laboratory. Each sample was contained in a 4 cm diameter x 1 cm thick aluminum case with 0.2 mm aluminum windows.

For the neutron energy below 2 keV, transmission measurements of low energy resolution were made at the flight path of 56.32 m, using an 11.1 cm diameter x 0.635 cm thick ^{6}Li-glass detector. Above 2 keV, the high

resolution transmission measurement was made for ^{137}Ba at 191.49 m, using five 11.1 cm diameter x 1.27 cm thick ^{6}Li-glass detectors. The energy calibration was made using the energies of sharp resonances present in the beam filters; 5.9035 keV of Al, 3.360 keV and 71.191 keV of Pb[7].

Analysis and results

The transmission data were analyzed with the multi-level Breit Wigner formula incorporated in a least-squares fitting program. The resonance spins and radiation widths Γ_γ were adopted from BNL-325[7] when they are available. Otherwise, the spin statistical weight factor g = 0.5 was used and the Γ_γ values were assumed to be 150 meV, 80 meV and 55 meV for ^{135}Ba, ^{137}Ba and ^{138}Ba, respectively. The nuclear radii could not be obtained in the present experiments and were simply adjusted in order to represent the transmission values in the off-resonance region.

The experimental transmission data for ^{135}Ba, ^{137}Ba and ^{138}Ba are shown in Fig. 1. Numerical values of our resonance parameters will be published separately, but main results can be summarized as follows:

Our resonance energies are in good agreement with the data by Alves et al.[1] and Bilpuch et al.[5] but about 0.3 % lower than those of Van de Vyver and Pattenden[2]. Resonance energies by Musgrove et al.[3,4] are systematically higher than the present data because their values are based on the old standard values of 5.906 keV for Aluminum while the recent value for this resonance is 5.9035 keV. Our neutron widths are also in good agreement with the previous data although their energy regions were limited and isotope assignments for some resonances were made often in error.

The cumulative sums of reduced neutron widths are plotted in Figs. 2 and 3 for ^{135}Ba and ^{137}Ba, respectively. These plots are almost insensitive to weak levels. The solid straight lines drawn in the figures are the values of s-wave strength functions S_0. The previous values of the s-wave strength functions for ^{135}Ba and ^{137}Ba are given in Table 1 together with the recommended values in BNL-325 and our results. Corrections for missing small resonances were not made to determine the average level spacings D_0. Our observed average level spacing for ^{135}Ba may be slightly high due to small values of D_0, but missing for resonances of ^{137}Ba are hardly expected in our measured energy region.

The apparent energy dependence of the strength function was observed in the case of ^{135}Ba. That is the reason why previous strength function

values, which were obtained only in the low energy region, were small. The similar energy dependences have been often observed in the many case such as Ag^{109}, Sm^{149} and Pb isotopes, but the reasonable explanation has not be made yet.

References

1) R.N. Alves, S. de Barros, P.L. Chevillon, J. Julien, J. Morgenstern and C. Samour : Nucl. Phys. A134 (1969) 118

2) R.E. Van de Vyver and N.J. Pattenden: Nucl. Phys. A177 (1971) 393

3) A.R. de L. Musgrove, B.J. Allen and R.L. Macklin : AAEC/E327 (1974)

4) A.R. de L. Musgrove, B.J. Allen, J.W. Boldeman and R.L. Macklin: Aust. J. Phys. 29 (1976) 157

5) E.G. Bilpuch, K.K. Seth, C.D. Bowman, R.H. Tabony, R.C. Smith and H.W. Newson: Annals Phys. 14 (1961) 387

6) A.R. de L. Musgrove, B.J. Allen, J.W. Boldeman and R.L. Macklin: Nucl. Phys. A252 (1975) 301

7) S.F. Mughabghab, M. Divadeenam and N.E. Holden: Neutron cross sections, vol. 1A, BNL-325, (4th ed.) (1981), Academic Press, New York

Table 1 Strength functions and average level spacings for ^{135}Ba and ^{137}Ba

| | ^{135}Ba | | ^{137}Ba | |
	S_0 $(\times 10^4)$	D_0 (eV)	S_0 $(\times 10^4)$	D_0 (eV)
Alves et al.	$0.80 \pm \begin{smallmatrix}0.35\\0.20\end{smallmatrix}$		~ 0.3	
Van de Vyver et al.	1.0 ± 0.3		0.33 ± 0.17	
Musgrove et al.		39.3 ± 3.0	0.57 ± 0.2	380 ± 70
BNL-325	0.9 ± 0.3	40 ± 7	0.41 ± 0.08	290 ± 40
Present	$1.33 \pm 0.22^{*}$	53 ± 4	0.51 ± 0.12	270 ± 28

* Large energy dependence is observed; $(0.75\pm0.16)\times10^{-4}$ in the energy region from 400 to 2800 eV and $(1.96\pm0.55)\times10^{-4}$ from 2800 to 4600 eV.
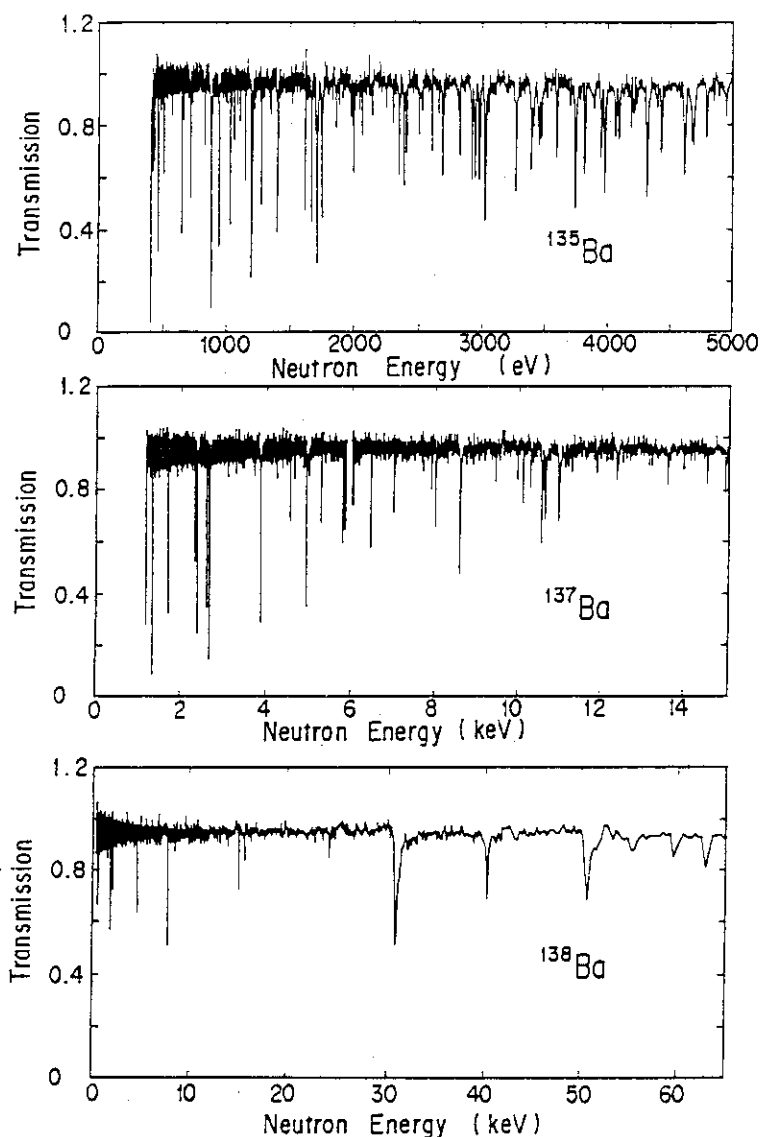
Fig. 1 Transmission data of ^{135}Ba, ^{137}Ba and ^{138}Ba. The data for ^{137}Ba arount 6 keV are obscured by the Al resonance in the flight path wimdow.
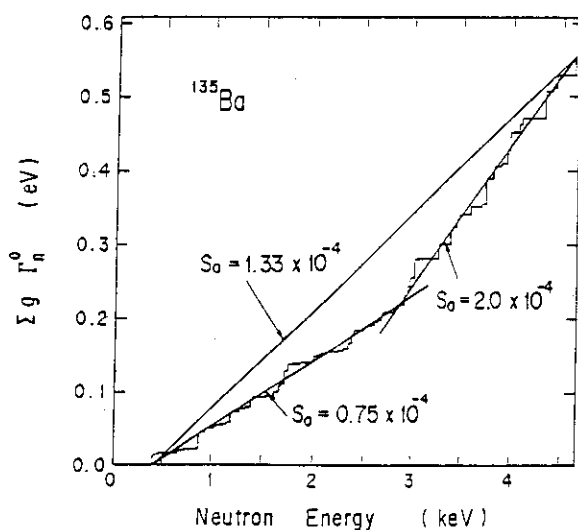
Fig. 2 The sum of the reduced neutron widths versus energy for ^{135}Ba
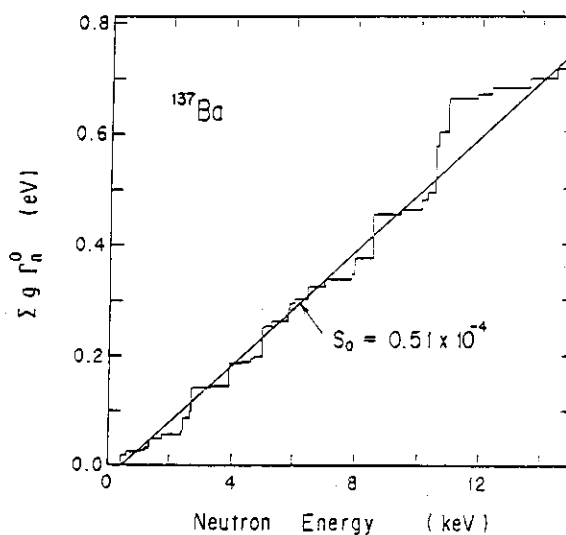
Fig. 3 The sum of the reduced neutron widths versus energy for ^{137}Ba

6.5 TRANSMISSION EFFICIENCY OF THE NEUTRON GUIDE TUBE WITH ALIGNMENT ERRORS

Masatoshi SUZUKI, Yuji KAWABATA, Hidetake TAKAHASHI
Masanobu SAKAMOTO[*]

Department of Research Reactor Operation and [*]Department of
Physics

Introduction

The neutron guide tube is able to lead slow neutrons from the neutron
source to the large beam hall over long distances without significant loss,
by means of total reflections of neutrons on the metallic mirror surfaces,
for instance Ni[1]. The practical usefulness of the neutron guide tubes in
large scale has been already established not only on the continuous
neutrons from the research reactors, for instance ILL in Grenoble, but also
on the pulsed neutrons from spallation sources.

The reconstruction program of JRR-3 (Japan Research Reactor-3, JAERI)
has the plan of the neutron guide tubes, which are two thermal neutron
guide tubes (57m and 58m long for the characteristic wave length 2Å) and
three cold neutron guide tubes (44m and 37m for 4Å and 27m for 6Å).

Experiment

A 1/10 scale model of the planned neutron guide tubes have been made,
in order to study the effects of the alignment errors on the neutron
transmissions, by using slow neutrons from the JAERI electron linac. The
energy analysis of the neutrons have been made by the time of flight (TOF)
method. The flight paths are 6m from the target to the entrance of the
model guide tube, and 2m from the entrance to the ^{3}He detector. The
experimental arrangement is schematically shown in Fig.1.

The internal cross-section of the 1/10 scale model is 2mm wide and 60mm
height, and the length of one unit is 300mm long. Six units make the 1.8m
long neutron guide tube for studying its characteristics. The neutron
mirror is made of Ni evaporated on the polished borosilicate glass, with
the thickness of more than 1000Å which is same with the planned guide tube.
The surface roughness measured by the stylus method is less than 100Å with
cut-off of 0.8mm. The guide tube units fabricated in the precision within

0.01mm are aligned precisely by the position adjuster with micrometer within 0.1mm.

Results

The neutron beam divergence have been measured by scanning the detector horizontally with 0.5mm step for the source neutron beam with 5mm slit and the transmitted beam through the straight guides with different length, as shown in Fig.2. Here, neutron counts means the total counts of which the wavelength is longer than 1Å. The enhanced peak of the transmitted neutrons through the guide tube with 6 units shows the effectiveness of the straight guide tube. In other words the straight guide tube with enough length can conduct the neutrons which may spread and cannot be used when the guide tube is short. The rates of transmitted neutrons against the neutrons incident to the guide tube are about 65% for 0.5 - 1.5Å in wavelength and about 100% for 1.5 - 2.5Å. In order to cancel the angular divergence of the incident neutron source, the all results of the transmission rate in this study are normalized to the observed results on the straight guide tube with 6 units, as can be seen in Fig.2.

The observed transmissions of the straight guide tube with abutment error are shown in Fig.3, in which the fourth unit in the guide tube is moved horizontally 20% and 10% of the internal width of the guide tube. The results for the curved guide tube with the characteristic wavelength 2Å are shown in Fig.4 and Fig.5, together with the calculated results of the analysis code 'NEUGT'[2], in which the fourth unit is moved horizontally 20%, 10% and 0% of the beam width to inner and outer side to the curved guide respectively.

In the case of the curves guide tube with the characteristic wavelength 2Å, the effects of the rotational adjustment error on the neutron transmission are also studied. The observed and calculated results are shown in Fig.6 and Fig.7 for A type and B type error for the fourth unit, as noted in Fig.1, in which the angle of the error is 0.05°. There is no essential difference between A type and B type, except the positional of the gap. However, Fig.5 and Fig.6 show that the transmission for A type alignment error is larger than that for B type. The reason is the abutment direction. Neutrons with garland reflections, which go near the outer wall, can go through the A type error because the unit on the lower reach goes outside. As the unit on the upper reach goes outside for B type, the

garland component cannot go through it.

Conclusion

The neutron transmission efficiencies of the 1/10 scale model guide tube have been studied experimentally in order to make clear the effects of the alignment errors. All of the experimental results agree well with the calculated results of 'NEUGT'. For 3Å neutron, the effects of the alignment errors on the transmission are summarized as follows,

(1) The horizontal abutment errors of 10% and 20% for the beam width on the straight guide tube the transmission decrease of 14% and 26% respectively.

(2) The abutment error of 10% and 20% on the curved guide tube give the decrease of 20% and 22% for inner side error, and 11% and 30% for outer side.

(3) The rotational adjustment errors of 0.05° on the curved guide tubes give the decrease of 11% for A type and 27% for B type.

References

1) M.Suzuki et al., JAERI-M 86-037
2) T.Harami et al., JAERI-M 85-092
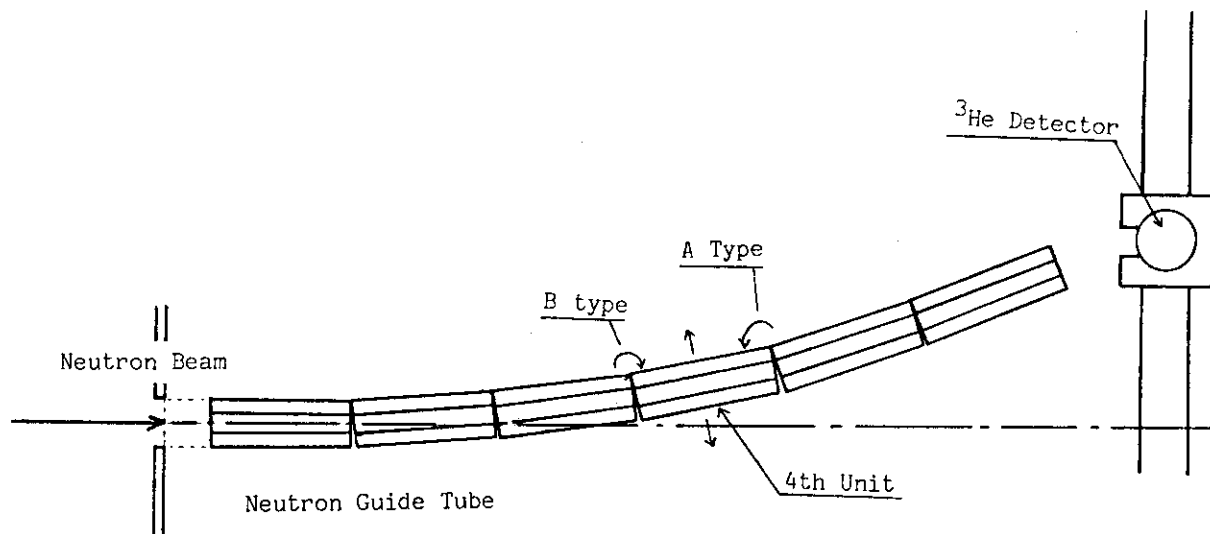
Fig.1 Experimental arrangement
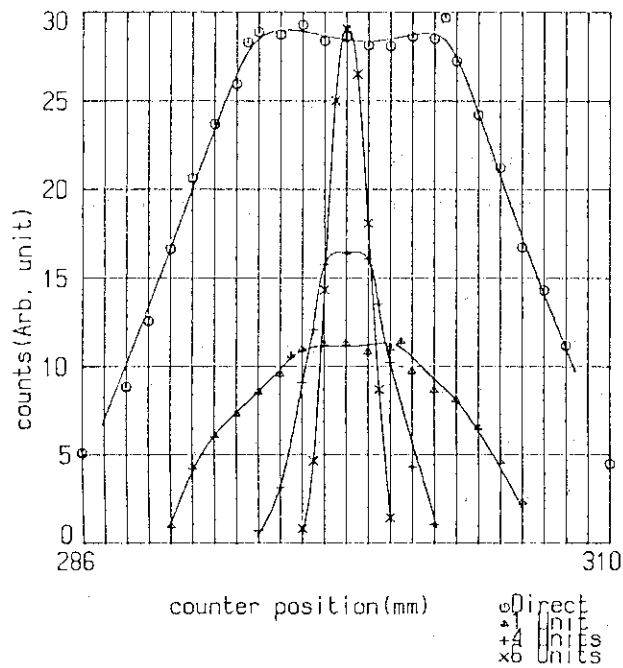
Fig.2 Effectiveness of the straight guide tube. The beam divergence from the straight guides with the different length and the source beam.
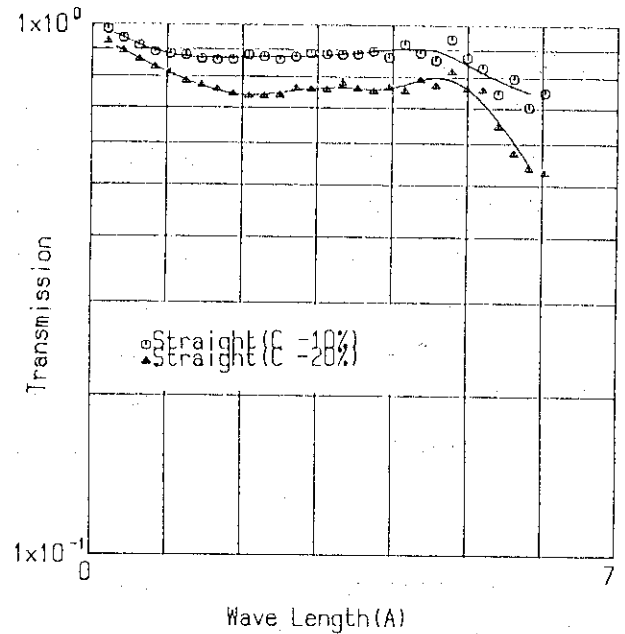
Fig.3 The neutron transmission of the straight guide tube with the horizontal abutment error. The errors are 20% and 10% of the beam width.
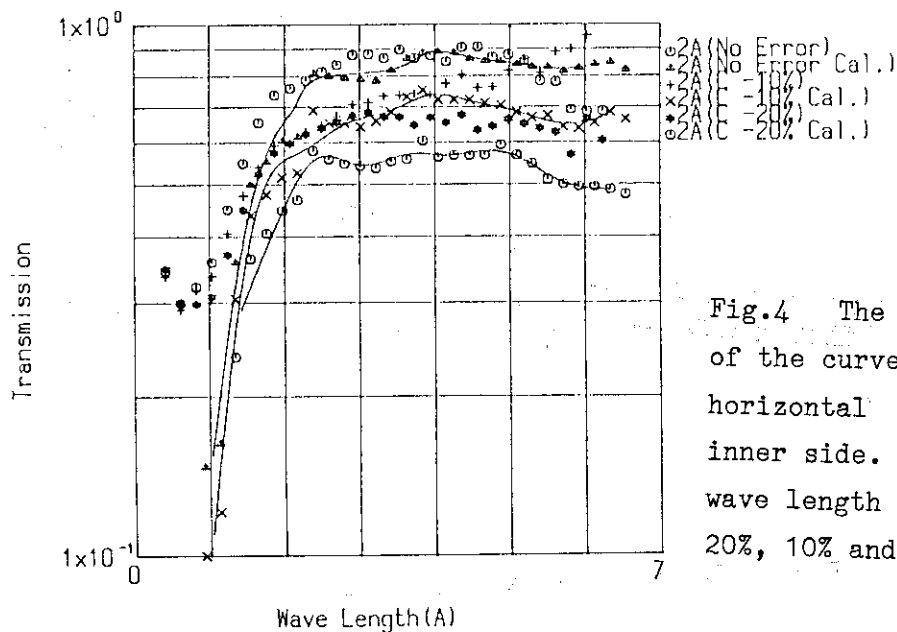
Fig.4 The neutron transmission of the curved guide tube with the horizontal abutment error to inner side. The characteristic wave length is 2A. The errors are 20%, 10% and 0% of the beam width.
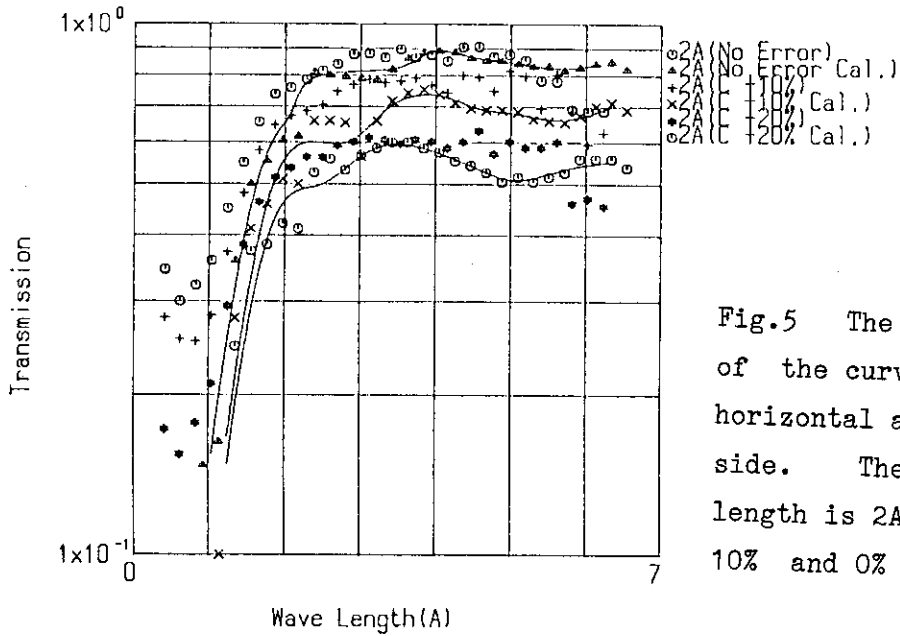
Fig.5 The neutron transmission of the curved guide tube with the horizontal abutment error to outer side. The characteristic wave length is 2A. The errors are 20%, 10% and 0% of the beam width.
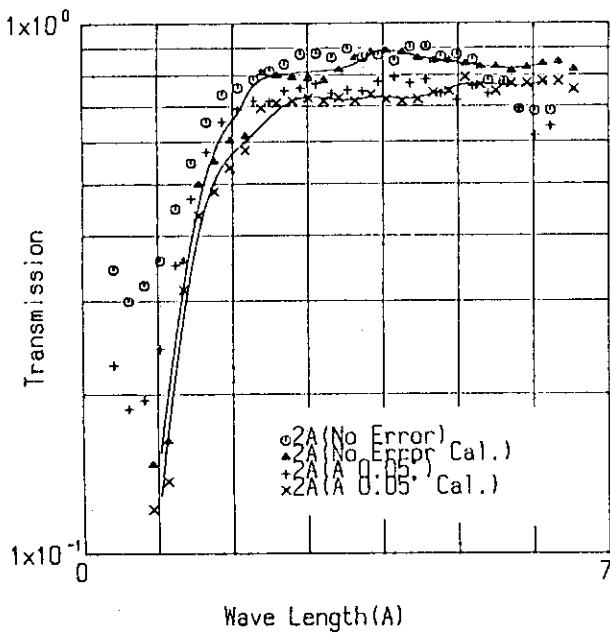
Fig.6 The neutron transmission of the curved guide tube with the rotational adjustment error of A type. The errors are 0.05° and 0°.
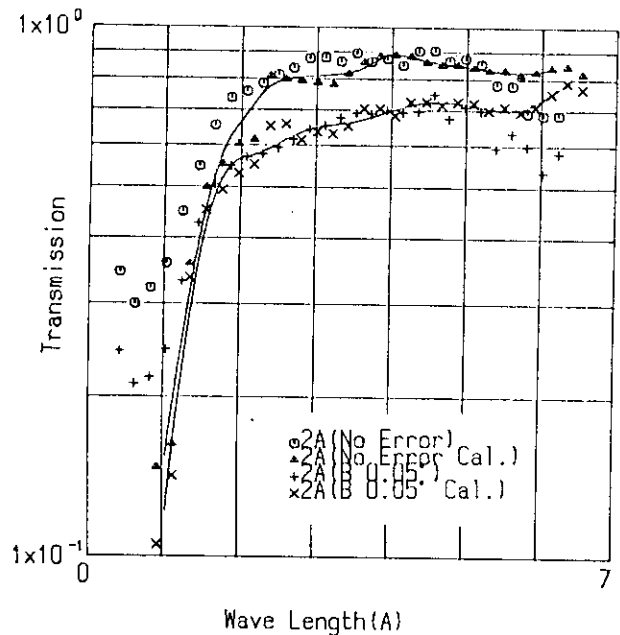
Fig.7 The neutron transmission of the curved guide tube with the rotational adjustment error of B type. The errors are 0.05° and 0°.

- 205~(206) -

Ⅶ PUBLICATIONS

7.1 Publications in Journals and Proceedings

1. Baba, Y.

   Studies on Surface Chemical States of Some Metals and Cermics
   Bombarded with Energetic Light-ions.

   JAERI 1304 (1987).

2. Baba, Y. and Sasaki, T.A.

   Surface Chemical Changes of TiC, TiN and TiO_2 by Light-ion
   Bombardments.

   J. Nucl. Mater. 145-147 (1987) 396.

3. Chiba, S., Yamanouti, Y., Mizumoto, M., Sugimoto, M., Hyakutake, M.,
   Iwasaki, S. and Kawaraswaki, Y.

   Measurement of the Fast Neutron Cross Sections at the JAERI Tandem
   Accelerator Facility.

   JAERI-M 87-025 (1987) 262.

   T

4. Fujita, H., Kato, N., Tachikawa, T., Sugimitsu, T., Kimura, K.,
   Ikeda, Y., Yamaguchi, H., Nakajima, Y., Sugiyama, Y., Tomita, Y.,
   Ikezoe, H., Ideno, K., Shikazono, N., Kubono, S. and Tanaka M.

   Spin-Orbit Interaction Deduced From Elastic and Inelastic Scattering
   of The $^{19}F + ^{16}O$ System.

   Submitted in Phys. Lett. B.

   T

5. Hanashima, S. and Minehara, E.

   Scaling of the Optical Parameters for the JAERI Tandem Accelerator

   Proc. SNEAP-85, Argonne, Illinois (1985).

   Rev. Sci. Instrum, 57(5)(1986) 787.

   T

6. Haruna, K., Maeta, H., Ohashi, K., and Koike, T.

   The Negative Thermal Expansion Coefficient of GaP Crystal at Low
   Temperature.

   J. Phys. C19 (1986) 5149.

7. N. Igata, K. Miyahara, C. Tada, D. Blasl, S. Hamada, T. Sawai,

H. Kayano and Y. Hosoi

Microstructure and Mechanical Properties of α-Particle Irradiated
Stainless Steels.

J. Nucl. Mat <u>141-143</u> (1986) 543.

8. Ikezoe, H., Shikazono, N., Tomita, Y., Ideno, K., Sugiyama, Y.,
    Takekoshi, E., Tachikawa, T. and Nomura, T.
    Measurements of Evaporation Residues to Investigate Lower Limiting
    Angular Momenta in Fusion Reactions.
    Nucl. Phys. <u>A456</u> (1986) 298.
    T

9. Ikezoe, H., Shikazono, N., Tomita, Y., Sugiyama, Y., Ideno, K.
    Coincidence Measurements of Light Particles and Evaporation
    Residues in the $^{16}O + ^{27}Al$ Reaction
    Nucl. Phys. <u>A462</u> (1987) 150.
    T

10. Ishida, I., Yoshiie, T., Kiritani, M., Sasaki, S., Iwase, A., Iwata, T.
     Observation of Defect Clusters in Masked Thin Foil Cu by He^{+} Ion
     Irradiation.
     Proc. XIth Int. Cong. on Electron Mycroscopy in Kyoto (1986) p.1281.
     V

11. Ishii, M., Ishii, T., Makishima, A. and Ogawa, M.,
     Yrast States of Two Quasi-Protons Coupled with Bosons.
     Proceedings of Int. Nucl. Phys. Conf. Harrougate U.K. (1986).
     T

12. Ishii, M., Makishima, A., Hoshi, M. and Ishii, T. Si Box: New Tool
     for In-Beam γ-Ray Spectroscopy through Heavy-Ion Fusion Reactions.
     Nuclei off the Line of Stability (ed. R.A. Meyer and D.S. Brenner,
     American Chemical Society, Washington D.C. 1986).
     T

13. Ishii, T., Ishii, M., Hoshi, M. and Ogawa, M., B(E2) Anomaly in
     Ground-State Band in $^{126,124}Ce$.
     Proceedings of Int. Nucl. Phys. Conf. Harrougate U.K. 1986.

     T

14. Iwamoto, A.
    Exciton-Model Approach to Fast-Particle Emission in Heavy-Ion
    Collisions.
    Phys. Rev. C35 (1987) 984.

15. Iwamoto, A. and Harada, K.
    Enhancement of the Subbarrier Fusion Reaction Due to Neck Formation
    Z. Phys. A326 (1987) 201.

16. Iwase, A., Sasaki, S., Iwata, T. and Nihira, T.
    Anomalous Reduction of Stage I Recovery in Nickel Irradiated with
    Heavy Ions in the Energy Range 100-120 MeV.
    Phys. Rev. Lett. 58 (1987) 3560.
    T

17. Iwase, A., Sasaki, S., Iwata, T. and Nihira, T.
    Defect Production and Recovery in Nickel Irradiated with Energetic
    Ions.
    J. Nucl. Mater. 141-143 (1986) 786.
    V

18. Iwata, T.
    Radiation Effect Studies in the Tandem Energy Region.
    Proceedings of Beijing International Symposium on Physics at Tandem,
    ed. J. Chenglie, L. Shounan, S. Zuxun and Z. Huangiao
    (World Scientific, 1987) p. 587.   T

19. Y. Kawarasaki et al.
    A Preparatory Study of Linac for the FEL Project at JAERI.
    Proc. of the 11 Meeting on Linac in Tsukuba (1986) 93.
    L

20. Kazumata, Y., Yugo, S. Kimura, T., Sato, T and Nakano, Y
    ESR of Pyro-Graphite Irradiated by Ions I.
    Low Energy Ion Bombardments.
    J. Phys. Chem. Solids 47 (1986) 617.
    V

21. Kazumata, Y., Yugo, S., Kimura, T and Nakano, Y.
    ESR of Pyro-Graphite Irradiated by Ions II.
    High Energy Ion Bombardments.
    J. Phys. Chem. Solids 47 (1986) 633.
    T

22. Kirchner, R., Klepper, O., Scherdt, D. and Sekine, T.
    Ion Source Development for the GSI On-Line Isotope Separator.
    Nucl. Instrm. & Methods B26 (1987) 23.

23. Komaki, Y., Ohno, S., Ohtsu, H., Itoh, H., Seguchi, T. and Iwasaki, M.
    Heavy Ion Track Registration in Polyvinylidene Fluoride.
    Nucl. Tracks Radiat. Meas. 11 (1986) 99.
    T

24. Kumagai, H., Fuse, M., Gotoh, E., Ohshima, M., Hashizume A., and
    Inamura, T.
    Parallel Plate Avalanche Counter - Application in the Coulomb
    Excitation Study.
    to be published in RIKEN Accel. Progr. Rep. 20 (1986).
    T

25. Kuroda, K., Noda, K., Ishii, Y., Saka, Y., Imura, T. and Watanabe, H.
    Microstructure of Ion-Irradiated Si_3N_4.
    Proc. 11th Int. Cong. on Electron Microscopy in Kyoto (Aug. 31 –
    Sep. 7, 1986) p. 1305-1306.
    V

26. Makishima A., Adachi M., Taketani H. and Ishii M., Yrast Band in
    Yrast Band in $^{138,136}Sm$ and ^{132}Nd.
    Phys Rev. C34 576 (1986).   T

27. Mashiko, K., Nobusaka, Y., Shoji, T., Isizaki, N. and Kawarasaki, Y.
    Status of the JAERI-Linac.
    Proceedings of the 11th Meeting on linac in Tsukuba (1986).

28. Minehara, E.
    A Compact High Voltage Isolation Transformer for the 350 kV Injector
    of the JAERI Tandem Accelerator.
    Nucl. Instrum. & Methods A249 (1986) 137.

29. Minehara, E., Oshima, M., Kikuchi, S., Inamura, T., Hashizume,
    A. and Kumahora, H.
    Signature Dependence Observed for M1 Transition between Rotational
    Levels Based on an $f_{7/2}$ Single-Particle State in ^{163}Dy.
    Phys. Rev. C35 (1987) 358.
    T

30. Minehara, E., Yoshida, T., Abe, S. Kanazawa, B., Tsukihashi, Y.,
    Horie, K. and Hanashima, S.
    An Extension to the 350 kV Negative Ion Injector for the JAERI
    Tandem Accelerator.
    Rev. Sci. Instrum. 38 (1987) 215.

31. Mizumoto, M.
    Nuclear Data related to Accelerator Applications.
    Proc. of the 1986 Seminar on Nuclear Data. JAERI-M 87-025 (1987).

32. Naramoto, H., Kikuchi, A. and Ozawa, K.
    Irradiation Effects with Heavy Ions on Alkali Halides (I)
    JAERI-M 84-129, 943.
    T

33. Noda, K., Ishii, Y., Matsui, H. and Watanabe, H.
    Irradiation Damage in Lithium Oxide.
    Advances in Ceramics (American Ceramic Society), submitted.
    T

34. Noda, K., Ishii, Y., Ohno, H., Watanabe, H. and Matsui, H.
    Irradiation Defects and Ion Conductivity of Lithium Oxide.
    Advances in Ceramics (American Ceramic Society), submitted.
    T

35. Ohkubo M.
Neutron Total Cross Section Measurements on Oxygen, Aluminum and
Carbon below 930 keV.
JAERI-M-86-193 (Jan. 1987).   L

36. Ohkubo M.
Reduction of Delayed Gamma Ray Backgrounds for a Pulsed Neutron Source.
Nucl. Instr. Methods A253 (1986) 43.
L

37. Ohno, S., Furukawa, K. and Soga, T.
Chemical Effectiveness of Elastic and Inelastic Energy Loss of He^+,
Ar^+ and Xe^+ Ions Bomberding Solid Potassium Nitrate.
Bull. Chem. Soc. Jpn., 59 (1986) 1947.

38. Oshima, M.
Electromagnetic Properties of Atomic Nuclei.
RCNP Report P-87 (1987) 40.
T

39. Sataka, M. and Kawatsura, K.
Characteristics of Gas Stripper Cell for Production of Multi-Charged
Ions.
JAERI-M 86-154 (1986).
V

40. Schutz, Y., Baktash, C., Lee, I.Y., Halbert, M.L., Hensley, D.C.,
Johnson, N.R., Oshima, M., Ribas, R., Lisle, J.C., Adler, L.A.
Honkanen, K., Sarantites, D.G., Larabee, A.J. and Saladin, J.X.
Search for Superdeformed Shapes in ^{144}Gd.
Phys. Rev. C 35 (1987) 348.
T

41. Sekine, T., Ichikawa, S. and Baba, S.
Triple Neutron Capture of ^{153}Eu in a Reactor: The Cross Sections of
^{154}Eu and ^{155}Eu.
Int. J. Appl. Red. Isotopes, in press.

42. Sekine, T., Cerny, J., Kirchner, R., Klepper, O., Koslowsky, V.T., Plochocki, A., Roechl, E., Schardt, D., Sherrill, B. and Brown, B.A.
The Beta Decay of ^{48}Mn: Gamow-Teller Quenching in fp-Shell Nuclei.
Nucl. Phys. <u>A467</u> (1987) 93.

43. Shinohara, N., Usuda, S., Ichikawa, S., Suzuki, T., Magara, M., Okashita, H., Yoshikawa, H., Horiguchi, T., Iwata, Y., Shibata, S. and Fujiwara, I.
Actinides Produced by ^{12}C + ^{242}Pu and ^{16}O + ^{238}U Reactions.
Phys. Rev. <u>C34</u> (1986) 909.   T

44. Soga, T., Furukawa, K. and Ohno, S.
Chemical Reaction Induced by Energetic Particles.
JAERI-M 86-112, p.100 (1986).
V

45. Soga, T., Furukawa, K. and Ohno, S.
Effects of the Deposited Energy Density on the Chemical Reaction.
Proc. 52nd Ann. Conf. Chem. Soc. Jpn., <u>1</u> (1986) 322.
V

46. Sugiyama, Y., Tomita, Y., Ikezoe, H., Ideno, K., Shikazono, N., Kato, N., Fujita, H., Sugimitsu, T. and Kubono, S.
Transfer Cross Sections For ^{28}Si + ^{58,82}Ni.
Phys. Lett. <u>B176</u> (1986) 302.
T

47. Tomimitsu, H., Kazumata, Y. and Sakai, E.
X-Ray Diffraction Topographic Observation of Silicon Single Crystals.
Irradiated with Energetic Heavy Ions (5).

48. Usuda, S.
Anion Excahnge Behaviour of the Transplutonium and Rare Earth Elements in Nitric Acid - Methyl Alcohol Media at Elevated Temperature.
J. Radioanal. Nucl. Chem. <u>111</u> (1987) 399.

49. Usuda, S.
Anion Exchange Behaviour of the Transplutonium Elements in Hydrochloric

Acid – Alcohol Media at Elevated Temperature.

J. Radioanal. Nucl. Chem. 111 (1987) 477.

50. Usuda, S. and Shinohara, N.

Simple Ion-Exchange System for Transplutonium Elements Synthesized by

Heavy-Ion Bombardments.

JAERI-M 86-188 (1987).

T

51. Usuda, S., Shinohara, N. and Yoshikawa, H.

Single Column Ion Exchange Separation of the Transplutonium Elements

from Uranium Targets Bombarded with Heavy Ions and Catcher Foils.

J. Radioanal. Nucl. Chem. 109 (1987) 353.

T

52. Electron Linac Group

Electron Linac Operation and Improvements.

JAERI-M 86-112 (1986) 18.

7.2 Contributions to Scientific and Technical Meetings

1. Aruga, T., Katano, Y. and Shiraishi, K.
   Microstructural Evolution in He-Preinjected Stainless Steel Irradiated with Electrons.
   Third International Conference on Fusion Reactor Materials, in Karlsruhe F.G. Germany (Oct. 4-8, 1987) (Accepted for presentation.).
   V

2. Baba, S., Hata, K., Sekine, T., Matsuoka, H., Nagame, Y. and Yokoyama, A.
   Nucleon Transfer Reactions in the System ^{37}Cl + ^{103}Rh.
   The 30th Symposium on Radiochemistry in Sendai (Oct. 22-24, 1986).
   T

3. Baba, Y. and Sasaki, T.A.
   Thermal Desorption of D_2 and He Implanted in TiO_2.
   Annual Meeting of the Atomic Energy Society of Japan in Nagoya (Apr. 1-3, 1987).

4. Chiba, S., Yamanouti, Y., Sugimoto, M., Furuta, Y., Mizumoto, M., Hyakutake, M. and Iwasaki, S.
   Measurement of Fast Neutron Scattering Cross Section of ^{118}Sn.
   Autumn Meeting of the Atomic Energy Society of Japan in Fukuoka (Oct. 16-18, 1986).
   T

5. Chiba, S., Yamanouti, Y., Mizumoto, M. Hyakutake, M. and Iwasaki, S.
   Measurement of the Elastic and Inelastic Scattering Cross Sections of ^{7}Li and En = 11.0 and 13.0 MeV.
   Annual Meeting of the Atomic Energy Society of Japan in Nagoya (Apr. 1-3, 1987).
   T

6. Fujita, H., Kato, N., Sugimitsu, T. and Sugiyama, Y.
   3-Body Cluster Coupled Channel Calculations for Elastic and

Inelastic Scattering of the ^{19}F + ^{12}C, ^{16}O Systems.
Symposium on Clustering Aspects in Nuclear Physics, INS. University
of Tokyo (Jan. 12-15, 1987).
T

7. Fujita, H., Kato, N., Sugimitsu, T. and Sugiyama, Y.
3-Body Cluster Coupled Channel Calculations for Elastic and
Inelastic Scattering of the ^{19}F + ^{12}C, ^{16}O Systems.
Annual Meeting of the Physical Society of Japan in Nagoya (Mar. 27-30,
1987)
T

8. Fujita, H., Kato, N., Tachikawa, T., Sugimitsu, T., Kimura, K.,
Ikeda, Y., Yamaguchi, H., Nakajima, Y., Sugiyama, Y., Tomita, Y.,
Ikezoe, H., Ideno, K., Shikazono, N., Kubono, S. and Tanaka, M.
Spin-Orbit Interaction Deduced from Elastic and Inelastic Scattering
of ^{19}F + ^{16}O system.
International Conf. on Nuclear Physics, Harrogate, U.K. (Aug. 1986).
T

9. Fujita, H., Kato, N., Tachikawa, T., Sugimitsu, T., Kimura, K.,
Ikeda, Y., Yamaguchi, H., Nakajima, Y., Sugiyama, Y., Tomita, Y.,
Ikezoe, H., Ideno, K., Shikazono, N., Kubono, S. and Tanaka, M.
Elastic and Inelastic Scattering of The System ^{19}F + ^{16}O.
Annual Meeting of the Physical Society of Japan in Tokyo (Mar. 29 -
Apr. 1, 1986).
T

10. Hanashima, S. and Minehara, E.
Control System for the JAERI Tandem Accelerator.
7th Tandem Conference in West Berlin, West Germany (Apr. 6-10, 1987).
T

11. Hanashima, S., Ohuchi, I., Kanda, K., Tsukihashi, Y., Horie, K. and
Minehara, E.
Improvement of the Control System for the JAERI Tandem Accelerator.
Annual Meeting of Physical Society of Japan in Nagoya (Mar. 28 -
Apr. 1, 1987).   T

12. Haruna, K., Maeta, H., Ohashi, K. and Koike, T.
    The Negative Thermal Expansion Coefficient in High Energy Ion
    Irradiated Semiconductors Materials.
    Autumn Meeting of Japan Applied Physical Society in Sapporo (Sept. 30, 1986).
    T

13. Haruna, K., Maeta, H., Ohashi, K. and Koike, T.
    The Negative Thermal Expansion Coefficient in High Energy Ion
    Irradiated Si and InP Crystals.
    Annual Meeting of Physical Society of Japan in Tokyo (Mar 29 – Apr. 1,
    1986).
    T

14. Ishida, I., Yoshiie, T., Sasaki, S., Iwase, A., Iwata, T. and Kiritani,
    M.
    Distribution of Primary Damage and Point Defect Clusters along the Depth
    Direction in He$^+$ Ions Irradiated Cu.
    Spring Meeting of Japan Institute of Metals in Tokyo (Mar. 31 – Apr.
    3, 1987).
    V

15. Ideno, K., Yokota, W., Tomita, Y., Ikezoe, H., Sugiyama, Y., Hanashima,
    S.
    Scission in the Reactions of $^{35}Cl + ^{46}Ti$ and $^{37}Cl + ^{48}Ti$.
    Autumn Meeting of the Japan Physical Society in Kobe (Oct. 7-10, 1986).

16. Ishii M., Ishii T., Hoshi M. and Ogawa M.,
    Collective Motion in Very Ligh Rare-Earth Nuclei.
    The RCNP Symposium at the Osaka University, (July 1986).
    T

17. Ishii M., Ishii T., Ogawa M. and Hoshi M.,
    g-Factors of High-Spin States in $^{136,138}Sm$ and ^{132}Nd.
    Autumn Meeting of the Japan Physical Socity in Kobe (Oct. 7-10, 1986).
    T

18. Ishii T., Ishii M., Ogawa M. and Hoshi M.,
    Yrast States of Two Quasi-Prontons Coupled with Boson, Autumn
    Meeting of the Japan Physical Society in Kobe (Oct. 7-10, 1986).

19. Ishii, T., Ishii, M., Ogawa, M. and Hoshi, M.
    Electromagnetic Properties of Very Light Rare-Earth Nuclei.
    The "KIKEN" Nuclear Structure Symposium on IBM and related Topics in
    Kyoto, (Jan. 1987).
    T

20. Iwamoto, A.
    Exciton Model and Moving Source Model.
    Autumn Meeting of Physical Society of Japan in Kobe (Oct. 7-10, 1986).

21. Iwamoto, A.
    Width of the Mass Distribution in Heavy-Ion-Induced Fusion-Fission
    Reaction.
    Annual Meeting of Physical Society of Japan in Nagoya (Mar. 27-30,
    1987).

22. Iwase, A., Sasaki, S., Iwata, T. and Nihira, T.
    Defect Production and Recovery in FCC Metals Irradiated with energetic
    Ions (IV).
    Autumn Meeting of the Physical Society of Japan in Nishinomiya
    (Sep. 27-30, 1986).   T   V

23. Iwase, A., Sasaki, S. Iwata, T. and Nihira, T.
    Anomalous Reduction of Stage I Recovery in Nickel Irradiated with
    Energetic Heavy Ions.
    The Joint Seminar on Atomic Physics, Solid State Physics and Material
    Science in the Energy Region of TANDEM Accelerator in Tokai (Jan. 8-
    10, 1987).   T   V

24. Katano, Y., Ohno, H. and Katsuta, H.
    Damage Structure in Al_2O_3 Single Crystal Irradiated with He-Ions.
    Autumn Meeting of Japan Institute of Metals in Nagoya (Oct. 4-6, 1986).
    V

25. Katano, Y., Ohno, H. and Katsuta, H.
    Damage Structure in Al_2O_3 Single Crystal Irradiated with He-Ions.
    Third International Conference on Fusion Reactor Materials. (Oct.
    4-8, 1987) in Karlsruhe,

(Accepted for presentation)

V

26. Kawatsura, K., Ootuka, A., Sataka, M., Komaki, K., Naramoto, H., Ozawa, K., Nakai, Y. and Fujimoto, F.
Radiative Electron Capture for $Cl^{16+,17+}$ Ions on He Target.
Tenth International Conference on Atomic Physics in Tokyo (Aug. 25-29, 1986).
T

27. Kawatsura, K., Ootuka, A., Sataka, M., Komaki, K., Naramoto, H., Sugizaki, Y., Ozawa, K., Nakai, Y. and Fujimoto, T.
Continuum X Rays during Ion-Atom Collisions.
International Seminar on Dynamic Processes of Highly Charged Ions in Susono (Aug. 21-23, 1986).
T

28. Kawatsura, K., Sataka, M., Naramoto, H., Ozawa, K., Nakai, Y., Ootuka, A., Komaki, K. and Fujimoto, F.
Performance of the High Resolution X-Ray Crystal Spectrometer.
Autumn Meeting of the Physical Society of Japan in Nishinomiya (Sept. 27-30, 1986)
T

29. Kawatsura, K., Sataka, M., Naramoto, H., Ozawa, K., Nakai, Y., Ootuka, A., Komaki, K. and Fujimoto, F.
REC X Rays in Heavy Ion-Atom Collisions (I).
Autumn Meeting of the Physical Society of Japan in Nishinomiya (Sept. 27-30, 1986).
T

30. Kawatsura, K., Sataka, M., Ootuka, A., Komaki, K., Naramoto, H., Ozawa, K., Nakai, Y., Fujimoto, F. and Ishii, K.
Energy and Lifetime Mesurements in Highly Ionized Chlorine.
U.S. - Japan Joint Seminar on Interactions of Highly Ionized Atoms Produced by Ion-Atom Collisions in Kobe   (Mar. 16-20, 1987).
T

31. Kawatsura, K., Ootuka, A., Sataka, M., Komaki, K., Naramoto, H., Ozawa, K., Nakai, Y. and Fujimoto, F.
    Radiative Electron Capture in Heavy Ion and He Collisions.
    U. S. - Japan Joint Seminar on Interactions of Highly Ionized Atoms Produced by Ion-Atom Collisions in Kobe (Mar. 16-20, 1987).
    T

32. Kawatsura, K., Sataka, M., Naramoto, H., Sugizaki, Y., Nakai, Y., Ootuka, A., Komaki, K. and Fujimoto, F.
    REC X Rays in Heavy Ion-Atom Collisions (II).
    Annual Meeting of the Physical Society of Japan in Nagoya (Mar. 27-30, 1987).
    T

33. Kazumata, Y., Naramoto, H. and Kikuchi, A.
    Lattice Defects in SiC Irradiated by Ions.
    Annual Meeting of Physical Society of Japan in Nagoya (Mar. 27-30, 1987).

34. Kuroda, K., Noda, K., Ishii, Y., Saka, H., Imura, T. and Watanabe, H.
    Microstructure of Ion-Irradiated Si_3N_4.
    11th Int. Cong. on Electron Microscopy in Kyoto (Aug. 31 - Sep. 7, 1986).
    V

35. Maeta, H. Haruna, K., Ohashi, K., Ono, F.
    A Study of Radiation Mechanism in High Emergy Ion Irradiated Materials by X-ray Diffraction.
    Spring Meeting of Physical Society of Japan in Tokyo (Mar. 29 - Apr. 1, 1986).
    T

36. Magara, M., Shinohara, N., Usuda, S., Ichikawa, S., Suzuki, T., Okashita, H., Yoshikawa, H., Iwata, Y., Horiguchi, T., Shibata, S. and Fujiwara, I.
    Decay of ^{245}Cf.
    The 30th Symposium on Radiochemistry in Sendai (Oct. 22-24, 1986).
    T

37. Minehara, E., and Hanashima, S.
    JAERI Negative Ion Injectors.
    Seventh Tandem Conference in West Berlin   (Apr. 6-10, 1987).

38. Minehara, E., Pardo, R., Billquist, P. and Evans, W.
    Design of the ATLAS PIIECR Ion Source.
    Eleventh International Conference on Cyclotrons and their
    Applications in Tokyo   (Oct. 13-17, 1986).

39. Miyahara, K., Okazaki, Y., Motizuki, H., Hosoi, Y. and Kayano, H.
    Microstructure and Mechanical Properties of α-Particle Irradiated
    Fe-Cr-Mn Alloy.
    99th Meeting of Japan Institure of Metals in Nagoya (Oct. 20-22, 1986).

40. Mizumoto, M., Yamanouti, Y., Sugimoto, M., Chiba, S
    and Kawarasaki, Y.
    Measurements of Gamma-ray Spectrum from Aluminum.
    Annual Meeting of the Atomic Energy Society Meeting of Japan in
    Nagoya   (Apr. 1-3, 1987).
    V

41. Mizumoto, M. and Zhao Wenrong
    ^{148}Sm Resonance Parameter Measurements
    Autumn Meeting of the Atomic Energy Society Meeting of Japan in
    Fukuoka   (Oct. 16-18, 1986).
    L

42. Nagame, Y., Magara, M., Matsuoka, H., Sekine, T., Hata, K., Baba, S.
    and Yokoyama, A.
    Formation and Deexcitation of the ^{105}Ag Compound Nuclears.
    The 30th Symposium on Radiochemistry in Sendai (Oct. 22-24, 1986).
    T

43. Nakata, K., Takamura, S., Kobiyama, M. and Masaoka, I.
    Measurements of Damage Distribution of Ion-Irradiation by Electrical
    Resistivity.
    Autumn Meeting of Japan Institute of Metals in Nagoya (Oct. 20-22,
    1986).
    T

44. Naramoto, H., Kawatsura, K. Sataka, M., Sugizaki, Y., Nakai, Y.,
    Ozawa, K., Yamaguchi, S. and Fujino, Y.
    Development of Elastic Recoil Detection Analysis using High Energy
    Heavy Ions.
    Annual Meeting of Physical Society of Japan in Nagoya (Mar. 27-30,
    1987).
    T

45. Noda, K., Ishii, Y., Matsui, H., Suzuki, S. and Watanabe, H.
    Ion Conductivity of Oxygen Ion Irradiated Li_2O.
    Autumn Meeting of Atomic Energy Society of Japan in Fukuoka
    (Oct. 16-18, 1986).
    T

46. Noda, K., Ishii, Y., Ohno, H. Watanabe, H. and Matsui, H.
    Irradiation Defects and Ion Conductivity of Lithium Oxide.
    Symposium on Fabrication and Properties of Lithium Ceramics,
    89th Annual Meeting of the American Ceramic Society in Pittsburgh
    (April 27-29, 1987).
    T

47. Ogawa, M., Ishii, T., Ishii, M. and Hoshi, M.,
    B(E2) Anomaly in Ground - State Bands of ^{126}Ce and ^{124}Ce.
    Spring Meeting of the Japan Physical Society in Tokyo (April 1, 1986).
    T

48. Ohno, S.
    Radiation Chemistry.
    8th Meeting on Radiation Applications in Tokyo (Jan. 30, 1987).

49. Ohno, S.
    Microdosimetory of Ion Beams.
    Yayoi Symposium on Beam Technology and Radiation Chemistry
    (Dec. 13, 1986).

50. Ohtsuki, T., Sueki, K., Nakahara, H., Kohno, I., Shinohara, N.,
    Magara, M. and Nagame, Y.
    Configuration of Mass Yield Curves in Low Energy Fission of Actinide

Elements.

The 30th Symposium on Radiochemistry in Sendai (Oct. 22-24, 1986).

T

51. Ootuka, A., Kawatsura, K., Komaki, K., Fujimoto, F., Kouchi, N. and Shibata, H.

Effect of Molecular Ion Irradiation on Inner-Shall Ionization of Aluminum.

Annual Meeting of the Physical Society of Japan in Nagoya (Mar. 27-30, 1987).

V

52. Oshima, M.

Signature Dependence Observed for Transition Probabilities of ^{161,163}Dy.

RIKEN Symposium on Electromagnetic Transitions and Nuclear Structure in Saitama (Mar. 25, 1986).

T

53. Oshima, M.

Electromagnetic Properties of Atomic Nuclei.

RCNP Symposium on Nuclear Physics at High-Spin States in Osaka (July 20-22, 1986).

T

54. Oshima, M., Minehara, E., Ichikawa, S., Iimura, H., Inamura, T., Hashizume, A. and Kusakari, H.

M1 and E2 Transition Probabilities of the Ground-State Rotational Band in ^{161,161}Dy.

Annual Meeting of Physical Society of Japan in Nagoya (Mar. 27-30, 1987).

T

55. Sagara, A., Kamada, K., Sasaki, T.A., Baba, Y., Kitajima, M. and Yamaguchi, S.

Surface Segregation and Evaporation of Li in Al-Li Alloy.

Annual Meeting of the Atomic Energy Society of Japan in Nagoya (Apr. 1-3, 1987).

56. Sasaki, S., Iwase, A. and Iwata, T.
    Cascade Damage in Molybdenum by Heavy-Ion Irradiation with Energy Range
    of Around 100 MeV.
    Spring Meeting of Japan Institute of Metals in Tokyo (Mar. 31 - Apr.
    3, 1987).
    T

57. Sasaki, S., Iwase, A. and Iwata, T.
    Cascade Damage in Molybdenum by The Irradiation with Heavy-Ions from
    JAERI-Tandem Accelerator.
    Autumn Meeting of Japan Institute of Metals in Nagoya (Oct. 20-22,
    1986).
    T

58. Sasaki, S., Iwase, A. and Iwata, T.
    Cascade Damage in Molybdenum by High Energy Ion Irradiation.
    Annual Meeting of the Physical Society of Japan in Nagoya (Mar.
    27-30, 1987).
    T

59. Sasaki, T.A. and Baba, Y.
    Surface Chemical Changes of TiC, TiN and TiO_2 by Light-ion
    Bombardments.
    Seventh International Conference on Plasma-Surface
    Interactions in Controlled Fusion Devices in Princeton
    (May 5-9, 1986).

60. Sasaki, T.A. and Baba, Y.
    Surface Chemical Changes and Thermal Desorption of Implanted
    Hydrogen for Metal Oxides Bombarded with Hydrogen Ion.
    Autumn Meeting of the Atomic Energy Society of Japan in Fukuoka
    (Oct. 16-18, 1986).

61. Sasaki, T.A., Baba, Y., Sagara, A. and Kamada, K.
    Chemical State of Lithium Segregated on Surface of Al-Li Alloy.
    Annual Meeting of the Atomic Energy Society of Japan in Nagoya
    (Apr. 1-3, 1987).

62. Sataka, M., Ootuka, A., Kawatsura, K., Komaki, K., Naramoto, H., Nakai, Y., Fujimoto, F. and Ishii, K.
    Beam-Foil Spectroscopy of Multi-Charged Chlorine Ions (III)
    Autumn Meeting of the Physical Society of Japan in Nishinomiya (Sept. 27-30, 1986).
    T

63. Sataka, M., Ozawa, K., Kawatsura, K., Ootuka, A., Komaki, K., Naramoto, H., Nakai, Y., Fujimoto, F., Kikuchi, A. and Ishii, K.
    Beam-Foil Spectroscopy of Multi-Charged Chlorine Ions.
    Tenth International Conference on Atomic Physics in Tokyo (Aug. 25-29, 1986).
    T

64. Sekine, T., Cerny, J., Kirchner, R., Klepper, O., Koslowsky, V. T., Plochocki, A., Roeckl, E., Schardt, D., Sherrill, B. and Brown, B. A.
    The Beta Decay of ^{48}Mn: Gamow-Teller Quenching in fp-Shell Nuclei.
    The 30th Symposium on Radiochemistry in Sendai (Oct. 22-24, 1986).

65. Sugita, M.
    Coexistence of Bands in the Doubly Even Tin Isotopes.
    Autumn Meeting of Physicsl Society of Japan (Oct. 7-10, 1986).

66. Sugita, M. and Otsuka, T.
    Gamma Instability and Triaxiality in the O(6) Limit of the IBM.
    Annual Meeting of Physical Society of Japan in Nagoya (Oct. 1987).

67. Sugiyama, Y.
    DWBA Approach to the Molecular Resonance Observe in the ^{12}C + ^{12}C System.
    Symposium on Clustering Aspects in Nuclear Physics, INS, University of Tokyo (Jan. 12-15, 1986).

68. Sugiyama, Y.
    Heavy-Ion Spectrograph "ENMA" and Heavy-Ion Nuclear Reaction.
    Friday Seminar in JAERI (Nov. 7, 1985).
    T

69. Sugiyama, Y., Tomita, Y., Ikezoe, H., Ideno, K., Shikazono, N.,
    Kato, N., Fujita, H., Sugimitsu, T. and Kubono, S.
    Transfer Cross Sections for ^{28}Si + ^{58,62}Ni near the Coulomb Barrier.
    Autumn Meeting of the Physical Society of Japan in Kobe (Oct. 7-10,
    1986).
    T

70. Takahashi, M., Takeda, M., Baba, Y. and Sasaki, T.A.
    Characterization of Thermal Decomposition Product of $K_3[Sb(OX)_3]nH_2O$.
    Spring Meeting of Chemical Society of Japan in Kyoto (Apr. 1-4, 1986).

71. Takeuchi, S., Isii, T., Ikezoe, H., Ohkubo. M. and Shikazono, N.
    Development of Coaxial-Quarter-Wave-Line-Type Superconducting
    Niobium Accelerating Cavity.
    Spring Meeting of the Physical Society of Japan in Nagoya (Mar. 30,
    1987).

72. Usuda, S.
    Rapid Ion-Exchange Separation of Actinides.
    International Conference on Methods and Applications of Radioanalytical
    Chemistry in Kona, Hawaii (Apr. 5-10, 1987).

73. Yokoyama, A., Shinohara, A., Saito, T., Wakamatsu, S., Baba, H., Hata,
    K., Nagame, Y., Ichikawa, S. and Baba, S.
    Nucleon Transfer Reaction in the Systems of ^{197}Au + ^{16}O 6.6-MeV/u and
    8.8-MeV/u.
    Annual Meeting of the Physical Society of Japan in Nagoya (Mar. 27-30,
    1987).
    T

VIII PERSONNEL AND COMMITTEES

(April 1986 — March 1987)

8.1 Personnel

Department of Physics

	Naomoto	Shikazono	Director
	Yoichi	Suto	Administrative Manager

Accelerators Division

Scientific Staff	Michio	Maruyama*
	Shiro	Kikuchi
	Suehiro	Takeuchi
	Eisuke	Minehara
	Susumu	Hanashima
Technical Staff	Chiaki	Kobayashi**
(Tandem, V.D.G.)	Isao	Ohuchi
	Yutaka	Sato
	Tadashi	Yoshida
	Susumu	Kanda
	Katsuzo	Horie
	Satoshi	Tajima
	Yoshihiro	Tsukihashi
	Shinichi	Abe
	Shuhei	Kanazawa
Technical Staff	Katuo	Mashiko**
(Linac)	Yukio	Nobusaka
	Tokio	Shoji
	Nobuhiro	Ishizaki

Nuclear Physics Laboratory

Scientific Staff	Mitsuhiko	Ishii***

* Head, Accelerators Division

** Leader, Technical Staff

*** Head, Nuclear Physics Laboratory

Nuclear Physics Laboratory (continued)

Scientific Staff	Yoshiaki	Tomita
	Yasuharu	Sugiyama
	Akira	Iwamoto
	Kazumi	Ideno
	Hiroshi	Ikezoe
	Masumi	Ohshima
	Takaharu	Ohtsuka (~ December, 1986)
	Tetsuro	Ishii

Linac Laboratory

Scientific Staff	Yuuki	Kawarasaki*
	Makio	Ohkubo
	Motoharu	Mizumoto
	Yoshimaro	Yamanouchi
	Masayoshi	Sugimoto
	Satoshi	Chiba

Solid State Physics Laboratory I

Scientific Staff	Yukio	Kazumata**
	Hiroshi	Naramoto
	Hiroshi	Tomimitsu

Solid State Physics Laboratory II

Scientific Staff	Tadao	Iwata***
	Saburo	Takamura
	Hiroshi	Maeta
	Mitsuo	Watanabe
	Teruo	Kato
	Shigemi	Sasaki
	Akihiro	Iwase
	Terufumi	Yokota

* Head, Linac Laboratory
** Head, Solid State Physics Laboratory I
*** Head, Solid State Physics Laboratory II

Solid State Physics Laboratory III
  Scientific Staff   Masanobu   Sakamoto

Atomic and Molecular Physics Laboratory
  Scientific Staff   Yohta   Nakai*
                             Kiyoshi   Kawatsura
                             Masao   Sataka
                             Yasuaki   Sugizaki

Department of Chemistry
  Nuclear Chemistry Laboratory
    Scientific Staff   Tadashi   Yamamoto**
                             Toshio   Suzuki
                             Shigekazu   Usuda
                             Nobuaki   Kono
                             Shin-ichi   Ichikawa
                             Nobuo   Shinohara
                             Masaaki   Magara

  Analytical Chemistry Laboratory
    Scientific Staff   Yuji   Baba

  Physical Chemistry Laboratory
    Scientific Staff   Mutsuhide   Komaki

  Solid State Chemistry Laboratory
    Scientific Staff   Kazuhiko   Izui***
                             Shin-ichi   Ohno
                             Teikichi   Sasaki
                             Shigemi   Furuno
                             Takeshi   Soga
                             Katsutoshi Furukawa
                             Kiichi   Hojou

  * Head, Atomic and Molecular Physics Laboratory
 ** Head, Nuclear Chemistry Laboratory
*** Head, Solid State Chemistry Laboratory

Department of Radioisotope Production

  Production Development Division

    Scientific Staff   Sumiko   Baba

                       Hiromitsu   Matsuoka

                       Kentaro   Hata

                       Toshiaki   Sekine

                       Yuichiro   Nagame

Department of Fuels and Materials Research

  Physical Matallurgy Laboratory

    Scientific Staff   Akimichi   Hishinuma*

                       Takeo   Aruga

                       Shozo   Hamada

                       Tomotsugu   Sawai

                       Kenji   Suzuki

                       Katsumaro   Fukai

  Fuel Property Laboratory

    Scientific Staff   Hitoshi   Watanabe**

                       Kenji   Noda

                       Yoshinobu   Ishii

  Function Materials Laboratory

    Scientific Staff   Hiroji   Katsuta***

                       Hideo   Ohno

                       Takanori   Nagasaki

                       Yoshio   Katano

Department of Reactor Engineering

  Reactor Instrumentation Laboratory

    Scientific Staff   Eiji   Sakai

Radioisotope and Nuclear Engineering School

                       Kensuke   Shiraishi

   * Head, Physical Matellurgy Laboratory

  ** Head, Fuel Property Laboratory

*** Head, Function Materials Laboratory

Department of Health Physics

    Technical Staff   Shoji   Izawa*

                           Toshihiro Miyamoto

                           Takeo   Seki

* Chief of Radiation Control Group, Department of Health Physics

8.2 Tandem Steering Committee

(Chairman)	Toyojiro	Fuketa	(Deputy Director General, Tokai Research Establishment)
	Shojiro (-August, 1986)	Matsuura	(Director, Department of Reactor Engineering)
	Yoshihiko (August, 1986-)	Kaneko	(Deputy Director, Department of Reactor Engineering)
	Tatuo	Kondo	(Director, Department of Fuels and Materials Research)
	Naomoto	Shikazono	(Director, Department of Physics)
	Kaoru	Ueno	(Director, Department of Chemistry)
	Masatoshi	Tanaka	(Director, Department of Thermonuclear Fusion Research)
	Eiji	Shikata	(Director, Department of Radioisotopes)
(Secretary)	Masashi	Iizumi	(Deputy Director, Department of Physics)
(Secretary)	Michio	Maruyama	(Head, Accelerators Division)
(Secretary)	Yoichi	Suto	(Administrative Manager, Department of Physics)

8.3 Tandem Consultative Committee

(Chairman)	Shigeru	Mori	(Vice President)
(Vice Chairman)	Toyojiro	Fuketa	(Deputy Director General, Tokai Research Establishment)
(Vice Chairman)	Naomoto	Shikazono	(Director, Department of Physics)
	Hiromichi	Kamitsubo	(Principal Scientist, Institute of Physical and Chemical Research)
	Kōji	Nakai	(Professor, National Laboratory for High Energy Physics)
	Hiroyasu	Ejiri	(Professor, Osaka University)
	Shiori	Ishino	(Professor, University of Tokyo)
	Hiroyuki	Tawara	(Associate Professor, Institute of Plasma Physics, Nagoya University)
	Kohzoh	Masuda	(Professor, University of Tsukuba)
	Shiro	Iwata	(Professor, Kyoto University)
	Ichiro	Fujiwara	(Professor, Otemon Gakuin University)
	Kenji	Sumita	(Professor, Osaka University)
	Itsuro	Kimura	(Professor, Kyoto University)
(Secretary)	Masashi	Iizumi	(Deputy Director, Department of Physics)
(Secretary)	Michio	Maruyama	(Head, Accelerators Division)
(Secretary)	Yoichi	Suto	(Administrative Manager, Department of Physics)

8.4 Tandem Program Advisory Committee

(Chairman)	Naomoto	Shikazono	(Director, Department of Physics)
	Masashi	Iizumi	(Deputy Director, Department of Physics)
	Hirokazu	Umezawa	(Deputy Director, Department of Radio-isotopes)
	Shoji	Izawa	(Chief, Radiation Control Group, Department of Health Physics)
	Hitoshi	Watanabe	(Head, Fuel Property Laboratory, Department of Fuels and Materials Research)
	Tadashi	Yamamoto	(Head, Nuclear Chemistry Laboratory, Department of Chemistry)
	Yohta	Nakai	(Head, Atomic and Molecular Physics Laboratory, Department of Physics)
	Mitsuhiko	Ishii	(Head, Nuclear Physics Laboratory, Department of Physics)
	Yuuki	Kawarasaki	(Head, Linac Laboratory, Department of Physics)
	Michio	Maruyama	(Head, Accelerators Division, Department of Physics)
	Chiaki	Kobayashi	(Leader, Tandem Operation Group, Department of Physics)

− 237 ∼ (238) −

Ⅸ CO – OPERATIVE RESEARCHES

Title		Co-Operation Institution
1.6	Observation of Spontaneous Emission of Radiation at a Visible wave Length	Nuclear Engineering Research Laboratory, The University of Tokyo
2.2	Radiative Electron Capture in Heavy Ion and He Collisions	College of General Education, The University of Tokyo*
2.3	X-Ray Emission from Foil-Excited Chlorine Beams	College of General Education, The University of Tokyo*
2.4	Molecular Effect of Al $K\alpha$ Satellite X-Ray Yields from a Thin Al Target for H^+ and H_2^+ Ion Impact	College of General Education, The University of Tokyo*
2.5	Beam-Foil Spectra of Chlorine Ions In High Energy Region (IV)	Department of Engineering Science, Kyoto University College of General Education, The University of Tokyo*
2.6	Elastic Recoil Detection Analysis with High Energy Heavy Ions	Department of Nuclear Engineering, Tohoku University*
2.8	Construction of an Apparatus for Study of Heavy-Ion Induced Chemical Reactions	Nuclear Engineering Laboratory The University of Tokyo
3.1	A Study of X-ray Diffraction of Heavy Ion Irradiated LiF and Gap Crystals	Faculty of Engineering, Tamagawa University* College of Liberal Arts and Sciences, Okayama University*
3.2	Damage Distribution of Heavy-Ion Irradiation in Metals Studied by Electrical Resistivity Measurements	Faculty of Engineering, Ibaraki University*
3.3	The Effect of High Density Electron Excitation and Electron-Phonon Interaction on the Defect Production in Nickel Irradiated with 100 MeV Heavy Ions	Faculty of Engineering, Ibaraki University*
3.6	Micorstructure and Mechanical Properties of He Irradiated Fe-Cr-Mn alloy	Faculty of Engineering, Nagoya University*

3.8 Ion Conductivity Change of Li_2O by
Oxygen Ion Irradiation

Faculty of Engineering,
Nagoya University[*]

3.10 Irradiation Damage of Ion-Irradiated
Si_3N_4

Faculty of Engineering,
Nagoya University[*]

4.1 Decay Property of ^{245}Cf.

Faculty of Science, Tokyo
Metropolitan University
Faculty of Science, Hiroshima
University
Faculty of Science,
The University of Tokyo
Otemon Gakuin University

4.2 A Helium-Jet Recoil-Transport System
for Studies of Short-Lived Actinide
Nuclides

Faculty of Science, Tokyo
Metropolitan University
Faculty of Science, Hirosima
University
Faculty of Science,
The University of Tokyo
Otemon Gakuin University

4.3 On-Line Mass Separation of the
Monoxides In the Light Rare-Earth
Region

Faculty of Science,
Osaka University[*]

4.4 Decay Spectroscopy of ^{130}Pr, ^{128}Pr,
^{124}La, ^{122}La and the New Isotope
^{121}La

Faculty of Science,
Osaka University

4.5 Proton Induced Fission of Actinide
Elements

Faculty of Science Tokyo
Metropolitan University

4.6 Statistical Decay ^{105}Ag Compound
Nucleus

Faculty of Science
Osaka University,
Faculty of Science Tokyo
Metropolitan University

4.7 Measurement of Fission Fragment
Isotopic Distribution by ISOL

Faculty of Science,
Osaka University[*]

4.9 Nucleon Transfer Reaction of the
^{16}O + ^{197}Au System in the Energy
Region Below 10-MeV/u

Faculty of Science
Osaka University[*]

5.1 Transfer Cross Sections For
^{16}O + $^{148,152}Sm$ Near The Coulomb
Barrier

Faculty of Science
Kyushu University

* Travel Expense is supplied by JAERI